Let's enjoy Scientific English!

Naoko Nakagawa

学術研究出版

Let's enjoy Scientific English!

Naoko Nakagawa

学術研究出版

はじめに

本書は，立教大学の理学部で，５年間にわたり，科学英語の授業をしていた時に作成したプリントや教材として用いたものをまとめたものです．私は，物理学科，化学科，生命理学科の３学科の科学英語の授業を担当していましたが，授業の Reading 練習に用いた論文は，ノーベル賞受賞者の方々の論文だけでなく，私が在籍していた物理学科の教員の方の論文や，自分が過去に執筆した論文も扱っていました．独自に作成したプリントも多数あります．５年経ったところで，一度これらをまとめておきたいと思いました．

科学は国境のない普遍的な学問です．globalization が加速化している昨今においては，科学の分野においても，自分が考えたことを，日本国内のみならず海外にも発信し，また，海外の情報を正確に入手することが重要であり，そのためには共通語である英語を使いこなしていくことが必要不可欠です．問題提起をし，仮説を立て，それを検証する，その世界共通の論理的な展開を，共通語である英語で発信できるようになれば，さらに多くの可能性が拓けることでしょう．理系こそ英語を身につけて，世界に羽ばたいてほしいと思います．しかし，授業をしていく中で，理系の学生さんの中には，英語に苦手意識を持っていらっしゃる方が多いのは事実です．実際，私の周りの研究者の方々にも，英語に苦手意識を持っている方は少なからずいらっしゃいます．これはもしかしたら，大学に入るまでの我が国の英語教育にも問題があるのかもしれません．一方で，いくら英語を聴いたり話したりすることに堪能であっても，伝える内容がなければ意味がありません．逆に科学分野の知識を持った方達が，共通語である英語をコミュニケーションツールとして臆することなく情報発信できるようになれば，もっと楽しい世界が広がることでしょう．そのような，これから社会に飛び立つ学生を応援する気持ちを込めて，私は授業をしていました．

I think “English” is a communication tool to enable information exchange with others as well as a means to develop friendships not only in Japan but also in foreign countries. I would like to teach the Scientific English class with a positive way of thinking so that the students will share information, original ideas, and techniques with confidence when they will become scientists or engineers in the future. Never give up and seize your dream with your own hands!

本書は，授業をしながら限られた時間の中でまとめたものですので，かなり雑駁なところもありますが，科学英語の授業では，科学の分野で必要とされる「論理的に展開する」ということを念頭におきながら，英語の Writing, Reading, Listening, Speaking のスキル向上をはかっていましたので，本書も Writing, Reading, Listening, Speaking の章に分けて構成しました．本書が，これから社会に飛びたち科学分野で活躍するであろう学生の一助となれば，これほどの喜びはありません．

2018 年 9 月 15 日　　立教大学 4207 室にて

中川　直子

目　次

Chapter 1

Reading

科学英語論文を読んでみよう

1－1　英語論文の構造

Reading や Writing のセクションに入る前に，まず，科学英語論文の構造について学んでいきましょう．皆さんがそれぞれの専門の研究室に入って研究を始めると，必ずといっていいほど，英語で書かれた科学論文を読むようになります．日本語で書かれた論文だけを読むよりも，世界の共通語である英語で書かれた論文を探した方が間違いなく幅広い分野を探せます．そして，ご自分も新たに論文を書いて情報発信ができればなおのこと良いです．ここに例として挙げているのは私が以前書いた論文です．論文と言ってもこれはレター（letter）といって，通常の論文は 8 ページから 20 ページに及ぶこともありますが，それをぎゅっと圧縮して 5 ～ 6 ページに短くまとめたものです．短くて内容が一般的なので例としてここに挙げました．論文でもレターでもその構造は変わりません．まず論文の最初のページの上の左端はこの論文が掲載された雑誌名とページ番号などが記されています．そして次に書かれているのが論文のタイトルです．その次に記載されているのが，著者，この論文の場合，私が書いた論文ですので，最初に第一著者である私の名前を記載します．この論文は私が書いた論文ですが，他にも論文執筆や研究に深くかかわった方がいれば，その方たちの名前を列記します．彼らは共著者と呼びます．そしてその下に第一著者および共著者たちの所属を書きます．そしていよいよ本論文に入っていきますが，科学英語論文では，必ずと言っていいほど，つぎのような構造に沿って書かれます．Abstract（概要）→ Introduction（研究の背景）→ Materials and Method（研究に用いた材料と方法）→ Results（結果）→ Discussion（考察）→ Conclusions（結論）→ Acknowledgment（謝辞）→ References（参考文献）です．

Abstract（概要）

Abstract（概要）はこの論文に書かれている内容を短くまとめたセクションで，どのような研究を行ったのか，そしてどのような結果が得られたのかが端的にまとめられています．他の研究者が概要の部分を読んで，この論文を読もうかどうかを決める部分ともいわれており，論文の中で一番重要な部分といっても過言ではありません．この後に載せた，私が以前書いたこの論文内容について説明します．私たちが家庭で使っている一人一日当たりの水使用量のトレンドをみていましたら，近年，その使用量が減っているということに気が付いたのです．そこで，これは家庭で使われている節水機器，例えば，最近はトイレや洗濯機も節水型になっていますし，節水機器の普及によって水使用量が減ってきているのではないかと考え，自分でモデル式を考えて，シミュレーションを行い，シミュレーション結果と実測値との比較をし，将来予測も行ったという論文内容です．ですから私の書いた論文の Abstract（概要）では，家庭用水使用量が家庭の節水機器の普及によって漸減していると仮定して，節水機器の普及率と節水率より, 定量的なシミュレーションを行ったこと, そして結果として, シミュレーションによって実際の水量データ推移が精度よく再現でき，今のトレンドだと 2025 年には 1997 年のピーク時よりも 9％減り，2050 年には 10% 減ることが予想されることを 300 字以内で端的にまとめています．用いられる英文の時制としては過去形, 現在形, そして現在完了形が用いられます．Abstract（概要）の下に書かれているのは，Keywords（キーワード）といって，この論文に出てくる重要単語をいくつか羅列して，他の研究者がこの分野の論文を読みたいと思った時に検索しやすくします．

Introduction（研究の背景）

本論文に入り，まず書かれているのは Introduction（研究の背景）です．ここでは，この領域では今までどのような研究がなされていてどこまで進んでいるか，どんなことがまだわかっていないか，それゆえの本研究の必要性を書き，本研究の目的や，本論文に記載してあるのはどこからどこまでの範囲かを書きます．英文の時制は過去形や現在形，現在完了形が用いられます．今までの研究に関しては，詳しく書いていると紙面を費やしてしまうので，参考文献を示して読者が詳しく知りたいときは参考文献を論文の最後に列記します．参考文献の引用のしかたは掲載される雑誌によって異なりますが，例に挙げた論文では，例えば英文の終わりに（Yamada *et al.* ,2004）と記載されています．これは山田さん他何名かの研究者（山田ら）が 2004 年に出版された論文ということで *et al.* は通常イタリック（斜体）にして記載します．この内容について詳しく知りたい場合は論文の最後にある References の中にある

Yamada K, Tanaka K, Sato Y, Higashi Y. 2004. The structure analysis of domestic water demands ac-

cording to the size of the households. *Proceedings of Environmental System.* JSCE.32: 403-406 (in Japanese).

を検索して調べればいいのです．この項目の見方については後ほど出てくる references の項目で説明します．

Materials and Method（研究に用いた材料と方法）

ここでは，実験に用いた材料やその実験方法が書かれています．私が書いた論文は，家庭で使われる水の量が近年漸減していることに着目してシミュレーションを行った内容で，実験を行ったわけではなく，特に材料となるものは用いていないので，Methodology（方法）というセクションにして，考案したモデルの説明をしています．実験などを行ったときは論文を書くよりも前に行われていますので，英文の時制は過去形で書かれるのが一般的です．また，誰が実験したかは第一著者や共著者であることが明白ですので，物を主語にした（無生物主語といいます）受動態の文章で書かれることが多いです．科学英語のモットーは concise and factual（簡潔かつ事実に基づいている）ですので，なるべく無駄な情報は省くのです．

Results（結果）

例に挙げた論文にもあるように，このセクションでは，本研究によって得られた結果を表や図を用いて説明します．用いられる英文の時制については，過去形や現在形を用います．図や表を説明するときには現在形で書きます．得られた結果に関しては通常過去形で書きますが，通常の英文でもそうですが普遍的な事実を述べる時には現在形で書きます．

Discussion（考察）

このセクションでは結果から考えられる考察を書きます．用いられる英文の時制は現在形が多いですが，予測に関しては未来形も使います．例に挙げた論文でも，得られた結果から考えた今後の予測に関しては未来形が用いられています．また，考察ですので，たぶんこうだろうと憶測が入ることもあり，不確かさを表す助動詞，may, could, would などが用いられることもあります．また，例に挙げた論文のように，Results（結果）と Discussion（考察）を一つのセクションにまとめて Results and Discussion とすることも多いです．例に挙げている論文もそのような形式をとっています．

Conclusions（結論）

本研究のまとめを行います．Abstract（概要）のように，短くまとめる場合が多いです．本研究はどのようなことを目的として行い，結果としてどのようなことが得られたのか，そして今後の展望について端的にまとめます．このセクションで用いられる英文の時制は過去形，現在形が主ですが，今後の展望を述べる時には未来形も用いられます．

Acknowledgment（謝辞）

研究を遂行する際には，国やどこかの機関から助成金などの支援を受けているケースが多いので，ある機関のプロジェクトの一環として行った場合は，プロジェクト名や研究補助金を受けている機関の名前を明記してこのセクションで謝辞を述べます．

References（参考文献）

Introduction（研究の背景）のところで述べたように，研究の背景を述べる時には，その研究で参照されている先行研究について，参考文献を引用しながら，詳しい内容についてはこの参考文献を調べてくださいという意味で参考文献を載せます．参考文献を列記するときの書式は，雑誌によって異なりますが，例えば Introduction（研究の背景）のところで引用した，

Yamada K, Tanaka K, Sato Y, Higashi Y. 2004. The structure analysis of domestic water demands according to the size of the households. *Proceedings of Environmental System.* JSCE.32: 403-406 (in Japanese).

について説明しますと，各項目はピリオドで区切られており，最初に書かれているのが著者の名前です．ファーストネームはイニシャルのみで表す時が多いです．本文中では Yamada *et al.* だけでしたが，この References（参考文献）のセクションでは共著者も含めて全員分の名前を書きます．次の 2004 とあるのは出版された西暦です．そして次に書かれている“The structure analysis of domestic water demands according to the size of the households”は引用した論文の題名，次にイタリック（斜体）で書かれている“*Proceedings of Environmental System*”は論文が掲載されている雑誌名，次の“JSCE”はこの論文を発行している団体名，次に書かれている“32: 403-406”は 32 巻（または号）の 403-406 ページ目に載っているという意味です．最後に引用した文献が日本語で書かれている場合は“(in Japanese)”と付け加えます．このようにして，どの論文から引用したものなのかがはっきりとわかるようにするのです．

論文名　ページ番号

Hydrological Research Letters **3**, 22–26 (2009)
Published online in J-STAGE (www.jstage.jst.go.jp/browse/HRL). DOI: 10.3178/HRL.3.22

Influence of water-related appliances on projected domestic water use in Tokyo

タイトル

Naoko Nakagawa[1]*, Masahiro Otaki[2], Toshiya Aramaki[3] and Akira Kawamura[1]

著者ら

[1]*Dept. of Civil and Environmental Engineering, Tokyo Metropolitan University, 1-1 Minami-Ohsawa, Hachioji, Tokyo, 192-0397, Japan*
[2]*Dept. of Human Environmental Sciences, Ochanomizu University, 2-1-1, Otsuka, Bunkyo-ku, Tokyo, 112-8610, Japan*
[3]*Dept. of Regional Development Studies, Toyo University, 1-1-1 Izumino, Itakura, Oura, Gumma, 374-0193, Japan*

著者らの所属

Abstract: 概要

In this study, the amount of domestic water use was quantified by estimating the usage rates of various water-related appliances. Tokyo Metropolis was selected as a case study because it was relatively easy to obtain detailed data from Tokyo Waterworks Bureau. In the analysis, the calculations for domestic water use reproduced actual usage figures from 1998 to 2006. From the maximum domestic water use per capita in 1997 the projected reduction was estimated to be 9% by 2025 and 10% by 2050. In addition, our results indicate that water use for both bath and toilet is expected to remain high in the future. We performed a simulation assuming that a 6 L-type toilet is installed by all consumers, with the results suggesting that domestic water use per capita per day could reduce to around 200 L. It was therefore concluded that the replacement of a conventional toilet with a water-saving-type toilet is one of the most effective solutions for reducing domestic water use.

KEYWORDS domestic water use; projection; Tokyo; water related appliances; water saving

INTRODUCTION

研究の背景，はじめに

The amount of water supply per capita in Japan increased with economic growth until reaching a plateau in the 1990s, and has since decreased over the last 4–5 years (Ministry of Land, Infrastructure, Transport and Tourism, 2008). The amount of domestic water use per capita in Tokyo also shows a gradual decrease over the last 6–7 years, as shown in Figure 1 (Tokyo Waterworks Bureau, 1980–2008). One reason for this trend is that newer appliances with advanced water saving technology, such as dishwashers and water-saving washing machines, have been developed and supplied to the market in which the usage rates of basic water-related appliances, such as flushing toilets and private baths, have approached a degree of saturation.

The domestic water use per capita is known to be influenced by various factors, such as water charges, household income, household size, climate, precipitation, consciousness about water saving and so on (Aramaki *et al.*, 2004; Yamada *et al.*, 2004; Murase *et al.*, 2005). For example, the pattern of domestic water use has been analyzed according to household size (Yamada *et al.*, 2004). The relationship between water charge and domestic water use has also been analyzed (Murase *et al.*, 2005). However, the models in previous papers have not considered the decreasing trend of domestic water use per capita. It is most likely that the use of advanced water-saving appliances has greatly influenced the downward trend of domestic water use per capita in recent years because the use reduction achieved by these appliances is significant. This trend was also seen in a study of water use in California (CALFED Bay-Delta Program, 2006).

The present study undertook a projection of domestic water use in Tokyo, incorporating simulated usage of a range of water-related appliances including advanced water-saving appliances. In other words, the decreasing trend of domestic water use per capita in recent years was expressed by modeling the introduction of advanced water-saving appliances. The amount of domestic water use per capita was calculated according to the proposed model from 1998 to 2006 and compared with Tokyo's actual data (Figure 1) for that time period setting the parameter at the base year of 1997. The parameters were then used to project water use until 2050.

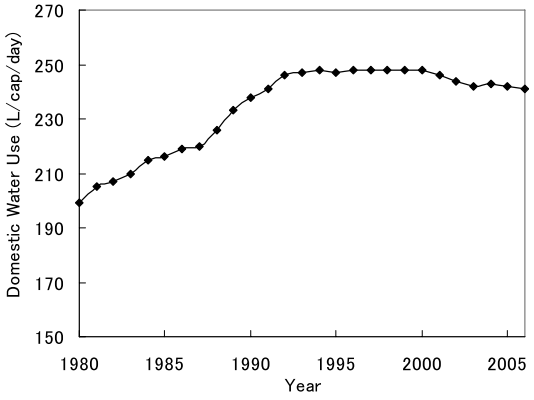

Figure 1. Changes in domestic water use per capita in Tokyo.

図のキャプションは図の下に書く

Correspondence to: Naoko Nakagawa, Department of Civil and Environmental Engineering, Tokyo Metropolitan University, 1-1, Minamiosawa, Hachioji city, Tokyo, 192-0397, Japan. E-mail: nakanaok@tmu.ac.jp.

Received 17 March 2009
Accepted 11 June 2009

MATERIALS and METHOD

METHODOLOGY ← 方法

Estimation of future domestic water use in Tokyo

The domestic water use per capita in Tokyo reached a plateau in 1997, at 248 L/cap/day (Tokyo Waterworks Bureau, 1980–2008). Its subsequent reduction was assumed to result from new water-saving appliances being used in households. Based on this assumption, the amount of water use per capita was calculated for each purpose, classified into kitchen (cooking and dish washing), laundry, toilet, bathing and 'face wash and others' usage. Then, the projected future domestic water use per capita was estimated as the total amount of water consumed for each purpose as shown in Eq. (1).

$$\text{Domestic water use (L/cap/day)} = \sum_{i=1}^{n}[\{b_i \times (1 - a_i) + (1 - b_i)\} \times Q_i] \quad (1)$$

where, i is the purpose of water use in household, a_i is the saving rate of each water-saving appliance, b_i is the usage rate of each water-saving appliance, Q_i is virtual maximum water use for each water use category assuming the water-saving appliances are not used.

The values for a_i are shown in Table I. The saving rate a_i of dishwasher, 24 hours bath, water-saving-type shower, and water-saving tap plug indicate the reduced amount of water for each purpose after introducing these water-related appliances. The saving rate a_i of full automatic washing machine and drum-type washing machine indicate the difference compared to the conventional water tank type washing machine. The saving rate a_i of 10 L-type toilet, 8 L-type toilet, and 6 L-type toilet indicate the difference compared to the conventional 13 L-type toilet. The amount of water use is increased by introducing bidet with a fountain of warm water. Therefore, the domestic water use per capita is assumed to increase 1 L/day when the bidet with a fountain of warm water is introduced.

In order to obtain b_i, past records of usage rates of conventional and water-saving appliances for household water use were used in order to project future trends of usage. Figure 2 shows the domestic usage rates of conventional and water-saving appliances obtained from the field survey of domestic water use that is conducted by the Tokyo Waterworks Bureau every three years. Usage rates shown in this figure for conventional appliances, that is bathtubs, showers, washing machines and flushing toilets, were nearly 100%. Changes in water use occurred due to the use of dishwashers, fully automatic washing machines, 10 L low-flush toilets (10 L indicates 10 liters of water per flush), '24-hour baths' (these are defined as systems offering purification, disinfection, heat insulation, and circulation), water-saving tap plugs and bidets, and each of these were considered in this analysis. The water-saving appliances for which usage rates have been increasing include fully automatic washing machines, dishwashers, and toilets which incorporate a bidet (for washing with a fountain of warm water). Future trends of usage for these appliances were projected by a logistic function using the least-square method. Saturation values of the logistic curve for the usage rate of each water-related appliance were tentatively assumed as shown in Table II considering information about past condition of usage rate. The usage rates of these water-related appliances were obtained from a website (Association of 24 hours bath system, 2008) and an interview survey. According to an interview survey

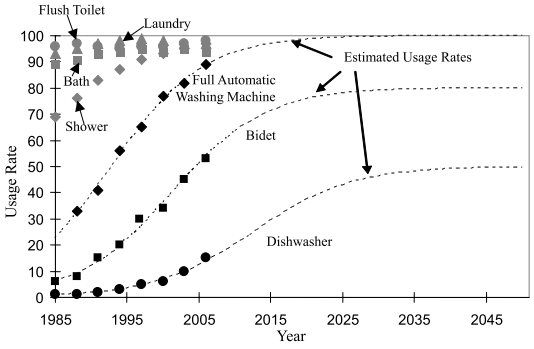

Figure 2. Usage rates of water-related appliances and projected usage rates (Tokyo Waterworks Bureau, 1980–2008).

キャプションは文章にしない

大文字，The はつけない

表のキャプションは表の上に書く
キャプションは文章にしない

Table I. Water-saving rate of appliances.

Ⓟurpose	Ⓦater-related appliances	Saving rate (%)	Source
Kitchen	Dishwasher	80	(Nagasaki Prefecture Government, 2009)
Laundry	Full automatic washing machine	14	(Takada *et al.*, 2005)
	Drum-type washing machine	33	(kain, 2008)
Bath, Shower	24 hours bath	50	Interview survey at the association of 24 hours bath system
	Water-saving-type shower	20	(Nagasaki Prefecture Government, 2009)
Toilet	10 L-type toilet	23	Interview survey at TOTO LTD
	8 L-type toilet	38	Interview survey at TOTO LTD
	6 L-type toilet	53	Interview survey at TOTO LTD
	Bidet with a fountain of warm water	1 L increase*	(Nagasaki Prefecture Government, 2009)
Face wash and others	Water-saving tap plug	50	(Tokyo Waterworks Bureau, 2008)

* '1 L increase' means domestic water use per capita is assumed to increase 1 L/day when the bidet with a fountain of warm water is introduced.

Table II. Saturation usage values for the logistic function of each water-related appliance used in the model.

Purpose	Water-related appliances	Saturation usage value (%)
Kitchen	Dishwasher	50
Laundry	Full automatic washing machine	100
Bath, Shower	24 hours bath	5
Toilet	10 L-type toilet	80
	6 L-type toilet	80
	Bidet with a fountain of warm water	80
Face wash and others	Water-saving tap plug	50

at TOTO Ltd., the usage rate of water-saving toilets has reached about 60% over 30 years. Therefore, the usage rate of a 10 L-type toilet was assumed to be 60% following its introduction to the market in 1994. The future trends for these appliances were also projected by a logistic function with the least-square method as shown in Figures 3(a) and 3(b). Moreover, other water-related appliances, such as drum-type washing machines and water-saving showers have been introduced. However, these appliances were not considered due to their low usage rate and because their use is not currently increasing rapidly.

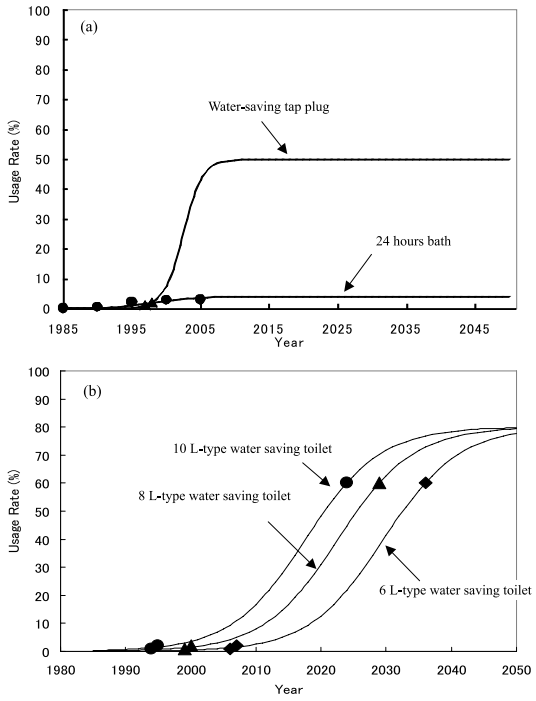

Figure 3. (a) Projected usage rates of 24-hours bath and water-saving tap plug (24-hours Bath System, interview survey at TOTO Ltd.) (b) Projected usage rates of the 6 L, 8 L, and 10 L-type water-saving toilets (6 L, 8 L, and 10 L means the amount of water per flush)

Q_i was determined by the water used per capita for each purpose in 1997 (kitchen, 55.6 L; laundry, 54.2 L; toilet, 59.7 L; bath, 65.3 L; and hand basin and other usages, 20.0 L). Water use for cooking was assumed not to change.

結果と考察

RESULTS AND DISCUSSION

The first projection of domestic water use per capita based on equation (1) is shown in Figure 4. Compared to the actual domestic water use in Tokyo between 1998 and 2006, as obtained from the Tokyo Waterworks Bureau, the calculated amount of the domestic water use per capita per day is accurate to within plus or minus 1%, as shown in Figure 5. According to the model expressed by equation (1), the reduction rate from the maximum water demand in 1997 is projected to be 9% in 2025 and 10% in 2050. A breakdown of the projected domestic water use figures for 2025 and 2050 is shown in Table III.

It is expected that water use for baths and toilets will be substantial in Japan, even in the future, according to past trends of usage rates. It is difficult for people to reduce water usage for bathing from a hygienic point of view. On the other hand, reducing water used in the toilet will contribute to reducing the level of domestic water use in the future.

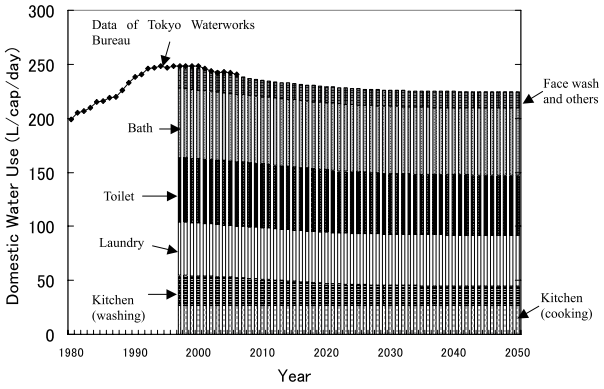

Figure 4. Results of the projection of domestic water use per capita per day.

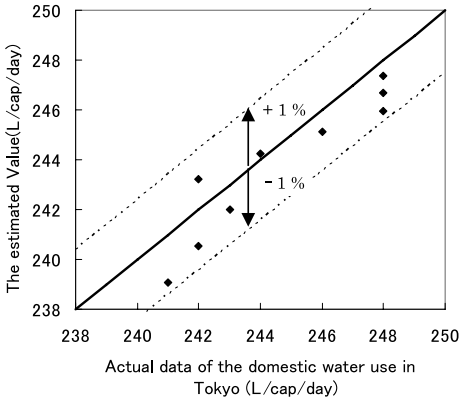

Figure 5. Comparison of the actual data of the domestic water use in Tokyo and the estimated values.

Table III. Breakdown of projected domestic water use.

	Kitchen (cooking)	Kitchen (washing)	Laundry	Toilet	Bath	Face wash and others	Total
Amount of water use in 1997 (L/cap/day)	27.3	27.3	49.5	59.5	64.5	19.8	247.9
Projected water use in 2025 (L/day/cap)	27.3	18.9	47.3	56.4	62.1	14.9	226.8
Reduction rate	0.0%	30.7%	4.7%	5.3%	3.7%	24.9%	8.5%
Projected water use in 2050 (L/day/cap)	27.3	17.4	47.2	55.0	62.1	14.9	223.9
Reduction rate	0.0%	36.1%	4.8%	7.5%	3.7%	24.9%	9.7%

Therefore the second simulation was performed by replacing the 10 L-type toilet with a 6 L-type toilet, and the results are shown in Figure 6. It was found that if the 6 L-type toilet is adopted in Japan according to the projected usage rate as shown in Figure 3 (b), a take-up rate which could be achieved through advertising campaigns and water policy, the domestic water use per capita per day would reduce to around 200 L. In this case the reduction rate is then projected to be 11% by 2025 and 17% by 2050, with 1997 set as the base year.

Here, the market saturation values of first projection shown in Table II were tentatively set from past conditions of usage rate. If the usage rate of 6 L-type toilet, dish washer, and water-saving tap plug will be 100% and the drum-type washing machine with high saving rate (as shown in Table I) will be replaced with the full automatic washing machine as shown in Table IV in the assumption of a scenario where aggressive water saving is accompanied by water conserving policy until 2050, then the total amount of domestic water use would reduce to 171.2 L/cap/day as shown in Table IV. In this case, the water use for toilet and kitchen were significantly reduced; and the reduction rate is projected to be 31% by 2050, with 1997 set as the base year. Therefore it is considered that high efficient water use can be achieved without compromising sanitary living standards, by implementing above-mentioned water-saving appliances.

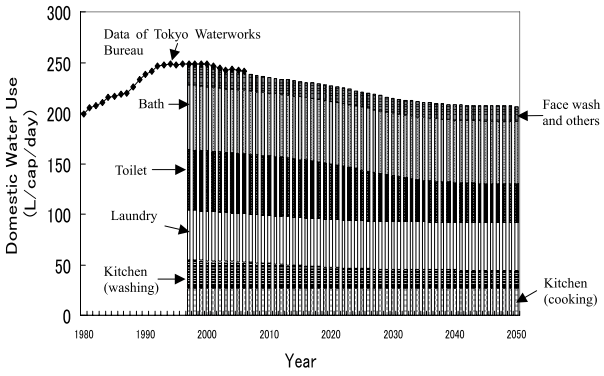

Figure 6. Results of the projection of domestic water use per capita with the 6 L-type toilet instead of the 10 L-type toilet.

CONCLUSIONS ◀･･ 結論

This paper aims to quantify the amount of domestic water use needed in the future by estimating usage rates of various water-related appliances. Tokyo Metropolis was selected as a case study. The results of this study show that the calculated amount of domestic water use reproduced the actual amount of water use between 1998 and 2006 accurately and the reduction rate is projected to be 9% by 2025 and 10% by 2050 with 1997 set as the base year. The model was developed to reflect the present market uptake trends of water-related appliances. In addition, it was considered that the amount of water used for flushing toilets would be substantial even in the future. From the results of a simulation performed by replacing the 10 L-type toilet with a 6 L-type toilet, it was found that the domestic water use per capita per day would reduce to around 200 L. The replacement of a conventional toilet with a water-saving-type toilet is hence one effective solution for reducing domestic water use in the future.

ACKNOWLEDGEMENTS ◀･･ 謝辞

This paper presents the results of the research

Table IV. Breakdown of projected domestic water use with aggressive water saving accompanied by water conservation policy.

	Kitchen (cooking)	Kitchen (washing)	Laundry	Toilet	Bath	Face wash and others	Total
Water-related appliances	–	Dish washer	Drum-type washing machine	6 L-type toilet	24 hours bath	Water-saving tap plug	
Saturation usage value	–	100	100	100	5	100	
Amount of water use in 1997 (L/cap/day)	27.3	27.3	49.6	59.5	64.5	19.8	247.9
Projected water use in 2050 (L/day/cap)	27.3	5.8	37.8	28.2	62.1	10.0	171.2
Reduction rate	0.0%	78.8%	23.8%	52.6%	3.7%	49.5%	31.2%

project “Developing an Integrated Water Cycle Model for Sustainability Assessment of World Water Resources” performed by the Ministry of Education, Culture, Sports, Science and Technology and the research project “Solutions for the water-related problems in Asian metropolitan areas” supported by the Tokyo Metropolitan Government. The authors are grateful to the members of the Tokyo Waterworks Bureau and TOTO LTD for providing valuable data.

REFERENCES ◄··· 参考文献

Aramaki T, Suzuki M, Hanaki K. 2004. International analysis and projection of domestic water use. *Journal of Global Environment Engineering* **10**: 1–10.

Japan, Association for 24 hours bath system. April 1, 2008. *Number of shipments*. http://24furo.v.wol.ne.jp/database/04/index.htm. [June 16, 2009] (in Japanese).

Japan, Ministry of Land, Infrastructure, Transport and Tourism. August 21, 2007. *Transition of the amount of water usage for life*. http://www.mlit.go.jp/tochimizushigen/mizsei/c_actual/images/03-02.gif. [June 7, 2009] (in Japanese).

Japan, Nagasaki Prefecture Government. May 28, 2009. *Results of the field survey of water-saving appliances*. http://www.pref.nagasaki.jp/suido/download/pdf/riyou06.pdf. [June 7, 2009] (in Japanese).

Japan, Tokyo Waterworks Bureau. June 8, 2009. *How to use water efficiently*. http://www.waterworks.metro.tokyo.jp/customer/life/g_jouzu.html. [June 7, 2009] (in Japanese).

Japan, Tokyo Waterworks Bureau. *Annual documents of domestic water use in Tokyo*. 1980–2008. http://www.waterworks.metro.tokyo.jp/customer/life/g_jouzu.html. [June 7, 2009] (in Japanese).

Japan. kain. May 16, 2009. *The amount of the water used of a washing machine*. http://www.seikatu-cb.com/kiwami/siyous01.html. [June 7, 2009] (in Japanese).

Murase M, Nakamura A, Kawasaki H. 2005. An analysis for demand structure and price of domestic water supply. *Proceedings of Hydraulics Engineering*. JSCE. **49**: 475–480 (in Japanese).

Takada J, Tasaka H, Usui S. 2005. Actual water consumption according to the purpose in an ordinary house. *The Collected Lectures of the 56th National Symposium on Water Supply Technology*. 66–67 (in Japanese).

Yamada K, Tanaka K, Sato Y, Higashi Y. 2004. The structure analysis of domestic water demands according to the size of the households. *Proceedings of Environmental System*. JSCE. **32**: 403–406 (in Japanese).

USA, CALFED Bay-Delta Program. 2006. *Water Use Efficiency Comprehensive Evaluation Final Report*. http://www.calwater.ca.gov/content/Documents/library/WUE/2006_WUE_Public_Final.pdf. [June 7, 2009]

1－2　科学論文のリーディング（Reading）のコツ

リーディングの授業では，ノーベル賞を受賞された日本人の方々が書かれた論文や宇宙に関するものを題材として，科学論文のリーディングの仕方を学んでいきましょう．

科学英語論文Reading のコツ

1．専門用語を正確に把握する．
科学分野でよく出てくる専門用語の中には，それ以外の分野とは違う使われ方をしている単語が少なからず存在します．例えば，「value」という単語．これは通常は「価値」という意味で用いられますが，科学論文では「値，数値」という意味で用いられることがほとんどです．「conductor」という単語もそうです．科学論文では，電気や熱を通す「伝導体」という意味で用いられますが，日常生活においては「案内人」や「指揮者」という意味で用いられることが多いです．もともと，「導くもの」という意味を持っているのですね．科学論文を読むときに，「conductor」を「案内人」とか「指揮者」などの意味で解釈してしまうと，内容が分からなくなってしまいます．ですから，科学論文を読む上でまず大事なことは専門用語をしっかりと把握することです．

2．科学英語はほとんど S+V+O+C の文型で，複雑な文はないので（なぜなら，科学英語は concise〈簡潔な〉and factual〈事実に基づく〉がモットー）素早く，どれが主語でどれが述語になるのかを見つけましょう．

3．サイトトランスレーションと呼びますが，英文を関係代名詞や不定詞の前で区切って，前から（戻らずに）英語の語順で訳していくと早く読めるようになると思います．是非試してみてください．

4．英文を音読してみるとよいです．知らない専門用語に出会ったとき，その単語の読み方も一緒に確認して，間違えたまま覚えないようにすると長い目で見れば効率がよいです．例えば，ion, nitro の“ i ”は [ai] と発音するので気を付けましょう．日本語では「イオン」，「ニトロ」と呼んでいるので紛らわしいですが，しっかりと覚えていきましょう．音読することで英語が脳により強くインプットされ，これはスピーキングの際にも役立つというメリットもあります．

1–3　リーディング（Reading）練習の題材

Electrical Conductivity in Doped Polyacetylene

ドープされたポリアセチレンの電気伝導度

ここに紹介するのは，2000 年にノーベル化学賞を受賞された，白川英樹博士の論文です．

導電性ポリマーを作り出したのが白川英樹博士です．ある日，白川博士のところに，ポリアセチレンの合成をしてみたいという研究生が来ました．その研究生は，白川先生が渡したメモに記載された触媒量の単位を間違えて，フラスコに多く入れたのです．想像もしていなかったキラキラと光るフィルム上のポリアセチレンができました．白川博士はその後アメリカに渡った後，そのフィルムにヨウ素を添加して，電気伝導度を測ったところ，驚いたことにその値が何桁も上がりました．この発見を述べた論文を読んでみましょう．

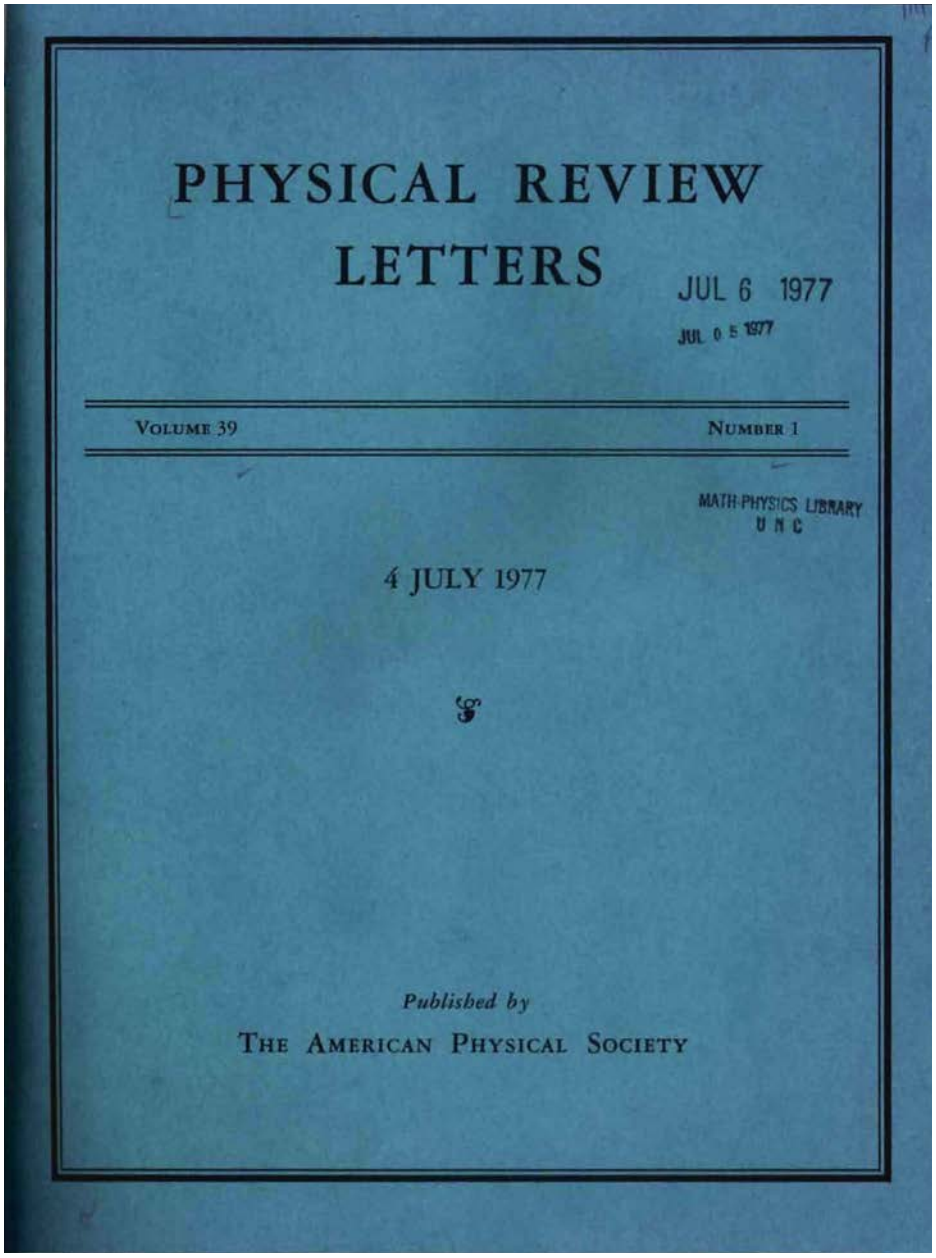

PHYSICAL REVIEW
LETTERS

VOLUME 39 NUMBER 1

4 JULY 1977

Published by
THE AMERICAN PHYSICAL SOCIETY

VOLUME 39, NUMBER 17 PHYSICAL REVIEW LETTERS 24 OCTOBER 1977

Metals, edited by D. H. Douglass (Plenum, New York and London, 1976), and by C. M. Varma and R. C. Dynes, *ibid.*

[9]We have chosen 0.5 eV somewhat arbitrarily to define $D_2^<$. It is the energy near the F.S., scattering within which leads to over 90% of most of the anomalies.

[10]W. Kohn, Phys. Rev. Lett. 2, 393 (1959); A. W. Overhauser, Phys. Rev. Lett. 4, 415 (1960).

Electrical Conductivity in Doped Polyacetylene

C. K. Chiang, C. R. Fincher, Jr., Y. W. Park, and A. J. Heeger

Department of Physics and Laboratory for Research on the Structure of Matter, University of Pennsylvania, Philadelphia, Pennsylvania 19104

and

H. Shirakawa,[a] E. J. Louis, S. C. Gau, and Alan G. MacDiarmid

Department of Chemistry and Laboratory for Research on the Structure of Matter, University of Pennsylvania, Philadelphia, Pennsylvania 19104

(Received 23 June 1977)

Doped polyacetylene forms a new class of conducting polymers in which the electrical conductivity can be systematically and continuously varied over a range of eleven orders of magnitude. Transport studies and far-infrared transmission measurements imply a metal-to-insulator transition at dopant concentrations near 1%.

We find that films of the semiconducting polymer, polyacetylene, show a dramatic increase in electrical conductivity when doped with controlled amounts of the halogens chlorine, bomine, or iodine, and with arsenic pentafluoride (AsF_5). The concentration dependence in combination with far-infrared transmission data suggests the occurrence of a metal-insulator transition as a function of dopant concentration.

Polyacetylene is one of the simplest linear conjugated polymers with a single-chain structure as shown in Fig. 1. Each carbon is σ bonded to one hydrogen and two neighboring carbon atoms consistent with sp^2 hybridization. The π electrons are therefore available to delocalize into a band. In the idealized situation of a uniform chain, the resulting conduction band would give rise to metallic behavior. However, such a system is unstable with respect to bond alternation, which causes the formation of an energy gap in the electronic spectrum. Studies of π-π^* transitions in short-chain polyenes show that the frequencies do not fall as n^{-2} as expected for a free-electron picture, but appear to saturate at $\Delta E_{(n\ \mathrm{large})}^{\pi-\pi^*} \simeq 2.4$ eV.[1] Bond alternation is present in the polymer and would be expected to lead to semiconducting behavior. However, Ovchinnikov[1] has stimmated the bond-alternation energy gap to be too small and attributed the observed value to Coulomb correlation effects, i.e., a Hubbard gap.

In a series of studies Shirakawa and co-workers[2-6] succeeded in synthesizing high-quality polycrystalline films of $(CH)_x$, and developed techniques for controlling the *cis/trans* content.[4,5] These materials are semiconductors[6]; the *trans* isomer is the thermodynamically stable form at room temperature.

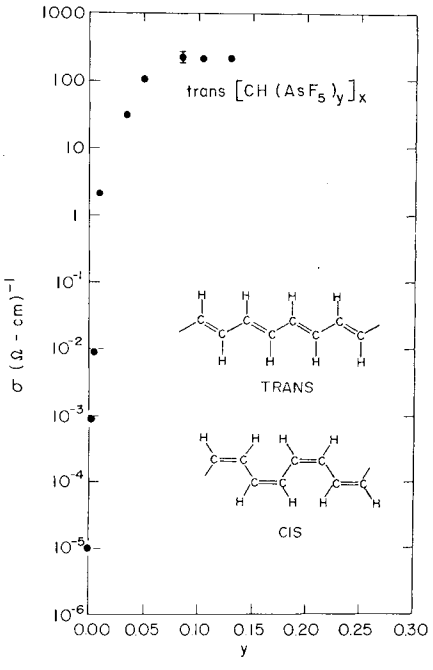

FIG. 1. Electrical conductivity of *trans*-$(CH)_x$ as a function of (AsF_5) dopant concentration. The *trans* and *cis* polymer structures are shown in the inset.

VOLUME 39, NUMBER 17 PHYSICAL REVIEW LETTERS 24 OCTOBER 1977

Polyacetylene crystalline films were prepared with the techniques developed by Shirakawa and co-workers[2-6] in the presence of a Zeigler catalyst. X-ray diffraction and scanning-electron micrograph studies show that films of any *cis* and *trans* composition are crystalline and consist of matted fibrils. The *cis*/*trans* content was controlled by thermal isomerization.[4,5] Details of preparation and characterization are published elsewhere.[7,8]

Samples used in the electrical conductivity study were cut from polymer films approximately 0.1–0.5 mm in thickness. Platinum wires and Electroday were used to make electrical contacts to the films which were treated with the vapor of the dopant at room temperature, *in vacuo*, for 3–4 hours. Their resistance was monitored at at intervals. Final compositions of the doped $(CH)_x$ were determined either by the elemental analysis (Galbraith Laboratories, Inc.) of a piece of reference film placed just below the film whose conductivity was being measured and/or by the increase in weight of the reference film during doping. All conductivity measurements used four-probe dc techniques. Far-ir (400–20 cm^{-1}) transmission measurements were made on films of both pure and doped polyacetylene with use of Grubb-Parsons Michelson interferometer with a helium-cooled gallium-doped germanium bolometer detector. Measurements in the middle ir utilized a Perkin-Elmer 225.

Figure 1 shows the room-temperature electrical conductivity of polyacetylene as a function of AsF_5 concentration; the initial sample was *trans*-rich [*trans* content (95–97)%]. After an initial steep rise over about seven orders of magnitude, the values appear to saturate at 220 Ω^{-1} cm^{-1}. Similar results have been obtained for halogen dopants; e.g., *trans*-$(CHI_{0.20})_x$ yields σ(300 K) $\simeq 160$ Ω^{-1} cm^{-1}.[7-9] The highest-room-temperature results to date have been obtained by doping *cis*-$(CH)_x$ with AsF_5 to yield *cis*-$[CH(AsF_5)_{0.14}]_x$ with $\sigma(300\ K) = 560$ Ω^{-1} cm^{-1}[8]—a value comparable to that obtained with *single crystals* of the organic metal tetrathiafulvalene-tetracyanoquinodimethane (TTF-TCNQ). The concentration dependences observed in all cases studied thus far are similar to Fig. 1; an initial steep rise over many orders of magnitude followed by a leveling off at concentrations above a few percent.

These results suggest that the residual conductivity in "pure" $(CH)_x$ is probably due to residual impurities or defects at very low levels. The extreme sensitivity to impurities is demonstrated in Fig. 1. Moreover, the residual conductivity can be compensated by trace amounts of donor doping. Exposure of "pure" $(CH)_x$ to vapor of the donor, NH_3, causes the conductivity of *trans*-$(CH)_x$ to fall more than four orders of magnitude ($< 10^{-9}$ Ω^{-1} cm^{-1}) without detectable weight increase. Subsequent reaction of the compensated film with AsF_5 brings the conductivity back up to metallic levels—an overall change of eleven orders of magnitude.

Far-infrared transmission data were taken on samples of varying concentrations of iodine and AsF_5 with qualitatively similar results. The data for a series of iodinated samples are shown in Fig. 2 for $y = 0.0$, 0.9, 2.0, and 6.0 at.%. In the case of the 6% sample, there is no observable transmission throughout the ir down to 20 cm^{-1}, implying a continuous excitation spectrum; i.e., metallic. For the 2% sample, the transmission was zero at the high end of the spectrum (4000 cm^{-1} to 300 cm^{-1}), but increases below 300 cm^{-1} to about 60% by 40 cm^{-1}, implying an energy gap at low frequencies. The far-ir transmission through the 0.9% sample is near 90% with no significant change from an undoped sample. The inset to Fig. 2 shows the absorption coefficient α (uncorrected for reflection) at 40 cm^{-1} as a function of dopant concentration. The transition is sharp with a critical concentration (n_c) in the range (2–3)%. Similar results have been obtained with AsF_5 although n_c appears to be slightly smaller. The values for n_c as inferred from the ir and dc transport measurements are in agreement.

Although the initial $(CH)_x$ is crystalline, disor-

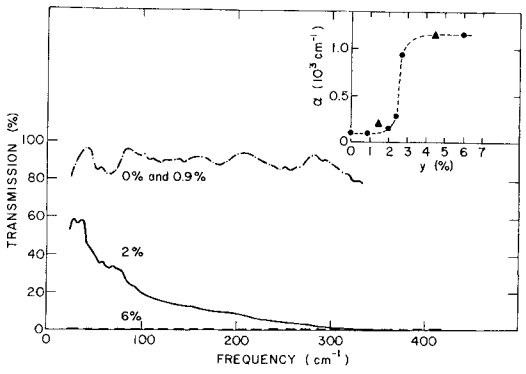

FIG. 2. Far-infrared (20–400 cm^{-1}) transmission of iodine-doped polyacetylene (sample temperature was 77 K). The inset shows the absorption coefficient (uncorrected for reflection) at 40 cm^{-1} vs concentration (solid points, *trans* polymer; triangles, *cis* polymer).

der may play an important role in the doped polymer. In general, we find that plots of $\ln\sigma$ vs $1/T$ do not give straight-line behavior. Plotting the data as $\ln\sigma$ vs $T^{-1/4}$ (or $T^{-1/2}$) tends to give more nearly straight-line behavior at least in the low-concentration range below n_c where the results are typical of transport in disordered and amorphous systems.[10] Variable-range hopping[11] between localized states leads to temperature dependences of the form $\sigma \propto \exp[-(T_0/T)^{1/(d+1)}]$, where d is the dimensionality of the transport (e.g., $d=3$ for three-dimensional motion, etc.).

A qualitative change in the temperature dependence of the dc conductivity is observed at the critical concentration as shown in Fig. 3, where we plot $\sigma(T)/\sigma(300\ \mathrm{K})$ vs T on a linear scale. At low concentrations the curves appear thermally activated with generally upward curvature. Above n_c, the curvature changes and the conductivity decreases slowly with decreasing temperature, heading toward zero approximately linearly in T.

As an initial point of view we treat this transition as similar to that seen in heavily doped semiconductors. If this is the case, one expects the halogen and AsF_5 dopants to act as acceptors with localized hole states in the gap, with the hole bound to the acceptor in a hydrogenlike fashion. For low concentrations, one expects the combination of impurity ionization and variable-range hopping to lead to a combination of activated processes as observed experimentally. However, as extensively discussed by Mott[12] and others,[13] if the concentration is increased to a critical level, then the screening from carriers will destroy the bound states giving an insulator-to-metal transition. This will occur when the screening length becomes less than the radius of the most tightly bound Bohr orbit of the hole and acceptor in the bulk dielectric[12];

$$n_c^{1/3} \simeq (4a_{\mathrm{H}})^{-1}\left(\frac{m^*}{m\epsilon}\right)^2,$$

where a_{H} is the Bohr radius, ϵ is the dielectric constant of the medium, and m^*/m is the ratio of the band mass to the free-electron mass. Assuming $m^*/m \simeq 1$ and using $\epsilon \simeq 3$ from far-ir reflection measurements, we estimate that $n_c \simeq 2 \times 10^{20}\ \mathrm{cm}^{-3}$. Since the density of carbon atoms is about $2\times10^{22}\ \mathrm{cm}^{-3}$, n_c would be at about 1%, assuming one carrier per dopant. The excellent agreement with our experimental results is fortuitous in view of the much over-simplified model. However, the scale is correct; the transition occurs at about 1% because of the relatively small dielectric constant. Although we have discussed the metal-insulator transition from the point of view of simple semiconductor theory, the relative importance of Coulomb correlation effects must be considered.[2]

The polymer structure of polyacetylene implies strong π overlap along the chain with weaker interchain coupling since the intrachain carbon-carbon–bond length is about 1.4 Å whereas the interchain spacing is 3.6 Å.[2-5] Thus we expect the resulting metal to be anisotropic, and possibly quasi–one-dimensional. The temperature dependence of the conductivity above n_c is consistent with that expected for a disordered one-dimensional metal.[14] Since all states are localized in such a system,[15] the static conductivity goes to zero at $T=0$ K. However, when the electron-phonon interaction is taken into account, phonon-assisted diffusion through the localized states leads to finite conductivity with a temperature dependence determined by the number of thermal phonons in the modes to which the conduction electrons are strongly coupled.[14] In addition interfibril contact may be playing a role. Studies of the temperature dependence of the conductivity of polycrystalline $(SN)_x$[16,17] and organic conductors

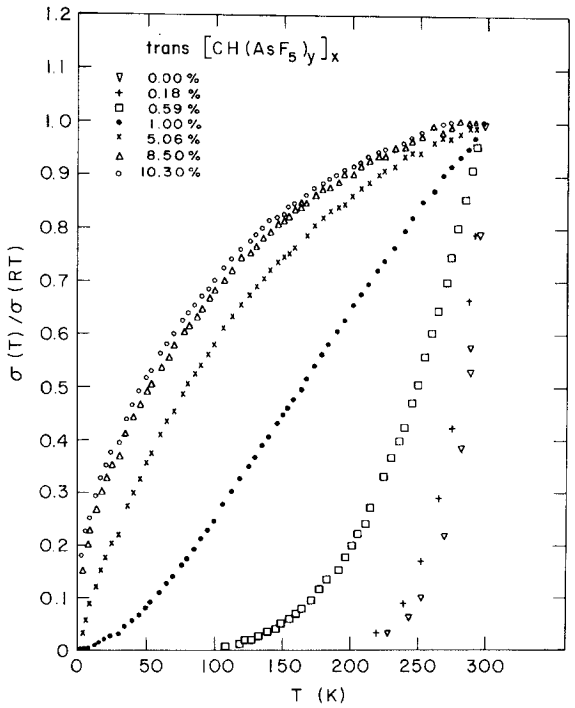

FIG. 3. Temperature dependence of the normalized conductivity at several doping levels (AsF_5).

such as TTF-TCNQ[18] often show monotonically decreasing conductivity even though the single-crystal data indicate metallic behavior.

In the metallic state, the carrier mobility may be estimated from $\sigma = ne\mu$, where n is the carrier density, e is the electronic charge, and μ is the mobility. Using $\sigma = 560\ \Omega^{-1}\ \mathrm{cm}^{-1}$ for *cis*-$[CH(AsF_5)_{0.14}]_x$ and assuming one carrier per AsF_5, we find $\mu \simeq 1\ \mathrm{cm}^2/\mathrm{V\ sec}$—surprisingly high when compared with typical polymer photoconductors[19] ($\mu \sim 10^{-7}\ \mathrm{cm}^2/\mathrm{V\ sec}$) or even with copper metal ($\mu \sim 20\ \mathrm{cm}^2/\mathrm{V\ sec}$). Given the anisotropic polymer structure and the fibrous nature of the low-density as-grown films,[2-6] higher conductivities may be expected from aligned films of $(CH)_x$ derivatives.

In summary, we have shown that doped polyacetylene forms a new class of conducting polymers in which the electrical conductivity can be systematically and continuously varied over a range of eleven orders of magnitude. Transport studies and far-ir transmission measurements imply a metal-insulator transition at dopant concentrations near 1%. We have obtained room-temperature conductivities for polycrystalline films of the doped polymer comparable to that found on single crystals of the organic metal TTF-TCNQ. Use of different dopants and replacement of the H atoms in $(CH)_x$ with organic or inorganic groups should lead to a large new class of conducting polymers with electrical properties that can be controlled over the full range from insulator to semiconductor to metal.

This work was supported by the Office of Naval Research.

[a]Permanent address: Tokyo Institute of Technology, Tokyo, Japan.

[1]For a summary of these data and detailed references, see A. A. Ovchinnikov, Usp. Fiz. Nauk 108, 81 (1973) [Sov. Phys. Usp. 15, 575 (1973)].

[2]H. Shirakawa and S. Ikeda, Polym. J. 2, 231 (1971).

[3]H. Shirakawa, T. Ito, and S. Ikeda, Polym. J 4, 460 (1973).

[4]T. Ito, H. Shirakawa, and S. Ikeda, J. Polym. Sci. Polym. Chem. Ed. 12, 11 (1974).

[5]T. Ito, H. Shirakawa, and S. Ikeda, J. Polym. Sci. Polym. Chem. Ed. 13, 1943 (1975).

[6]H. Shirakawa, T. Ito, and S. Ikeda, unpublished.

[7]H. Shirakawa, E. J. Louis, A. G. MacDiarmid, C. K. Chiang, and A. J. Heeger, to be published.

[8]C. K. Chiang, M. A. Druy, S. C. Gau, A. J. Heeger, E. J. Louis, A. G. MacDiarmid, Y. W. Park, and H. Shirakawa, to be published. The conductivity of doped $(CH)_x$ is electronic. No increase in resistance was observed after passing enough current through the sample that the integrated charge exceeded by a factor of 10 the amount needed to cause complete polarization, if conduction were by an ionic mechanism.

[9]The more recent iodination experiments involving *trans*-$(CH)_x$ yield significantly improved electrical properties ($\sigma = 160\ \Omega^{-1}\ \mathrm{cm}^{-1}$) as compared with earlier results (Ref. 7) ($\sigma = 30\ \Omega^{-1}\ \mathrm{cm}^{-1}$). This increase may be related to the rate of iodination leading to more uniform doping through the thickness of the films. Detailed studies of the effects of film thickness, reaction rate, etc., are underway.

[10]H. Fritchie, in *Electronic Properties of Materials*, edited by R. H. Bube (McGraw-Hill, New York, 1972), Chap. 13; A. K. Jonscher, J. Vac. Sci. Technol. 8, 135 (1971); R. S. Allgaier, J. Vac. Sci. Technol. 8, 113 (1971); R. M. Hill, Philos. Mag. 23, 59 (1971).

[11]N. F. Mott, Philos. Mag. 19, 835 (1969); N. F. Mott, in *Festkörperprobleme*, edited by J. H. Queisser (Pergamon, New York, 1969), Vol. 9, p. 22; V. Ambegaokar, B. I. Halperin, and J. S. Langer, Phys. Rev. B 4, 2612 (1971).

[12]N. F. Mott, Adv. Phys. 21, 785 (1972).

[13]See, for example, J. M. Ziman, *Principles of the Theory of Solids* (Cambridge Univ. Press, Cambridge, England, 1972), 2nd ed., p. 168–170.

[14]A. A. Gogolin, V. I. Mel'nikov, and E. I. Rashba, Zh. Eksp. Teor. Fiz. 69, 327 (1975) [Sov. Phys. JETP 38, 620 (1974)].

[15]N. F. Mott and W. D. Twose, Adv. Phys. 10, 107 (1961).

[16]M. M. Labes, Pure Appl. Chem. 12, 275 (1966).

[17]A. A. Bright, M. J. Cohen, A. F. Garito, and A. J. Heeger, C. M. Mikulski, and A. G. MacDiarmid, Appl. Phys. Lett. 26, 612 (1975).

[18]L. B. Coleman, Ph.D. thesis, University of Pennsylvania, 1975 (unpublished).

[19]W. D. Gill, J. Appl. Phys. 43, 5033 (1972).

Electrical Conductivity in Doped Polyacetylene

Vocabulary

electrical conductivity	電気伝導度
dope	ドープする（結晶の性質を変えるために少量の不純物を添加すること）
Polyacetylene	ポリアセチレン
conducting polymer	電導性ポリマー
eleven orders of magnitude	11桁
transport	輸送
in combination with~	～と共に，～と結合して
far-infrared	遠赤外線の
transmission	透過
imply	示唆する
metal-to-insulator	金属・絶縁体の
transition	遷移
dopant concentrations	ドーパント濃度（不純物の濃度）
semiconducting	半導体の
polymer	ポリマー，重合体
dramatic	急激な
halogens	ハロゲン族元素
chlorine	塩素
bromine	臭素
iodine	ヨウ素
arsenic pentafluoride (AsF5)	５フッ化ヒ素
suggest	示す，示唆する
conjugated polymer	共役系高分子（単結合と二重結合が交互に連なっている高分子のこと）
single-chain	単鎖
σ bond	σ結合
neighboring	隣接した

consistent with~	～と一致して
hybridization	混成
π electron	π 電子
be available~	～できる
delocalize	非局在化する
idealized situation	理想状態
a uniform chain	１本鎖
conduction band	伝導体バンド
metallic	金属の
unstable	不安定な
with respect to	～に関して
bond alternation	結合交替（単結合と二重結合が交互になること）
energy gap	エネルギーギャップ
electronic spectrum	電子スペクトル
π-π* transitions	π-π* 遷移
short-chain	短鎖の
polyene	ポリエン
frequencies	周波数
free-electron	自由電子
saturate	飽和する
estimate	推測する
attribute~to ―	～を―によって説明する
the observed value	観測値，測定値
Coulomb correlation effects	クーロン相関効果
i.e.	例えば，すなわち
in a series of ~	一連の～
succeeded in ~	～に成功する
cis/trans	シス－トランス
content	含有率，内容
semiconductor	半導体
***trans* isomer**	トランス異性体

thermodynamically	熱力学的に
stable	安定な
crystalline	結晶の，結晶体から成る
Polyacetylene crystalline films	ポリアセチレン結晶フィルム
catalyst	触媒
X-ray diffraction	X線回折
scanning-electron micrograph	走査型電子顕微鏡写真
matted fibrils	絡み合った微小繊維
thermal isomerization	熱異性化
Electroday	電極（=electrode）
in vacuo	真空中で
four-probe dc techniques	４端子直流法
interferometer	干渉計
germanium bolometer detector	ゲルマニウムボロメーター検出器
middle ir	中波長赤外線
e.g.	例えば
yield	もたらす，与える，引き起こす
comparable to~	～に匹敵する
organic metal	有機金属
tetrathiafulvalene-tetracyanoquinodimethane (TTF-TCNQ)	テトラチアフルバレン－テトラシアノキノジメタン（TTF-TCNQ）
followed by~	続いて～になる
due to~	～による
residual	残りの
residual impurities	残留不純物
demonstrate	論証する
compensate	補填する
exposure	曝露
subsequent	その後の，それ以降の

p.1098

Electrical Conductivity in Doped Polyacetylene

ドープされたポリアセチレンの電気伝導度

Abstract（概要）

Doped polyacetylene forms a new class of conducting polymers in which the electrical conductivity can be systematically and continuously varied over a range of eleven orders of magnitude. Transport studies and far-infrared transmission measurements imply a metal-to-insulator transition at dopant concentrations near 1%.

We find that films of the semiconducting polymer, polyacetylene, show a dramatic increase in electrical conductivity when doped with controlled amounts of the halogens chlorine, bromine, or iodine, and with arsenic pentafluoride (AsF_5).

The concentration dependence in combination with far-infrared transmission data suggests the occurrence of a metal-insulator transition as a function of dopant concentration.

Polyacetylene is one of the simplest linear conjugated polymers with a single-chain structure as shown in Fig. 1. Each carbon is σ bonded to one hydrogen and two neighboring carbon atoms consistent with sp^2 hybridization. The π electrons are therefore available to delocalize into a band.

In the idealized situation of a uniform chain, the resulting conduction band would give rise to metallic behavior. However, such a system is unstable with respect to bond alternation, which causes the formation of an energy gap in the electronic spectrum.

Studies of π - π * transitions in short-chain polyenes show that the frequencies do not fall as n^{-2} as expected for a free-electron picture, but appear to saturate at $\Delta E_{(n\ large)}{}^{\pi-\pi^*} \simeq 2.4$ eV.[1]

Bond alternation is present in the polymer and would be expected to lead to semiconducting behavior. However, Ovchinnikov[1] has estimated the bond-alternation energy gap to be too small and attributed the observed value to Coulomb correlation effects, i.e., a Hubbard gap.

In a series of studies Shirakawa and co-workers[2-6] succeeded in synthesizing high-quality polycrystalline films of $(CH)_x$, and developed techniques for controlling the *cis/trans* content.[4,5] These materials are semiconductors[6] ; the *trans* isomer is the thermodynamically stable form at room temperature.

Polyacetylene crystalline films were prepared with the techniques developed by Shirakawa and co-workers[2-6] in the presence of a Zeigler catalyst.

X-ray diffraction and scanning-electron micrograph studies show that films of any *cis* and *trans* composition are crystalline and consist of matted fibrils.

The *cis/trans* content was controlled by thermal isomerization. [4,5] Details of preparation and characterization are published elsewhere.[7,8]

Samples used in the electrical conductivity study were cut from polymer films approximately 0.1-0.5 mm in thickness. Platinum wires and Electroday were used to make electrical contacts to the films which were treated with the vapor of the dopant at room temperature, *in vacuo* , for 3-4 hours. Their resistance was monitored at intervals.

Final compositions of the doped $(CH)_x$ were determined either by the elemental analysis (Galbraith Laboratories, Inc.) of a piece of reference film placed just below the film whose conductivity was being measured and/or by the increase in weight of the reference film during doping. All conductivity measurements used four-probe dc techniques.

Far-ir (400-20 cm^{-1}) transmission measurements were made on films of both pure and doped polyacetylene with use of Grubb-Parsons Michelson interferometer with a helium-cooled gallium-doped germanium bolometer detector.

Measurements in the middle ir utilized a Perkin-Elmer 225.

Figure 1 shows the room-temperature electrical conductivity of polyacetylene as a function of AsF_5 concentration; the initial sample was *trans*-rich [*trans* content (95-97) %].

After an initial steep rise over about seven orders of magnitude, the values appear to saturate at 220 $\Omega^{-1}cm^{-1}$.

Similar results have been obtained for halogen dopants; e.g., *trans*-$(CHI_{0,20})_x$, yields σ (300 K) ≃ 160 $\Omega^{-1}cm^{-1}$.[7-9]

The highest-room-temperature results to date have been obtained by doping *cis*-$(CH)_x$, with AsF_5 to yield *cis*-$[CH(AsF_5)_{0,14})]_x$ with σ (300 K) = 560 $\Omega^{-1}cm^{-1}$ [8]—a value comparable to that obtained with *single crystals* of the organic metal tetrathiafulvalene-tetracyanoquinodimethane(TTF-TCNQ).

The concentration dependences observed in all cases studied thus far are similar to Fig. 1; an initial steep rise over many orders of magnitude followed by a leveling off at concentrations above a few percent.

These results suggest that the residual conductivity in "pure" $(CH)_x$ is probably due to residual impurities or defects at very low levels.

The extreme sensitivity to impurities is demonstrated in Fig. 1.

Moreover, the residual conductivity can be compensated by trace amounts of donor doping.

Exposure of "pure" $(CH)_x$ to vapor of the donor, NH_3 causes the conductivity of *trans*-$(CH)_x$ to fall more than four orders of magnitude ($<10^{-9}$ $\Omega^{-1}cm^{-1}$) without detectable weight increase.

Subsequent reaction of the compensated film with AsF_5 brings the conductivity back up to metallic levels—an overall change of eleven orders of magnitude.

Far-infrared transmission data were taken on samples of varying concentrations of iodine and AsF_5 with qualitatively similar results.

The data for a series of iodinated samples are shown in Fig. 2 for y=0.0, 0.9, 2.0, and 6.0 at. % .

In the case of the 6% sample, there is no observable transmission throughout the ir down to 20 cm^{-1}, implying a continuous excitation spectrum; i.e., metallic.

For the 2% sample, the transmission was zero at the high end of the spectrum (4000 cm^{-1} to 300 cm^{-1}), but increases below 300 cm^{-1} to about 60% by 40 cm^{-1}, implying an energy gap at low frequencies.

The far-ir transmission through the 0.9% sample is near 90% with no significant change from an undoped sample.

遠赤外線透過

The inset to Fig. 2 shows the absorption coefficient α (uncorrected for reflection) at 40 cm^{-1} as a function of dopant concentration.

The transition is sharp with a critical concentration (n_c) in the range (2-3)%.

Similar results have been obtained with AsF_5, although n_c, appears to be slightly smaller.

The values for n_c as inferred from the ir and dc transport measurements are in agreement.

Although the initial $(CH)_x$ is crystalline, disorder may play an important role in the doped polymer.

p.1101　四角で囲ってある部分

In summary, we have shown that doped polyacetylene forms a new class of conducting polymers in which the electrical conductivity can be systematically and continuously varied over a range of eleven orders of magnitude.

Transport studies and far-ir transmission measurements imply a metal-insulator transition at dopant concentrations near 1%.

We have obtained room-temperature conductivities for polycrystalline films of the doped polymer comparable to that found on single crystals of the organic metal TTF-TCNQ.

Use of different dopants and replacement of the H atoms in $(CH)_x$ with organic or inorganic groups should lead to a large new class of conducting polymers with electrical properties that can be controlled over the full range from insulator to semiconductor to metal.

This work was supported by the Office of Naval Research.

Protein and Polymer Analyses up to *m/z* 100 000 by Laser Ionization Time-of-flight Mass Spectrometry

レーザーイオン化飛行時間質量分析法による*m/z* 100 000までのタンパク質やポリマーの分析

こちらの論文は，2002 年にノーベル化学賞を受賞した田中耕一博士の論文です．

田中博士が開発した分析方法は，生命の辞書を逆引きした技術と言われています．ヒトゲノム解読の結果病気や退室に関連する様々な遺伝情報が明らかにされましたが，一方では働きのわからない遺伝子も多く残されました．もし，遺伝子から作られた，タンパク質の方から，その性質や役割を突き止めることができれば，逆にわからなかった遺伝情報を明らかにできるかもしれない．また，タンパク質の解析をすることで，新しい薬の開発や病気診断，予防にも役立てられると考え，タンパク質を分析することが必要と考えました．

タンパク質を分析するには分子を一つずつイオンにして分析することが必要であり，田中博士はレーザーを照射してタンパク質を分析する，レーザーイオン化飛行時間質量分析法という方法を用いていましたが，タンパク質のような高分子は，レーザーの熱でバラバラになってしまい，イオン化するのが困難でした．そこで，何か特別な物質を混ぜて分子を保護してイオン化できないかと考えました．

ある日，質量分析計に導入するサンプルを調整している時に，加える試薬を間違え，グリセリンを混ぜてしまいました．捨てるのももったいないのでそのまま測ることにしました．するとどうでしょう，グリセリンを混ぜたおかげで，これまでできなかった，高分子をイオン化することに成功したのです．この「最高の失敗」を述べた論文を読んでみましょう．

Protein and Polymer Analyses up to *m/z* 100 000 by Laser Ionization Time-of-flight Mass Spectrometry

タイトル

Koichi Tanaka†, Hiroaki Waki, Yutaka Ido, Satoshi Akita, Yoshikazu Yoshida and Tamio Yoshida

著者ら

Shimadzu Corporation, Nishinokyo-Kuwabaracho, Nakagyo-ku, Kyoto 604, Japan

SPONSOR REFEREE: T. Matsuo, Osaka University, Osaka, Japan

Hitherto, ^{252}Cf plasma desorption mass spectrometry (PDMS) has been used to study peptides and proteins in the molecular weight range from 1 kDa to 35 kDa.[1,2] Fast atom bombardment mass spectrometry (FABMS) and secondary ion mass spectrometry (SIMS) have been applied to the analyses of proteins and polymers molecules.[3,4] On the other hand, in the area of laser desorption time-of-flight (TOF) mass spectrometry (MS), though there have been many papers on analyses of organic compounds, the molecular weight of these compounds has been relatively low.[5]

For the purpose of investigating the mass spectrometry of high-mass molecular organic compounds, we developed a laser ionization TOF mass spectrometer. To assess the utility of this spectrometer for high masses, we evaluated and tried the mass spectrometer on various organic compounds.[6,7] This spectrometer was able to obtain useful spectra up to *m/z* 100 000. Typical spectra of proteins and polymers with molecular weights up to 25 kDa are shown in this paper.

EXPERIMENTAL

実験，方法

Apparatus

The construction of the laser ionization TOF mass spectrometer (Shimadzu LAMS-50K) is shown in Fig. 1. A nitrogen laser (wavelength: 337 nm, pulse width: about 15 ns, pulse energy: 4 mJ max.) was used for sample ionization. The sample, mounted on the sample holder, was capable of small movements in the plane perpendicular to the ion axis. The magnification image of the sample surface could be observed on the TV monitor. These features provided reliable analysis of the selected area. The ion acceleration voltage of 5 kV was applied to the sample holder.

Generally, TOF-MS has the following characteristics: very high transmission; measurement times of less than a few hundreds of μs; unlimited mass range, low mass resolution.

A new "gradient electric field type ion reflector"[8] for a TOF mass spectrometer has been developed in order to improve mass spectral resolution by time focusing. The TOF mass separation system was designed to select the "reflection type" (above-mentioned) or the "linear type" (without reflecting electric field). For ion detection, a micro channel plate (MCP) was used, which was equipped with an ion to electron converter in order to improve the sensitivity of detection for high-mass ions.

† Author to whom correspondence should be addressed.

Two TOF systems were constructed. The first system utilized a digital wave memory and accumulation circuits. This system could accumulate the spectrum data of 8 K words within 1 ms. In the first place, a "one shot" TOF spectrum was stored into the wave memory, in the subsequent accumulating circuits the spectrum was accumulated in sequence. The second system utilized a constant fraction discriminator (CFD) and a multi-stop time-to-digital converter (TDC). The time intervals between "start" and "stop" pulses were measured with a time resolution of 1 ns. In these experiments, the first system (AD method) was only used.

The measuring circuit was controlled with a microprocessor [Intel 80286, Intel, CA, USA], and the TOF spectrum obtained with those measurement systems could be provided with various processes, e.g., smoothing, background subtraction, peak detection and mass number calibration.

Sample preparation

We investigated the method of sample preparation to increase the yield of high-mass ions and to prolong the production time. As a result, it was found that the yield of ions and the sustained production time largely depended on the method of sample preparation and that the "ultra fine metal plus liquid matrix method", described below, was extremely effective.

A sample was made into a solution having a concentration of about 10 μg/10 μL using distilled water as the solvent. About 10 μL of this sample solution was dripped onto the sample holder. On the other hand, an ultra fine metal powder ((UFP), in these experiments, we used cobalt powder of about 300 Å diameter purchased from Vacuum Metallurgical Co. in Japan) and glycerol were dissolved with organic solvents, e.g., ethanol and acetone. About 10 μL of this solution was also dripped onto the sample holder. A mixture of the two solutions was then vacuum dried for a short time to remove volatile compounds of the solution. The sample holder, with sample, was then introduced into the mass spectrometer to start analysis. This sample preparation method was simple with preparation times of less than a few minutes.

Data acquisition

Several one-shot spectra were accumulated from a single sample introduction to produce the final spectrum, giving total data acquisition times of 2 or 4 min; in some cases two or more significant spectra were

CCC-0951-4198/88/0151-0153 $1.50

掲載された雑誌名

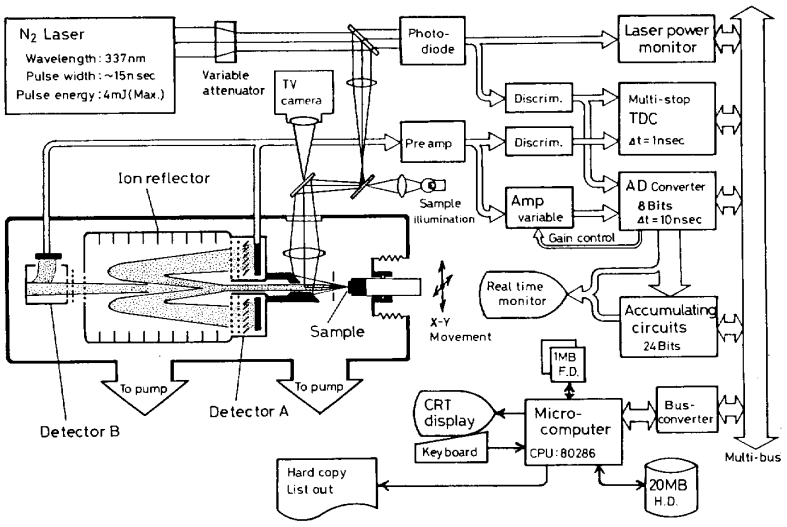

Figure 1. Construction of the laser ionization TOF mass spectrometer.

obtained from a single sample introduction. The final spectrum data were smoothed and sometimes background was subtracted and the position of the peak tops determined. Mass number calibrations were carried out by using cationized molecular ion peaks ($[M+Na]^+$) of poly(ethylene glycol) ((PEG); mixture of PEG 200, 400, 600, 1000, 1500 and 2000) as measures of isotopically averaged mass (chemical mass).

結果と考察

RESULTS AND DISCUSSION

This mass spectrometer was successfully applied to the detection of high-mass molecular ions, e.g., lysozyme, mol. wt 14306 Da (Fig. 2); chymotrypsinogen, mol. wt 25717 Da (Fig. 3); poly(propylene glycol) (PPG), average mol. wt 4 kDa (Fig. 4); and PEG20K, average mol. wt ca 20 kDa (Fig. 5).

It was impossible to detect high-mass molecular ions from these samples without using the "ultra fine metal plus liquid matrix method" for sample preparation.

UFP has the following features in comparison with bulk: high photo-absorption, low heat capacity, and extremely large surface area per unit volume. "Rapid heating" of the sample was used as a volatility enhancement technique of organic compounds[9] and it was achieved by irradiating a pulsed laser on the sample surface. We suppose that UFP in the sample enhances the speed of sample heating, by laser irradiation, due to the above mentioned features. Consequently, molecular ions are formed more easily. By the addition of glycerol to the sample, molecules of the sample are replenished to the laser beam irradiation position and it is considered that the ion formation is allowed to continue for a long time.

Figure 2 shows the singly- and many of the doubly-charged cluster ions of lysozyme. Quasi-molecular ions (may be mostly in the form of $[M+Cation]^+$) of lysozyme were also clearly found.[10] This mass spectrometer could detect $[n\times M+Cation]^+$ and $[n\times M+2\times Cation]^{2+}$ ($n=1$–7) of lysozyme. As far as we know, ions of $m/z \geq 100000$ are the highest organic ion yet observed by laser ionization/desorption mass spectrometry.

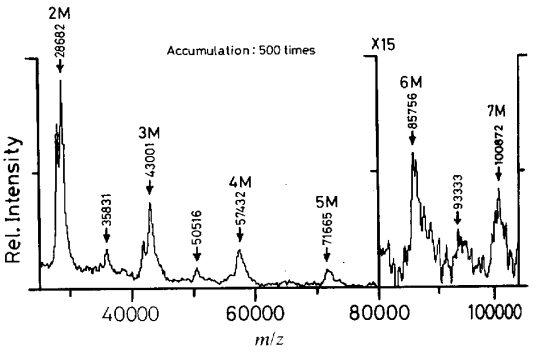

Figure 2. Laser ionization mass spectrum of lysozyme from chicken egg white, mol. wt 14306 Da.

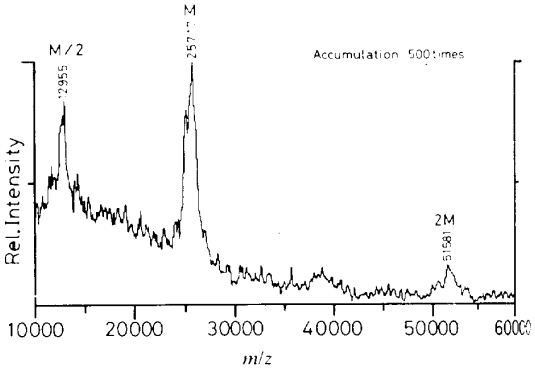

Figure 3. Laser ionization mass spectrum of chymotrypsinogen, mol wt 25717 Da.

Figure 3 shows the singly- and doubly-charged quasi-molecular ions and the cluster ion of chymotrypsinogen. This spectrometer was also capable of detecting the quasi-molecular ion of carboxypeptidase-A (mol. wt 34472 Da),[10] bovine insulin (mol. wt 5733 Da),[6] cytochrome-C (mol. wt 12384 Da)[7] and so on.

The widths of all the peaks associated with the molecule (over 1000 Da wide in most cases) were broader than those expected from the distribution of isotopes in the molecule. The origin of these observed broad peaks is uncertain. Impurities in the sample, together with adduct ions $[M+Na]^+$, $[M+K]^+$ and $[M+H]^+$, as well as metastable peaks arising from these ions, are all possible contributors.

Figure 4 shows cationized molecular ion peaks $[M+Na]^+$ of PPG having the nonlinear structure. The intensity of fragment peaks was so weak compared to that of the molecular ions that it was easy to calculate the average molecular weight from this spectrum. Figure 5 shows the molecular ion region spectrum of PEG20K. Each peak for the different polymerization (n) is not separated. It is supposed, however, that the shape of this spectrum shows the distribution envelope of PEG20K molecules.

We observed the spectrum about 10 times for each sample above. Those peak tops, taken in all cases to be the cationized molecular ion $[M+Na]^+$, allowed the molecular weight to be determined within ±1%.

In conclusion, analytically useful spectra from proteins and polymers with molecular weights as high as 34 kDa were obtained by using the laser ionization TOF mass spectrometer. The time required to obtain such spectra was very short compared with PDMS and comparable to liquid SIMS.[3]

The methods commonly used at present for molecular weight determination of proteins and polymers are sodium dodecyl sulfate poly-acrylamide gel electrophoresis (SDS-PAGE), gel permeation chromatography (GPC) and viscosity method. These methods normally allow a molecular weight determination precision of ca±10%. The precision may be influenced by other properties of the molecule such as conformational state and hydrophobicity. In addition, with these latter techniques, the measurement times are considerably longer. In comparison with these methods, the precision of this laser ionization TOF mass spectrometer was at least one order of magnitude higher and its measurement time was one or two orders shorter.

We developed the method of sample preparation ("ultra fine metal plus liquid matrix method") to be able to form high-mass molecular ions up to at least 34 kDa for laser ionization mass spectrometry. Theoretically, TOF-MS has no limitation of mass range and this spectrometer was capable of detecting organic ions up to m/z 100 000. Further improvements on this method of sample preparation should be promising, enabling the detection of high-mass molecular ions over 34 kDa.

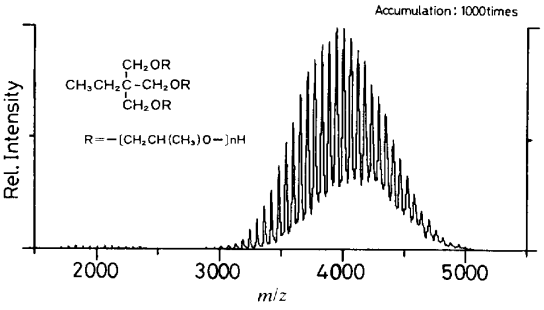

Figure 4. Laser ionization mass spectrum of poly(propylene glycol), average mol. wt 4 kDa (PPG4K).

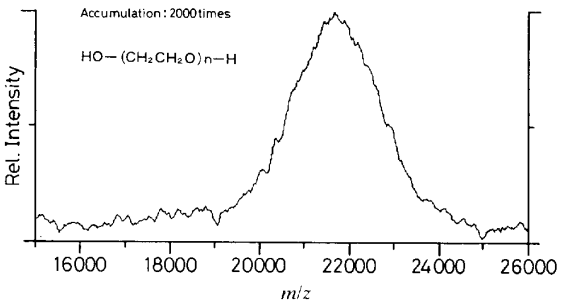

Figure 5. Laser ionization mass spectrum of poly(ethylene glycol), average mol. wt ca 20 kDa (PEG20K).

REFERENCES ← 参考文献

1. P. Roepstorff and B. Sundquist, in *Mass Spectrometry in Biomedical Research*, ed. by S. J. Gaskell, p. 269, Wiley, Chichester (1986).
2. R. D. Macfarlane, *40th Annual Pittsburgh Conf. & Exposition*, p. 612 (1988).
3. M. Barber and B. N. Green, *Rapid Commun. Mass Spectrom.* **1**, 80 (1987).
4. I. V. Bletsos, D. M. Hercules, J. H. Magill, D. van Leyen, E. Niehuis and A. Benninghoven, *Anal. Chem.* **60**, 938 (1988).
5. C. L. Wilkins, D. A. Weil, C. L. C. Yang and C. F. Ijames, *Anal. Chem.* **57**, 520 (1985).
6. K. Tanaka, Y. Ido, S. Akita, Y. Yoshida and T. Yoshida, *12th Proc. Japanese Soc. for Medical Mass Spectrom.* p. 219 (1987).
7. T. Yoshida, K. Tanaka, Y. Ido, S. Akita and Y. Yoshida, *Mass Spectroscopy (Japan)*, **36**, 59 (1988).
8. Y. Yoshida, *US Pat.* 4625112 (1986).
9. R. J. Beuhler, E. Flanigan, L. J. Green and L. Friedman, *J. Am. Chem. Soc.* **12**, 3990 (1974).
10. K. Tanaka, Y. Ido, S. Akita, Y. Yoshida and T. Yoshida, *Proc. 2nd Japan-China Joint Sympos. on Mass Spectrom.* p. 185 (1987).

Received 6 June 1988; accepted 6 June 1988.

Protein and Polymer Analyses up to *m/z* 100 000 by Laser Ionization Time-of-flight Mass Spectrometry

Vocabulary

polymer	ポリマー，重合体
analyses	分析（analysisの複数形）
laser Ionization	レーザーイオン化
time-of-flight	飛行時間
mass spectrometry	質量分析法
hitherto	今までは
desorption	脱離，脱着
peptide	ペプチド（二個以上のアミノ酸のペプチド結合によってできた化合物）
kDa	キロダルトン，１kDa=分子量1000
bombardment	照射，衝撃
organic	有機の
assess	評価する
utility	有用性
m/z	質量数/イオンの電荷数,つまりイオンの質量
spectra	スペクトル
Apparatus	実験器具
mass spectrometer	質量分析計
be mounted on ~	～に乗せられた
perpendicular to~	～に垂直に
magnification image	拡大図
feature	特徴
acceleration voltage	加速電圧
characteristics	特性，特徴
transmission	伝達，透過

resolution	分解能
electric field	電界，電場
reflector	反射器
above-mentioned	上述した
detection	検出
be equipped with~	～が取り付けられている
converter	変換器
sensitivity	感度
accumulation	累積，蓄積
circuits	回路
accumulate	蓄積する
subsequent	その次の，その後の
in sequence	次々と
constant fraction discriminator	定数・少数分別器
time-to digital converter	時間デジタル変換器
interval	間隔
mass number calibration	質量数補正
EXPERIMENTAL	
Sample preparation	試料作製，試料調整，試料準備
yield	収率
prolong	延長する
production time	生成時間
sustain	持続させる
ultra fine metal plus liquid matrix method	金属超粉末プラス液体マトリクス法
distill	蒸留する
distilled water	蒸留水
solvent	溶媒
drip	滴下する
ultra fine metal powder (UFP)	金属超微粉末
cobalt	コバルト

Å	オングストローム（10^{-10}）
diameter	直径
purchase	購入する
vacuum	真空の
metallurgical	冶金の
glycerol	グリセリン，グリセロール
dissolve	溶解する
organic solvent	有機溶媒
ethanol	エタノール
acetone	アセトン
mixture	混合物
volatile	揮発性の
compound	化合物
remove	除去する
mass	質量
spectrometer	分析計
RESULTS AND DISCUSSION	
e.g.	例えば
lysozyme	リゾチーム
chymotrypsinogen	キモトリプシノーゲン
poly (propylene glycol)(PPG)	ポリ（プロピレングリコール）
detect	検出する
UPF	金属超微粉末（ultra fine metal powder）
in comparison with~	～と比較して
bulk	バルク
photo-absorption	光吸収
heat capacity	熱容量
volatility	揮発性
enhancement	促進
irradiating	照射

replenish	補充する
最後の部分	
form	形成する
high-mass molecular ions	高分子量イオン
theoretically	理論的には
detect	検出する
organic ion	有機物イオン
improvement	改良
be promising	有望である

Protein and Polymer Analyses up to *m/z* 100 000 by Laser Ionization Time-of-flight Mass Spectrometry

レーザーイオン化飛行時間質量分析法による *m/z* 100 000 までのタンパク質やポリマーの分析

Hitherto,^{252}Cf plasma desorption mass spectrometry(PDMS) has been used to study peptides and proteins in the molecular weight range from 1kDa to 35 kDa.[1,2]

Fast atom bombardment mass spectrometry (FABMS) and secondary ion mass spectrometry(SIMS) have been applied to the analyses of proteins and polymers molecules.[3,4]

On the other hand, in the area of laser desorption time-of flight (TOF) mass spectrometry (MS), though there have been many papers on analyses of organic compounds, the molecular weight of these compounds has been relatively low.[5]

For the purpose of investigating the mass spectrometry of high-mass molecular organic compounds, we developed a laser ionization TOF mass spectrometer.

To assess the utility of this spectrometer for high masses, we evaluated and tried the mass spectrometer on various organic compounds.[6,7]

This spectrometer was able to obtain useful spectra up to *m/z* 100000.

Typical spectra of proteins and polymers with molecular weights up to 25kDa are shown in this paper.

EXPERIMENTAL

Apparatus

The construction of the laser ionization TOF mass spectrometer (Shimadzu LAMS-50K) is shown in Fig.1.

A nitrogen laser (wavelength:337 nm, pulse width: about 15 ns, pulse energy: 4 mJ max.) was used for sample ionization.

The sample, mounted on the sample holder, was capable of small movements in the plane perpendicular to the ion axis.

The magnification image of the sample surface could be observed on the TV monitor.

These features provided reliable analysis of the selected area.

The ion acceleration voltage of 5 kV was applied to the sample holder.

Generally, TOF-MS has the following characteristics: very high transmission; measurement times of less than a few hundreds of μs; unlimited mass range, low mass resolution.

A new“gradient electric field type ion reflector ”[8] for a TOF mass spectrometer has been developed in order to improve mass spectral resolution by time focusing.

The TOF mass separation system was designed to select the “reflection type ”(above-mentioned) or the “ linear type” (without reflecting electric field).

For ion detection, a micro channel plate (MCP) was used, which was equipped with an ion to electron converter in order to improve the sensitivity of detection for high-mass ions.

Two TOF systems were constructed.

The first system utilized a digital wave memory and accumulation circuits.

This system could accumulate the spectrum data of 8K words within 1 ms.

In the first place, a “one shot” TOF spectrum was stored into the wave memory, in the subsequent accumulating circuits the spectrum was accumulated in sequence.

The second system utilized a constant fraction discriminator (CFD) and a multi-stop time-to digital converter (TDC).

The time intervals between “start” and “stop” pulses were measured with a time resolution of 1 ns.

In these experiments, the first system (AD method) was only used.

The measuring circuit was controlled with a micro-processor [Intel 80286,Intel,CA,USA], and the TOF could be provided with various processes, e.g., smoothing, background subtraction, peak detection and mass number calibration.

Sample preparation

We investigated the method of sample preparation to increase the yield of high-mass ions and to prolong the production time.

As a result, it was found that the yield of ions and the sustained production time largely depended on the method of sample preparation and that the “ultra fine metal plus liquid matrix method”, described below, was extremely effective.

A sample was made into a solution having a concentration of about 10 μg/10 μL using distilled water as the solvent.

About 10 μL of this sample solution was dripped onto the sample holder.

On the other hand, an ultra fine metal powder ((UFP),in these experiments, we used cobalt powder of about 300 Å diameter purchased from Vacuum metallurgical Co. in Japan) and glycerol were dissolved with organic solvents, e.g., ethanol and acetone.

About 10 μL of this sample solution was also dripped onto the sample holder.

A mixture of the two solutions was then vacuum dried for a short time to remove volatile compounds of the solution.

The sample holder, with sample, was then introduced into the mass spectrometer to start analysis.

This sample preparation method was simple with preparation times of less than a few minutes.

RESULTS AND DISCUSSION

This mass spectrometer was successfully applied to the detection of high-mass molecular ions, e.g., lysozyme, mol. Wt 14306 Da (Fig.2); chymotrypsinogen, mol. Wt 25717 Da (Fig.3); poly (propylene glycol)(PPG), average mol. Wt 4 kDa(Fig.4); and PEG20K,average mol. wt ca 20 kDa(Fig.5).

It was impossible to detect high-mass molecular ions from these samples without using the “ultra fine metal plus liquid matrix method” for sample preparation.

UFP has the following features in comparison with bulk: high photo-absorption, low heat capacity, and extremely large surface area per unit volume.

“Rapid heating” of the sample was used as a volatility enhancement technique of organic compounds and it was achieved by irradiating a pulsed laser on the sample surface.

We suppose that UFP in the sample enhances the speed of sample heating, by laser irradiation, due to the above mentioned features.

Consequently, molecular ions are formed more easily.

By the addition of glycerol to the sample, molecules of the sample are replenished to the laser beam irradiation position and it is considered that the ion formation is allowed to continue for a long time.

最後の部分

We developed the method of sample preparation (“ultra fine metal plus liquid matrix method”) to be able to form high-mass molecular ions up to at least 34 KDa for laser ionization mass spectrometry.

Theoretically, TOF-MS has no limitation of mass range and this spectrometer was capable of detecting organic ions up to *m/z* 100 000.

Further improvements on this method of sample preparation should be promising, enabling the detection of high-mass molecular ions over 34 kDa.

Molecular Structure of Nucleic Acids

核酸の分子構造

こちらの論文は，1962 年にノーベル生理・医学賞受賞したワトソン博士とクリック博士の論文です．

親から子へ受け継がれる遺伝情報を収めた物質が DNA（デオキシリボ核酸）です．この物質の 2 重らせん構造（double helix structure）を解き明かしたのが，ワトソン博士とクリック博士だといわれています．このネイチャーに掲載されたほぼ 1 ページの論文が，DNA が二重らせん構造をしていることの第一報で，DNA の構造を細かく説明しています．これ以降，この発見は生化学に限らず，医学，薬学，農学，及び工学に大きな進歩をもたらしたといわれています．この，短いながらも科学史上の一大発見を述べた論文を読んでみましょう．

equipment, and to Dr. G. E. R. Deacon and the captain and officers of R.R.S. *Discovery II* for their part in making the observations.

[1] Young, F. B., Gerrard, H., and Jevons, W., *Phil. Mag.*, **40**, 149 (1920).
[2] Longuet-Higgins, M. S., *Mon. Not. Roy. Astro. Soc., Geophys. Supp.*, **5**, 285 (1949).
[3] Von Arx, W. S., Woods Hole Papers in Phys. Oceanog. Meteor., **11** (3) (1950).
[4] Ekman, V. W., *Arkiv. Mat. Astron. Fysik.* (*Stockholm*), **2** (11) (1905).

MOLECULAR STRUCTURE OF NUCLEIC ACIDS

A Structure for Deoxyribose Nucleic Acid

WE wish to suggest a structure for the salt of deoxyribose nucleic acid (D.N.A.). This structure has novel features which are of considerable biological interest.

A structure for nucleic acid has already been proposed by Pauling and Corey[1]. They kindly made their manuscript available to us in advance of publication. Their model consists of three inter-twined chains, with the phosphates near the fibre axis, and the bases on the outside. In our opinion, this structure is unsatisfactory for two reasons: (1) We believe that the material which gives the X-ray diagrams is the salt, not the free acid. Without the acidic hydrogen atoms it is not clear what forces would hold the structure together, especially as the negatively charged phosphates near the axis will repel each other. (2) Some of the van der Waals distances appear to be too small.

Another three-chain structure has also been suggested by Fraser (in the press). In his model the phosphates are on the outside and the bases on the inside, linked together by hydrogen bonds. This structure as described is rather ill-defined, and for this reason we shall not comment on it.

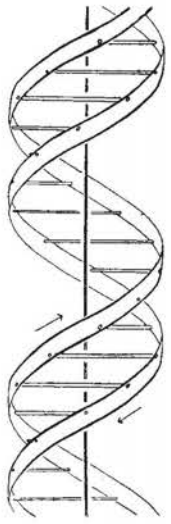

This figure is purely diagrammatic. The two ribbons symbolize the two phosphate—sugar chains, and the horizontal rods the pairs of bases holding the chains together. The vertical line marks the fibre axis

We wish to put forward a radically different structure for the salt of deoxyribose nucleic acid. This structure has two helical chains each coiled round the same axis (see diagram). We have made the usual chemical assumptions, namely, that each chain consists of phosphate di-ester groups joining β-D-deoxy-ribofuranose residues with 3′,5′ linkages. The two chains (but not their bases) are related by a dyad perpendicular to the fibre axis. Both chains follow right-handed helices, but owing to the dyad the sequences of the atoms in the two chains run in opposite directions. Each chain loosely resembles Furberg's[2] model No. 1; that is, the bases are on the inside of the helix and the phosphates on the outside. The configuration of the sugar and the atoms near it is close to Furberg's 'standard configuration', the sugar being roughly perpendicular to the attached base. There is a residue on each chain every 3·4 A. in the z-direction. We have assumed an angle of 36° between adjacent residues in the same chain, so that the structure repeats after 10 residues on each chain, that is, after 34 A. The distance of a phosphorus atom from the fibre axis is 10 A. As the phosphates are on the outside, cations have easy access to them.

The structure is an open one, and its water content is rather high. At lower water contents we would expect the bases to tilt so that the structure could become more compact.

The novel feature of the structure is the manner in which the two chains are held together by the purine and pyrimidine bases. The planes of the bases are perpendicular to the fibre axis. They are joined together in pairs, a single base from one chain being hydrogen-bonded to a single base from the other chain, so that the two lie side by side with identical z-co-ordinates. One of the pair must be a purine and the other a pyrimidine for bonding to occur. The hydrogen bonds are made as follows: purine position 1 to pyrimidine position 1; purine position 6 to pyrimidine position 6.

If it is assumed that the bases only occur in the structure in the most plausible tautomeric forms (that is, with the keto rather than the enol configurations) it is found that only specific pairs of bases can bond together. These pairs are: adenine (purine) with thymine (pyrimidine), and guanine (purine) with cytosine (pyrimidine).

In other words, if an adenine forms one member of a pair, on either chain, then on these assumptions the other member must be thymine; similarly for guanine and cytosine. The sequence of bases on a single chain does not appear to be restricted in any way. However, if only specific pairs of bases can be formed, it follows that if the sequence of bases on one chain is given, then the sequence on the other chain is automatically determined.

It has been found experimentally[3,4] that the ratio of the amounts of adenine to thymine, and the ratio of guanine to cytosine, are always very close to unity for deoxyribose nucleic acid.

It is probably impossible to build this structure with a ribose sugar in place of the deoxyribose, as the extra oxygen atom would make too close a van der Waals contact.

The previously published X-ray data[5,6] on deoxy-ribose nucleic acid are insufficient for a rigorous test of our structure. So far as we can tell, it is roughly compatible with the experimental data, but it must be regarded as unproved until it has been checked against more exact results. Some of these are given in the following communications. We were not aware of the details of the results presented there when we devised our structure, which rests mainly though not entirely on published experimental data and stereo-chemical arguments.

It has not escaped our notice that the specific pairing we have postulated immediately suggests a possible copying mechanism for the genetic material.

Full details of the structure, including the conditions assumed in building it, together with a set of co-ordinates for the atoms, will be published elsewhere.

We are much indebted to Dr. Jerry Donohue for constant advice and criticism, especially on inter-atomic distances. We have also been stimulated by a knowledge of the general nature of the unpublished experimental results and ideas of Dr. M. H. F. Wilkins, Dr. R. E. Franklin and their co-workers at

King's College, London. One of us (J. D. W.) has been aided by a fellowship from the National Foundation for Infantile Paralysis.

J. D. Watson
F. H. C. Crick
Medical Research Council Unit for the Study of the Molecular Structure of Biological Systems,
Cavendish Laboratory, Cambridge.
April 2.

[1] Pauling, L., and Corey, R. B., *Nature*, **171**, 346 (1953); *Proc. U.S. Nat. Acad. Sci.*, **39**, 84 (1953).
[2] Furberg, S., *Acta Chem. Scand.*, **6**, 634 (1952).
[3] Chargaff, E., for references see Zamenhof, S., Brawerman, G., and Chargaff, E., *Biochim. et Biophys. Acta*, **9**, 402 (1952).
[4] Wyatt, G. R., *J. Gen. Physiol.*, **36**, 201 (1952).
[5] Astbury, W. T., Symp. Soc. Exp. Biol. 1, Nucleic Acid, 66 (Camb. Univ. Press, 1947).
[6] Wilkins, M. H. F., and Randall, J. T., *Biochim. et Biophys. Acta*, **10**, 192 (1953).

Molecular Structure of Deoxypentose Nucleic Acids

While the biological properties of deoxypentose nucleic acid suggest a molecular structure containing great complexity, X-ray diffraction studies described here (cf. Astbury[1]) show the basic molecular configuration has great simplicity. The purpose of this communication is to describe, in a preliminary way, some of the experimental evidence for the polynucleotide chain configuration being helical, and existing in this form when in the natural state. A fuller account of the work will be published shortly.

The structure of deoxypentose nucleic acid is the same in all species (although the nitrogen base ratios alter considerably) in nucleoprotein, extracted or in cells, and in purified nucleate. The same linear group of polynucleotide chains may pack together parallel in different ways to give crystalline[1-3], semi-crystalline or paracrystalline material. In all cases the X-ray diffraction photograph consists of two regions, one determined largely by the regular spacing of nucleotides along the chain, and the other by the longer spacings of the chain configuration. The sequence of different nitrogen bases along the chain is not made visible.

Oriented paracrystalline deoxypentose nucleic acid ('structure *B*' in the following communication by Franklin and Gosling) gives a fibre diagram as shown in Fig. 1 (cf. ref. 4). Astbury suggested that the strong 3·4-A. reflexion corresponded to the internucleotide repeat along the fibre axis. The ~ 34 A. layer lines, however, are not due to a repeat of a polynucleotide composition, but to the chain configuration repeat, which causes strong diffraction as the nucleotide chains have higher density than the interstitial water. The absence of reflexions on or near the meridian immediately suggests a helical structure with axis parallel to fibre length.

Diffraction by Helices

It may be shown[5] (also Stokes, unpublished) that the intensity distribution in the diffraction pattern of a series of points equally spaced along a helix is given by the squares of Bessel functions. A uniform continuous helix gives a series of layer lines of spacing corresponding to the helix pitch, the intensity distribution along the nth layer line being proportional to the square of J_n, the nth order Bessel function. A straight line may be drawn approximately through

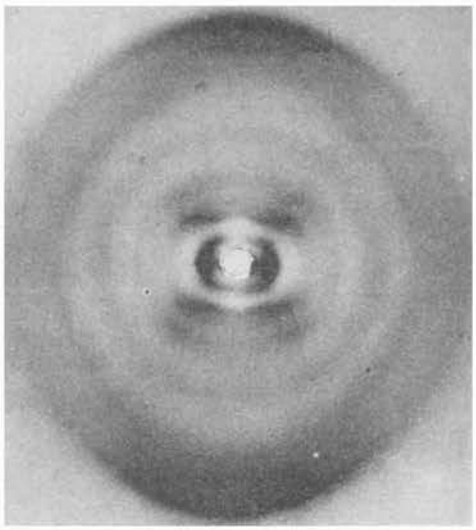

Fig. 1. Fibre diagram of deoxypentose nucleic acid from *B. coli*. Fibre axis vertical

the innermost maxima of each Bessel function and the origin. The angle this line makes with the equator is roughly equal to the angle between an element of the helix and the helix axis. If a unit repeats n times along the helix there will be a meridional reflexion (J_0^2) on the nth layer line. The helical configuration produces side-bands on this fundamental frequency, the effect[5] being to reproduce the intensity distribution about the origin around the new origin, on the nth layer line, corresponding to C in Fig. 2.

We will now briefly analyse in physical terms some of the effects of the shape and size of the repeat unit or nucleotide on the diffraction pattern. First, if the nucleotide consists of a unit having circular symmetry about an axis parallel to the helix axis, the whole diffraction pattern is modified by the form factor of the nucleotide. Second, if the nucleotide consists of a series of points on a radius at right-angles to the helix axis, the phases of radiation scattered by the helices of different diameter passing through each point are the same. Summation of the corresponding Bessel functions gives reinforcement for the inner-

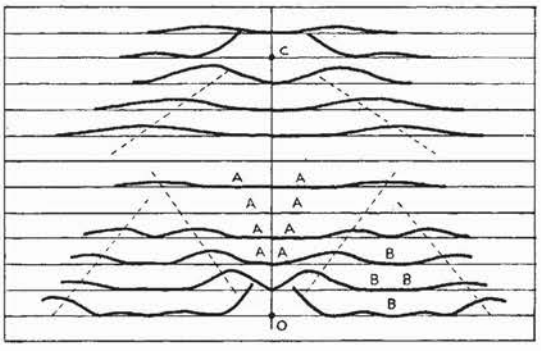

Fig. 2. Diffraction pattern of system of helices corresponding to structure of deoxypentose nucleic acid. The squares of Bessel functions are plotted about 0 on the equator and on the first, second, third and fifth layer lines for half of the nucleotide mass at 20 A. diameter and remainder distributed along a radius, the mass at a given radius being proportional to the radius. About C on the tenth layer line similar functions are plotted for an outer diameter of 12 A.

Molecular Structure of Nucleic Acids

Vocabulary

deoxyribose nucleic acid (D.N.A.)	デオキシリボ核酸（D.N.A.）
manuscript	論文
intertwined	絡み合っている
unsatisfactory	不満足
X-ray diagram	Ｘ線回折図
free acid	遊離した（核）酸
negatively charged	負に帯電した
phosphate	リン酸基
repel	反発する
van der Waals distance	ファンデルワールス距離
ill-defined	不明確である
radically	根本的に
helical	螺旋状の
assumption	仮定
phosphate di-ester group	リン酸基ジエステル
residue	残基
linkage	結合
base	塩基
dyad	一対，２分子
fibre axis	繊維軸
helix (helices)	螺旋 （複数形）
sequence	順序，配列
configuration	配列
perpendicular to	～に垂直である
phosphorus atom	リン原子
cation	陽イオン
purine bases	プリン塩基

pyrimidine bases	ピリミジン塩基
hydrogen-bonded	水素結合
side by side	相接して（隣り合って）
identical	同一の
plausible	もっともらしい
tautomeric	互変異性体の
keto	ケト
enol	エノール
specific	特殊な
adenine	アデニン
thymine	チミン
guanine	グアニン
cytosine	シトシン
unity	1，一致
ribose	リボース
rigorous	厳密な
compatible with	適合する
devise	考え出す
rest on	頼る
stereo-chemical	立体化学的な
postulate	仮定する
genetic	遺伝の
co-ordinate	座標
be indebted	恩義を受けている
inter-atomic distance	原子間距離
fellowship	奨学金
National Foundation for Infantile Paralysis	国立小児麻痺研究財団

Molecular Structure of Nucleic Acids

核酸の分子構造

We wish to suggest a structure for the salt of deoxyribose nucleic acid (D.N.A.). This structure has novel features which are of considerable biological interest.

A structure for nucleic acid has already been proposed by Pauling and Corey [1]. They kindly made their manuscript available to us in advance of publication.

Their model consists of three intertwined chains, with the phosphates near the fibre axis, and the bases on the outside. In our opinion, this structure is unsatisfactory for two reasons:

(1) We believe that the material which gives the X-ray diagrams is the salt, not the free acid. Without the acidic hydrogen atoms it is not clear what forces would hold the structure together, especially as the negatively charged phosphates near the axis will repel each other.

(2) Some of the van der Waals distances appear to be too small.

Another three-chain structure has also been suggested by Fraser (in the press). In his model the phosphates are on the outside and the bases on the inside, linked together by hydrogen bonds. This structure as described is rather ill-defined, and for this reason we shall not comment on it.

We wish to put forward a radically different structure for the salt of deoxyribose nucleic acid. This structure has two helical chains each coiled round the same axis (see diagram).

We have made the usual chemical assumptions, namely, that each chain consists of phosphate di-ester groups joining β-D-deoxyribofuranose residues with 3',5' linkages.

The two chains (but not their bases) are related by a dyad perpendicular to the fibre axis. Both chains follow right-handed helices, but owing to the dyad the sequences of the atoms in the two chains run in opposite directions.

Each chain loosely resembles Furberg's[2] model No. 1; that is, the bases are on the inside of the helix and the phosphates on the outside. The configuration of the sugar and the atoms near it is close to Furberg's 'standard configuration', the sugar being roughly perpendicular to the attached base.

There is a residue on each chain every 3.4 A. in the z-direction. We have assumed an angle of 36° between adjacent residues in the same chain, so that the structure repeats after 10 residues on each chain, that is, after 34 A. The distance of a phosphorus atom from the fibre axis is 10 A. As the phosphates are on the outside, cations have easy access to them.

The structure is an open one, and its water content is rather high. At lower water contents we would expect the bases to tilt so that the structure could become more compact.

The novel feature of the structure is the manner in which the two chains are held together by the purine and pyrimidine bases.

The planes of the bases are perpendicular to the fibre axis. They are joined together in pairs, a single base from the one chain being hydrogen-bonded to a single base from the other chain, so that the two lie side by side with identical z-co-ordinates.

One of the pair must be a purine and the other a pyrimidine for bonding to occur. The hydrogen bonds are made as follows: purine position 1 to pyrimidine position 1; purine position 6 to pyrimidine position 6.

If it is assumed that the bases only occur in the structure in the most plausible tautomeric form (that is, with the keto rather than the enol configurations) it is found the only specific pairs of bases can bond together. These pairs are: adenine (purine) with thymine (pyrimidine) , and guanine(purine) with cytosine (pyrimidine).

In other words, if an adenine forms one member of a pair, on either chain, then on these assumptions the other member must be thymine; similarly for guanine and cytosine.

The sequence of bases on a single chain does not appear to be restricted in any way. However, if only specific pairs of bases can be formed, it follows that if the sequence of bases on one chain is given, then the sequence on the other chain is automatically determined.

It has been found experimentally[3,4] that the ratio of the amounts of adenine to thymine, and the ratio of guanine to cytosine, are always very close to unity for deoxyribose nucleic acid.

It is probably impossible to build this structure with a ribose sugar in place of the deoxyribose, as the extra oxygen atom would make too close a van der Waals contact.

The previously published X-ray data[5,6] on deoxyribose nucleic acid are insufficient for a rigorous test of our structure. So far as we can tell, it is roughly compatible with the experimental data, but it must be regarded as unproved until it has been checked against more exact results.

Some of these are given in the following communications. We were not aware of the details of the results presented there when we devised our structure, which rests mainly though not entirely on published experimental data and stereo-chemical arguments.

It has not escaped our notice that the specific pairing we have postulated immediately suggests a possible copying mechanism for the genetic material.

Full details of the structure, including the conditions assumed in building it, together with a set of co-ordinates for the atoms, will be published elsewhere.

We are much indebted to Dr. Jerry Donohue for constant advice and criticism, especially on inter-atomic distance. We have also been stimulated by a knowledge of the general nature of the unpublished experimental results and ideas of Dr. M.H.F. Wilkins, Dr. R.E. Franklin and their co-workers at king's College, London. One of us (J.D.W.) has been aided by a fellowship from the National Foundation for Infantile Paralysis.

Application of microbial risk assessment on a residentially-operated Bio-toilet

家庭用バイオトイレにおける微生物リスク評価の適用

こちらの論文は，2006 年に私が執筆した論文です．現在の水循環システムは，もともと作物が育つために必要な栄養分を豊富に含んでいる屎尿を，農地に還元せずに水環境に排出してしまっていることから，水環境は富栄養化し，農地はリンやカリウムなどの栄養分が枯渇しているという現状を鑑みて，もっと環境に配慮した持続的な衛生（屎尿処理）を考えようと考え出された，持続的な衛生システム（sustainable sanitation system）に関する論文です．

この持続的な衛生システムを実現するには排出元のトイレが重要で，当初は水を使わず屎尿の栄養分を農地還元できるバイオトイレに着目していました．しかし，このバイオトイレは病原微生物が混入した場合も衛生学的に安全といえるのか？そのような疑問から微生物リスク評価をバイオトイレに適用して，その衛生学的安全性を評価した内容となっています．この論文のイントロの部分や実験の部分，結論部分を読んでみましょう．

479 © IWA Publishing 2006 Journal of Water and Health | 04.4 | 2006

掲載された雑誌名

Application of microbial risk assessment on a residentially-operated Bio-toilet

論文タイトル

Naoko Nakagawa, Hana Oe, Masahiro Otaki and Katsuyoshi Ishizaki

著者ら

ABSTRACT

概要

The Sustainable Sanitation System is a new wastewater treatment system that incorporates a non-flushing toilet (Bio-toilet) that converts excreta into a reusable resource (as fertilizer or humus for organic agriculture) and reduces the pollution load to environments of the rivers, the lakes, and the sea. However, the risk of exposure to pathogens should be considered, because excrement is stored in the Bio-toilet. The aim of the present work is to analyze the health risk of dealing with the matrix (excreta and urine mixed with sawdust) of the Bio-toilet. Therefore, the fate of pathogenic viruses was investigated using coliphages as a virus index, and the modeling of the die-off rate in matrix was introduced. Then the microbial risk assessment was applied to a Bio-toilet that was actually used in a residential house; the infection risks of rotavirus and enterovirus as reference pathogens were calculated.

According to the lab-scale experiment using coliphages for investing the die-off rate of viruses in the Bio-toilet, Qβ had a higher die-off, which was greatly influenced by the water content and temperature. On the other hand, T4 showed a lower rate and was independent of water content. Therefore, these two phages' data were used as critical examples, such as viruses having high or low possibilities of remaining in the Bio-toilet during the risk assessment analysis.

As the result of the risk assessment, the storage time required for an acceptable infectious risk level has wide variations in both rotavirus and enterovirus cases depending on the phage that was used. These were 0–260 days' and 0–160 days' difference, respectively.

Key words | Bio-toilet, die-off rate, microbial risk assessment, sustainable sanitation system

Naoko Nakagawa (corresponding author)
Masahiro Otaki
Dept. of Human Environmental Sciences,
Ochanomizu Univ., 2-1-1 Otsuka,
Bunkyo-ku 112-8610,
Tokyo, Japan
Tel.: +81-3-59785748
Fax: +81-3-59782049
E-mail: *urbanoasis@pop11.odn.ne.jp*

Hana Oe
Graduate School of Frontier Sciences,
University of Tokyo, 7-3-1, Hongo,
Bunkyo-ku 113-0033,
Tokyo, Japan

Katsuyoshi Ishizaki
Research Institute for a Sustainable Future,
Waseda University513 Tsurumaki-chou,
Waseda, Shinjuku-Ku,
Tokyo 169-8050,
Japan

INTRODUCTION

はじめに．研究の背景

The Sustainable Sanitation System that was developed by this research is a new wastewater treatment system; it incorporates a non-flushing toilet (Bio-toilet) that converts excreta into a reusable resource (as fertilizer or humus for organic agriculture) and reduces the pollution load to environments of the rivers, the lakes, and the sea.

The Sustainable Sanitation System was launched with the support of the Japanese government named CREST, as a project called "Research on the Development of Sustainable Sanitation Systems and their Introduction in the Water Cycle System." It will be undertaken from 2002 to 2007 in Japan, with the assistance of a US$4 million research budget from CREST. The objective of the System is to protect human health and the environment while reducing the use of water and recycling nutrients.

The elimination of black water from the residential wastewater stream by using a non-water carriage toilet will reduce the pollution load from a household. Therefore, the Bio-toilet – which does not use water and can recycle nutrients – is one of the key components in implementing the Sustainable Sanitation System. However, the risk of exposure to pathogens should be considered, because excrement remains in the Bio-toilet for long periods of time.

doi: 10.2166/wh.2006.028

In this research, to analyze the health risk of using the Bio-toilet, the microbial risk assessment was applied to a Bio-toilet that was actually operating in a residential house; rotavirus and enterovirus were selected as reference pathogens to discuss the hygienic safety of the Bio-toilets. For the microbial risk assessment, the fate of pathogenic viruses was investigated using coliphages as a virus index; the modeling of the die-off rate was then introduced. A number of environmental conditions will speed up or slow down the time it takes for a pathogen to die, depending on the characteristics of the condition. The major factors considered important for die-off are temperature, moisture, nutrients, other organisms, sunlight and PH (Winblad *et al.* 1998). We considered die-off rate as mainly depending on temperature and moisture. Therefore, this paper also describes the modeling of the die-off rate using temperature and water content parameters concerning model viruses.

MATERIAL AND METHODS ◀…… 研究の材料と方法

Bio-toilet

The Bio-toilet uses sawdust as an artificial soil matrix to decompose excreta into compost, and even to form gas and humus. Inside the tank itself, a motor gently stirs sawdust or chips; in the sawdust, the water content of the excreta evaporates as a result of the heat produced by the heater and the biological activity. After the organic material is composted, it is disposed of as waste material, along with the sawdust, for use as a fertilizer. All that remains following this process are small amounts of phosphorus, minerals, salt, and humus (Nakagawa *et al.* 2001).

Figure 1 shows the structure of the Bio-toilet. The excreta are placed in the sawdust in the tank, where it ferments and decomposes as it is agitated slowly by a screw-shaped rotating mechanism. The Bio-toilet has a structure whereby sawdust is sent out, in small amounts, from the excreta inlet side to the removal opening on the side. A ventilation fan installed beside the Bio-toilet keeps the interior of the house almost completely free of the smell of the excreta. The fermentation and decomposition reduce the volume of the excreta until it can finally be used as fertilizer in dry conditions. One such Bio-toilet was installed in the house cooperating with this research and was used by three people.

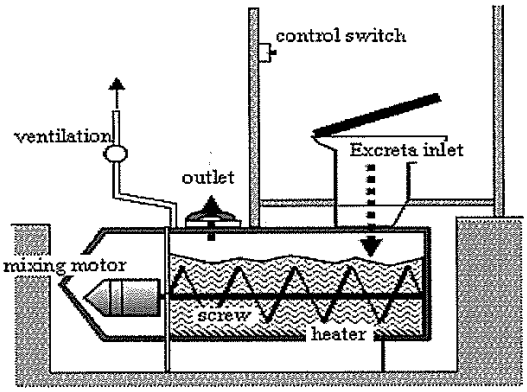

Figure 1 | The Bio-toilet.

Experimental procedure

Bacteriophage Qβ and Bacteriophage T4 were selected as model viruses. After the injection of these model organisms into the Bio-toilet media, it was stirred well by hand for 5 minutes. Then amounts of between 0.1–0.2 g of the media were sampled at predetermined intervals. These samples were then injected into 10 ml 3w/v% beef extra solution (pH 9.7) and mixed well for 1 minute, in order to elute microorganisms. Coliphages were measured by a double agar method using *E.coli* K12 as a host bacteria for Qβ, and *E.coli* C as a host for T4 (Otaki 2003).

The die-off rate is defined as follows.

$$-\log N/N_0 = kt \quad (1)$$

where
N: concentrations of phages [no./g],
N_0: concentrations of phages [no./g],
k: die-off rate,
t: storage time of phage in media (in [min] or [day]).

Modeling of the die-off rate

Based on the experimental data, the effect of temperature and water content on the die-off rate (k) profiles for a range of the temperature and water content were simulated. With respect to Qβ, the effect of the temperature on k was estimated by using the Arrhenius equation (Lopez *et al.* 2004) and the effect of the water content was expressed by

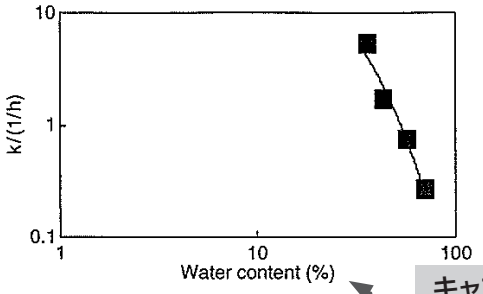

Figure 2 | The effect of water content on $K(Q\beta$ case).

キャプションは文章にしない

the following equation from the experimental data as shown in Figure 2.

$$\ln k = A \ln W + B \tag{2}$$

where

$$A = \frac{1}{\ln\left(\frac{50}{70}\right)} \ln\left(\frac{k_{50\%,T}}{k_{70\%,T}}\right)$$

$$B = \ln(k_{50\%,T}) - \ln(50)A$$

$$k_{70\%,T} = k_{s70\%} \exp\left[-\left(\frac{E_{70\%}}{R}\right)\left(\frac{1}{T+273} - \frac{1}{T_s+273}\right)\right]$$

$$k_{70\%,T} = k_{s50\%} \exp\left[-\left(\frac{E_{50\%}}{R}\right)\left(\frac{1}{T+273} - \frac{1}{T_s+273}\right)\right]$$

ks: k at T = 50°C ($ks_{50\%} = 0.895$(1/h), $ks_{70\%} = 0.274$(1/h)),
Ts: standard temperature 50 (Fujita 1995),
R: gas constant (8.314(J/mol/K)),
E: activation energy (J/mol) ($E_{50\%} = 110000$ (J/mol), $E_{70\%} = 70000$ (J/mol)),
Then, k was expressed by temperature T and water content W as follows

$$k_{Q\beta} = k_{50\%,T}\left(\frac{W}{50}\right)^{\alpha} \tag{3}$$

where

$$\alpha \frac{1}{\ln\left(\frac{50}{70}\right)} \ln\left(\frac{k_{50\%,T}}{k_{70\%,T}}\right)$$

$$+\left[-\left(\frac{\mathrm{E50\% - E70\%}}{R}\right)\left(\frac{1}{T+273} - \frac{1}{T_s+273}\right)\right]$$

T4 was found to be independent of water content, from the measurement results shown in Figure 5. Therefore, it is considered that only temperature effects k. Therefore, k is estimated by using just the Arrhenius equation as follows.

$$k_{T4} = ks \exp\left[-\frac{E}{R}\left(\frac{1}{T+273} - \frac{1}{Ts+273}\right)\right] \tag{4}$$

Being similar to the case of $k_{Q\beta}$,
ks: k at $T = 50$°C ($ks_{50\%} = 0.06$ (1/h), $ks_{70\%} = 0.046$ (1/h)),
Ts: standard temperature 50°C,
R: gas constant (8.314(J/mol/K)),
E: activation energy (J/mol), ($E_{50\%} = 130000$ (J/mol), $E_{70\%} = 80000$ (J/mol)).

Measurement of the temperature and the water content in the Bio-toilet actually operated

This Bio-toilet has been used for three years. When 30 months had passed since its installation, the temperature and the water content in the Bio-toilet were measured.

The temperature was measured two times at eight sampling points as shown in Figure 3.

With respect to the water content (w), the matrix was sampled seven times (once per day for one week) at each sampling point from eight locations and each was analyzed. The water content was measured by finding the weight (M) of the sawdust and the weight (Md) after drying at a temperature of 105°C. The water content is defined by the following equation.

$$(\%) = \frac{M - Md}{M} \times 100 \tag{5}$$

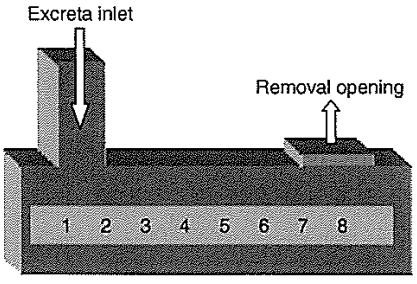

Figure 3 | The location of the sampling points.

Microbial risk assessment methods

Risk assessment is a powerful tool for evaluating the influence of hazardous agents on humans. This method consists of 4 parts. These are Hazard identification, Dose-Response assessment, Exposure assessment and Risk characterization.

Hazard Identification

From the results of the previous study, it was found that pathogenic viruses have potentially high risks and the control of them must be a key issue, rather than that of pathogenic microorganisms (Nakagawa *et al.* 2003). Therefore, rotavirus and enterovirus, which are representative waterborne pathogenic viruses, were selected as reference pathogens for this case study. According to the literature (Haas *et al.* 1999; Epstein 1998; Charles *et al.* 1999) concentrations of pathogens in feces and the duration of excretion of these pathogens are shown in Table 1. The volume of excreta is assessed to be 150 g per person, per day. The capacity of the media is 250 l. The density of the sawdust is 0.27 kg/l. The die-off rate of the pathogenic virus was based on the experimental data from the phage model described above. With respect to the period that pathogenic viruses are discharged into the Bio-toilet, it is considered to be the duration of pathogen excrement, as shown in Table 1.

Dose-response assessment

Several models that show the relation between the intake dose of the pathogen and the microbial risk have been proposed by Haas (Haas 1983), and Rose (Rose *et al.* 1991); the appropriate infective model, shown in Table 2, was used.

Table 1 | Concentration of pathogen in feces and duration of excreting pathogenic viruses (Haas *et al.* 1999; Epstein 1998; Charles *et al.* 1999).

Agent	Concentration of pathogen in faces	Duration of exreting pathogen
Rotavirus	$\sim 10^{10}$ (No./g)	5–9 days
Enterovirus	$\sim 10^{6}$ (No./g)	2–4 weeks

Table 2 | Parameters and models in dose-response of pathogens (Haas 1983; Rose *et al.* 1991)

最初の文字は大文字，'The' は つけない

Agent	Used model	Parameters
Rotavirus	β-model	$a = 0.232$, $\beta = 0.247$
Enterovirus	Log-normal	$GM = 250$, $GSD = 73$

Exposure assessment

In this house, cooperating with the research study, the residents remove matrix from the Bio-toilet and use it as a fertilizer periodically. Therefore, in this risk assessment, it was considered that resident exposure to pathogenic viruses was significant when they withdrew the compost from the Bio-toilet. Therefore, the volume of sawdust attached to the hand of the person after handling the sawdust should be estimated. In our laboratory, a survey of 14 persons was implemented. The examinee replaced the used media by hand, with and without gloves, and then the weight of the attached media was measured. We tested the media, which had three different water contents (20%, 50% and 80%).

Risk characterization

According to the results of the dose-response and exposure assessment, the infection risk of each agent was estimated using Monte Carlo techniques. The screw-shaped mixer in the Bio-toilet rotates twice to the left and twice to the right for one minute, usually every eight hours. Therefore, it is thought that pathogenic viruses in the excreta that entered the sawdust are gradually diffused while undergoing this repeated back-and-forth motion. It is important to know how long it takes the fastest-moving pathogenic microorganism to reach the removal port's opening, from the time it entered the Bio-toilet from the excreta inlet.

According to a previous study using 500 plastic balls with a diameter of 2–3 mm each, the quickest one appeared in 6 days with a median of 22 days (Kinoshita 1994). This result indicated the storage time of the pathogenic viruses in the Bio-toilet and was used in the risk assessment.

The computer simulation was performed by dividing the Bio-toilet into six sections so that the fastest-moving pathogenic microorganism was exposed for six days after

entering the Bio-toilet. In addition, a calculation was implemented where we supposed the pathogenic viruses diffused into adjacent sections equally, after being inactivated in each section.

The risk assessment was implemented in two kinds of cases. One was known as the "Actual case" where the estimated value of k in each section using the model of Qβ in the Bio-toilet was applied. On the other hand, the other case was called the "Worst case" and indicated that k in all sections of the Bio-toilet were similar to the value in the first section, where k was estimated to be at a minimum because of high water content and low temperatures (see Figure 7).

RESULTS AND DISCUSSION ◀····· 結果と考察

Measurement results and calculated model of the die-off rate constant using the model viruses

Figures 4 and 5 show the data and model of the die-off rates of Qβ and T4, respectively.

The closed circles and squares show the measurement results. Higher temperatures caused high die-off rate in both phage cases. In the case of Qβ, a dependence of water content on the die-off rate was also seen. However, it wasn't observed in the T4 case, as shown in Figure 5. Qβ is an RNA virus and T4 is a DNA virus; therefore, the difference in structure is considered to be one of the reasons for this phenomenon. However, the mechanism explaining this phenomenon hasn't yet been learned.

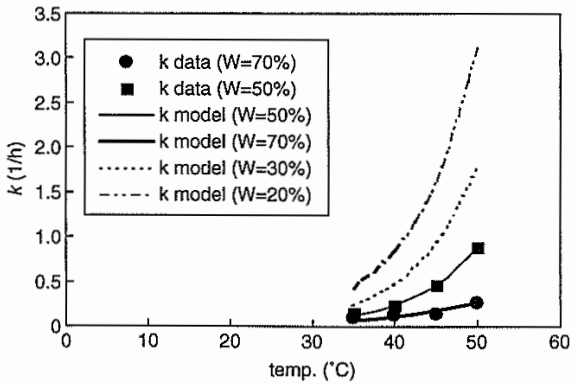

Figure 4 | The effect of temperature on die-off rate K (Qβ case).

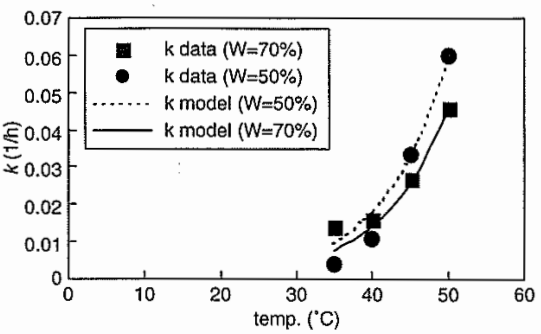

Figure 5 | The effect of temperature on die-off rate k (T4 case).

The lines in these figures show the calculated model of k concerning Qβ and T4, respectively. The line at 20% and 30% of the water content were also estimated in the case of Qβ as shown in Figure 4.

The measurement results of the temperature and the water content in the Bio-toilet actually operated

Figure 6 shows the measured temperature and water content in the Bio-toilet. The locations of each sampling point are indicated in Figure 6; they correspond to the numbers in Figure 3. The sampling point No.1 which is the point of the excreta inlet was considered to have the highest risk of a pathogen because the temperature was at the lowest, while water content was at the highest. The temperature of a middle point was around 60 degrees centigrade and it was considered that the risk of a pathogen becomes lower.

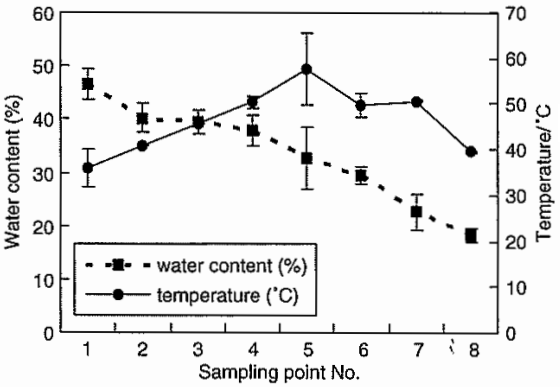

Figure 6 | Measurement result of the temperature and water content in the Bio-toilet in the house cooperating the research. (• Error bar means 95% confidential intervals).

Estimation of the die-off rate in the Bio-toilet in the house cooperating with the research

The die-off rate k of the pathogenic virus in the Bio-toilet was estimated according to the modeling of k (Equations (3) and (4)). Qβis an RNA virus and T4 is a DNA virus; both rotavirus and enterovirus are RNA viruses. In this way, the fates of rotavirus and enterovirus were assessed to be similar to that of Qβ, rather than that of T4. Therefore, k of rotavirus and enterovirus in the Bio-toilet was estimated from k model of Qβ, as shown in Figure 7.

Results of the exposure assessment

Figure 8 shows the results of this survey. The higher the water content was, the larger the volume of media was attached to the hand. The relationship between them was exponential, and the distribution of these volumes at each water content was assessed to have log-normal distribution, judging from a maximum likelihood method and likelihood ratio test (Haas *et al.* 1999). The median of the distribution (without gloves) was used as the volume of the exposure in the computer simulation.

Results of the risk calculation

Figure 9 shows the results of the risk calculation in the cases of rotavirus and enterovirus. Except for the worst case of rotavirus, the health risk of human infection from pathogenic viruses was almost zero less than 2.229×10^{-308} which is the minimum value which can be calculated in MS

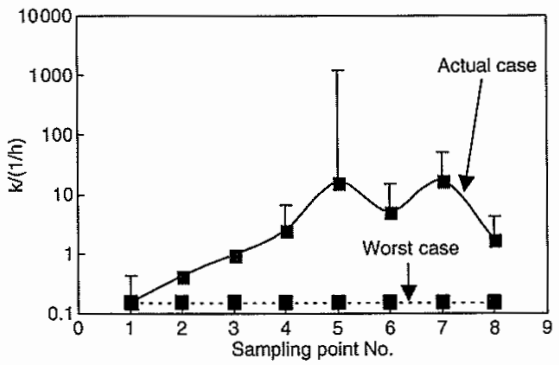

Figure 7 | Estimated k of rotavirus in the Bio-toilet. (* Error bar means 95% confidential intervals).

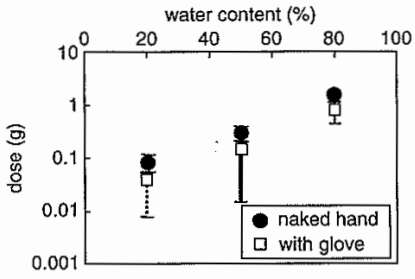

Figure 8 | Result of the survey for amount of the media attached to hand.

Excel 2003, in the case of both rotavirus and enterovirus. Even in the worst case of rotavirus, the infection risk was low. Figures 10 and 11 show the results of the risk calculation in the cases of rotavirus and enterovirus when applying the estimated value of k to each section from the model of T4. From the view point of structure, size, and type of gene, Qβ was assumed to be a better indicator than T4 for rotavirus and enterovirus. However, it is necessary to consider the "worst case scenario" when using an indicator with high resistance in the Bio-toilet, like T4. Figure 10 indicates that there is a high risk when a rotavirus is discharged into the Bio-toilet; the annual risk P_{annual} due to event frequency is shown below.

$$P_{annual} = 1 - (1 - p)^n \quad (6)$$

where

p: single exposure risk,

n: frequency of event

This residence exchanges the Bio-toilet's matrix every four months. Therefore, in order to reduce annual risk to an acceptable level (i.e. 1×10^{-4} per year (Regli *et al.* 1988), the probability of infection must be 3.33×10^{-5}.

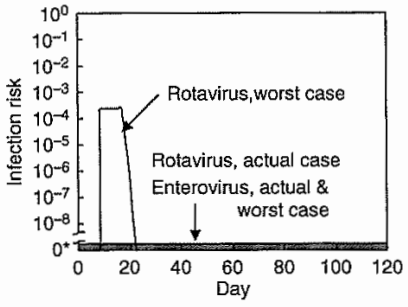

Figure 9 | Result of the risk assessment. (using Qβdie-off rate, rotavirus and enterovirus case) (0 * : less than minimum value which can be calculated).

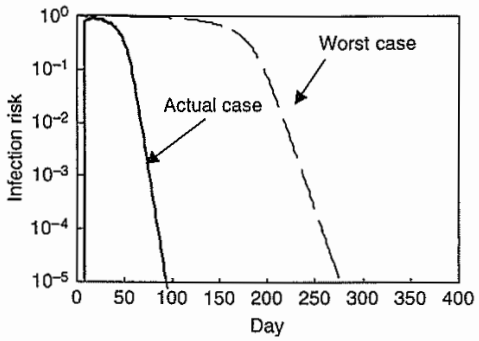

Figure 10 | Result of the risk assessment (using t4 die-off rate, rotavirus case).

The risk decreases gradually after the rotavirus stops entering, but it takes about 70 days before the risk is set at an acceptable level, and about 260 days in a "worst case scenario". In other words, it is best not to remove the compost for at least 90 days in this Bio-toilet, if diarrhea by rotavirus takes place to a person using this Bio-toilet and a rotavirus is discharged into the Bio-toilet. The infection risk of enterovirus decreases rapidly compared with that of rotavirus, in spite of its long period of excretion pathogenic viruses (Table 1), as shown in Figure 11. Acceptable levels of risk exposure occur after about 50 days in actual cases; however, 160 days is the conservative, "worst case scenario". Thus, if an indicator with a low die-off rate (like T4) is used in the risk assessment, the infection risk becomes considerably high.

The storage time of the pathogenic virus required for the Bio-toilet

The die-off rate k of the model virus Qβwas used as the parameters of temperature and water content, as shown

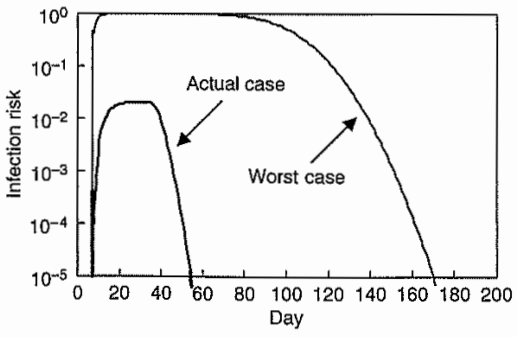

Figure 11 | Result of the risk assessment (using T4 die-off rate, enterovirus case).

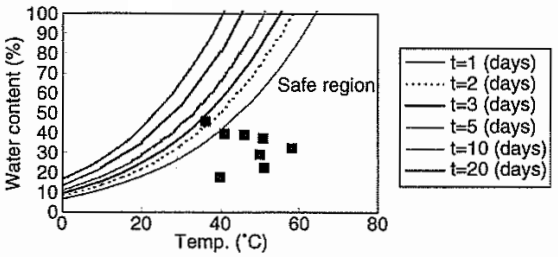

Figure 12 | The region of the safety level of the infection risk (rotavirus case using Qβdie-off rate).

in Equation (3). In the existing study, the removal ratio ($\log N/N_0$) required for the Bio-toilet is 11.5 for rotavirus and 6.5 for enterovirus, in order to hold down the annual risk to 1×10^{-4}(Nakagawa *et al.* 2003). There is a relation between removal ratio, the die-off rate, and storage time, as shown in Equation (1). Therefore, the required die-off rate was calculated in case of each storage time t to achieve these removal ratios by Equation (1). Then, the temperature and water content to achieve each k by Equation (3) was calculated. The result of the case of rotavirus is shown in Figure 12. The right-hand side of each curve of each storage time t indicates the region of safety levels of infection risk. The measurement results in terms of temperature and water content in each of the sample points of the Bio-toilet (as shown in Figure 3) are also shown in Figure 12 (square mark). From this figure, the required storage time is more than three days, in order to hold down the risk of infection risk for the year to 1×10^{-4}.

If the toilet is not heated mechanically, there is a risk that some of the material does not reach these high temperatures. In that case the risk will be substantially higher and a much longer storage time will be required to reach a safety level.

CONCLUSIONS ◀····· 結論

In this research, the fate of pathogenic viruses in a Bio-toilet was estimated according to the fate of coliphages. The experimental data of coliphage Qβ showed a higher die-off rate and more dependence on water content. On the other hand, that of T4 showed a lower die-off rate and was independent of water content. A risk assessment was

applied to the actual Bio-toilet condition according to the data derived in the house cooperating with the research.

As the results of the risk assessment, according to the actual data of water content and temperature in the Bio-toilet and the empirical die-off model of Qβ－which was assumed to be similar to many enteric viruses – the infection risks were estimated to be at sufficiently safe levels in this research. However, it was also indicated that there was the possibility of a high risk of infection caused by inappropriate use of the Bio-toilet in the presence of a highly resistant virus like coliphage T4.

In addition, the required storage time of the pathogenic viruses in the Bio-toilet can be estimated from the results of the risk assessment.

ACKNOWLEDGEMENTS ◀…… 謝辞

This research presents the results of the research project "Research on the Development of Sustainable Sanitation Systems and their Introduction in the Water Cycle System," which is Core Research for Evolutional Science and Technology (CREST), as performed by the Japan Science and Technology Agency.

REFERENCES ◀…… 参考文献

Epstein, E. 1998 Pathogenic health aspects of land application. *Bio Cycle* **39**(9), 62–67.

Fujita, K. 1995 *The technology of the composting*. Gihodo Shuppan Co., Ltd., pp. 72–74 (written in Japanese).

Haas, C. 1983 Estimation of risk due to low doses of micro-organisms: A comparison of alternative methodologies. *J. of Epidemiology* **18**, 573.

Haas, C. N., Rose, J. B. & Gerba, C. P. 1999 *Quantitative Microbial Risk Assessment*. John Wiley.

Kinosshita, M. 1994 *The Experiment Report on the Speed of Contents in Bio-toilet* (Private Report).

Lopez Zavala, M. A., Funamizu, N. & Takakuwa, T. 2004 Temperature effect on aerobic biodegradation of feces using sawdust as a matrix. *Water Research* **38**(9), 2405–2415.

Nakagawa, N., Otaki, M. & Ishizaki, K. 2001 The technical trend at the low environmental load type toilets. *Proceedings of IWA 2nd World Water Congress, Japan Science and Technology Agency*, Japan, pp. 240–248.

Nakagawa, N., Yamakoshi, K., Oe, H. & Otaki, M. 2003 Microbial risk assessment of the composting toilet. *Journal of Japan Society and Civil Engineering* **748**(VII-29), 91–98 (in Japanese).

Otaki, M. 2003 The fate of pathogenic micro-organisms in composting toilet and risk assessment. *Proceedings of the 1st International Symposium on Sustainable Sanitation*. Japan Science and Technology Agency, pp. 41–48.

Regli, S., Amirtharajah, A., Borup, B., Hibler, C., Hoff, J. & Tobin, R. 1988 Panel discussion on the implications of regulatory changes for water treatment in the United States. In *Advances in Giardia Research*, (ed. P. M. Walls, *et al.*). University of Calgary Press, Calgary, pp. 275–286.

Rose, J. B. & Gerba, C. P. 1991 Use of risk assessment for development of microbial standards. *Wat. Sci. Tech.* **24**(2), 29.

Winblad, U., Esrey, S. A., Gough, J., Rapaport, D., Sawyer, R. & Simpson-Hébert, M. 1998 *Ecological Sanitation*. Swedish International Development Cooperation Agency, Stockholm.

Available online May 2006

Application of microbial risk assessment on a residentially-operated Bio-toilet

Vocabulary

Sustainable Sanitation System	持続的な衛生システム
wastewater treatment system	排水処理システム
incorporate	組み込む
non-flushing toilet	水を使わないトイレ
Bio-toilet	バイオトイレ
convert	変える
excreta	排泄物，糞便
reusable	再利用できる
fertilizer	肥料
humus	堆肥，腐植土
organic	有機の
pollution load	汚濁負荷
exposure	曝露
pathogen	病原菌
excrement	排泄物，糞便
matrix	担体
sawdust	おがくず
urine	尿
fate	消長
coliphage	大腸菌ファージ
index	指標
die-off rate	不活化率
microbial risk assessment	微生物リスク評価
residential house	居住している住宅
infection risk	感染リスク
rotavirus	ロタウイルス
enterovirus	エンテロウイルス
reference pathogen	指標病原微生物
Qβ,T4	大腸菌ファージの一種
water content	含水率
phage	ファージ
critical	限界の，臨界の
storage time	滞留時間
acceptable	許容できる

variation	変化
procedure	手順
Bacteriophage	細菌ウイルスの通称，ファージ
model virus	指標ウイルス
injection	注入
media	担体
be stirred	撹拌された
predetermined	あらかじめ決めた
3w/v%	３％の（下記参考）
beef extra solution	ビーフエキス液
elute	溶出する，抽出する
microorganism	微生物
double agar method	２層寒天培地法
***E.coli* K12**	大腸菌（糞便性大腸菌）の一種
host	宿主
***E.coli* C**	大腸菌（糞便性大腸菌）の一種
derive	導く
empirical	実験の
assume	仮定する，
enteric	腸管系の
indicate	示唆する
inappropriate	不適切な
resistant	耐性のある

ファージ：特定のバクテリアに溶菌作用や分解作用を起こさせるウイルスの総称

３w/v%：wはweightの略でvはvolumeの略．100 mL中に３gということ．

Application of microbial risk assessment on a residentially-operated Bio-toilet

ABSTRACT

The Sustainable Sanitation System is a new wastewater treatment system that incorporates a non-flushing toilet (Bio-toilet) that converts excreta into a reusable resource (as fertilizer or humus for organic agriculture) and reduces the pollution load to environments of **the rivers, the lakes, and the sea.**

However, the risk of exposure to pathogens should be considered, because excrement is stored in the Bio-toilet.

The aim of the present work is to analyze the health risk of dealing with the matrix (excreta and urine mixed with sawdust) of the Bio-toilet.

Therefore, the fate of pathogenic viruses was investigated using coliphages as a virus index, and the modeling of the die-off rate in matrix was introduced.

Then the microbial risk assessment **was applied to** a Bio-toilet that was actually used in a residential house; the infection risks of rotavirus and enterovirus as reference pathogens were calculated.

According to the lab-scale experiment using coliphages for investigating the die-off rate of viruses in the Bio-toilet, Qβ had a higher die-off, which was greatly influenced by the water content and temperature.

On the other hand, T4 showed a lower rate and **was independent of** water content.

Therefore, these two phages' data were used as critical examples, **such as** viruses having high or low possibilities of remaining in the Bio-toilet during the risk assessment analysis.

As the result of the risk assessment, **the storage time required** for an acceptable infectious risk level has wide variations in both rotavirus and enterovirus cases **depending on** the phage that was used.

These were 0–260 days' **and** 0–160 days' difference**, respectively.**

MATERIAL AND METHODS

Experimental procedure

Bacteriophage Qβ and Bacteriophage T4 were selected as model viruses.

After the injection of these model organisms into the Bio-toilet media, it was stirred well by hand for 5 minutes.

Then amounts of between 0.1–0.2 g of the media were sampled at predetermined intervals.

These samples were **then** injected into 10 ml 3w/v% beef extra solution (pH 9.7) and mixed well for 1 minute, **in order to** elute microorganisms.

Coliphages were measured by a double agar method using *E.coli* K12 as a host bacteria for Qβ, and *E.coli* C as a host for T4 (Otaki 2003).

The die-off rate is defined **as follows**.

$$-\log N/N_0 = kt \qquad (1)$$

where

N: concentrations of phages [no./g],

N_0: initial concentrations of phages [no./g],

k: die-off rate,

t: storage time of phage in media (in [min] or [day])

CONCLUSIONS

In this research, the fate of pathogenic virus in Bio-toilet was estimated **according to** the fate of coliphages.

The experimental data of coliphage Qβ showed a higher die-off rate and more **dependent on** water content.

On the other hand, that of T4 showed a lower die-off rate and **was independent of** water content.

A risk assessment **was applied to** the actual Bio-toilet condition **according to** the data **derive**d in the house cooperating the research.

As the results of the risk assessment, **according to** the actual data of water content and temperature in the Bio-toilet and the **empirical** die-off model of Qβ – which was **assume**d to be similar to many enteric viruses – the infectious risks were estimated to be at sufficiently safe levels in this research.

However, it was also **indicate**d that there was the possibility of a high risk of infection caused by inappropriate use of the Bio-toilet in the presence of a highly resistant virus like coliphage T4.

In addition, **the required storage time** of the pathogenic viruses in the Bio-toilet can be estimated from the results of the risk assessment.

Detection of the Characteristic Pion-Decay Signature in Supernova Remnants

超新星残骸中での，特徴的なパイ中間子崩壊サインの検出

この論文は，私が所属している立教大学理学部物理学科の教員の方の論文で，2013 年にサイエンス誌（ネイチャーと並ぶ有名な専門雑誌）の“今年のブレイクスルー”として選ばれた論文の中で次点に輝いた論文です．

宇宙に降り注ぐ宇宙線の大部分を占める陽子成分は，超新星残骸で生成されているという示唆は今までにもあったものの，決定的な証拠はありませんでした．この問題の解決には，高エネルギーガンマ線の観測が重要な役割を果たします．高エネルギーの陽子や原子核が周囲のガスと衝突すると，中性パイ中間子が生成し，それがすぐに崩壊して特有なエネルギーのガンマ線を出すからです．超新星残骸から，この特徴的な放射（ガンマ線）が観測されれば，それは宇宙線の陽子成分が超新星残骸で生成することの決定的な証拠になるのです．

この論文のアブストラクトおよびイントロダクションの途中までを読んでみましょう．

Science
AAAS

Detection of the Characteristic Pion-Decay Signature in Supernova Remnants

M. Ackermann *et al.*

Science **339**, 807 (2013);
DOI: 10.1126/science.1231160

Science (print ISSN 0036-8075; online ISSN 1095-9203) is published weekly, except the last week in December, by the American Association for the Advancement of Science, 1200 New York Avenue NW, Washington, DC 20005.

16. N. P. Ong, *Phys. Rev. B* **43**, 193 (1991).
17. P. L. Taylor, *Proc. R. Soc. Lond. A Math. Phys. Sci.* **275**, 209 (1963).
18. J. W. Orenstein *et al.*, *Phys. Rev. B* **42**, 6342 (1990).
19. Z. Schlesinger *et al.*, *Phys. Rev. B* **41**, 11237 (1990).
20. H. L. Liu *et al.*, *J. Phys. Condens. Matter* **11**, 239 (1999).
21. D. van der Marel *et al.*, *Nature* **425**, 271 (2003).
22. C. C. Homes *et al.*, *Nature* **430**, 539 (2004).
23. T. Valla *et al.*, *Science* **285**, 2110 (1999).
24. S. Kasahara *et al.*, *Phys. Rev. B* **81**, 184519 (2010).
25. H. Shishido *et al.*, *Phys. Rev. Lett.* **104**, 057008 (2010).
26. N. Doiron-Leyraud *et al.*, *Eur. Phys. J. B* **78**, 23 (2010).
27. J. S. Brooks, *Rep. Prog. Phys.* **71**, 126501 (2008).
28. M. A. Tanatar, J. Paglione, C. Petrovic, L. Taillefer, *Science* **316**, 1320 (2007).
29. R. Settai *et al.*, *J. Phys. Condens. Matter* **13**, L627 (2001).
30. A. McCollam, S. R. Julian, P. M. C. Rourke, D. Aoki, J. Flouquet, *Phys. Rev. Lett.* **94**, 186401 (2005).
31. J. S. Kim, D. Hall, K. Heuser, G. R. Stewart, *Solid State Commun.* **114**, 413 (2000).
32. N. Kimura *et al.*, *Physica B* **281-282**, 710 (2000).
33. R. Daou, C. Bergemann, S. R. Julian, *Phys. Rev. Lett.* **96**, 026401 (2006).
34. M. Takashita *et al.*, *J. Phys. Soc. Jpn.* **65**, 515 (1996).
35. R. Hlubina, T. M. Rice, *Phys. Rev. B* **51**, 9253 (1995).
36. A. Rosch, *Phys. Rev. Lett.* **82**, 4280 (1999).
37. J. M. Ziman, *Electrons and Phonons* (Clarendon Press, Oxford, UK, 1960).
38. S. S. Adler *et al.*; PHENIX Collaboration, *Phys. Rev. Lett.* **91**, 182301 (2003).
39. T. Schäfer, *Phys. Rev. A* **76**, 063618 (2007).
40. C. Cao *et al.*, *Science* **331**, 58 (2011).
41. D. A. Teaney, *arXiv*:0905.2433v1.
42. P. K. Kovtun, D. T. Son, A. O. Starinets, *Phys. Rev. Lett.* **94**, 111601 (2005).
43. A. V. Andreev, S. A. Kivelson, B. Spivak, *Phys. Rev. Lett.* **106**, 256804 (2011).
44. A. Kaminski *et al.*, *Phys. Rev. B* **71**, 014517 (2005).

Acknowledgments: We are pleased to acknowledge the help of M. Baenitz, M. Nicklas, and C. Klausnitzer of the Max Planck Institute for the Chemical Physics of Solids in Dresden, where the high-temperature resistivity measurements on $Sr_3Ru_2O_7$ were performed, and useful discussions with J. Orenstein, S. A. Kivelson, C. A. Hooley, and J. Zaanen. The research was supported by the UK Engineering and Physical Sciences Research Council. H.S. gratefully acknowledges fellowships from the Canon Foundation Europe and Marubun Research Promotion Foundation, and A.P.M. acknowledges the receipt of a Royal Society–Wolfson Merit Award.

Supplementary Materials

www.sciencemag.org/cgi/content/full/339/6121/804/DC1
Materials and Methods
Supplementary Text
Fig. S1
Tables S1 to S10
References (*45*–*65*)

18 July 2012; accepted 27 November 2012
10.1126/science.1227612

Detection of the Characteristic Pion-Decay Signature in Supernova Remnants

M. Ackermann,[1] M. Ajello,[2] A. Allafort,[3] L. Baldini,[4] J. Ballet,[5] G. Barbiellini,[6,7] M. G. Baring,[8] D. Bastieri,[9,10] K. Bechtol,[3] R. Bellazzini,[11] R. D. Blandford,[3] E. D. Bloom,[3] E. Bonamente,[12,13] A. W. Borgland,[3] E. Bottacini,[3] T. J. Brandt,[14] J. Bregeon,[11] M. Brigida,[15,16] P. Bruel,[17] R. Buehler,[3] G. Busetto,[9,10] S. Buson,[9,10] G. A. Caliandro,[18] R. A. Cameron,[3] P. A. Caraveo,[19] J. M. Casandjian,[5] C. Cecchi,[12,13] Ö. Çelik,[14,20,21] E. Charles,[3] S. Chaty,[5] R. C. G. Chaves,[5] A. Chekhtman,[22] C. C. Cheung,[23] J. Chiang,[3] G. Chiaro,[24] A. N. Cillis,[14,25] S. Ciprini,[13,26] R. Claus,[3] J. Cohen-Tanugi,[27] L. R. Cominsky,[28] J. Conrad,[29,30,31] S. Corbel,[5,32] S. Cutini,[33] F. D'Ammando,[12,34,35] A. de Angelis,[36] F. de Palma,[15,16] C. D. Dermer,[37] E. do Couto e Silva,[3] P. S. Drell,[3] A. Drlica-Wagner,[3] L. Falletti,[27] C. Favuzzi,[15,16] E. C. Ferrara,[14] A. Franckowiak,[3] Y. Fukazawa,[38] S. Funk,[3]* P. Fusco,[15,16] F. Gargano,[16] S. Germani,[12,13] N. Giglietto,[15,16] P. Giommi,[33] F. Giordano,[15,16] M. Giroletti,[39] T. Glanzman,[3] G. Godfrey,[3] I. A. Grenier,[5] M.-H. Grondin,[40,41] J. E. Grove,[37] S. Guiriec,[14] D. Hadasch,[18] Y. Hanabata,[38] A. K. Harding,[14] M. Hayashida,[3,42] K. Hayashi,[38] E. Hays,[14] J. W. Hewitt,[14] A. B. Hill,[3,43] R. E. Hughes,[44] M. S. Jackson,[30,45] T. Jogler,[3] G. Jóhannesson,[46] A. S. Johnson,[3] T. Kamae,[3] J. Kataoka,[47] J. Katsuta,[3] J. Knödlseder,[48,49] M. Kuss,[11] J. Lande,[3] S. Larsson,[29,30,50] L. Latronico,[51] M. Lemoine-Goumard,[52,53] F. Longo,[6,7] F. Loparco,[15,16] M. N. Lovellette,[37] P. Lubrano,[12,13] G. M. Madejski,[3] F. Massaro,[3] M. Mayer,[1] M. N. Mazziotta,[16] J. E. McEnery,[14,54] J. Mehault,[27] P. F. Michelson,[3] R. P. Mignani,[55] W. Mitthumsiri,[3] T. Mizuno,[56] A. A. Moiseev,[20,54] M. E. Monzani,[3] A. Morselli,[57] I. V. Moskalenko,[3] S. Murgia,[3] T. Nakamori,[47] R. Nemmen,[14] E. Nuss,[27] M. Ohno,[58] T. Ohsugi,[56] N. Omodei,[3] M. Orienti,[39] E. Orlando,[3] J. F. Ormes,[59] D. Paneque,[3,60] J. S. Perkins,[14,21,20,61] M. Pesce-Rollins,[11] F. Piron,[27] G. Pivato,[10] S. Rainò,[15,16] R. Rando,[9,10] M. Razzano,[11,62] S. Razzaque,[22] A. Reimer,[3,63] O. Reimer,[3,63] S. Ritz,[62] C. Romoli,[10] M. Sánchez-Conde,[3] A. Schulz,[1] C. Sgrò,[11] P. E. Simeon,[3] E. J. Siskind,[64] D. A. Smith,[52] G. Spandre,[11] P. Spinelli,[15,16] F. W. Stecker,[14,65] A. W. Strong,[66] D. J. Suson,[67] H. Tajima,[3,68] H. Takahashi,[38] T. Takahashi,[58] T. Tanaka,[3,69]* J. G. Thayer,[3] J. B. Thayer,[3] D. J. Thompson,[14] S. E. Thorsett,[70] L. Tibaldo,[9,10] O. Tibolla,[71] M. Tinivella,[11] E. Troja,[14,72] Y. Uchiyama,[3]* T. L. Usher,[3] J. Vandenbroucke,[3] V. Vasileiou,[27] G. Vianello,[3,73] V. Vitale,[57,74] A. P. Waite,[3] M. Werner,[63] B. L. Winer,[44] K. S. Wood,[37] M. Wood,[3] R. Yamazaki,[75] Z. Yang,[29,30] S. Zimmer[29,30]

Cosmic rays are particles (mostly protons) accelerated to relativistic speeds. Despite wide agreement that supernova remnants (SNRs) are the sources of galactic cosmic rays, unequivocal evidence for the acceleration of protons in these objects is still lacking. When accelerated protons encounter interstellar material, they produce neutral pions, which in turn decay into gamma rays. This offers a compelling way to detect the acceleration sites of protons. The identification of pion-decay gamma rays has been difficult because high-energy electrons also produce gamma rays via bremsstrahlung and inverse Compton scattering. We detected the characteristic pion-decay feature in the gamma-ray spectra of two SNRs, IC 443 and W44, with the Fermi Large Area Telescope. This detection provides direct evidence that cosmic-ray protons are accelerated in SNRs.

A supernova explosion drives its progenitor material supersonically into interstellar space, forming a collisionless shock wave ahead of the stellar ejecta. The huge amount of kinetic energy released by a supernova, typically 10^{51} ergs, is initially carried by the expanding ejecta and is then transferred to kinetic and thermal energies of shocked interstellar gas and relativistic particles. The shocked gas and relativistic particles produce the thermal and nonthermal emissions of a supernova remnant (SNR). The mechanism of diffusive shock acceleration (DSA) can explain the production of relativistic particles in SNRs (*1*). DSA generally predicts that a substantial fraction of the shock energy is transferred to relativistic protons. Indeed, if SNRs are the main sites of acceleration of the galactic cosmic rays, then 3 to 30% of the supernova kinetic energy must end up transferred to relativistic protons. However, the presence of relativistic protons in SNRs has been mostly inferred from indirect arguments (*2*–*5*).

A direct signature of high-energy protons is provided by gamma rays generated in the decay of neutral pions (π^0); proton-proton (more generally nuclear-nuclear) collisions create π^0 mesons, which usually quickly decay into two gamma rays (*6*–*8*) (schematically written as $p + p \rightarrow \pi^0 +$ other products, followed by $\pi^0 \rightarrow 2\gamma$), each having an energy of $m_{\pi^0}c^2/2 = 67.5$ MeV in the rest frame of the neutral pion (where m_{π^0} is the rest mass of the neutral pion and c is the speed of light). The gamma-ray number spectrum, $F(\varepsilon)$, is thus symmetric about 67.5 MeV in a log-log representation (*9*). The π^0-decay spectrum in the usual $\varepsilon^2F(\varepsilon)$ representation rises steeply below ~200 MeV and approximately traces the energy distribution of parent protons at energies greater than a few GeV. This characteristic spectral feature (often referred to as the "pion-decay bump") uniquely identifies π^0-decay gamma rays and thereby high-energy protons, allowing a measurement of the source spectrum of cosmic rays.

Massive stars are short-lived and end their lives with core-collapse supernova explosions. These explosions typically occur in the vicinity of molecular clouds with which they interact. When cosmic-ray protons accelerated by SNRs penetrate into high-density clouds, π^0-decay gamma-ray emission is expected to be enhanced because of more frequent *pp* interactions relative to the interstellar medium (*10*). Indeed, SNRs

interacting with molecular clouds are the most luminous SNRs in gamma rays (*11*, *12*). The best examples of SNR-cloud interactions in our galaxy are the SNRs IC 443 and W44 (*13*), which are the two highest-significance SNRs in the second Fermi Large Area Telescope (LAT) catalog (2FGL) (*14*) and are thus particularly suited for a dedicated study of the details of their gamma-ray spectra. The age of each remnant is estimated to be ~10,000 years. IC 443 and W44 are located at distances of 1.5 kpc and 2.9 kpc, respectively.

We report here on 4 years of observations with the Fermi LAT (4 August 2008 to 16 July 2012) of IC 443 and W44, focusing on the sub-GeV part of the gamma-ray spectrum—a crucial spectral window for distinguishing π^0-decay gamma rays from electron bremsstrahlung or inverse Compton scattering produced by relativistic electrons. Previous analyses of IC 443 and W44 used only 1 year of Fermi LAT data (*15*–*17*) and were limited to the energy band above 200 MeV, mainly because of the small and rapidly changing LAT effective area at low energies. A recent update to the event classification and background rejection (so-called Pass 7) provides an increase in LAT effective area at 100 MeV by a factor of ~5 (*18*), enabling the study of bright, steady sources in the galactic plane below 200 MeV with the Fermi LAT. Note that the gamma-ray spectral energy distribution of W44 measured recently by the AGILE satellite falls steeply below 1 GeV, which the authors interpreted as a clear indication for the π^0-decay origin of the gamma-ray emission (*19*). Also, a recent analysis of W44 at high energies (above 2 GeV) has been reported (*20*), revealing large-scale gamma-ray emission attributable to high-energy protons that have escaped from W44. Here, we present analyses of the gamma-ray emission from the compact regions delineated by the radio continuum emission of IC 443 and W44.

The analysis was performed using the Fermi LAT Science Tools (*21*). We used a maximum likelihood technique to determine the significance of a source over the background and to fit spectral parameters (*22*, *23*). For both SNRs, additional sources seen as excesses in the background-subtracted map have been added to the background model (*24*) and are shown as diamonds in Fig. 1—one in the case of IC 443, three in the case of W44. The inclusion of these sources had no influence on the fitted spectrum of the SNRs. Three close-by sources (2FGL J1852.8+0156c, 2FGL J1857.2+0055c, and 2FGL J1858.5+0129c) have been identified with escaping cosmic rays from W44 (*20*). These 2FGL sources have been removed from the background model (see below) in order to measure the full cosmic-ray content of W44.

Figure 2 shows the spectral energy distribution obtained for IC 443 and W44 through maximum likelihood estimation. To derive the flux points, we performed a maximum likelihood fitting in 24 independent logarithmically spaced energy bands from 60 MeV to 100 GeV. The normalization of the fluxes of IC 443 and W44, and those of neighboring sources and of the galactic diffuse model, was left free in the fit for each bin. In both sources, the spectra below ~200 MeV are steeply rising, clearly exhibiting a break at ~200 MeV. To quantify the significances of the spectral breaks, we fit the fluxes of IC 443 and W44 between 60 MeV and 2 GeV—below the high-energy breaks previously found in the 1-year spectra (*15*, *16*)—with both a single power law of the form $F(\varepsilon) = K(\varepsilon/\varepsilon_0)^{-\Gamma_1}$ and a smoothly broken power law of the form $F(\varepsilon) = K(\varepsilon/\varepsilon_0)^{-\Gamma_1}\left[1 + (\varepsilon/\varepsilon_{\rm br})^{(\Gamma_2-\Gamma_1)/\alpha}\right]^{-\alpha}$ with $\varepsilon_0 = 200$ MeV. The spectral index changes from Γ_1 to Γ_2 ($>\Gamma_1$) at the break energy $\varepsilon_{\rm br}$. The smoothness of the break is determined by the parameter α, which was fixed at 0.1 (Table 1). We define the test-statistic value (*TS*) as $2\ln(\mathcal{L}_1/\mathcal{L}_0)$, where $\mathcal{L}_{1/0}$ corresponds to the likelihood value for the source/no-source hypothesis (*24*). The detection significance is given by $\sim\sqrt{TS}$. The smoothly broken power law model yields a significantly larger *TS* than a single power law, establishing the existence of a low-energy break. The improvement in log likelihood when comparing the broken power law to a single power law corresponds to a formal statistical significance of 19σ for the

[1]Deutsches Elektronen Synchrotron (DESY), D-15738 Zeuthen, Germany. [2]Space Sciences Laboratory, University of California, Berkeley, CA 94720, USA. [3]W. W. Hansen Experimental Physics Laboratory, Kavli Institute for Particle Astrophysics and Cosmology, Department of Physics, and SLAC National Accelerator Laboratory, Stanford University, Stanford, CA 94305, USA. [4]Università di Pisa and Istituto Nazionale di Fisica Nucleare, Sezione di Pisa, I-56127 Pisa, Italy. [5]Laboratoire AIM, CEA-IRFU/CNRS/Université Paris Diderot, Service d'Astrophysique, CEA Saclay, 91191 Gif-sur-Yvette, France. [6]Istituto Nazionale di Fisica Nucleare, Sezione di Trieste, I-34127 Trieste, Italy. [7]Dipartimento di Fisica, Università di Trieste, I-34127 Trieste, Italy. [8]Rice University, Department of Physics and Astronomy, MS-108, Post Office Box 1892, Houston, TX 77251, USA. [9]Istituto Nazionale di Fisica Nucleare, Sezione di Padova, I-35131 Padova, Italy. [10]Dipartimento di Fisica e Astronomia "G. Galilei," Università di Padova, I-35131 Padova, Italy. [11]Istituto Nazionale di Fisica Nucleare, Sezione di Pisa, I-56127 Pisa, Italy. [12]Istituto Nazionale di Fisica Nucleare, Sezione di Perugia, I-06123 Perugia, Italy. [13]Dipartimento di Fisica, Università degli Studi di Perugia, I-06123 Perugia, Italy. [14]NASA Goddard Space Flight Center, Greenbelt, MD 20771, USA. [15]Dipartimento di Fisica "M. Merlin" dell'Università e del Politecnico di Bari, I-70126 Bari, Italy. [16]Istituto Nazionale di Fisica Nucleare, Sezione di Bari, 70126 Bari, Italy. [17]Laboratoire Leprince-Ringuet, École Polytechnique, CNRS/IN2P3, 91128 Palaiseau, France. [18]Institut de Ciències de l'Espai (IEEE-CSIC), Campus UAB, 08193 Barcelona, Spain. [19]INAF—Istituto di Astrofisica Spaziale e Fisica Cosmica, I-20133 Milano, Italy. [20]Center for Research and Exploration in Space Science and Technology (CRESST) and NASA Goddard Space Flight Center, Greenbelt, MD 20771, USA. [21]Department of Physics and Center for Space Sciences and Technology, University of Maryland Baltimore County, Baltimore, MD 21250, USA. [22]Center for Earth Observing and Space Research, College of Science, George Mason University, Fairfax, VA 22030, resident at Naval Research Laboratory, Washington, DC 20375, USA. [23]National Research Council Research Associate, National Academy of Sciences, Washington, DC 20001, resident at Naval Research Laboratory, Washington, DC 20375, USA. [24]INFN and Dipartimento di Fisica e Astronomia "G. Galilei," Università di Padova, I-35131 Padova, Italy. [25]Instituto de Astronomía y Física del Espacio, Parbelló n IAFE, Cdad. Universitaria, C1428ZAA Buenos Aires, Argentina. [26]ASI Science Data Center, I-00044 Frascati (Roma), Italy. [27]Laboratoire Univers et Particules de Montpellier, Université Montpellier 2, CNRS/IN2P3, Montpellier, France. [28]Department of Physics and Astronomy, Sonoma State University, Rohnert Park, CA 94928, USA. [29]Department of Physics, Stockholm University, AlbaNova, SE-106 91 Stockholm, Sweden. [30]Oskar Klein Centre for Cosmoparticle Physics, AlbaNova, SE-106 91 Stockholm, Sweden. [31]Royal Swedish Academy of Sciences Research Fellow, funded by a grant from the K. A. Wallenberg Foundation. [32]Institut Universitaire de France, 75005 Paris, France. [33]Agenzia Spaziale Italiana (ASI) Science Data Center, I-00044 Frascati (Roma), Italy. [34]IASF Palermo, 90146 Palermo, Italy. [35]INAF–Istituto di Astrofisica Spaziale e Fisica Cosmica, I-00133 Roma, Italy. [36]Dipartimento di Fisica, Università di Udine and Istituto Nazionale di Fisica Nucleare, Sezione di Trieste, Gruppo Collegato di Udine, I-33100 Udine, Italy. [37]Space Science Division, Naval Research Laboratory, Washington, DC 20375, USA. [38]Department of Physical Sciences, Hiroshima University, Higashi-Hiroshima, Hiroshima 739-8526, Japan. [39]INAF Istituto di Radioastronomia, 40129 Bologna, Italy. [40]Max-Planck-Institut für Kernphysik, D-69029 Heidelberg, Germany. [41]Landessternwarte, Universität Heidelberg, Königstuhl, D-69117 Heidelberg, Germany. [42]Department of Astronomy, Graduate School of Science, Kyoto University, Sakyo-ku, Kyoto 606-8502, Japan. [43]School of Physics and Astronomy, University of Southampton, Highfield, Southampton SO17 1BJ, UK. [44]Department of Physics, Center for Cosmology and Astro-Particle Physics, Ohio State University, Columbus, OH 43210, USA. [45]Department of Physics, Royal Institute of Technology (KTH), AlbaNova, SE-106 91 Stockholm, Sweden. [46]Science Institute, University of Iceland, IS-107 Reykjavik, Iceland. [47]Research Institute for Science and Engineering, Waseda University, 3-4-1, Okubo, Shinjuku, Tokyo 169-8555, Japan. [48]CNRS, IRAP, F-31028 Toulouse Cedex 4, France. [49]GAHEC, Université de Toulouse, UPS-OMP, IRAP, 31028 Toulouse, France. [50]Department of Astronomy, Stockholm University, SE-106 91 Stockholm, Sweden. [51]Istituto Nazionale di Fisica Nucleare, Sezione di Torino, I-10125 Torino, Italy. [52]Université Bordeaux 1, CNRS/IN2p3, Centre d'Études Nucléaires de Bordeaux Gradignan, 33175 Gradignan, France. [53]Funded by contract ERC-StG-259391 from the European Community. [54]Department of Physics and Department of Astronomy, University of Maryland, College Park, MD 20742, USA. [55]Mullard Space Science Laboratory, University College London, Holmbury St. Mary, Dorking, Surrey RH5 6NT, UK. [56]Hiroshima Astrophysical Science Center, Hiroshima University, Higashi-Hiroshima, Hiroshima 739-8526, Japan. [57]Istituto Nazionale di Fisica Nucleare, Sezione di Roma "Tor Vergata," I-00133 Roma, Italy. [58]Institute of Space and Astronautical Science, JAXA, 3-1-1 Yoshinodai, Chuo-ku, Sagamihara, Kanagawa 252-5210, Japan. [59]Department of Physics and Astronomy, University of Denver, Denver, CO 80208, USA. [60]Max-Planck-Institut für Physik, D-80805 München, Germany. [61]Harvard-Smithsonian Center for Astrophysics, Cambridge, MA 02138, USA. [62]Santa Cruz Institute for Particle Physics, Department of Physics, and Department of Astronomy and Astrophysics, University of California, Santa Cruz, CA 95064, USA. [63]Institut für Astro- und Teilchenphysik and Institut für Theoretische Physik, Leopold-Franzens-Universität Innsbruck, A-6020 Innsbruck, Austria. [64]NYCB Real-Time Computing Inc., Lattingtown, NY 11560, USA. [65]Department of Physics and Astronomy, University of California, Los Angeles, CA 90095, USA. [66]Max-Planck-Institut für Extraterrestrische Physik, 85748 Garching, Germany. [67]Department of Chemistry and Physics, Purdue University Calumet, Hammond, IN 46323, USA. [68]Solar-Terrestrial Environment Laboratory, Nagoya University, Nagoya 464-8601, Japan. [69]Department of Physics, Graduate School of Science, Kyoto University, Sakyo-ku, Kyoto 606-8502, Japan. [70]Department of Physics, Willamette University, Salem, OR 97031, USA. [71]Institut für Theoretische Physik and Astrophysik, Universität Würzburg, D-97074 Würzburg, Germany. [72]NASA Postdoctoral Program Fellow. [73]Consorzio Interuniversitario per la Fisica Spaziale, I-10133 Torino, Italy. [74]Dipartimento di Fisica, Università di Roma "Tor Vergata," I-00133 Roma, Italy. [75]Department of Physics and Mathematics, Aoyama Gakuin University, Sagamihara, Kanagawa 252-5258, Japan.

*To whom correspondence should be addressed. E-mail: funk@slac.stanford.edu (S.F.); ttanaka@cr.scphys.kyoto-u.ac.jp (T.T.); uchiyama@slac.stanford.edu (Y.U.)

low-energy break in IC 443 and 21σ for that in W44, when assuming a nested model with two additional degrees of freedom.

To determine whether the spectral shape could indeed be modeled with accelerated protons, we fit the LAT spectral points with a π^0-decay spectral model, which was numerically calculated from a parameterized energy distribution of relativistic protons. Following previous studies (*15*, *16*), the parent proton spectrum as a function of momentum p was parameterized by a smoothly broken power law in the form of

$$\frac{dN_p}{dp} \propto p^{-s_1}\left[1+\left(\frac{p}{p_{\rm br}}\right)^{\frac{s_2-s_1}{\beta}}\right]^{-\beta} \quad (1)$$

Best-fit parameters were searched using χ^2-fitting to the flux points. The measured gamma-ray spectra, in particular the low-energy parts, matched the π^0-decay model (Fig. 2). Parameters for the underlying proton spectrum are $s_1 = 2.36 \pm 0.02$, $s_2 = 3.1 \pm 0.1$, and $p_{\rm br} = 239 \pm 74$ GeV c^{-1} for IC 443, and $s_1 = 2.36 \pm 0.05$, $s_2 = 3.5 \pm 0.3$, and $p_{\rm br} = 22$ GeV c^{-1} for W44 (statistical errors only). In Fig. 3 we show the energy distributions of the high-energy protons derived from the gamma-ray fits. The break $p_{\rm br}$ is at higher energies and is unrelated to the low-energy pion-decay bump seen in the gamma-ray spectrum. If the interaction between a cosmic-ray precursor (i.e., cosmic rays distributed in the shock upstream on scales smaller than ~0.1R, where R is the SNR radius) and adjacent molecular clouds were responsible for the bulk of the observed GeV gamma rays, one would expect a much harder energy spectrum at low energies (i.e., a smaller value for the index s_1), contrary to the Fermi observations. Presumably, cosmic rays in the shock downstream produce the observed gamma rays; the first index s_1 represents the shock acceleration index with possible effects due to energy-dependent propagation, and $p_{\rm br}$ may indicate the momentum above which protons cannot be effectively confined within the SNR shell. Note that $p_{\rm br}$ results in the high-energy break in the gamma-ray spectra at ~20 GeV and ~2 GeV for IC 443 and W44, respectively.

The π^0-decay gamma rays are likely emitted through interactions between "crushed cloud" gas and relativistic protons, both of which are highly compressed by radiative shocks driven into molecular clouds that are overtaken by the blast wave of the SNR (*25*). Filamentary structures of synchrotron radiation seen in a high-resolution radio continuum map of W44 (*26*) support this picture. High-energy particles in the "crushed cloud" can be explained by reacceleration of the preexisting galactic cosmic rays (*25*) and/or freshly accelerated particles that have entered the dense region (*20*). The mass of the shocked gas

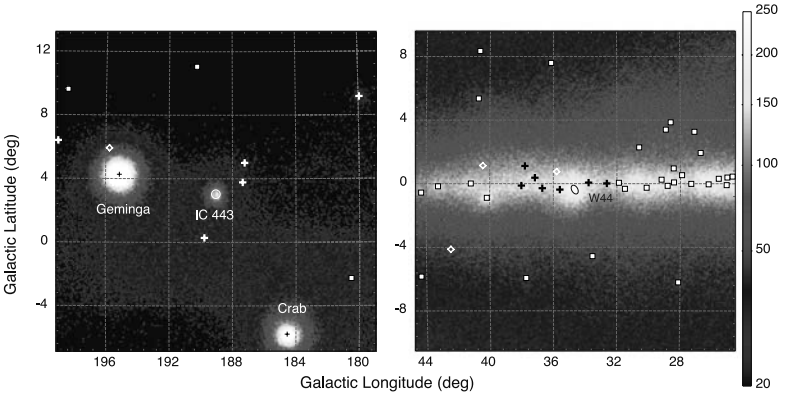

Fig. 1. Gamma-ray count maps of the 20° × 20° fields around IC 443 (**left**) and W44 (**right**) in the energy range 60 MeV to 2 GeV. Nearby gamma-ray sources are marked as crosses and squares. Diamonds denote previously undetected sources. For sources indicated by crosses and diamonds, the fluxes were left as free parameters in the analysis. Events were spatially binned in regions of side length 0.1°, the color scale units represent the square root of count density, and the colors have been clipped at 20 counts per pixel to make the galactic diffuse emission less prominent. Given the spectra of the sources and the effective area of the LAT instrument, the bulk of the photons seen in this plot have energies between 300 and 500 MeV. IC 443 is located in the galactic anti-center region, where the background gamma-ray emission produced by the pool of galactic cosmic rays interacting with interstellar gas is rather weak relative to the region around W44. The two dominant sources in the IC 443 field are the Geminga pulsar (2FGL J0633.9+1746) and the Crab (2FGL J0534.5+2201). For the W44 count map, W44 is the dominant source (subdominant, however, to the galactic diffuse emission).

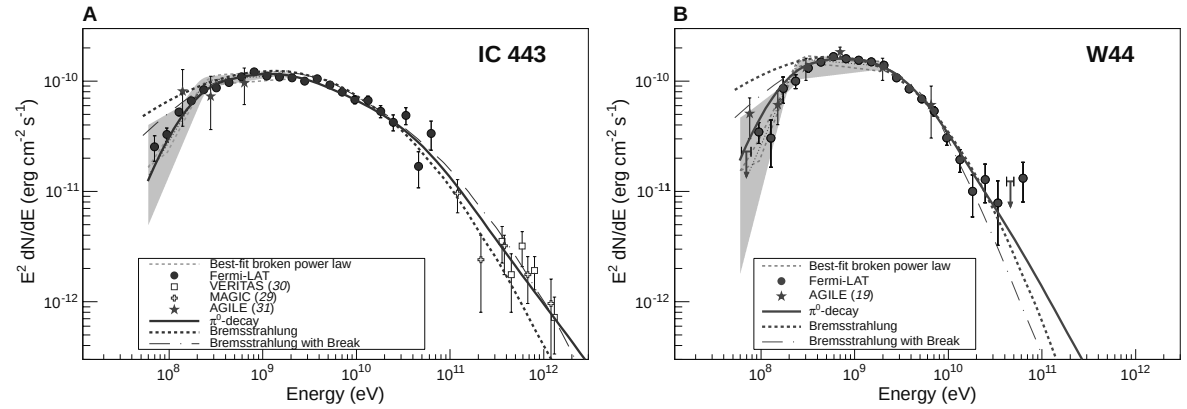

Fig. 2. (**A** and **B**) Gamma-ray spectra of IC 443 (A) and W44 (B) as measured with the Fermi LAT. Color-shaded areas bound by dashed lines denote the best-fit broadband smooth broken power law (60 MeV to 2 GeV); gray-shaded bands show systematic errors below 2 GeV due mainly to imperfect modeling of the galactic diffuse emission. At the high-energy end, TeV spectral data points for IC 443 from MAGIC (*29*) and VERITAS (*30*) are shown. Solid lines denote the best-fit pion-decay gamma-ray spectra, dashed lines denote the best-fit bremsstrahlung spectra, and dash-dotted lines denote the best-fit bremsstrahlung spectra when including an ad hoc low-energy break at 300 MeV c^{-1} in the electron spectrum. These fits were done to the Fermi LAT data alone (not taking the TeV data points into account). Magenta stars denote measurements from the AGILE satellite for these two SNRs, taken from (*31*) and (*19*), respectively.

(~1 × 10^3 $M_\odot$ and ~5 × 10^3 $M_\odot$ for IC 443 and W44, respectively, where $M_\odot$ is the mass of the Sun) is large enough to explain the observed gamma-ray luminosity. Because the "crushed cloud" is geometrically thin, multi-GeV particles are prone to escape from the dense gas, which may explain the break p_{br}.

Escaped cosmic rays reaching the unshocked molecular clouds ahead of the SNR shock can also produce π^0-decay gamma rays (*27*, *28*). Indeed, the gamma rays emitted by the escaped cosmic rays in the large molecular complex that surrounds W44 (total extent of 100 pc) have been identified with three close-by sources (*20*), which led us to remove them from the model in the maximum likelihood analysis, as mentioned above. With this treatment, the measured fluxes below 1 GeV contain small contributions from the escaped cosmic rays, but this does not affect our conclusions. The escaped cosmic rays may significantly contribute to the measured TeV fluxes from IC 443 (*29*, *30*). Emission models could be more complicated. For example, the cosmic-ray precursor with a scale of ~0.1R at the highest energy could interact with the adjacent unshocked molecular gas, producing hard gamma-ray emission. This effect is expected to become important above the LAT energy range.

We should emphasize that radiation by relativistic electrons cannot account for the gamma-ray spectra of the SNRs as naturally as radiation by relativistic protons can (*23*). An inverse-Compton origin of the emission was not plausible on energetic grounds (*11*). The most important seed photon population for scattering is the infrared radiation produced locally by the SNR itself, with an energy density of ~1 eV cm^{-3}, but this is not large enough to explain the observed gamma-ray emission. Unless we introduce in an ad hoc way an additional abrupt break in the electron spectrum at 300 MeV c^{-1} (Fig. 2, dash-dotted lines), the bremsstrahlung models do not fit the observed gamma-ray spectra. If we assume that the same electrons are responsible for the observed synchrotron radiation in the radio band, a low-energy break is not expected to be very strong in the radio spectrum, and thus the existing data do not rule out this scenario. The introduction of the low-energy break introduces additional complexity, and therefore a bremsstrahlung origin is not preferred. Although most of the gamma-ray emission from these SNRs is due to π^0 decay, electron bremsstrahlung may still contribute at a lower level. The Fermi LAT data allow an electron-to-proton ratio K_{ep} of ~0.01 or less, where K_{ep} is defined as the ratio of dN_e/dp and dN_p/dp at p = 1 GeV c^{-1} (figs. S2 and S3).

Finding evidence for the acceleration of protons has long been a key issue in attempts to elucidate the origin of cosmic rays. Our spectral measurements down to 60 MeV enable identification of the π^0-decay feature, thus providing direct evidence for the acceleration of protons in SNRs. The proton momentum distributions, well constrained by the observed gamma-ray spectra, are yet to be understood in terms of acceleration and escape processes of high-energy particles.

Table 1. Spectral parameters in the energy range of 60 MeV to 2 GeV for power-law (PL) and broken power-law (BPL) models. TS = 2 ln($\mathcal{L}_1/\mathcal{L}_0$) is the test-statistic value.

Model	K (cm^2 s^{-1} MeV^{-1})	Γ_1	Γ_2	ε_{br} (MeV)	TS
IC 443					
PL	11.7 (±0.2) × 10^{-10}	1.76 ± 0.02	—	—	21,651
BPL	11.9 (±0.6) × 10^{-10}	0.57 ± 0.25	$1.95^{+0.02}_{-0.02}$	245^{+16}_{-15}	22,010
W44					
PL	13.0 (±0.4) × 10^{-10}	1.71 ± 0.03	—	—	6,920
BPL	15.8 (±1.0) × 10^{-10}	0.07 ± 0.4	$2.08^{+0.03}_{-0.03}$	253^{+11}_{-11}	7,351

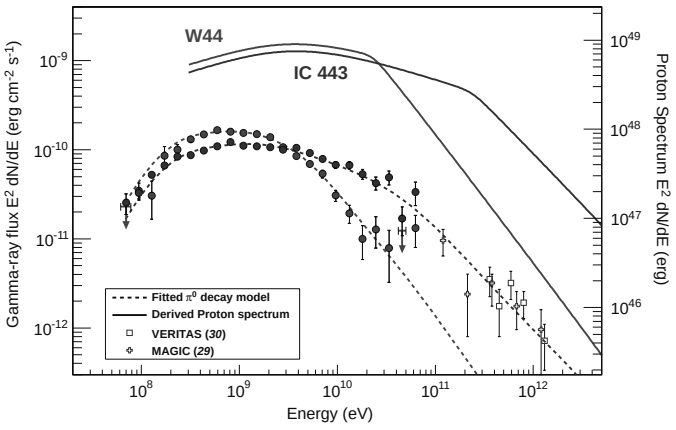

Fig. 3. Proton and gamma-ray spectra determined for IC 443 and W44. Also shown are the broadband spectral flux points derived in this study, along with TeV spectral data points for IC 443 from MAGIC (*29*) and VERITAS (*30*). The curvature evident in the proton distribution at ~2 GeV is a consequence of the display in energy space (rather than momentum space). Gamma-ray spectra from the protons were computed using the energy-dependent cross section parameterized by (*32*). We took into account accelerated nuclei (heavier than protons) as well as nuclei in the target gas by applying an enhancement factor of 1.85 (*33*). Note that models of the gamma-ray production via *pp* interactions have some uncertainty. Relative to the model adopted here, an alternative model of (*6*) predicts ~30% less photon flux near 70 MeV; the two models agree with each other to better than 15% above 200 MeV. The proton spectra assume average gas densities of n = 20 cm^{-3} (IC 443) and n = 100 cm^{-3} (W44) and distances of 1.5 kpc (IC 443) and 2.9 kpc (W44).

References and Notes

1. M. A. Malkov, L. O'C. Drury, *Rep. Prog. Phys.* **64**, 429 (2001).
2. J. S. Warren *et al.*, *Astrophys. J.* **634**, 376 (2005).
3. Y. Uchiyama, F. A. Aharonian, T. Tanaka, T. Takahashi, Y. Maeda, *Nature* **449**, 576 (2007).
4. E. A. Helder *et al.*, *Science* **325**, 719 (2009).
5. G. Morlino, D. Caprioli, *Astron. Astrophys.* **538**, A81 (2012).
6. C. D. Dermer, *Astron. Astrophys.* **157**, 223 (1986).
7. L. O'C. Drury, F. A. Aharonian, H. J. Völk, *Astron. Astrophys.* **287**, 959 (1994).
8. T. Naito, F. Takahara, *J. Phys. G* **20**, 477 (1994).
9. F. W. Stecker, *NASA Spec. Publ. 249* (1971).
10. F. A. Aharonian, L. O'C. Drury, H. J. Völk, *Astron. Astrophys.* **285**, 645 (1994).
11. A. A. Abdo *et al.*, *Astrophys. J.* **706**, L1 (2009).
12. D. J. Thompson, L. Baldini, Y. Uchiyama, http://arxiv.org/abs/1201.0988 (2012).
13. M. Seta *et al.*, *Astrophys. J.* **505**, 286 (1998).
14. P. L. Nolan *et al.*, *Astrophys. J. Suppl. Ser.* **199**, 31 (2012).
15. A. A. Abdo *et al.*, *Science* **327**, 1103 (2010).
16. A. A. Abdo *et al.*, *Astrophys. J.* **712**, 459 (2010).
17. J. Lande *et al.*, *Astrophys. J.* **756**, 5 (2012).
18. M. Ackermann *et al.*, *Astrophys. J. Suppl. Ser.* **203**, 4 (2012).
19. A. Giuliani *et al.*, *Astrophys. J.* **742**, L30 (2011).
20. Y. Uchiyama *et al.*, *Astrophys. J.* **749**, L35 (2012).
21. http://fermi.gsfc.nasa.gov/ssc/
22. The region model fitted to the data includes the SNR of interest (IC 443 or W44), background point sources from the 2FGL catalog (*14*), the galactic diffuse emission (ring_2year_P76_v0.fits), and a corresponding isotropic component (isotrop_2year_P76_source v0.txt).
23. J. R. Mattox *et al.*, *Astrophys. J.* **461**, 396 (1996).
24. See supplementary materials on *Science* Online.
25. Y. Uchiyama, R. D. Blandford, S. Funk, H. Tajima, T. Tanaka, *Astrophys. J.* **723**, L122 (2010).
26. G. Castelletti, G. Dubner, C. Brogan, N. E. Kassim, *Astron. Astrophys.* **471**, 537 (2007).
27. S. Gabici, F. A. Aharonian, S. Casanova, *Mon. Not. R. Astron. Soc.* **396**, 1629 (2009).
28. Y. Ohira, K. Murase, R. Yamazaki, *Mon. Not. R. Astron. Soc.* **410**, 1577 (2011).
29. J. Albert *et al.*, *Astrophys. J.* **664**, L87 (2007).
30. V. A. Acciari *et al.*, *Astrophys. J.* **698**, L133 (2009).
31. M. Tavani *et al.*, *Astrophys. J.* **710**, L151 (2010).

32. T. Kamae, N. Karlsson, T. Mizuno, T. Abe, T. Koi, *Astrophys. J.* **647**, 692 (2006).
33. M. Mori, *Astropart. Phys.* **31**, 341 (2009).

Acknowledgments: The Fermi LAT Collaboration acknowledges support from a number of agencies and institutes for both development and the operation of the LAT as well as scientific data analysis. These include NASA and the U.S. Department of Energy (United States); CEA/Irfu and IN2P3/CNRS (France); ASI and INFN (Italy); MEXT, KEK, and JAXA (Japan); and the K. A. Wallenberg Foundation, the Swedish Research Council, and the National Space Board (Sweden). Additional support from INAF in Italy and CNES in France for science analysis during the operations phase is also gratefully acknowledged. Fermi LAT data are available from the Fermi Science Support Center (http://fermi.gsfc.nasa.gov/ssc).

Supplementary Materials
www.sciencemag.org/cgi/content/full/339/6121/807/DC1
Materials and Methods
Figs. S1 to S3
References (*34*–*39*)

5 October 2012; accepted 12 December 2012
10.1126/science.1231160

Crystalline Inorganic Frameworks with 56-Ring, 64-Ring, and 72-Ring Channels

Hsin-Yau Lin,[1] Chih-Yuan Chin,[1] Hui-Lin Huang,[1] Wen-Yen Huang,[1] Ming-Jhe Sie,[1] Li-Hsun Huang,[1] Yuan-Han Lee,[1] Chia-Her Lin,[2] Kwang-Hwa Lii,[3] Xianhui Bu,[4] Sue-Lein Wang[1]*

The development of zeolite-like structures with extra-large pores (>12-membered rings, 12R) has been sporadic and is currently at 30R. In general, templating via molecules leads to crystalline frameworks, whereas the use of organized assemblies that permit much larger pores produces noncrystalline frameworks. Synthetic methods that generate crystallinity from both discrete templates and organized assemblies represent a viable design strategy for developing crystalline porous inorganic frameworks spanning the micro and meso regimes. We show that by integrating templating mechanisms for both zeolites and mesoporous silica in a single system, the channel size for gallium zincophosphites can be systematically tuned from 24R and 28R to 40R, 48R, 56R, 64R, and 72R. Although the materials have low thermal stability and retain their templating agents, single-activator doping of Mn^{2+} can create white-light photoluminescence.

Crystalline open-framework materials are of interest because of their rich structural chemistry and their use ranging from conventional catalysis, gas separation, and ion exchange to modern high-tech low-*k* materials, zeolite-dye microlasers, high-capacity H_2 and CO_2 gas storage (*1*–*4*), and potential lanthanide-free phosphor materials for light-emitting diodes (*5*–*7*). Their functions are mainly attributed to properties related to pore size. Therefore, pore engineering goals such as enlarging the channels, changing channel shape and connectivity, or modifying the wall composition are critical for creating new materials.

For many years, various zeolite-like structures have been synthesized using both simple and complex preparative techniques. In 1982, the discovery of $AlPO_4$-based zeolite structures (*8*) inspired the synthesis of open-framework metal phosphates. Soon after, the crystal structure of an iron phosphate mineral known as cacoxenite (*9*) was solved, revealing that the structure contained notably large channels with a free diameter of 1.4 nm and openings encircled by 36 polyhedra (36R). These discoveries led to increasing interest in pure tetrahedral and mixed polyhedral frameworks with extra-large channels (table S1). Later, many landmark structures were synthesized

[1]Department of Chemistry, Frontier Research Center on Fundamental and Applied Sciences of Matters, National Tsing Hua University, Hsinchu 30013, Taiwan. [2]Department of Chemistry, Chung-Yuan Christian University, Chungli 320, Taiwan. [3]Department of Chemistry, National Central University, Chungli 320, Taiwan. [4]Department of Chemistry and Biochemistry, California State University, Long Beach, CA 90840, USA.
*To whom correspondence should be addressed. E-mail: slwang@mx.nthu.edu.tw

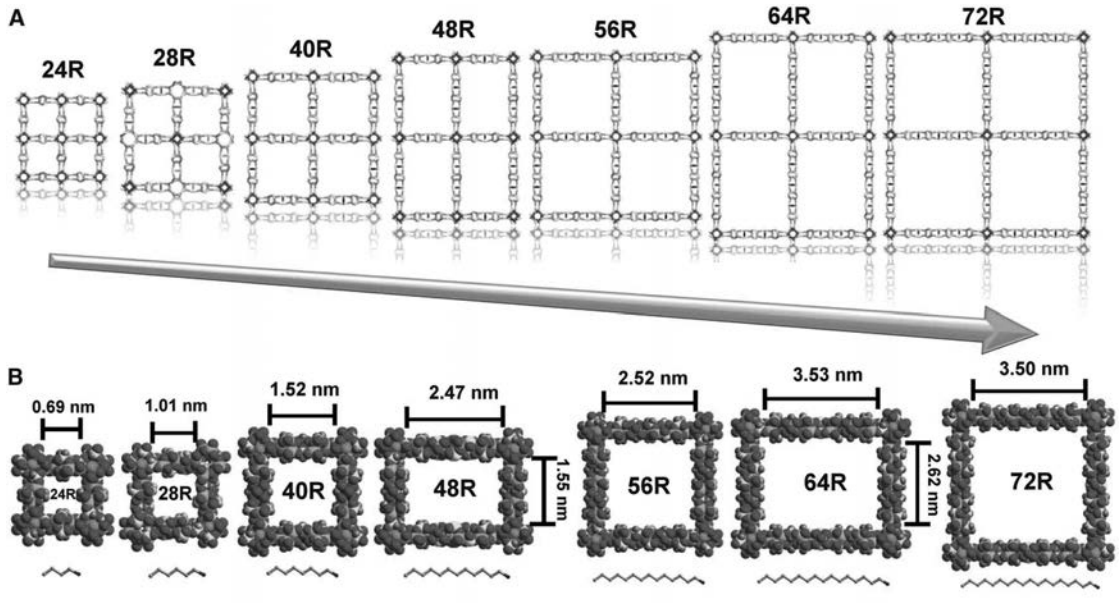

Fig. 1. Systematic expansion of structures with extra-large channels. (**A**) Channel ring size ranging from 24R to 72R. (**B**) Pore diameters spanning the micro and meso regimes. The templates are alkyl monoamines (using a ball-and-stick model) with carbon chain lengths ranging from 4C to 18C.

Detection of the Characteristic Pion-Decay Signature in Supernova Remnants

Vocabulary

（Abstractの部分）	
pion	π 中間子
supernova	超新星
remnant	残骸
cosmic ray	宇宙線
relativistic	相対論な
galactic	銀河系の
unequivocal	明白な
encounter	遭遇する
interstellar	星間の
neutral	中性の
compelling way	説得力のある方法
acceleration	加速
identification	同定
bremsstrahlung	制動放射
Inverse Compton scattering.	逆コンプトン散乱
spectra	Spectrum（スペクトル）の複数形
（Introductionの部分）	
progenitor	最初の，元祖の，創始者
supersonically	超音速で
collisionless	衝突のない
ejecta	噴出物，排出物，散乱物
kinetic energy	運動エネルギー
thermal energy	熱エネルギー
emission	放射，排出
diffusive shock acceleration (DSA)	衝撃波統計加速（フェルミ加速）

predict	予測する，予想する
substantial	かなりの，たくさんの
fraction	破片，分数
infer	推論する，推測する
schematically	図式的に，概要的に
frame	系（座標系）
rest frame	静止系
rest mass	静止系での質量
symmetric	対称の，対称性の，つりあった
parent	原因となる，元の，
proton	陽子
bump	＝hump（こぶ）
thereby	それによって，それに関して
short-lived	短命の，はかない
core-collapse	核がつぶれた（崩壊した）
vicinity	付近
penetrate	入り込む，浸透する，貫く
medium	媒体
luminous	明るい，光を発する，輝く
dedicated	専用の，特定の，
kpc	1000パーセク，1pc=3.085677581×10^{16}
rejection	排除
interpret	解釈する
attributable~	～のせいで
analyses	Analysisの複数形
delineate	描写する, 叙述する，輪郭を描く
continuum	連続

Detection of the Characteristic Pion-Decay Signature in Supernova Remnants

(Abstract)

Cosmic rays are particles (mostly protons) accelerated to relativistic speeds. Despite wide agreement that supernova remnants (SNRs) are the sources of galactic cosmic rays, unequivocal evidence for the acceleration of protons in these objects is still lacking.

When accelerated protons encounter interstellar material, they produce neutral pions, which in turn decay into gamma rays. This offers a compelling way to detect the acceleration sites of protons.

The identification of pion-decay gamma rays has been difficult because high-energy electrons also produce gamma rays via bremsstrahlung and inverse Compton scattering.

We detected the characteristic pion-decay feature in the gamma-ray spectra of two SNRs, IC 443 and W44, with the Fermi Large Area Telescope. This detection provides direct evidence that cosmic-ray protons are accelerated in SNRs.

(Introduction)

A supernova explosion drives its progenitor material supersonically into interstellar space, forming a collisionless shock wave ahead of the stellar ejecta. The huge amount of kinetic energy released by a supernova, typically 10^{51} ergs, is initially carried by the expanding ejecta and is then transferred to kinetic and thermal energies of shocked interstellar gas and relativistic particles.

The shocked gas and relativistic particles produce the thermal and nonthermal emissions of a supernova remnant (SNR). The mechanism of diffusive shock acceleration (DSA) can explain the production of relativistic particles in SNRs (*1*). DSA generally predicts that a substantial fraction of the shock energy is transferred to relativistic protons.

Indeed, if SNRs are the main sites of acceleration of the galactic cosmic rays, then 3 to 30% of the supernova kinetic energy must end up transferred to relativistic protons. However, the presence of relativistic protons in SNRs has been mostly inferred from indirect arguments (*2*–*5*).

A direct signature of high-energy protons is provided by gamma rays generated in the decay of neutral pions (π^0); proton-proton (more generally nuclear-nuclear) collisions create π^0 mesons, which usually quickly decay into two gamma rays (*6–8*) (schematically written as $p + p \rightarrow \pi^0$ +other products, followed by $\pi^0 \rightarrow 2\gamma$), each having an energy of $m_{\pi 0} c^2/2$=67.5 MeV in the rest frame of the neutral pion (where $m_{\pi 0}$ is the rest mass of the neutral pion and *c* is the speed of light).

The gamma-ray number spectrum, $F(\varepsilon)$, is thus symmetric about 67.5 MeV in a log-log representation (*9*). The π^0-decay spectrum in the usual $\varepsilon^2 F(\varepsilon)$ representation rises steeply below ~200 MeV and approximately traces the energy distribution of parent protons at energies greater than a few GeV.

This characteristic spectral feature (often referred to as the “pion-decay bump”) uniquely identifies π^0-decay gamma rays and thereby high-energy protons, allowing a measurement of the source spectrum of cosmic rays.

Massive stars are short-lived and end their lives with core-collapse supernova explosions. These explosions typically occur in the vicinity of molecular clouds with which they interact.

When cosmic-ray protons accelerated by SNRs penetrate into high-density clouds, π^0-decay gamma-ray emission is expected to be enhanced because of more frequent *pp* interactions relative to the interstellar medium (*10*).

Indeed, SNRs interacting with molecular clouds are the most luminous SNRs in gamma rays (*11, 12*). The best examples of SNR-cloud interactions in our galaxy are the SNRs IC 443 and W44 (*13*), which are the two highest-significance SNRs in the second Fermi Large Area Telescope (LAT) catalog (2FGL) (*14*) and are thus particularly suited for a dedicated study of the details of their gamma-ray spectra.

The age of each remnant is estimated to be ~10,000 years. IC 443 and W44 are located at distances of 1.5 kpc and 2.9 kpc, respectively.

We report here on 4 years of observations with the Fermi LAT (4 August 2008 to 16 July 2012) of IC 443 and W44, focusing on the sub-GeV part of the gamma-ray spectrum—a crucial spectral window for distinguishing π^0-decay gamma rays from electron bremsstrahlung or inverse Compton scattering produced by relativistic electrons.

Previous analyses of IC 443 and W44 used only 1 year of Fermi LAT data (*15*–*17*) and were limited to the energy band above 200 MeV, mainly because of the small and rapidly changing LAT effective area at low energies.

A recent update to the event classification and background rejection (so-called Pass 7) provides an increase in LAT effective area at 100 MeV by a factor of ~5 (*18*), enabling the study of bright, steady sources in the galactic plane below 200 MeV with the Fermi LAT.

Note that the gamma-ray spectral energy distribution of W44 measured recently by the AGILE satellite falls steeply below 1 GeV, which the authors interpreted as a clear indication for the π^0-decay origin of the gamma-ray emission (*19*).

153 Also, a recent analysis of W44 at high energies (above 2 GeV) has been reported
154 (*20*), revealing large-scale gamma-ray emission attributable to high-energy
155 protons that have escaped from W44. Here, we present analyses of the gamma-
156 ray emission from the compact regions delineated by the radio continuum
157 emission of IC 443 and W44.
158

Novel metalorganic chemical vapor deposition system for GaN growth

窒化ガリウム（GaN）成長のための新しい有機金属化学蒸着システム

この論文は，LED（Light Emitting Diode）の開発により，2014 年にノーベル物理学賞を受賞した，中村修二博士が書いたものです．LED そのものは共に受賞した赤崎博士によってすでに存在していましたが，中村博士が大量生産できる方法を考え出したのです．どのような方法をとったかというと，GaN（窒化ガリウム）を基板に蒸着させる時に，主流だけでなく副流も付加することで，それまでは困難といわれていた，サファイア基板上に GaN を直接成長させることに成功し，その結果，工程数を少なくコストも減らし，大量生産への道を切り拓いたといわれています．この方法に基づく装置と，作製された試料の性能の高さを述べている論文を読んでみましょう．

AIP | Applied Physics Letters

Novel metalorganic chemical vapor deposition system for GaN growth

Shuji Nakamura, Yasuhiro Harada, and Masayuki Seno

Citation: Applied Physics Letters **58**, 2021 (1991); doi: 10.1063/1.105239
View online: http://dx.doi.org/10.1063/1.105239
View Table of Contents: http://scitation.aip.org/content/aip/journal/apl/58/18?ver=pdfcov
Published by the AIP Publishing

Novel metalorganic chemical vapor deposition system for GaN growth

Shuji Nakamura, Yasuhiro Harada, and Masayuki Seno
Nichia Chemical Industries Ltd., 491 Oka, Kaminaka, Anan, Tokushima 774, Japan

(Received 28 September 1990; accepted for publication 10 February 1991)

A novel metalorganic chemical vapor deposition (MOCVD) system, which has two different flows, has been developed. One flow carries a reactant gas parallel to the substrate, and the other an inactive gas perpendicular to the substrate for the purpose of changing the direction of the reactant gas flow. The growth of a GaN film was attempted using this system, and a high quality, uniform film was obtained over a 2 in. sapphire substrate. The carrier concentration and Hall mobility are $1\times10^{18}/cm^3$ and 200 cm^2/V s, respectively, which are the highest for GaN films grown directly on a sapphire substrate by the MOCVD method.

Gallium nitride (GaN) is one of the most potential materials which can be used as a wide-gap semiconductor with applications for blue, violet, and ultraviolet light-emitting devices. For the fabrication of these optical devices, high quality GaN film is required. Usually, GaN film is grown on a sapphire substrate by the metalorganic chemical vapor deposition (MOCVD) method, and the grown layers usually show *n*-type conduction without any intentional doping. Recently, much progress has been achieved in the crystal quality of GaN film. Carrier concentration and Hall mobility, whose values were $(2–5)\times10^{17}/cm^3$ and 350–430 cm^2/V s, were obtained by the prior deposition of a thin AlN layer as a buffer layer before the growth of GaN film.[1-3] However, without the AlN buffer layer, the carrier concentration was around $2\times10^{19}/cm^3$ and the Hall mobility was only around 50 cm^2/V s in MOCVD growth without any intentional doping. To form a high quality film for the fabrication of optical devices, these values must be improved. In the previous investigations, a thin delivery tube was used to feed a reactant gas to the substrate for the purpose of obtaining a high gas velocity (around 5 m/s).[1-5] For this reason, it was very difficult to get a high quality film uniformly over the sapphire substrate.

A novel MOCVD reactor, which is shown in Fig. 1, was developed for the GaN growth. It has two different gas flows. One is the main flow which carries the reactant gas parallel to the substrate with a high velocity through the quartz nozzle. Another flow is the subflow which transports the inactive gas perpendicular to the substrate for the purpose of changing the direction of the main flow to bring the reactant gas into contact with the substrate (see Fig. 2). This subflow is very important. Without the subflow, a continuous film was not obtained and only few island growths were obtained on the substrate. The mixed gas of H_2 and N_2 was used as the subflow. We call this system a two-flow MOCVD (TF-MOCVD). The growth of GaN film was operated at atmospheric pressure. Sapphire with (0001) orientation (C face) was used as a substrate. Trinethylgallium (TMG) and ammonia (NH^3) were used as Ga and N sources, respectively. First, the substrate was heated at 1050 °C in a stream of hydrogen. Then, the substrate temperature was lowered to 1000 °C to grow the GaN film. During the deposition, the flow rates of H_2, NH_3, and TMG of the main flow were kept at 1.0 ℓ/min, 5.0 ℓ/min, and 54 μmol/min, respectively. The flow rates of H_2 and N_2 of the subflow were kept at 10 and 10 ℓ/min,

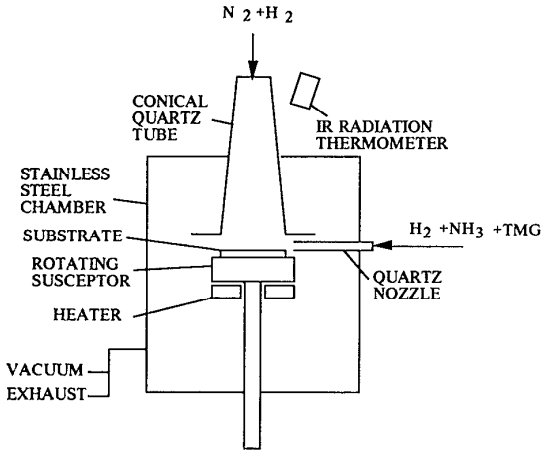

FIG. 1. Schematic novel MOCVD reactor for GaN growth.

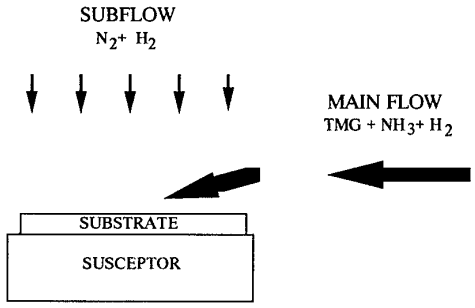

FIG. 2. Schematic principle figure of two-flow MOCVD.

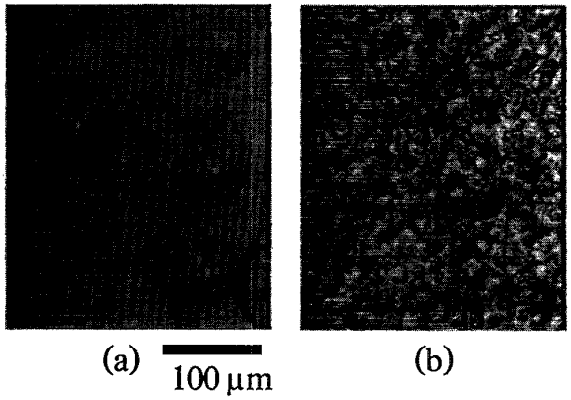

FIG. 3. Interference micrographs of the surface of the grown GaN film; (a) sample A, (b) sample B.

respectively. The growth time was 40 min. This sample was labeled sample A. Its thickness was about 3.0 μm. Another sample was labeled sample B, which was grown under the same condition as sample A except the flow rates of H_2 and N_2 of the subflow, which were changed to 10 and 0 ℓ/min, respectively. The thickness of sample B was about 2.5 μm.

Figure 3 shows the surface morphology of the grown GaN film. Normal hexagonal-like pyramid growths are observed on the surface of sample A. Many small distorted hexagonal-like pyramid growths are observed on the surface of sample B. Therefore, the surface morphology of the GaN film is affected by the flow rate of the subflow in this TF-MOCVD system. Figure 4 shows the thickness distribution of sample A. Good uniformity is obtained around the center. Hall measurement was performed by the van der Pauw method at room temperature. The results of sample A are shown in Fig. 5. The carrier concentration and Hall mobility are 1×10^{18}/cm^3 and 200 cm^2/V s, respectively. The distribution of the carrier concentration and the Hall mobility shows good uniformity. The value of the

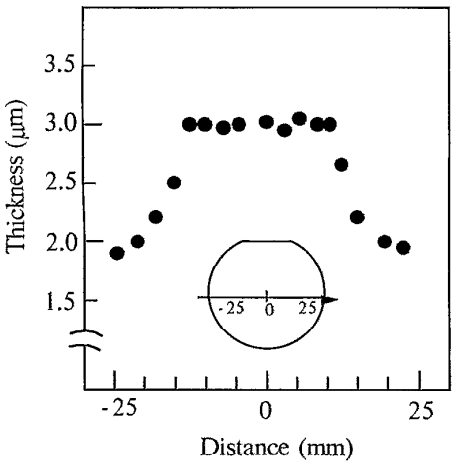

FIG. 4. Distribution of the thickness of the GaN film.

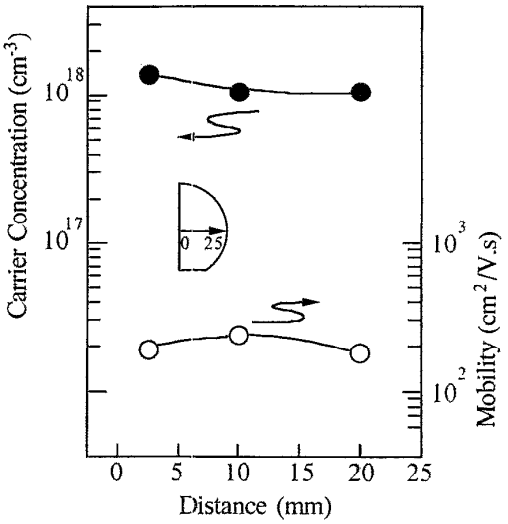

FIG. 5. Distribution of the carrier concentration and the Hall mobility.

Hall mobility is the highest one for GaN films grown directly on the sapphire substrate. The carrier concentration and the Hall mobility of sample B were 1×10^{19}/cm^3 and 40 cm^2/V s, respectively. The crystal quality of the GaN film was characterized by the double-crystal x-ray rocking curve (XRC) method. The full width at half maximum (FWHM) for (0002) diffraction from the GaN film of sample A is shown in Fig. 6. These values, about 5 min, are much better than ordinary values (about 8 min) obtained through the conventional MOCVD method. The FWHM of sample B is about 40 min.

In the TF-MOCVD system, the reactant gas flows parallel to the substrate. Thus, the lateral growth rate in the GaN growth by this system is larger in comparison with that by the conventional MOCVD system in which the reactant gas flows perpendicular or diagonally to the substrate. A continuous film is easily obtained by the present method. Also the crystal quality of the GaN film is improved.

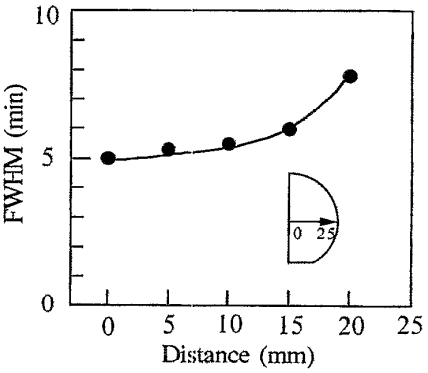

FIG. 6. Distribution of the FWHM of the XRC for (0002) diffraction.

In summary, a novel MOCVD system, which has two different flows, was developed. High quality, uniform GaN film was obtained on a 2 in. sapphire substrate using this system.

[1] H. Amano, N. Sawaki, I. Akasaki, and Y. Toyoda, Appl. Phys. Lett. **48**, 353 (1986).
[2] H. Amano, I. Akasaki, K. Hiramatsu, and N. Koide, Thin Solid Films **163**, 415 (1988).
[3] H. Amano, M. Kito, K. Hiramatsu, and I. Akasaki, Jpn. J. Appl. Phys. **28**, L2112 (1989).
[4] M. Hashimoto, H. Amano, N. Sawaki, and I. Akasaki, J. Cryst. Growth. **68**, 163 (1984).
[5] Y. Koide, H. Itoh, N. Sawaki, and I. Akasaki, J. Electrochem. Soc. **133**, 1956 (1986).

Published without author corrections

Novel metalorganic chemical vapor deposition system for GaN growth

Vocabulary

metalorganic chemical vapor deposition (MOCVD)	有機金属化学蒸着
Gallium nitride (GaN)	窒化ガリウム
reactant gas	反応ガス
parallel to ~	～に平行に
substrate	基板
inactive gas	不活化ガス
perpendicular to ~	～に垂直に
uniform	均一な
film	膜
2in.	２インチ（直径約５cm）
sapphire	サファイア
carrier concentration	キャリア濃度
Hall mobility	Hall測定による移動度
wide-gap semiconductor	ワイドギャップ半導体
ultraviolet	紫外線
light-emitting devices	発光デバイス
n-type conduction	ｎ型伝導
doping	ドーピング（不純物を入れてキャリアをつくること）
AlN layers	窒化アルミニウム層
buffer layer	緩衝層
delivery tube	配給管
velocity	速度
quartz nozzle	石英製ノズル
subflow	サブフロー
inactive gas	不活化ガス
continuous film	連続膜
atmospheric pressure	大気圧

(0001) orientation (C face)	（0001）方向（C面）
Tri-methylgallium (TMG)	トリメチルガリウム（TMG）
ammonia (NH_3)	アンモニア
flow rate	流速
growth time	成長時間
surface morphology	表面形態
Normal hexagonal-like pyramid	正６角形様のピラミッド
distribution	分布
uniformity	均一性
van der Pauw method	ファンデルポー法
crystal	結晶
double-crystal x-ray rocking curve (XRC) method	ダブルクリスタルX線ロッキングカーブ（XRC）法
full width at half maximum (FWHM)	半値全幅（FWHM）
diffraction	回折
conventional	従来の，既存の
lateral	側面の，横方向の
growth rate	成長率
in comparison with~	～と比較して
diagonally to~	～に対して斜めに

Novel metalorganic chemical vapor deposition system for GaN growth

窒化ガリウム(GaN) 成長のための新しい有機金属化学蒸着システム

Abstract

概要

A novel **metalorganic chemical vapor deposition (MOCVD)** system, which has two different flows, has been developed.

One flow carries a **reactant gas parallel to** the **substrate**, and the other an **inactive gas perpendicular to** the **substrate** for the purpose of changing the direction of the **reactant gas** flow.

The growth of a **GaN film** was attempted using this system, and a high quality, **uniform film** was obtained over a **2in. sapphire substrate**.

The **carrier concentration** and **Hall mobility** are 1×10^{18} /cm^3 and 200 cm^2/Vs, respectively, which are the highest for **GaN films** grown directly on a **sapphire substrate** by the **MOCVD** method.

Novel metalorganic chemical vapor deposition system for GaN growth

窒化ガリウム(GaN) 成長のための新しい有機金属化学蒸着システム

Gallium nitride (GaN) is one of the most potential materials which can be used as a **wide-gap semiconductor** with applications for blue, violet, and **ultraviolet light-emitting devices.**

For the **fabrication** of these **optical devices**, high quality **GaN film** is required.

Usually **GaN film** is grown on a sapphire **substrate** by the **metalorganic chemical vapor deposition (MOCVD)** method, and the grown layers usually show **n-type conduction** without any intentional **doping.**

Recently, much progress has been achieved in the crystal quality of **GaN film**.

Carrier concentration and **Hall mobility**, whose values were (2-5) × 10^{17} /cm^3 and 350-430 cm^2 /V s, were obtained by the prior **deposition** of a thin **AIN layers** as a **buffer layer** before the growth of **GaN film**.[1-3]

However, without the **AIN buffer layer**, the **carrier concentration** was around 2×10^{19} /cm^3 and the **Hall mobility** was only around 50 cm^2 /V s in **MOCVD** growth without any intentional **doping**.

To form a high quality **film** for the **fabrication** of **optical devices**, these values must be improved.

In the previous investigations, a **thin delivery tube** was used to feed a **reactant gas** to the **substrate** for the purpose of obtaining a high gas **velocity** (around 5 m/s).[1-5]

For this reason, it was very difficult to get a high quality **film uniformly** over the **sapphire substrate**.

A novel **MOCVD reactor**, which is shown in Fig.1, was developed for the GaN growth.

It has two different gas flows. One is the main flow which carries the **reactant gas** parallel to the **substrate** with a high **velocity** through the **quartz nozzle**.

Another flow is the **subflow** which transports the **inactive gas perpendicular to** the **substrate** for the purpose of changing the direction of the main flow to bring the **reactant gas** into contact with the **substrate** (see Fig.2).

This **subflow** is very important. Without the **subflow**, a **continuous film** was not obtained and only few island growths were obtained on the **substrate**.

The mixed gas of H_2 and N_2 was used as the **subflow**.

We call this system a **two-flow MOCVD(TF-MOCVD)**.

The growth of GaN **film** was operated at **atmospheric pressure**.

Sapphire with (0001) orientation (C face) was used as a **substrate**.

Tri-methylgallium (TMG) and **ammonia (NH_3)** were used as Ga and N sources, respectively.

First, the **substrate** was heated at 1050℃ in a stream of hydrogen.

Then, the **substrate** temperature was lowered to 1000℃ to grow the **GaN film**.

During the **deposition**, the **flow rates** of H_2 ,NH_3, and TMG of the main flow were kept at 1.0 L/min, 5.0 L/min, and 54μmol/min, respectively.

The flow rates of H_2 and N_2 of **subflow** were kept at 10 and 10 L/min, respectively.

The **growth time** was 40 min. This sample was labeled sample A. Its thickness was about 3.0μm.

Another sample was labeled sample B, which was grown under the same condition as sample A except the **flow rates** of H_2 and N_2 of **subflow**, which were changed to 10 and 0 L/min, respectively. The thickness of sample B was about 2.5μm.

Figure 3 shows the **surface morphology** of the grown GaN film. **Normal hexagonal-like pyramid** growths are observed on the surface of sample A.

Many small **distorted hexagonal-like pyramid** growths are observed on the surface of sample B.

Therefore, the **surface morphology** of the **GaN film** is affected by the **flow rate** of the **subflow** in this TF-MOCVD system.

Figure 4 shows the thickness **distribution** of sample A. Good uniformity is obtained around the center.

Hall measurement was performed by the **van der Pauw method** at room temperature.

The results of sample A are shown in Fig.5. The **carrier concentration** and the **Hall mobility** are $1\times 10^{18}/cm^3$ and 200 cm^2/Vs, respectively.

The **distribution** of the **carrier concentration** and the **Hall mobility** shows good **uniformity**.

The value of the **Hall mobility** is the highest one for **GaN films** grown directly on the **sapphire substrate**.

The **carrier concentration** and the **Hall mobility** of sample B were $1\times 10^{19}/cm^3$ and 40 cm^2/Vs, respectively.

The **crystal** quality of the **GaN film** was characterized by the **double-crystal x-ray rocking curve (XRC)** method.

The **full width at half maximum (FWHM)** for (0002) **diffraction** from the **GaN film** of sample A is shown in Fig.6.

These values, about 5 min, are much better than ordinary values (about 8 min) obtained through the **conventional** MOCVD method. The FWHM of sample B is about 40 min.

In the TF-MOCVD system, the **reactant gas** flows **parallel to** the **substrate**.

Thus, the **lateral growth rate** in the GaN growth by this system is larger **in comparison with** that by the **conventional** MOCVD system in which the **reactant gas** flows **perpendicular** or **diagonally to** the **substrate**.

A **continuous** film is easily obtained by the present method. Also the **crystal** quality of the **GaN film** is improved.

In summary, a novel MOCVD system, which has two different flows, was developed. High quality, uniform **GaN film** was obtained on a **2 in. sapphire substrate** using this system.

First Law of Thermodynamics

Vocabulary

thermodynamics	熱力学
net	実質の
transfer	移る
positive	正の，プラスの
negative	負の，マイナスの
by convention	慣例に従って
internal energy	内部エネルギー
fluid	流体
law of conservation of energy	エネルギー保存則
amount	量
equation	方程式
process	過程
isobaric process	等圧過程
isovolumic process	等積過程
undergo	経る
isothermal process	等温過程
ideal gas	理想気体
adiabatic process	断熱過程

Quiz

According to *the theory of relativity,* if an object is moving with velocity v it will become shorter. If the length of the object is L when it rests, its length while moving will be $L\sqrt{1-(v/c)^2}$,

where c is the speed of light (3.00×10^8 m/s).
How much shorter will a 10 meter object become if it is moving at 2/3 the speed of light ?

Chapter 2

Writing

英語で実験レポート（Experimental report）を書いてみよう

2－1　実験レポートの参考テキスト・レポート課題

英語の実験レポートの書き方

英語で実験レポートを書くときには，英語で書かれた実験の説明書を参考にするとよいです．しかし，通常の操作説明書は命令形の文章で書かれています．論文やレポートの場合はその命令形の文章を，物を主語にした（無生物主語）受動態に直せばいいのです．どうして主語を人にしないかというと，だれが実験したのかは著者か共同研究者であることは明らかで，不必要な情報だからです．科学英語は concise and correct がベスト！不必要な情報はなるべく省いて書かれるのが科学英語の特徴です．

Introduction（序文）

ここでは研究の目的を書きましょう．研究の必要性を書き加えるとさらに良いです．英文の時制は過去形や現在形，現在完了形が用いられます．

Materials and Method（実験材料と方法）

実験に用いた器具と実験方法を書きましょう．通常，論文やレポートでは，Method の部分は“物”を主語（無生物主語）にした受動態で書かれます．また，実験を行った場合は，過去に行っているので時制は過去形で書かれます．

Results（結果）

このセクションでは，実験によって得られた結果を表や図を用いて説明します．用いられる英文の時制については，過去形や現在形を用います．図や表を説明するときには現在形で書きます．得られた結果に関しては通常過去形で書きます．

Discussion（考察）

このセクションでは結果から考えられる考察を書きます．用いられる英文の時制は現在形が多いですが，予測に関しては未来形も使います．また，考察ですので，たぶんこうだろうと憶測が入ることもあり，不確かさを表す助動詞，may, could, would などが用いられることもあります．

Conclusions（結論）

この実験はどのようなことを目的として行い，結果としてどのようなことが得られたのかについて端的にまとめます．このセクションで用いられる英文の時制は過去形，現在形が主です．

References（参考文献）

１－１ 英語論文の構造のセクションでも述べたように，レポートを書く際に，参考にした文献がありましたら記載します．

それでは実際に実験レポートを英語で作成してみましょう．

次のような参考テキストを用意しました．これをもとに英語で実験レポートを作成しましょう．

Apparatus　実験器具

Electronic balance　電子天秤

10 mL graduated (measuring) cylinder　10 mL のメスシリンダー

Test tube holder (rack)　試験管立て

Retort stand, Clamp , Thermometer　スタンド，クランプ，温度計

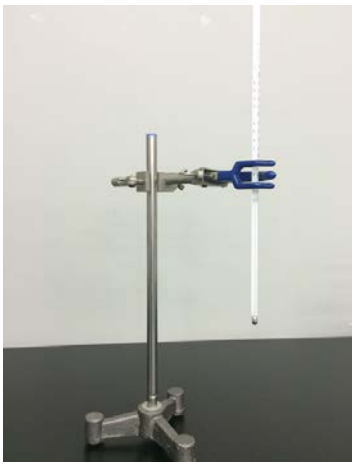

Distilled water , 1L Beaker, Heater stirrer

蒸留水，１Ｌビーカー，ヒータースターラー

Spatula , Marking pencil　薬さじ，マーカー

Solubility of Sugar in Water

INTRODUCTION

MATERIALS and METHOD

MATERIALS

Electronic balance …… 電子天秤
Thermometer …… 温度計
Heater stirrer …… ヒータースターラー
Spatula …… 薬さじ
Stirring rod …… ガラス棒
10 mL graduated (measuring) cylinder …… 10 mL のメスシリンダー
4 Test tubes …… 試験管 4 本
Retort stand …… スタンド
Test tube rack …… 試験管立て
Test tube holder …… 試験管ホルダー
1 L Beaker …… 1 L のビーカー
Clamp …… クランプ
Sugar …… 砂糖
Distilled wate …… 蒸留水
Marking pencil …… マーカー

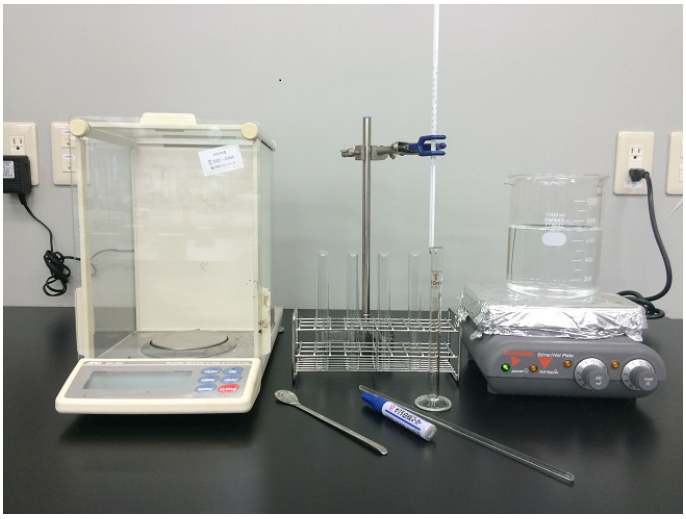

METHOD

１．Number the four test tubes using label tape as 1-4 and place them into the test tube rack.

2. Measure the quantities of sugar of 10.0 g, 13.0 g, 16.0 g and 19.0 g that are to be added to the test tubes 1-4 using the electronic balance and list these in a table as below:

Test Tube No.	Mass of Sugar (g)	Volume of distilled H_2O (mL)
1	10.0	5
2	13.0	5
3	16.0	5
4	19.0	5

（わかりやすいように表にまとめましたが，スペースをとるのでレポートには載せなくて結構です）

３. Use the 1 L beaker as a hot water bath and fill three quarter (3/4) of it with tap water. Place the water bath on the heater stirrer which is set at a medium temperature. Place test tube No.1, containing only 5 mL of water, in a clamp which attaches to the retort stand. Lower the test tube into the hot water bath. Add small amounts of sugar slowly to the test tube. The added sugar was dissolved before adding more. Heat the water bath continuously until the temperature reaches 90° C and adjust the heat to maintain this temperature.

４. Stir the sugar/water mixture with a glass stirring rod until the sugar completely dissolves. Loosen the clamp to remove the tube using a test tube holder. Stir the sugar solution continuously until you observe the first signs of crystallization. The temperature when crystallization begins is recorded in the data table.

５. Repeat steps 3 and 4 for all four test tubes. Record the temperatures for each mass of sugar in the data table.

RESULTS

表のキャプションは表の上に書く
名詞にして文章にはしない

項目の最初に
‘The’はつけない

Table 1.

Mass of Sugar (g)	Crystallization Temperature(℃)	Mass of sugar/100mL of H_2O (g/ 100 mL H_2O)
10.0	15	200.0
13.0	70	260.0
16.0	80	320.0
19.0	90	380.0

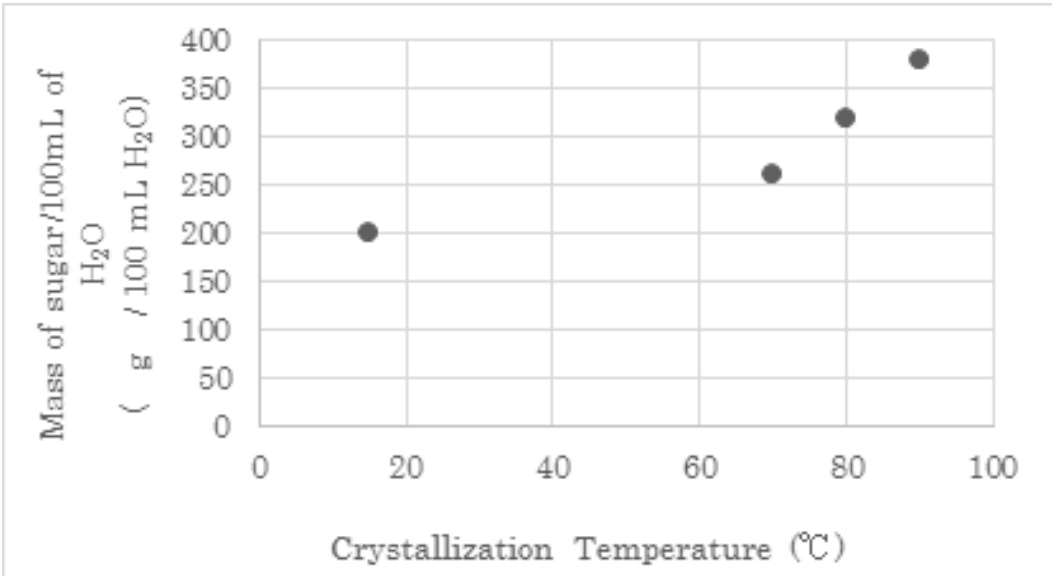

Figure 1. Crystallization temperature at different mass of sugar

図のキャプションは図の下に書く

DISCUSSION

CONCLUSIONS

Sugar dissolves more in hot water than in cold water. The hotter the water, the more the sugar dissolves.

レポート課題

このファイルをひな型として用いる場合は日本語の部分はすべて消して下さい.
多くても３ページ以内にまとめてください.

Student number
Name
学生番号と氏名を明記してください.

Title（題目）
参考テキストに書かれている「Solubility of Sugar in Water」でもいいですし，ご自分で考えた題目でも構いません.

Introduction（序文）
研究の目的を書いてください. ご自分で考えた研究の必要性を書き加えるとさらに良いです.

Materials and Method（実験材料と方法）
実験に用いた器具と実験方法を書いてください．通常，論文やレポートでは，Method の部分は“物”を主語（無生物主語）にした受動態で書かれます．また，実験を行った場合は，過去に行っているので時制は過去形で書かれます.
参考テキストの **METHOD** の **1.-5.** の部分は命令形で書かれていますので，これらの文を無生物主語にした受動態，過去形に書き変えてみましょう．例えば
１．Number the four test tubes using label tape as 1-4 and place them into the test tube rack.
この文を受動態に書き換えると
The four test tubes were numbered as 1-4 using label tape and placed into the test tube rack.
となりますね.
このようにして，**2.-5.** の文章も無生物主語にした受動態，過去形に書き換えましょう.

Results（結果）
結果を書いてください．表または図を入れるとさらに良いです．その際は表，図は Results の文章の下に入れ，表のキャプション（タイトル）は表の上に，図のキャプションは図の下に書きましょう．文章においては，例えば図 1（**Figure 1**）を入れる場合は，まず，「**Figure 1 shows the crystallization temperature at different mass of sugar.**」というように，その図が

何を表しているのかを最初に説明してください．そしてさらにグラフの説明をしてください．例えば「溶解した砂糖の量は 15℃から 70℃までは徐々に増加しているが 70℃から 90℃までは急激に増加している」というような結果を書いてください．

Discussion（考察）

ここでは，結果からさらに考えられることを書いてください．例えば「70℃のときの測定値が外れ値（outlier）に見えるのでもう一度測定する必要がある」など自由に書いて構いません．

Conclusion（結論）

ここではまとめを書いてください．参考テキストをそのまま写しても構いませんし，ご自分で考えた結論を書かれても構いません．

２–２　化学実験に使われる表現

実験で用いられる表現

調製する，合成する	A solution of 1.5 g of **X** and 3 g of **Y was prepared** and sealed in a test tube. **Z was prepared/synthesized** according to a method reported in the literature.
得る	All reagents and solvents **were obtained** from commercial sources and were used without further purification. The product **was obtained** with a 80 % yield. The product **was obtained** with a yield of 80 %. The yield of the product was 80 %.
加える	To a we**ll-stirre**d mixture of 100 ml of **X**, 15g of **Y was added** dropwise using a syringe. Approximately 5 g of **Z was added** to a well-stirred mixture of 100 ml of **X**.
処理する	**X was treated** with sulfuric acid. **X was processed** using100 ml of water.
入れる，導入する	Approximately 100 ml of benzene **was placed** in a 1-L round-bottomed flask. Hydrogen **was introduced** to the flask through a tube.
注ぐ	Water **was poured** into a beaker.
取り除く	Most of acetone **was removed at** atmospheric pressure.
撹拌する，移す	The resulting colorless solution **was stirred** for 2 min and then **transferred to** the reaction flask with a dry hypodermic syringe.
取り出す	A 1mL sample **was withdrawn** at 8-hr intervals (i.e. every 8 hours) from the reaction mixture.
加熱する	The mixture **was heated** for an additional 1.5 hr.
蒸発させる	When all the water **was evaporated,** solid crystals remained in the bottom of the flask.

抽出する,	The acidic solution **was extracted** with 200 mL quantities of dichloromethane.
希釈する, **洗浄する**	The organic layer **was diluted** with 250 mL of diethyl ether and **washed** with 100 mL of water.
乾燥する, **濃縮する**	The organic layer **was dried** over molecular sieves and then **concentrated** at 40 ℃ using an evaporator.
保管する	The product **was stored** overnight under vacuum.
集める	The orange solid product **was collected** on a glass filter.
記録する	The absorption spectra **were recorded** on a Hitachi UV-1000 spectrophotometer.
測定する	Melting points **were measured** using a melting point apparatus.
観測する	The formation of a crystalline compound **was observed** during the reaction.
保つ	The temperature of the solution was **kept (maintained)** at 50 ℃ throughout the experiment.
継続する	Heating **was continued** until the color of the metal changes.
増加する	**Increasing** the temperature by 10 ℃ did not change the yield. The temperature **was raised** to 100 ℃ to bring the reaction to completion.
減少する	The solubility of **X decreased** dramatically The reaction time **is reduced** by raising the temperature.
抑制する	Polymerization is retarded or **suppressed** by oxygen.
避ける	A temperature of 80 ℃ is required to **prevent** precipitation of the salt.
制御する	The pressure needs to **be controlled** to ensure safety during the experiment.
備える	The flask **was equipped** with a thermometer and a dropping funnel.
接続する	A thermometer **was attached** to the flask.
組み立てる	The apparatus **was set up** as described above.

２–３　ライティング（Writing）の為の文法

Writingのための英文法

冠詞

冠詞「the, a, an」は日本語にはないので，私たち日本人が英文を書く時にはついつい忘れがちですが，付け忘れると誤解を招くこともあるので，要注意です．例えば，マーク・ピーターセン著「日本人の英語」という本の中では,「a, an」という不定冠詞は単に名詞のアクセサリーではなく，冠詞をつけることで初めてその形が浮かび上がってくるものとして説明されています．例えば,

Last night, I ate chicken in the backyard.

と書かれていると，ネイティブイングリッシュの人間は，昨夜，裏庭で，（スーパーに売っているような鶏肉を使って）バーベキューでもしたのだな……と思いますが,

Last night, I ate a chicken in the backyard.

と書かれていると，昨夜，鶏を一羽（捕まえて，そのまま）裏庭で食べてしまった……と，血なまぐさい光景が目に浮かぶと書かれています．

私たち日本人は，英文を書くときに，冠詞をつけるべきかそれともつけないのか，つけるならば，the, a, an のどれを付けるべきかで悩むことが多いように思いますので，わかりやすいように下記のスケマティックにまとめてみました．以下に示すように，３つのステップで簡単に判断することができます．

ステップ１　その名詞は特定（限定）できますか？

まず冠詞の後にくる名詞が特定されているか否かを考えます．特定されているなら，その名詞が加算名詞であろうとなかろうと,「the」をつけます．

ステップ２　一方，その名詞が特定されていない場合，その名詞が加算名詞かを考えます,

ステップ３　単数形ならば冠詞は「a」, 母音から始まる単数形ならば冠詞は「an」，そして複数形や不可算名詞（information, equipment など）ならば無冠詞です（図中 × は無冠詞を表します）.

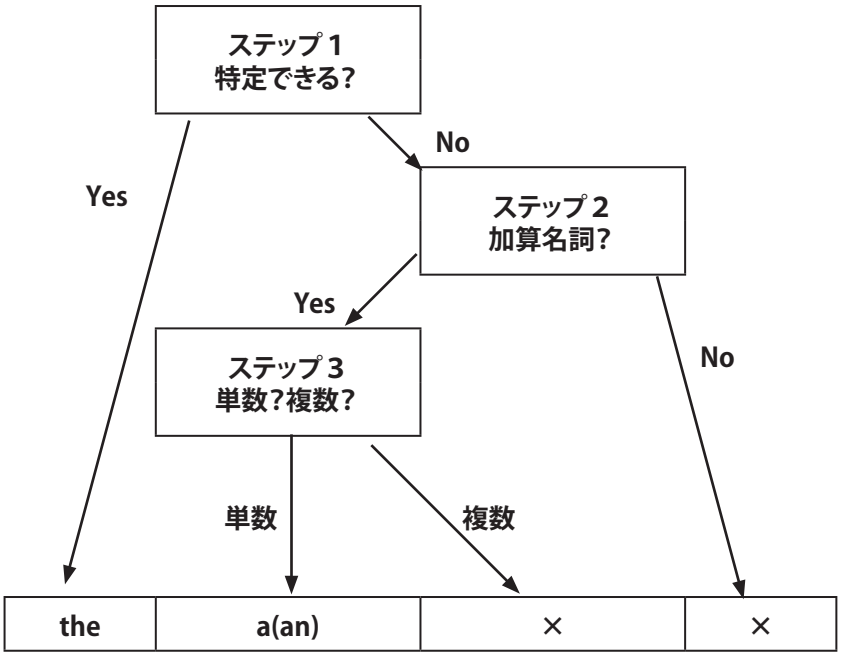
ステップ１
特定できる?
No
Yes
ステップ２
加算名詞?
Yes
No
ステップ３
単数?複数?
単数
複数
the
a(an)
×
×

２－４　文法に関する英単語

Vocabulary

単語	発音	意味
active voice		能動態
passive voice		受動態
article		冠詞
definite article		定冠詞
indefinite article		不定冠詞
tense		時制
upper case		大文字
lower case		小文字
noun		名詞
verb		動詞
adjective		形容詞
adverb		副詞
auxiliary		助動詞
modal auxiliary		may, could ,wouldなど
tentative verb		Seem, suggest, be likelyなど断定しない動詞
infinitive		不定詞
participle		分詞
gerund		動名詞
relative		関係詞
preposition		前置詞
open book style test		持ち込み可能テスト

Chapter 3

Listening

3－1　リスニング（Listening）のコツ

リスニングは単語とリエゾン(単語と単語のつなぎ)が聞き取れればだいたい理解できます.

学習方法の一例（Scientific American の Podcast など Transcript 付きの短いスキットを用意しましょう）

1．まず，vocabulary sheet なしで聴いてみる.
2．vocabulary　を確認してもう一度聴いてみる.
3．音声を聴きながら，トランスクリプトを音声と同じスピードで目を追う.
4．意味がわからなかった部分を確認する.
5．シャドーイングする.

シャドーイングとは内容は考えずに発音を追いかけながら音読すること.
英語のスピードに慣れる,英語のリズムやイントネーションがわかる,意味の区切りでのポーズの置き方がわかるなどのメリットがあります．自分で早くしゃべることができると早い英語も聴き取ることができます.

他には聴いた英語を dictation（書き取り）することも効果的な学習方法です.

3－2　リスニング（Listening）の練習題材

Muscle Mass Beats BMI as Longevity Predictor

寿命（**longevity**）の指標（**indicator**）としては，BMI（**body mass index**）よりも筋肉量（**muscle mass**）の方がいいという内容のポッドキャストです．

https://www.scientificamerican.com/podcast/episode/muscle-mass-beats-bmi-as-longevity-predictor1/

Vocabulary

BMI	body mass index（肥満度）
obesity	肥満
prescribe	指示する，処方する
shed the extra pounds	余分な体重（ポンド）を落とす
longevity	寿命
indicator	指標
muscle mass	筋肉量
analyze	分析する
a decade	10年
predict	予測する
odds	可能性，確率
correlation	相関
resistance training	筋トレ

Transcript

Doctors routinely measure a patient's body mass index, or **BMI**. And if that weight-to-height ratio points to **obesity**, the doc might **prescribe** exercise, to **shed the extra pounds**. But when it comes to **longevity**, a focus on weight loss may be misplaced. Because BMI isn't actually a very reliable **indicator** of life span. A more useful measure, some physicians say, might be **muscle mass.**

Researchers **analyzed** BMI and muscle mass data from more than 3,600 seniors in a long-term study. And they tracked which seniors had died, **a decade** later. Turns out BMI wasn't much good at **predicting** chance of death.

But muscle mass was: more muscle meant better **odds** of survival. The study appears in The American Journal of Medicine.

There's no cause-and-effect here—just **correlation** for now. But study author Preethi Srikanthan, of U.C.L.A., has this recommendation: "Get up and start moving. Focus on trying to maintain the maximum amount of **resistance training** that you can, and stop worrying so much about dropping calories." Which could take a little weight off your mind, too.

Quiz

１．医者は通常，何を健康の指標としているのか？

２．寿命を考えた場合は，どのような指標がよいのか？

３．研究者たちは何人の高齢者から **BMI** と筋肉量（**muscle mass**）のデータをとったのか？

４．データをとった高齢者の寿命から，どんなことがわかったのか？

５．U.C.L.A の Preethi Srikanthan さんはどんなことを推奨しているのか？

M Recycle Machine (Subcritical water reaction device)

今まで廃棄物とされていたものを，亜臨界水という高温高圧の水を用いて，その強い加水分解能力によって，肥料や飼料などの有価資源に変えることができる，Mリサイクルマシーンという装置があります．ここでは，この装置の宣伝用チラシ（flyer）を理解した後に，この装置のプロモーションビデオを観てみましょう．

Vocabulary

subcritical water	亜臨界水
critical point	臨界点
critical water	臨界水
hydrothermal reaction	水熱反応
organic molecule	有機分子
starch	でんぷん
protein	タンパク質
decompose	分解する
glucose	グルコース
amino acid	アミノ酸
low molecule	低分子
food waste	食品残渣
hydrolysis	加水分解
flammable waste	可燃性廃棄物
pressurized vessel	加圧容器
Incineration process	焼却処理
carbon dioxide	二酸化炭素
dioxin	ダイオキシン
nitrous oxide	N_2O，一酸化二窒素
sealing process	密封処理
processed products	処理済み産物
germ-free	無菌の
residual dioxin	残留ダイオキシン

heavy metal	重金属
safety standards	安全基準
raw garbage	生ごみ
architectural scrap wood	建築廃材
organic sludge	有機汚泥
polystyrene	ポリスチレン
shredder dust	シュレッダーゴミ
agricultural vinyl	農業ビニール
incineration ash	焼却灰

What is subcritical water?

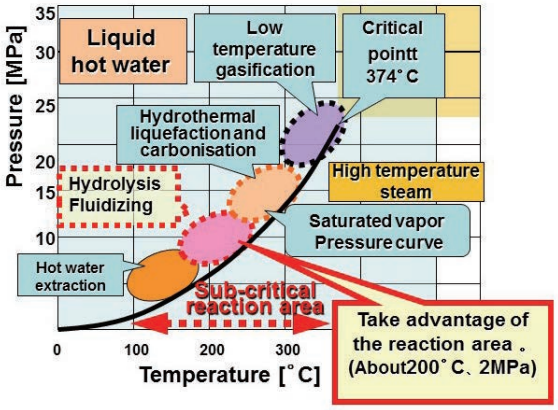

When the temperature and the pressure of water are raised to 374 ℃ and 22 Mpa (220 atmospheres), it becomes an uniform fluid that is neither steam nor water. This condition is called the critical point. Above this point, water is called super critical water. Moreover the hot water where temperature and pressure are lower than the critical point is called subcritical water, and the reaction from this water is called a hydrothermal reaction. Through this reaction the organic molecules such as starch and protein are decomposed into glucose and amino acid as well as being changed into a liquid form from solids. In conclusion this reaction is very safe, good for environment, and obtains valuable resource such as proteins from food waste by a quick and easy process.

To use this subcritical hydrolysis reaction makes recycling of waste easy and gentle on the environment.

What is M RECYCLING MACHINE【MRM】?

The MRM is a future type of subcritical water reactor that processes flammable waste by using high pressure and high temperature in a pressurized vessel.

There is no incineration process; therefore MRM doesn't generate carbon dioxide, dioxin, or nitrous oxide. Odors are not generated because of the sealed process.

This is very good for the prevention of the global warming gases and the protection of the environment. The resulting processed products are in a germ-free condition, with the residual dioxin and heavy metals below government safety standards.

The dimensions of MRM Ⅱ is 4.5 m in height, 8 m in length, and 2.5 m in width. Processing 2 ㎥ of waste takes about an hour. To operate MRM Ⅱ requires 2 to 3 people. The cost to process 2 ㎥ waste is about 3,000 yen including fuel and electricity.

It is able to recycle organic waste such as raw garbage, architectural scrap wood, organic sludge, polystyrene, shredder dust, agricultural vinyl, incineration ash, and any other flammable waste.

プロモーションビデオ

https://youtu.be/6KRp6qqwqDI

Vocabulary

disruption	破壊
verge of crisis	危機に瀕している
industrial waste	産業廃棄物
diversification	多様化
verbal	文字通り
troublesome	やっかいな，手に負えない
environmental pollution	環境汚染
toxic substances	有毒物質
livestock	家畜
sludge of sewage water	下水汚泥
filthy water	汚水
burn	燃やす
urban waste	都市ごみ
in step with the times	時代と協調した
uniform	一様な
critical point	臨界点
critical water	臨界水
hydrothermal reaction	水熱反応
starch	でんぷん
protein	タンパク質
glucose	グルコース
saccharides	糖類
acetic acid	酢酸
solvent	溶媒
closed process	密封処理=sealed process

germ-free	無菌の
scent-free	無香料の
sterilization	殺菌
deodorization	消臭
compost	コンポスト，堆肥
microbe	微生物
yeast	酵母（菌），イースト
funguses	真菌類
fertilizer	肥料

2017 Nobel in Chemistry for Seeing Biomolecules in Action

Scientific American という科学系の情報サイトのポッドキャスト「60-second　Science」では，最新の科学に関する研究成果が 1 分間程度の音声にまとめられています．その中には，毎年，スウェーデン王立科学アカデミーがノーベル賞を受賞した方々とその受賞内容を発表する様子もまとめられています．

ここでは，2017 年にノーベル化学賞を受賞した，溶液中の生体分子を高分解能で構造決定できるクライオ電子顕微鏡に関するポッドキャストを紹介します．

https://www.scientificamerican.com/podcast/episode/nobel-in-chemistry-for-seeing-biomolecules-in-action/

Vocabulary

cryo-electron microscopy	クライオ電子顕微鏡法
high-resolution	高分解能の，高解像度の
biomolecules	生体分子
secretary general	事務局長
honorary professor	名誉教授
Molecular Biology	分子生物学
exemplify	よい例となる，例示する
Zika virus	ジカウイルス

2017 Nobel in Chemistry for Seeing Biomolecules in Action

"The Royal Swedish Academy of Sciences has decided to award the 2017 Nobel Prize in Chemistry jointly to Jacques Dubochet, Joachim Frank and Richard Henderson…for developing **cryo-electron microscopy** for the **high-resolution** structure determination of **biomolecules** in solution."

Göran Hansson, **secretary general** of the Academy, at 5:53 this morning Eastern time.

Dubochet is **honorary professor** at the University of Lausanne in Switzerland. Frank is at Columbia University in New York. Henderson is at the Laboratory of **Molecular Biology** in Cambridge.

The technique has transformed electron microscopy from a technique that could be used to just see the shapes, the outer shapes, of molecules into one that is now used to see the details, the atoms inside the molecules.

Peter Brzezinski is a professor of biochemistry at Stockholm University and a member of the Nobel Committee for Chemistry.

"And the latest technical developments occurred very recently. So it's recent developments that you can actually see the details of these molecules. The technique is also relatively rapid, so once one has samples that can be studied the structure can be determined relatively rapidly. And this was **exemplified** last year when the structure of the **Zika virus** was determined in just a few months. And the structure shows the atomic details of the surface, which of course is important when developing drugs against the virus."

For an in-depth listen about the 2017 Nobel Prize in Chemistry, look for the Scientific American Science Talk podcast later today.

—Steve Mirsky

[The above text is a transcript of this podcast.]

Money to Burn

MIT の Open Course Ware に載っている化学実験のビデオです.

実験に登場するお札は本物か，ニセ札か？どうして灰も残らずお札は燃えてなくなったのでしょうか？

ビデオの途中までのトランスクリプトを載せました.

https://ocw.mit.edu/high-school/chemistry/demonstrations/videos/money-to-burn/

Vocabulary

burn	燃える
performing with~	～をする
dollar bill	ドル紙幣
flame	炎
thin air	虚空，何もない空
be engaging	魅力的
informative	役に立つ
ashes	灰
treated with~	～を処理する
nitrated	硝化された
soak	つける，ひたす
mixture	混合物
concentrated	濃縮された
Nitric acid	NHO_3
sulfuric acid	H_2SO_4
cellulose	セルロース，繊維素
reacts with~	～と反応する
nitrated cellulose	$C_6H_7(NO_2)_3O_5$
polymer	重合体，高分子化合物，ポリマー
nitro group	ニトロ基，-NO_2で表される原子団

molecules	分子
no doubt	きっと，おそらく
nitroglycerin	ニトログリセリン
tri nitro toluene (TNT)	トリニトロトルエン
explosive	爆発的な

Money to Burn

Hi I’m just again today. I’m going to be talking about a chemical demonstration.
I like to call ‘money to burn’ and chemist Dr. Bassam Shakhashiri here is actually going to be showing us the demo. He is the president of the American Chemical Society and is performing with demo right here at MIT. Let’s see if he has some money to burn.

What am I going to do now is reach in here and take a dollar bill and I’m going to put it in a flame just like that. Was that too fast? What we always do in science is to repeat the experiment. So I think what looks like a dollar bill is not a real dollar bill. I bring it close to the flame. Disappears into thin air. It looks like magic, right? I love magic. Magic is engaging but not informative.

How is that dollar bill burning up so quickly? Well, it’s actually not a dollar bill. it’s called flash paper and it’s paper that has been treated with chemicals to make it burn quickly and leave no ashes. A flash paper has been nitrated. Practically what that means is that you soak the paper in a mixture of concentrated nitric and sulfuric acid. The cellulose in the paper then reacts with the acid to produce nitrated cellulose and water. The reaction is this.

$$3HNO_3 + C_6H_{10}O_5 \rightarrow C_6H_7(NO_2)_3O_5 + 3H_2O$$

(nitric acid) (cellulose) (nitrated cellulose) (water)

So, nitric acid here mixes with the cellulose. Now this is actually just one unit in the big polymer, that is cellulose. It’s got lots a little units have $C_6H_{10}O_5$. So in this equation, I’m only writing one unit and that’s creating nitrated cellulose and water. Now the nitro group, the NO_2 is the reactive group and it can be very reactive depending on the molecule that it’s in. You’ve no doubt heard of nitroglycerin which looks like this. It’s an explosive liquid or TNT which actually stands for tri nitro toluene (TNT).It looks like this. So all these molecules have nitro groups in them and it’s the nitro or NO_2 groups that make these molecules explosive.

Why do onions make us cry ?

どうして玉ねぎを切ると涙が出るのでしょうか，そして涙が出るのを防ぐ方法は？

https://www.scientificamerican.com/video/why-do-onions-make-us-cry/

Vocabulary

pungent	鼻や舌を刺激する，ぴりっとする
be bound to	必ず
tear up	泣く
bulbous	球根状の
veggie	野菜
rupture	破裂させる
sturdy	丈夫な
swarm	大群
enzyme	酵素
sulfur	硫黄
sulfenic acids	スルフェン酸
volatile	揮発性の
irritating	ひりひりさせる
lachrymatory	涙を催させる
waft	ふわりと運ぶ，漂う
neuron	神経
duct	管，脈管
waterworks	水道
deactivate	非活性化する
collaborate	協力する
gene	遺伝子
shelf	棚
genetically	遺伝子的に

breeding	品種改良
grocery	食料雑貨
available	入手できる

Why do onions make us cry ?

Start chopping a **pungent** onion and before too long you're **bound to tear up.**
How exactly does this **bulbous veggie** have the power to make us cry?
The second you slice into an onion you change its chemistry.
Cutting an onion **ruptures** its cell walls.
You can think of these walls as **sturdy** balloons that hold in the cells contents.
When a knife breaks through, **swarms** of molecules and **enzymes** escape.
Some of those **enzymes** break down **sulfur** compounds present in the onion generating sulfenic acids in the process.
Other chemical reactions convert **sulfenic acids** into a **volatile** and **irritating** gas called onion **lachrymatory** factor.
When this gas **wafts** into your eyes, certain **neurons** instruct your tear **ducts** to flush out this potentially harmful substance.
Fortunately, there are a few tricks you can use to keep the **waterworks** to a minimum.
Storing the onion in the fridge or freezer for at least 30 minutes before chopping, slows down its **enzyme**s which should help prevent tears.
Briefly boiling an onion should have the same effect.
High heat can **deactivate** enzymes.
Another strategy is cutting the onion under running water to prevent the gas from reaching your eyes.
But the easiest solution is probably a pair of ski goggles or sunglasses.
Umm, if goggles or glasses don't work out so well, don't worry.
Scientists are trying to tackle the problem too.
Researchers in Japan and New Zealand have **collaborate**d to create a tear free onion.
They silenced one of the **gene**s that makes onion **lachrymatory** factor, the **volatile** gas that irritates your eyes.
But don't look for it on the **shelf**, this **genetically** modified product is not currently on the market.
Other researchers used traditional plant **breeding** to create the "Ever Mild", a yellow onion with really low levels of the **volatile** gas.
You can find it in some **grocery** stores.
But until these products are more widely **available**, we'll probably have to stick with Kleenex and sunglasses.

Have You Ever Seen an Atom?

あなたは原子を見たことがありますか？

https://www.youtube.com/watch?v=yqLlgIaz1L0

Vocabulary

atom	原子	**merge**	結合する
microscopes	顕微鏡	**every so often**	時々
ultra	超，極端な	**structure**	構造
chromosomes	染色体	**align**	配置
come up with	提案する	**granting**	与えている，許している
a whole host of	多数の	**awesome**	とてもよい，すごい
observe	観察する	**clarity**	明確，明快さ
fundamental	基礎的な	**analyze**	分析する
nanoparticle	ナノ粒子	**irregularities**	不規則，ふぞろい
platinum	白金，プラチナ，Pt	**dislocations**	ずれ
nanometers	10^{-9} m	**misalignment**	誤整列
tiny	とても小さな	**subtle**	わずかな，かすかな
angle	角度	**none the less**	それでもなお
reconstruction	復元，再建	**significantly**	かなり
unprecedented	かつてない,前例のない	**efficiency**	効率
blurry	ぼやけた，おぼろげな	**strength**	強さ
swarm	大群，昆虫などの群れ	**alloys**	合金

Have You Ever Seen an Atom?

Have you ever seen an atom?
Seeing everything is made of them you have.
But have you ever seen one of them on its own?
Over time microscopes have become more and more powerful allowing us to see deeper into the world of the ultra small.
Traditional light microscopes can be used to see things like these onion cells and the structures within them as they divide pulling apart the chromosomes.
The scientists have come up with a whole host of clever methods to observe far smaller things.
Using beams of electrons instead of light, we can generate detailed images of chromosomes themselves.
Recently groups of scientists around the world are becoming able to see material at the most fundamental scale, the atomic.
One group from the University of California in Los Angeles have been getting up close and personal with nanoparticles of platinum just a few nanometers across.
Each of the tiny dots you can see here are actually individual platinum atoms.
The researchers didn't stop at the two-dimensional picture.
By imaging over a hundred slices of nanoparticle at different angles then removing the noise by the special filter they're able to map the location of almost every atom.
The information was used to create a three-dimensional reconstruction of the whole particle in unprecedented detail.
It may look blurry but this particle is estimated to contain over twenty seven thousand atoms.
And so like flies in a swarm they appear to merge together.
Every so often though, we see the platinum atomic structure align granting awesome moment of clarity. This technique is being used to analyze tiny irregularities in the structure of the particle called dislocations.
Dislocations are subtle like the misalignment of the green and red layers of atoms in this particle.
But none the less they can significantly change the properties of materials with effects ranging from a change in the efficiency of LEDs to the strength of metal alloys.
Three-dimensional atomic scale imaging like this is bettering or understanding of the structure materials on this truly fundamental scale.

How Gene Therapy Targets Liver Cells

治療用の遺伝子情報を組み込んだウイルスを，異常な遺伝子を持つ細胞内に侵入させて治療することを遺伝子治療といいますが，このビデオは治療用ウイルスが肝臓の細胞に入って欠陥のある遺伝物質を取り換えるシーンが美しく映っています．さて，治療用ウイルスはどのようにしてマクロファージをすりぬけたのでしょうか？

https://www.scientificamerican.com/article/gene-therapy-video-how-targets-liver-video/

Vocabulary

virus	ウイルス	**binds to~**	～と結びつける
particle	粒子	**specifically**	特異的に
containing	含んでいる	**liver**	肝臓
therapeutic	治療（療法）上の	**envelope**	外皮，包被
gene	遺伝子	**merges with**	合体する
capillaries	毛細血管	**cell membrane**	細胞膜
pore	孔，毛穴	**load**	積む
macrophages	マクロファージ	**therapeutic DNA**	治療(療法)上のDNA
task	課された仕事	**penetrate**	侵入する
harmful	有害な	**nucleus**	核
coated with	被覆した，覆われた	**assure**	確かにする
protein	タンパク質	**function**	機能する，働く

How Gene Therapy Targets Liver Cells

Virus particles containing the therapeutic gene enter the liver with the blood stream.
Their target is the region where liver cells exchange matters with the blood, the small capillaries.
There are large pores in the capillary walls.
The liver cells are on the other side of these openings.
The capillaries also contain special cells, the macrophages.
Their task is to remove any foreign harmful particles.
They will try to do this also with the virus particles.
That is why the outside of the virus is coated with a protein that can bind specifically to liver cells.
Because of this protein, the virus will get passed the macrophages and reach the liver cells more quickly.
Once the virus particle binds to the liver cell, the viruses' envelope merges with the liver cells, cell membrane.
This allows the viruses load therapeutic DNA to penetrate the cell.
It will find a path to the cell's nucleus.
The virus proteins assured that therapeutic gene is taking into the genetic material on the liver cell.
This will enable the liver cell to function once again as a healthy cell.

What happen to your body after you die?

私たちの身体は，亡くなった後，どうなるのでしょうか.

https://www.scientificamerican.com/video/what-happens-to-your-body-after-you-die/

Vocabulary

Death sucks	誰も死を望んでいない，死はひどい
fascinating	魅了する
gross	ひどい
breathing	呼吸
oxygen	酸素
carbon dioxide	二酸化炭素
acidic	酸性
rupturing	破裂させる
sacs	嚢（袋）
enzymes	酵素
digest	消化する
creates	創る
blister-like	水ぶくれのような
fluid	流体
nutrient	栄養
fuel	燃料
army	軍隊
bacteria	バクテリア，細菌
fungi	菌類
further	さらに
liquefy	液化させる
organs	臓器，器官

muscles	筋肉
microbes	微生物
tissue	組織
bewildering	途方に暮れるほどの
array	整列，配列
chemicals	化学物質
Freon	フレオン（フロンガス）
coolant	クーラント（冷却液）
refrigerator	冷蔵庫
Benzene	ベンゼン
sulfur	硫黄
swamp	沼地
rotten egg	腐った卵
Carbon Tetrachloride	四塩化炭素（CCl_4）
extinguisher	消火器
maggot	ハエの幼虫
protein	たんぱく質
Hydroxyapatite	水酸化リン灰石（ハイドロキシアパタイト）
solace	慰め
vital	不可欠な，きわめて重要な
sprout	発芽する

What happen to your body after you die?

Death sucks! But what happens to your body after you die is fascinating. So we're going to show you. Don't worry, it won't be gross...much. Once a person's breathing stops the cells in their body stops receiving oxygen, But the cells continue to live for several minutes generating carbon dioxide. Carbon dioxide is acidic, and it builds up, rupturing sacs inside the cells. These sacs contain enzymes that begin to digest the cell from the inside out. This creates a blister-like fluid rich in nutrients. After about a week, those nutrients fuel an army of bacteria and fungi that further liquefy organs and muscles. The microbes that attack the tissue produce a bewildering array of chemicals and gasses. They include Freon, that's right, the coolant found in refrigerator. Benzene, a powerful component in gasoline. Sulfur, which smells of swamps and rotten eggs. And the molecule known as Carbon Tetrachloride, which was used in fire extinguishers and dry cleaning until scientists discovered it's highly toxic. At this point, there's very little flesh left, and it's consumed by...here it comes... maggots and beetles. Insects leave only bones behind. Over time, the protein in bone decomposes too, leaving just the bone mineral called Hydroxyapatite, which eventually turns to dust. We can take some solace in the fact that all those nutrients and chemicals, even the dust, provide vital substances that make soils fertile, sprouting plants and other new life after our lives have ended. Ashes to ashes, dust to dust.

How Does Meditation Change the Brain?

瞑想は物理的精神的な健康に良いと言われていますが，脳にどのような影響を与えるのでしょうか？

https://www.scientificamerican.com/video/how-does-meditation-change-the-brai2013-10-30/

Vocabulary

meditation	瞑想
relieve	和らげる，取り除く
neuroscientist	神経科学者
rewire	新しく設置する
neural circuit	神経回路
Pruning away	切り離す
mindfulness	サティ（仏教用語），注意，意識
sensation	感覚
ideally	理想的に
fluke	まぐれあたり
monk	僧侶
robust	強靭な
scatter	散らばる
synchronize	同時に起こる
wrinkly	しわの寄った
cortex	外皮，外層
sophisticated	洗練された
abstract	抽象的な
introspection	自己観察，自己反省
confirm	確かめる
hippocampus	海馬

seahorse	海馬
skull	頭蓋骨
crucial	重大な，決定的な
sustaining	持続する
shrink	委縮する
counteract	阻止する，和らげる，
decay	衰え
temporarily	一時的に
manipulate	操作する，操る
lifelong	一生の
outperform	上回る，しのぐ

How Does Meditation Change the Brain?

Researchers have known for decades that meditation can improve someone's physical and mental health. It can **relieve** stress, lower blood pressure and lift someone's mood. But only in the last few years have **neuroscientist**s taken a serious look at the changes in brain structure underlying some of meditation's benefits.

Like everything else we do, meditation **rewire**s our **neural circuits. Pruning away** the least used connections and strengthening the ones we exercise most.

Studies looking for signs of these changes usually focus on "**mindfulness** meditation" which challenges people to keep their attention fixed on the thoughts and **sensations** in the present moment.

Scientists acknowledge that these studies are small and not **ideally** designed, but at this point researchers have gathered enough evidence to be confident that their findings are not just **flukes**.

Experiments suggest that Buddhist **monks** have really **robust** connections between **scatter**ed regions of their brains, which allows for more **synchronize**d communication.

Expert meditators also seem to develop an especially **wrinkly cortex**: the brain's outer layer.

We depend on the **cortex** for many of our most **sophisticated** mental abilities like **abstract** thought and **introspection**.

Several studies have **confirm**ed that meditation can increase the volume and density of the **hippocampus**: a **seahorse**- shaped area of the brain in the middle of the **skull** that is absolutely **crucial** for memory.

And although areas of the brain responsible for **sustaining** attention usually **shrink** as we age, meditation **counteract**s this **decay.**

An increasing number of studies show that meditating for as little as 12 to 20 minutes a day for several weeks can sharpen the mind.

In these studies, meditators have scored higher on tests of attention and working memory, which is the ability to **temporarily** store and **manipulate** information in one's mind.

Some **lifelong** meditators in their 50s and 60s can even **outperform** twenty-something in tests of visual attention.

So if you're interested in trying meditation, you should probably start as soon as possible.

2015 Nobel Prize in Physiology or Medicine

Scientific American という科学系の情報サイトのポッドキャスト「60-second Science」では，最新の科学に関する研究成果が 1 分間程度の音声にまとめられています．その中には，毎年，スウェーデン王立科学アカデミーがノーベル賞を受賞した方々とその受賞内容を発表する様子もまとめられています．

ここでは，2015 年にノーベル生理・医学賞を受賞した，マラリアや回虫寄生虫による感染症に対する新療法についてのポッドキャストを紹介しましょう．

https://www.scientificamerican.com/podcast/episode/2015-nobel-prize-in-physiology-or-medicine1/

The 2015 Nobel Prize in Physiology or Medicine goes jointly to William C. Campbell and Satoshi Ōmura for their studies leading to novel therapies against infections caused by roundworm parasites and to Youyou Tu for her work developing a novel therapy against malaria

“The Nobel Assembly at the Karolinska Institute has today awarded the 2015 Nobel Prize in Physiology or Medicine, with one half jointly to William C. Campbell and Satoshi Ōmura for their discoveries concerning a novel therapy against infections caused by roundworm parasites and the other half to Youyou Tu for her discoveries concerning a novel therapy against malaria.”

Urban Lendahl of the Nobel Committee shortly after 5:30 this morning Eastern time.

Campbell is affiliated with Drew University in New Jersey. Ōmura is at Japan’s Kitasato University. Their work developed the drug Avermectin and later the closely related drug Ivermectin. The medications have led to the near eradication of the roundworm-caused diseases River Blindness and Lymphatic Filariasis, also known as Elephantiasis.

Youyou Tu is with the Academy of Chinese Medicine. Her studies led to the creation of the drug Artemisinin, which has lowered mortality rates from malaria. About half the world’s population have been living with the threat of these infections. Both types of drugs are examples of

natural products chemistry—that is, the efficacious compounds were isolated from organisms that naturally produce them or similar molecules and had exhibited therapeutic potential in screenings.

“The impact of Avermectin and Artemisinin goes far beyond reducing the disease burden of individuals.” Hans Forssberg of the Nobel Committee.

By allowing children to go to school and adults to go to work, the treatment helps them to escape poverty, which also contributes to economic growth of the community. The discoveries of the 2015 Nobel Laureates represent a paradigm shift in medicine, which has not only provided revolutionary therapies for patients suffering from devastating parasitic diseases, but has also promoted well-being and prosperity for both individuals and society. The global impact of their discovery and the resulting benefit to mankind is immeasurable.”

For an in-depth listen about the 2015 Nobel Prize in Physiology or Medicine, look for the Scientific American Science Talk podcast later today.

—Steve Mirsky

(The above text is a transcript of this podcast)

2014 Nobel Prize in Physics

2014 年に青色発光ダイオードの発明でノーベル物理学賞を受賞された３人の先生方の紹介と受賞内容について，スウェーデン王立科学アカデミーが発表している様子を映したビデオの途中までの単語とトランスクリプトを載せました.

http://www.scientificamerican.com/podcast/episode/blue-light-special-2014-nobel-prize-in-physics/

Vocabulary

invention	発明
blue light-emitting diode	青色発光ダイオード
energy-saving	省エネの
contain	含む
combine	結合する
energy efficiency	省エネ
lifetime	寿命
details	詳細
evolution	進化，発展
fuel	燃料
geometry	外形，幾何学
KVA	キロボルトアンペア
incandescent lighting	白熱灯
fluorescent lamp	蛍光灯
introduce	導入する
electricity consumption	消費電力
elimination	削除
civilization	文明
optical	光学の
retirement	引退

mercury	水銀
intermediate	中間の
possibility	可能性
accomplish	達成する
absorb	吸収する
convert	変える
hole	正孔子
transport	輸送する
charge	電荷
recombine	再結合する

2014 Nobel Prize in Physics

Staffan Normark:　This year's prize is about light.

The Royal Swedish Academy of Sciences has decided to award the 2014 Nobel Prize in physics to Professor Isamu Akasaki at Meijo University in Nagoya and Nagoya University, Japan; Professor Hiroshi Amano at Nagoya University, Japan; and Professor Shuji Nakamura at University of California Santa Barbara, for the **invention** of efficient **blue light-emitting diode**s, which has enabled bright and **energy-saving** white light sources.

Professor Per Delsing will now give us a short summary.（この後ちょっと省略）

Per Delsing:　Red and green LEDs have been around for many years, but the blue was really missing. This lamp **contain**s three LEDs: one red, one green, and one blue. If you **combine** these colors you get white light. This is something that Isaac Newton showed already in 1671. Thanks to the blue LED we can now get white light sources which have very high **energy efficiency** and very long **lifetime.** This LED technology is now replacing older technologies. In fact, many of you carry this technology in your pocket. The flashlight and also the screen of modern smartphones uses LED technology.

Professor Olle Inganäs will now continue and give you some of the **details.**

Olle Inganäs:　And we will continue to look at history of lighting, which has been around now for the last few million years of human **evolution**. We started out by burning **fuel**s inside lamps in a **geometry** quite similar to that lamp we see over there. However, that has mainly been used here at **KVA** using **incandescent lighting** and electrical light over the last hundred years or so, since Edison invented these things. The **fluorescent lamp** was **introduce**d somewhere in the early 20th century, and then we saw much, much later the arrival of the lighting element that we are now celebrating in this year's Nobel Prize. And what you see is, of course, an enormous increase of the power efficiency of the use of electrical energy in generating light.

Now something like a fourth of our **electricity consumption** in most industrialized economies goes to **elimination**. So these effects, having much more light for much less electricity, is really going to

have a big impact on our modern **civilization**. We see that impact. You see it in the streets, you see it on the cars, you see it in the lights.

You see it in new **optical** environments like this one from a festival of lights somewhere in Japan. And they're all based on the use of these light-emitting diodes. They come in different colors, not only white, but blue, red, and green, as we saw here, and they have not only the advantage, but much better using the electrical energy. They also give a very much longer lifetime; it may be 100 times longer than that of the standard incandescent lamp that is now being-going in **retirement.** Also it doesn't bring the **mercury** along that **intermediate** generation of fluorescent is contributing as a problem to industrial civilization.

So we will most certainly be able to use this technology. But it took a long while to arrive at this **possibility**. The red LEDs have been around since the early 1960s, the green LEDs some years later. Advances in semiconductor technology, using this band gap-semiconductors with different band gaps lies at the base of this. But the blue thing-the blue light-emitting diode was very, very difficult to **accomplish**. Not that there was a lack of effort. There was continuous efforts in industries to generate blue light-emitting diodes. Because today, with the advantage of having these available, we can generate all those colors, we can combine color-mixing with three different colors in the individual lamp, or we can use as you would find mostly maybe on the market today a blue or UV-emitting LED illuminating a thin layer, **absorb**ing this energy, and **convert**ing it to other colors.

The structure of these lamps are very similar to what you have at the base of your semiconductor electronics that's driving the information technology diode, a combination of semiconductor materials, where you have one layer carrying **hole**s, one layer carrying electrons. They **transport** these **charges** at two different energy levels, but when they meet in this intermediate layer, the active layer, they **recombine**, and when they fall into each other they turn up and turn light on. So this is the physical mechanism that lies at the heart of this device.

2015 Nobel Prize in Physics

Scientific American という科学系の情報サイトのポッドキャスト「60-second Science」では，最新の科学に関する研究成果が 1 分間程度の音声にまとめられています．その中には，毎年，スウェーデン王立科学アカデミーがノーベル賞を受賞した方々とその受賞内容を発表する様子もまとめられています．

こちらに紹介するのは，2015 年にノーベル物理学賞の受賞対象となった，ニュートリノ振動の発明内容についてのポッドキャストです．

https://www.scientificamerican.com/podcast/episode/2015-nobel-prize-in-physics/

“The Royal Swedish Academy of Sciences has decided to award the 2015 Nobel Prize in Physics to Takaaki Kajita and Arthur B. McDonald for the discovery of neutrino oscillations, which shows that neutrinos have mass.”

Göran Hansson, secretary general of the academy, a few minutes before 6 am Eastern time. Kajita is at the University of Tokyo. McDonald is with Queen’s University in Kingston, Canada.

“At this moment in this room there are more than a billion neutrinos, which travel almost at the speed of light.”

Anne L’Huillier is the chair of the Nobel physics committee.

“These elementary particles are the second most abundant in the universe, next to the photons, which are the particles of light. They are created in nuclear reactions, for example, in the sun, in stars. They interact very little with the environment, for example, they can go through Earth without being stopped.

There are three kinds of neutrinos. Electron-neutrinos, mu-neutrinos and tau-neutrinos. This year’s prize is awarded to the experimental discovery that neutrinos can change identity. For example, a mu-neutrino can become a tau-neutrino and vice versa. They oscillate.

The observations were made by two research groups, one at the Super-Kamiokande detector in Japan and the other at Sudbury Neutrino Observatory in Canada. The discovery implies that neutrinos, which were believed to be massless, do have a mass, even if very little. And since there are so many of them, it changes our view of the universe.

For an in-depth listen about the 2015 Nobel Prize in Physics, look for the Scientific American Science Talk podcast later this morning.

—Steve Mirsky [The above text is a transcript of this podcast.]

Physicists Model Mosh Moves

　ヘビーメタルのコンサートでの人の動きをモデル化して，アメリカ物理学会で発表した研究者がいました.

https://www.scientificamerican.com/podcast/episode/physicists-model-mosh-moves-13-03-27/

A heavy metal concert might be a tough place to think about physics, especially in the mosh pit, where some audience members dance violently. But the mosh pit itself is actually an interesting place to find physics in action. And not just force equals mass times acceleration.

Metal-loving Cornell researchers analyzed videos of mosh pits and mapped the motion of participants. They found that the collisions of moshers was similar to the motion of molecules in an ideal gas. Mosh dancers can also form what is called a circle pit, where they run collectively in a ring, creating a vortex pattern.

The scientists not only modeled mosh and circle pits, they also found how one type of motion transitions into the other. The presented their ongoing work at the American Physical Society's March Meeting. [Matthew Bierbaum et al., Mosh pits and Circle pits: Collective motion at heavy metal concerts]

But why bother to look at mosh pits in the first place? The physicists think their research may also apply to other extreme situations, which could help us understand collective human movement in panics and riots. So I say, rock on.

—Sophie Bushwick

[*The above text is a transcript of this podcast.*]

Are you alone in the Universe?

Scientific American というサイトでは，科学に関する様々な情報が面白いビデオにまとめられています．ここで紹介するのは，我々人類は宇宙の中で本当に唯一無二の存在なのかについてのビデオです．映像を観て想像力を働かせながら内容が把握できるとよいですね.

https://www.scientificamerican.com/video/are-we-alone-in-the-universe-inst 2012-11-15/

Vocabulary

astronomer	天文学者
eavesdrop	立ち聞きする，こっそり聞く
cosmos	宇宙
alien	異邦人
civilization	文明
beg	乞う
cosmic	宇宙の
desert	砂漠
inhabit	住む
galaxy	銀河
bunch	一団，束，群れ
fraction	分数，小部分，破片
planet	惑星
potentially	潜在的に
planetary system	惑星系
takes hold	定着する
intelligence	知能
species	種
broadcast	放送する
interstellar space	星間空間

survive	生き残る
detectable	検出可能な
microbe	微生物
slime molds	粘菌，変形菌
equation	方程式
last	続く
dying out	滅びること
self-destructing	自滅すること
billions	10億 （10^9）
Humankind	人類
close shave	危機一髪

Are you alone in the Universe?

Listen.
Do you hear anything? Me neither.
It's pretty deserted out here.
For the past 50 years, astronomers have been using radio dishes to eavesdrop on the cosmos.
They are listening for signals from alien civilizations.
But so far, it's been pretty silent.
That begs the question: Are we alone in a cosmic desert?

In 1961, astronomer Frank Drake, came up with a way to approach the question mathematically.
He created an equation that estimates how many alien cultures inhabit our galaxy.
The equation depends on a bunch of factors.
First, the number of new stars born each year
times the fraction of stars with planets
times the number of planets that could potentially support life in each planetary system
times the fraction of life-supporting planets where life actually takes hold
times the percentage of planets with life forms that develop intelligence
times the fraction of intelligent species that develop the ability to broadcast signals across interstellar space
times how long those civilizations are likely to survive, or at least how long they'll broadcast their signals into space.
Multiply all those together and you get "N"; the number of detectable civilizations in the galaxy.
It's a long equation and astronomers only have estimates for some of the factors;
the ones we can observe from Earth,
like how many stars are born each year.
On the other hand, we don't know much about how life develops on other worlds.
Many experts think that alien microbes and slime molds may be common.
But little green men? Not so much.
Perhaps the biggest question is the value of "L" in the Drake equation.
How long will a given civilization last before dying out or self-destructing?
"L" could be hundreds of years or it could be billions.

Humankind has only used technology like radio broadcasts for a century or so
and in that short time, we've already had a few close shaves.
So the lifetime of a given civilization could be rather short.
If that's the case, we may be alone in the cosmic desert after all.

For Scientific American's Instant Egghead, I'm John Matson.

Einstein and the Special Theory of Relativity

アインシュタインの特殊相対性理論のビデオです.

https://youtu.be/ajhFNcUTJI0

Vocabulary

exaggerate	大げさに言う
velocity	速度
switcheroo	突然の変化
simultaneous	同時の
perspective	視点，観点

Einstein and the Special Theory of Relativity

Around nineteen-hundred, all of physics, and particularly Einstein, was in trouble: they couldn't figure out how anything could move…

Now before you complain that I'm exaggerating, check out this cat !

You can clearly see that the cat is moving away from Einstein at a constant velocity… but do a little sliding switcheroo, and suddenly it looks like Einstein is the one moving. This is the "old-fashioned principle of relativity," but the point is that the switcheroo changes relative things, like position and velocity, and not absolute ones, like the separation of Einstein from his cat.

Now for the problem: before Einstein was even born, physicists showed that the speed of light was one of those absolute things which can't be changed by a switcheroo, so any switcheroo we do has to keep light moving at the same speed. But then it's obvious that we can't do our sliding switcheroo at all, which means we can't explain how anything other than light can move !

Ok, I spoke too soon… there is one solution - do you see it? We were assuming that our switcheroo had to keep every slice of time at the same, well, time. But there's no law of physics that says time is an absolute thing that can't be changed by switcheroos… so if we just rotate the slices of time while sliding them, then we can keep the speed of light the same, and explain how things can move, too.

Of course, Einstein didn't figure out this "special principle of relativity" in 1905 - it was already done by a guy named Lorentz ten years earlier. But Lorentz just thought this time-rotation was a mathematical trick…

and it took Einstein to step in, and, you guessed it, propose that "time-rotation" is real, that time really is relative, and that consequently, simultaneous events relative to one observer aren't simultaneous relative to another. Now that's a real switcheroo of perspective.

Units, Dimensions, and Scaling Arguments

ここに紹介するのは，MIT（マサチューセッツ工科大学）の **Open Course Ware** というサイトに載っている **Walter Lewin** 先生という熱血物理教師の授業を写したビデオで，単位や次元など物理学の基本的な事項を説明しています.

https://www.bing.com/videos/search?q=Units%2c+Dimensions%2c+and+Scaling+Arguments&&view=detail&mid=828D085903BE9312C5A5828D085903BE9312C5A5&&FORM=VDRVRV

Vocabulary

explore	探検する，探査する，調査する
fraction	破片
proton	陽子
span	わたる，拡がる
magnitude	大きさ
quantitatively	定量的に ↔ **qualitatively** 定性的に
define	定義する
definition	定義
evolve	発展する
derive	導く，ひきだす
be tailored	手直しされる
astronomers	天文学者
astronomical	天文学的な
mean distance	平均距離
metric	メートル法
uncivilized	未開の，文明から離れた
insult	侮辱する
drive you nuts	気ちがいにする
exclusively	もっぱら

decimal	10進法の
exception	例外
be conceived	考案された
Here we go	さあやってみよう
capital	大文字の
dimensions	次元
[L] divided by[T]	[L]/[T]
length to the power three	$[L]^3$
acceleration	加速度
time squared	$[T]^2$

Units, Dimensions, and Scaling Arguments

I'm Walter Lewin. I will be your lecturer this term.
In physics, we explore the very small to the very large.
The very small is a small fraction of proton and the very large is the universe itself.
They span 45 orders of magnitude, a 1 with 45 zeroes.
To express measurement quantitatively, we have to introduce units.
And we introduce for the unit of length, the meter; for the unit of time, the second; and for the unit of mass, the kilogram.
Now, you can read in your book how these are defined and how the definition evolved historically.
Now, there are many derived units which we use in our daily life for convenience and some are tailored toward specific fields. We have centimeters, we have millimeters, kilometers, we have inches, feet, miles. Astronomers even use the astronomical unit which is the mean distance between the earth and the sun and they use light-years which is the distance that light travels in one year. We have milliseconds, we have microseconds, we have days, weeks, hours, centuries, months…all derived unit.
For the mass, we have milligrams, we have pounds, we have metric tons. So lots of derived units exist.
Not all of them are very easy to work with. I find it extremely difficult to work with inches and feet. It's an extremely uncivilized system. I don't mean to insult you, but think about it,12 inches in a foot, three feet in a yard. Could drive you nuts.
I work almost exclusively decimal, and I hope you will do the same during this course but we may make some exceptions.

I will now first show you a movie, which is called "The Powers of Ten" It covers 40 orders of magnitude. It was originally conceived by a Dutch man named Kees Boeke in the early '50s. This is the second-generation movie, and you will hear the voice of Professor Morrison, who is a professor at MIT. "The Power of Ten", 40 orders of magnitude. Here we go.

（映画はカットされている）

I already introduced, as you see there, length, time, and mass, the three fundamental quantities

in physics. I will give this the symbol capital L for length, capital T for time, and capital M for mass.

All other quantities in physics can be derived from these fundamental quantities.

I ‘ll give you an example. I put a bracket around here. I say speed, and that means the dimensions of speed. The dimension of speed is the dimension of length divided by the dimension of time. So I can write for that: [L] divided by [T]. Whether it’s meters per second or inches per year that’s not what matters.

Volume would have the dimension of length to the power three.

Density would have the dimension of mass per unit volume. So that means length to the power three.

All-important on in our course is acceleration. We will deal a lot with acceleration.

Acceleration, as you will see, is length per time squared. The unit is meters per second squared. So you get length divided by time squared.

So all other quantities can be derived from these three fundamental. So now that we have agree on the units. We have the meter, the second and the kilogram.

Chapter 4

Speaking

4－1　英語で口頭発表（Oral presentation）をしてみよう

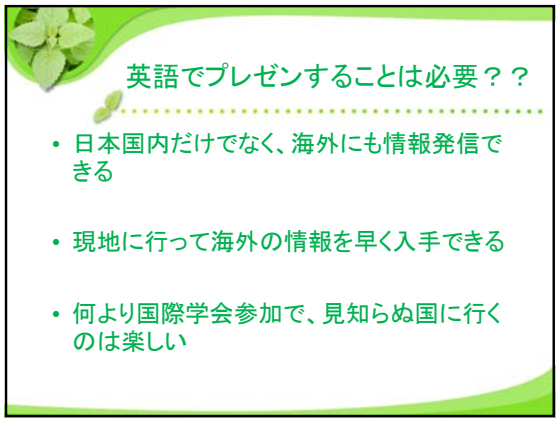

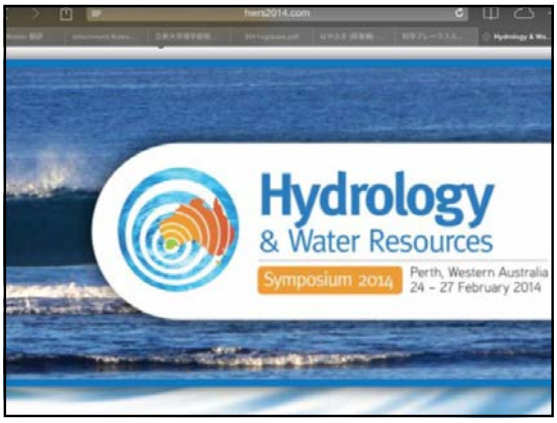

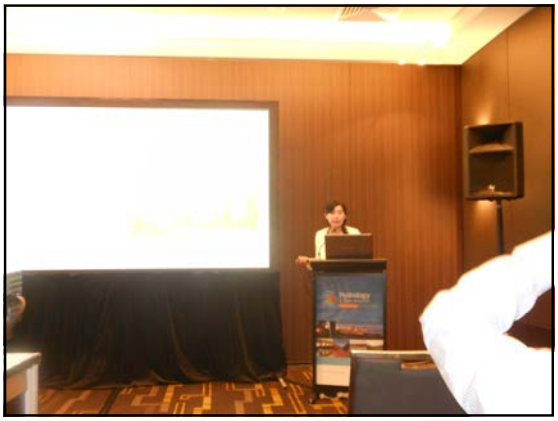

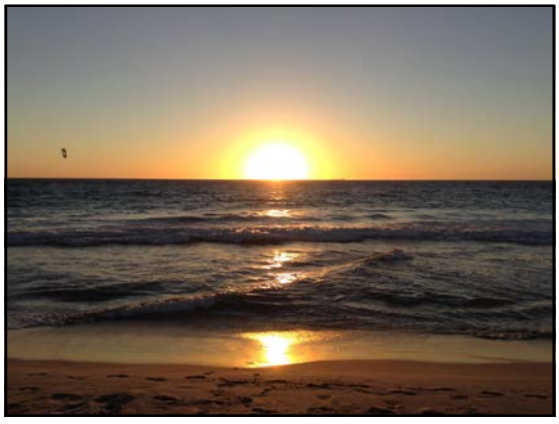

Thank you, Mr. chairman(Madam chairperson).

Good morning, ladies and gentleman.

I'm very glad to have the opportunity to give a presentation here today.

I'm Naoko Nakagawa from Tokyo Metropolitan University in(of) Japan.

ここでは最初に紹介した論文の内容を口頭発表した時に用いたプレゼンテーションファイルとスピーチを紹介します.

まず, あいさつをして, 自分の名前と所属を名乗ります.

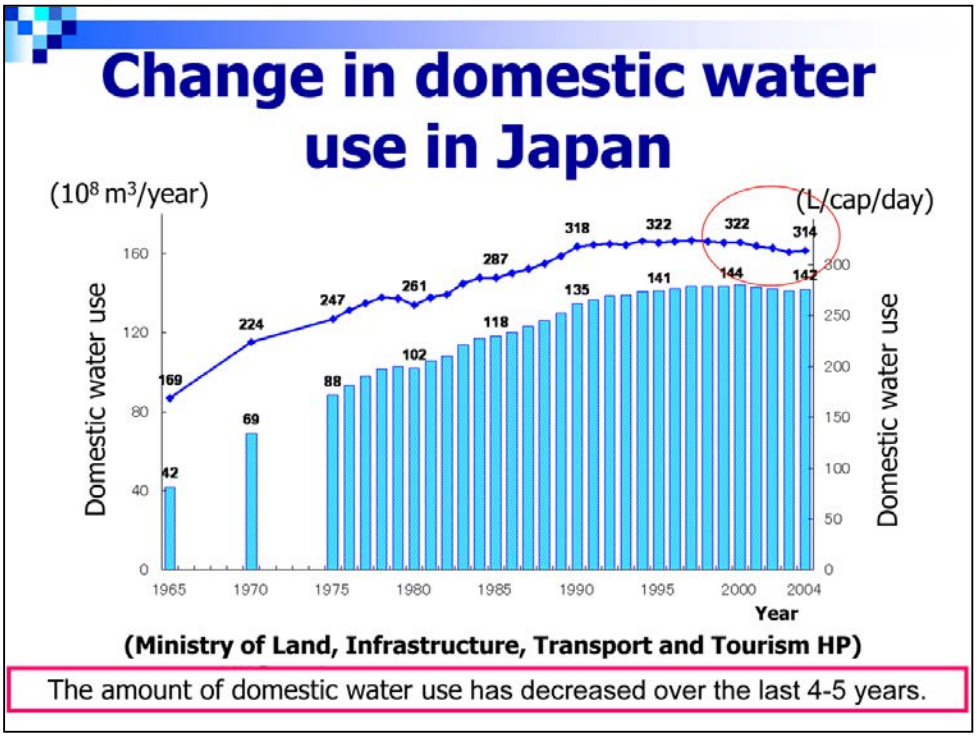

To begin with, I'd like to talk about the background of this study.

This figure shows the change in domestic water use in Japan.

The amount of water supply in Japan increased with economic growth until reaching a plateau in the 1990s, and has since decreased over the last 4-5 years.

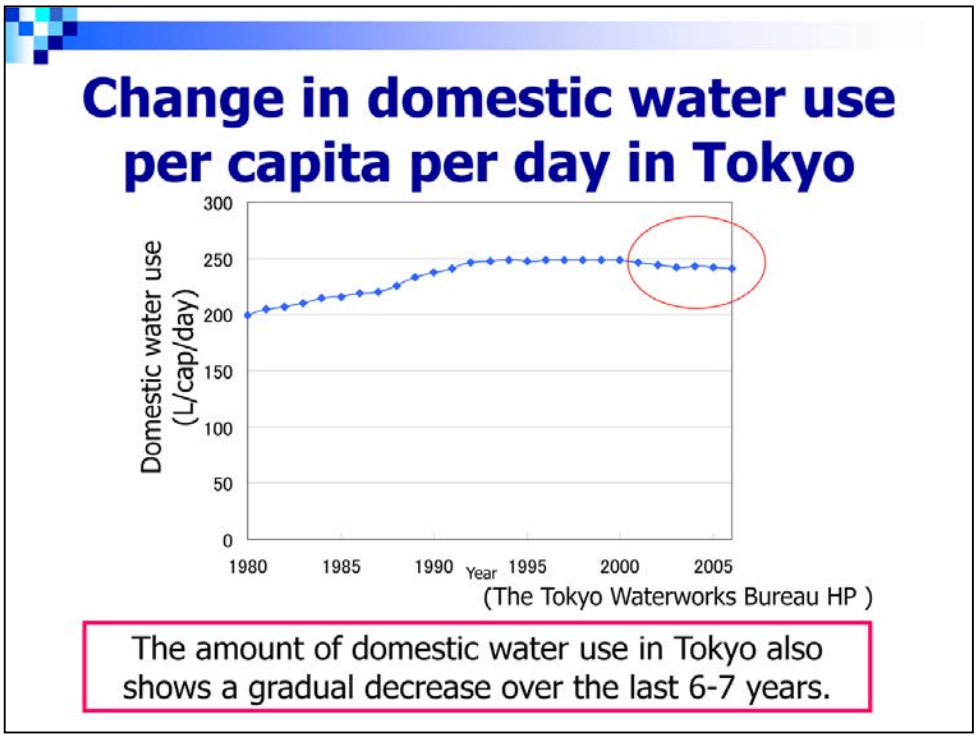

This figure shows the change in domestic water use per capita per day in Tokyo.

The amount of domestic water use in Tokyo also shows a gradual decrease over the last 6-7 years.

Therefore, I considered the reason of such tendency of decreasing in recent years in Japan.

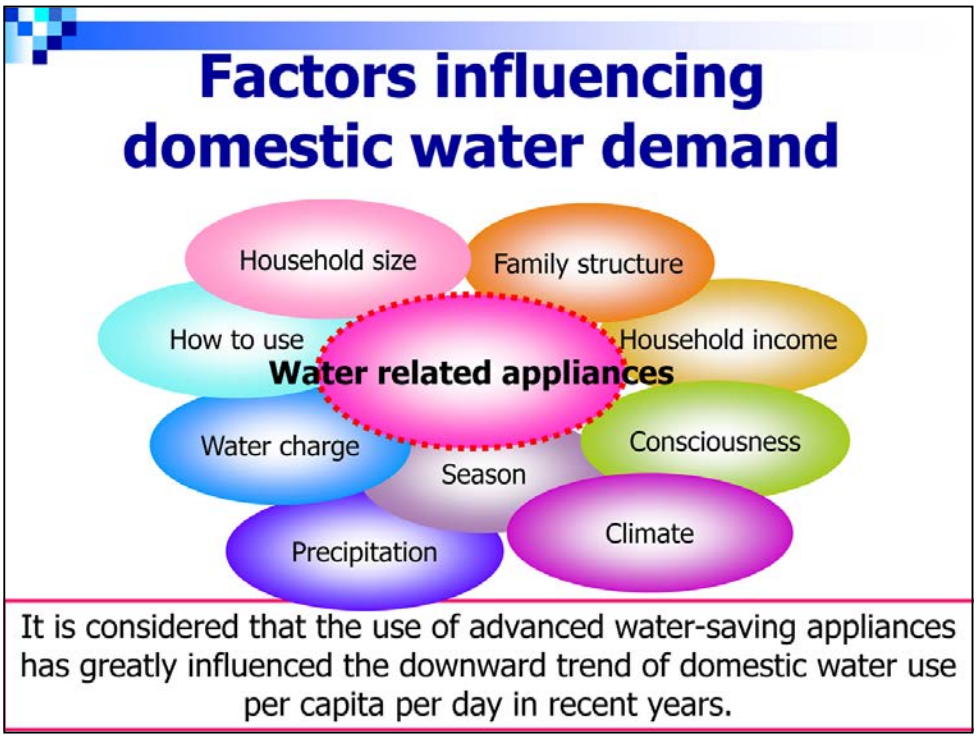

The domestic water use per capita is known to be influenced by various factors, such as water charge, household size, family structure, how to use it, water rate, etc.

But among these factors, it is considered that the use of advanced water-saving appliances has greatly influenced the downward trend of domestic water use per capita per day in recent years because the use reduction achieved by these appliance is significant.

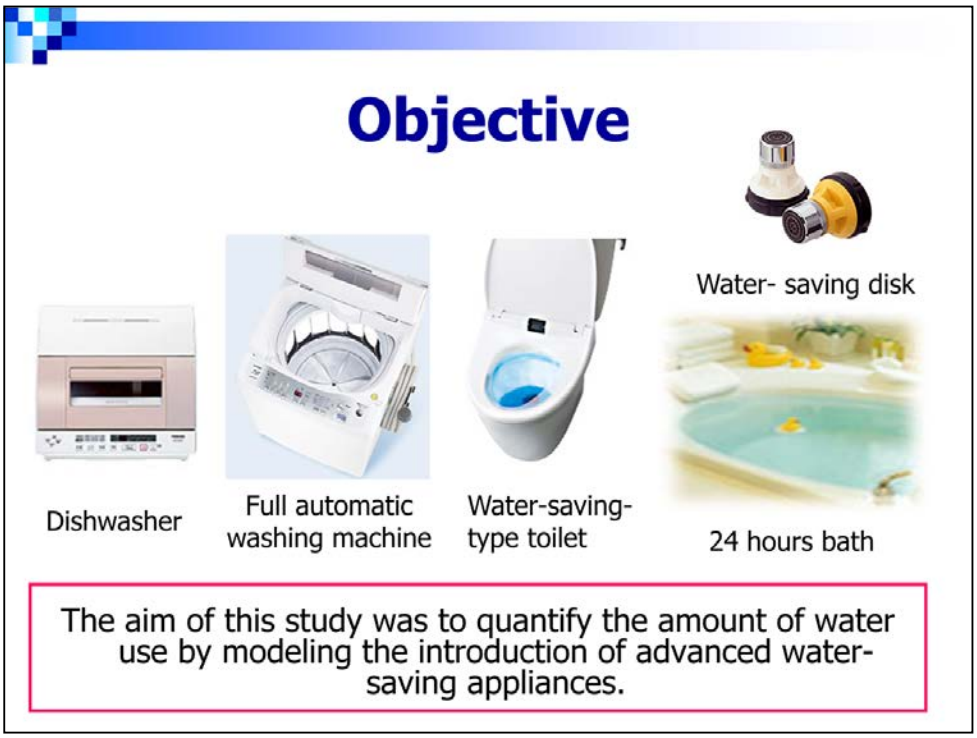

Therefore, the aim of this study was to quantify the amount of water use by modeling the introduction of advanced water-saving appliances.

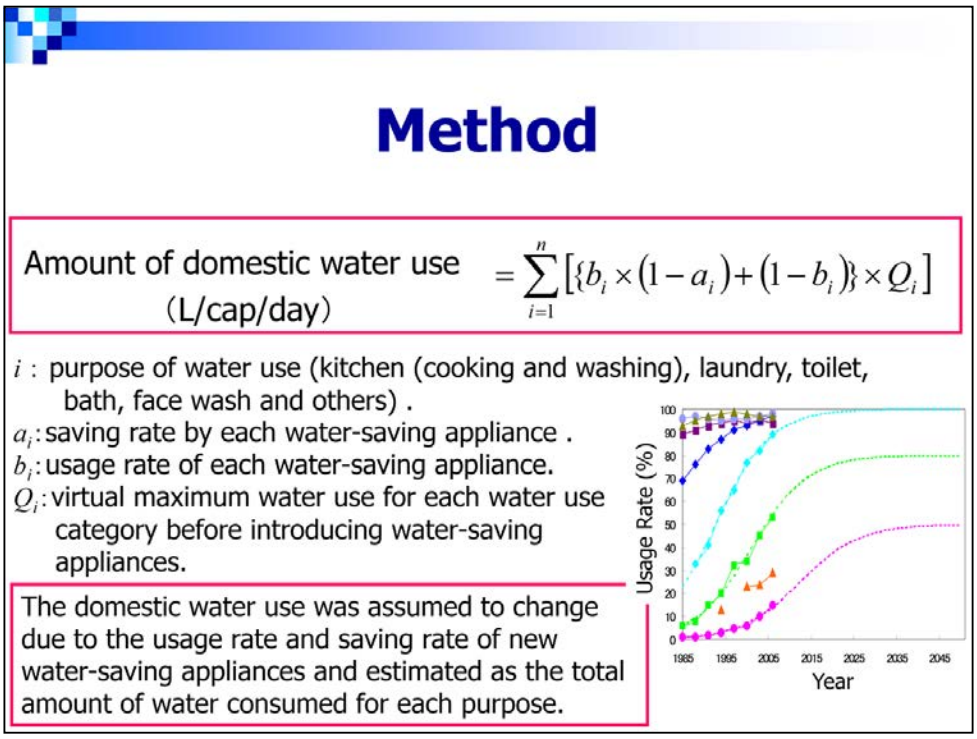

I considered such model for the domestic water use per capita per day.

According to this model, the domestic water use was assumed to change due to usage rate and saving rate of new water-saving appliances and estimated as the total amount of water consumed for each purpose.

where,

i is the purpose of water use in household,

ai is the saving rate by each water saving appliance,

bi is the usage rate of each water saving appliance,

Qi is the virtual maximum water use for each water use category before introducing water-saving appliances.

Hereafter ,I'd like to explain the usage rate and saving rate for each saving water appliance.

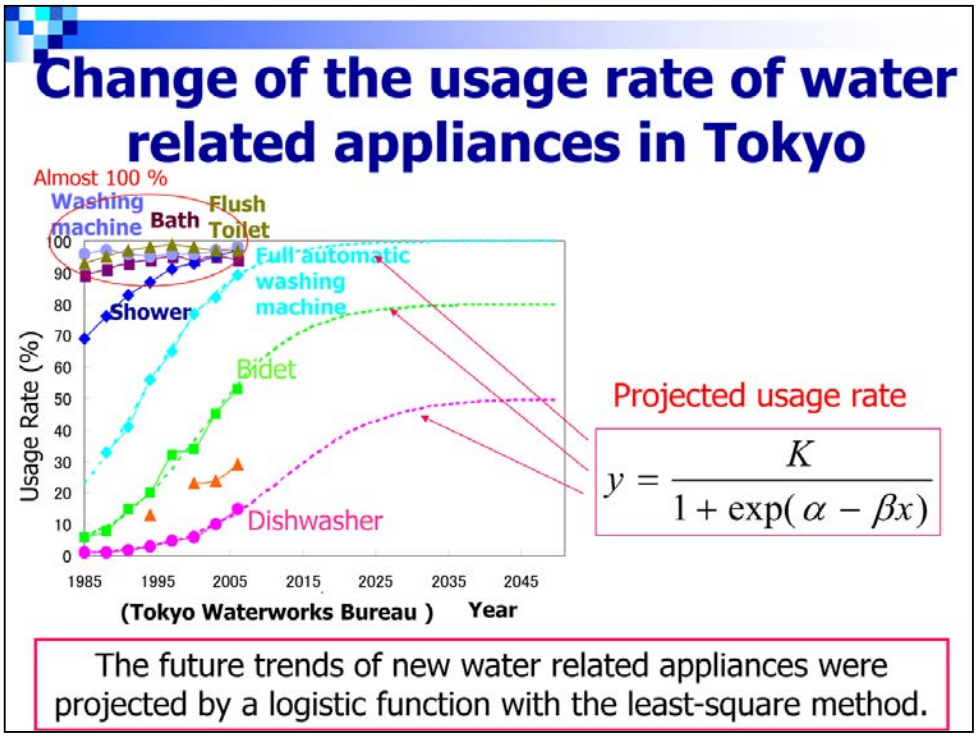

This figure shows the usage rates of conventional and new water related appliances obtained by the field survey of domestic water use conducted by the Tokyo Waterworks Bureau until 2006.

As shown in the figure, the usage rates of the conventional appliances, such as bathtubs, showers, washing machines and flushing toilets were nearly 100%.

New water related appliances whose usage rates have been increasing are full automatic washing machines, bidet (for washing with a fountain of warm water), dishwashers and so on.

The future trends of these appliances were projected by a logistic function with the least-square method.

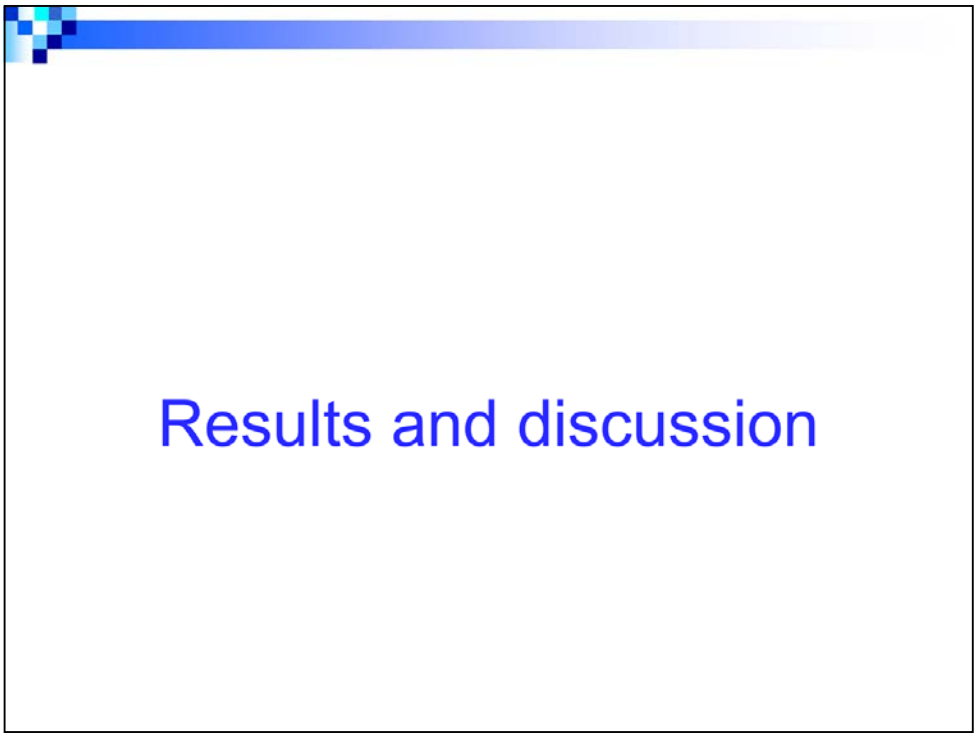

I’d like to talk about the results.

実際に用いたPPTファイルはもっと分量が多いのですが，ここでは省略して結果と考察にうつります．

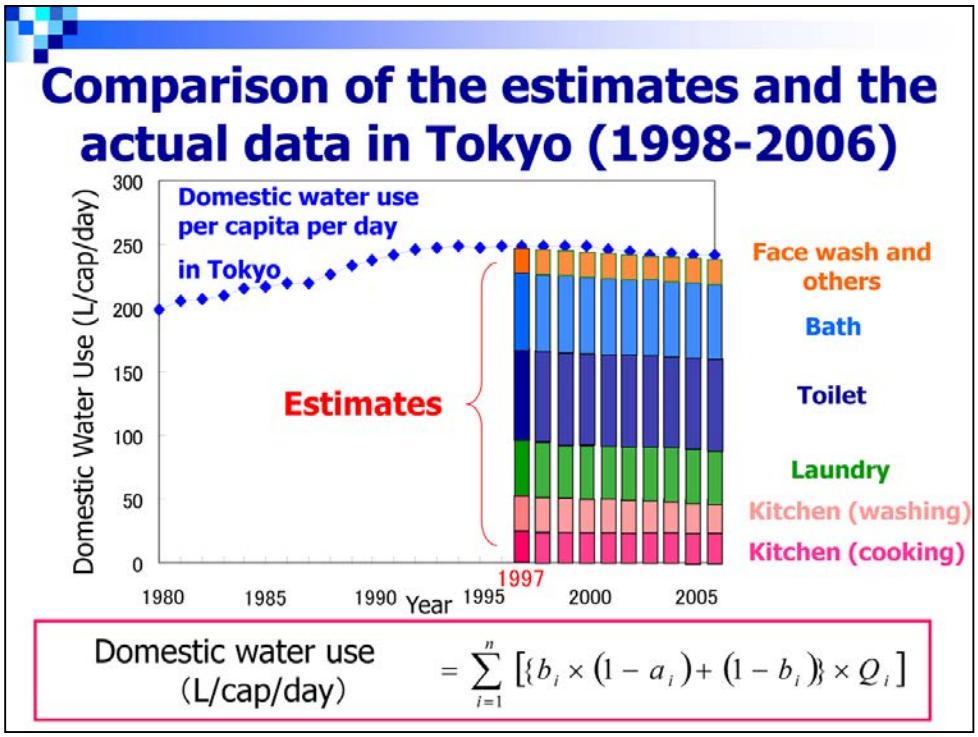

Here is the result.

This figure shows the change of domestic water use per capita per day in Tokyo.

Based on the model, the amount of domestic water use for each purpose was set to the actual amount of that in 1997 because this year was set as the base year.

Then, the amount of domestic water use was estimated based on this model until 2006.

And the estimated domestic water use from 1998 to 2006, during 9 years data, were compared with the actual data of Tokyo.

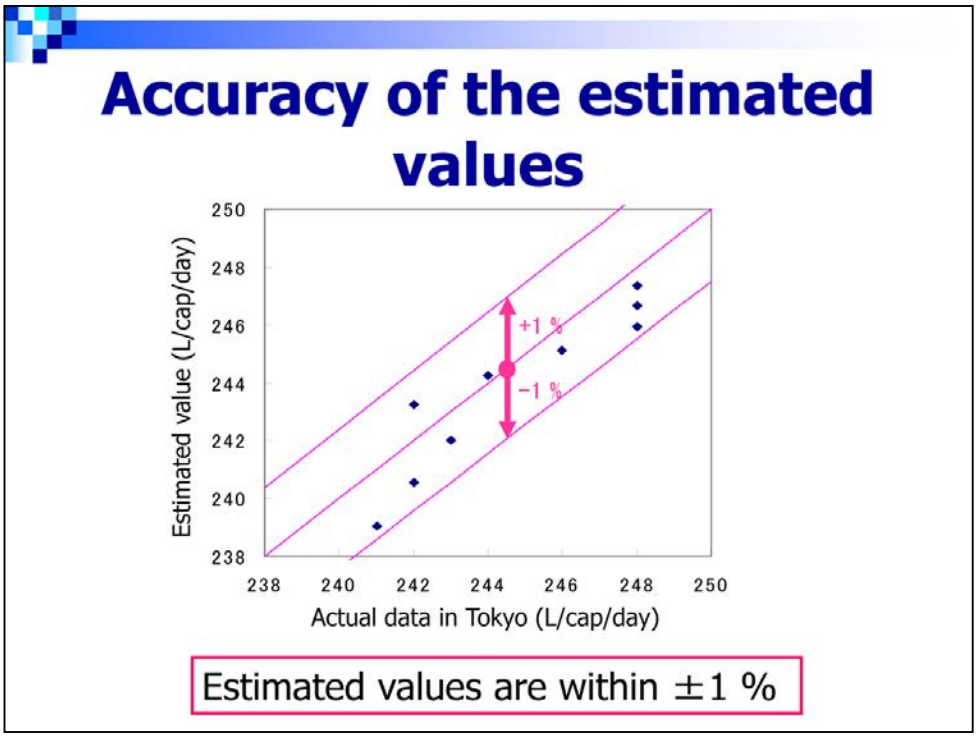

In this figure, the horizontal axis shows the actual data in Tokyo and **the vertical axis shows** the estimated values.

As shown in this figure, the estimated values are within plus or minus 1 % and it is found that the estimated amount of domestic water use per capita was corresponded to the actual amount of that very well in this decade.

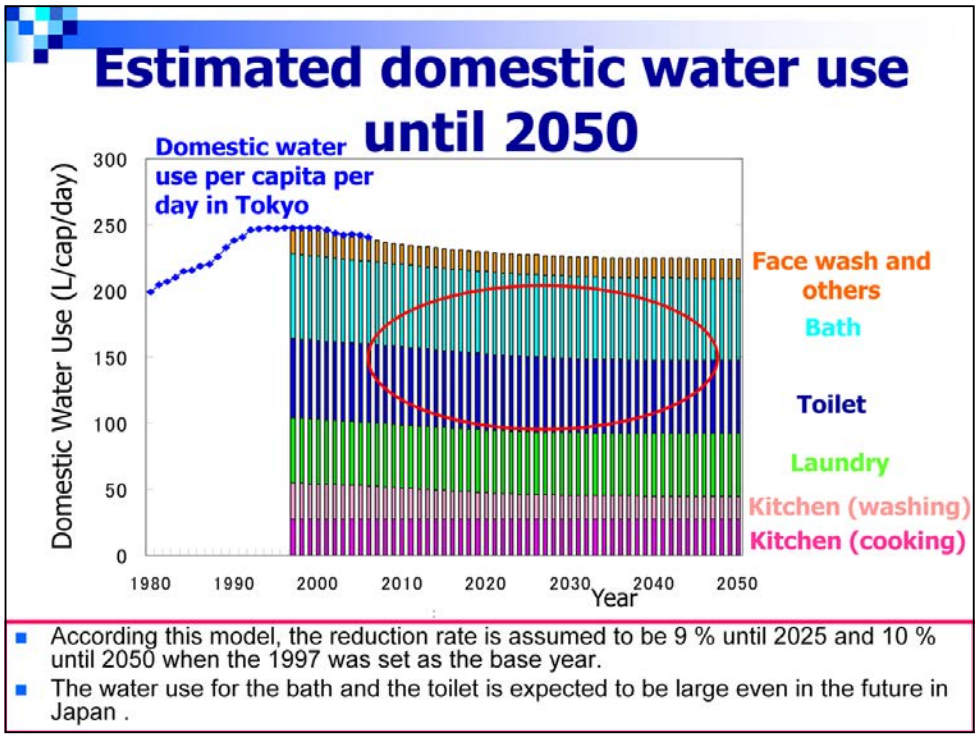

So, the domestic water use per capita per day was estimated until 2050 according to this model.

According to this model, the reduction rate is assumed to be 8 % until 2025 and 10 % until 2050 when the 1997 was set as the base year.

and it was considered that the water use for bath and toilet is expected to be large even in the future in Japan according to the present trend of the usage rate.

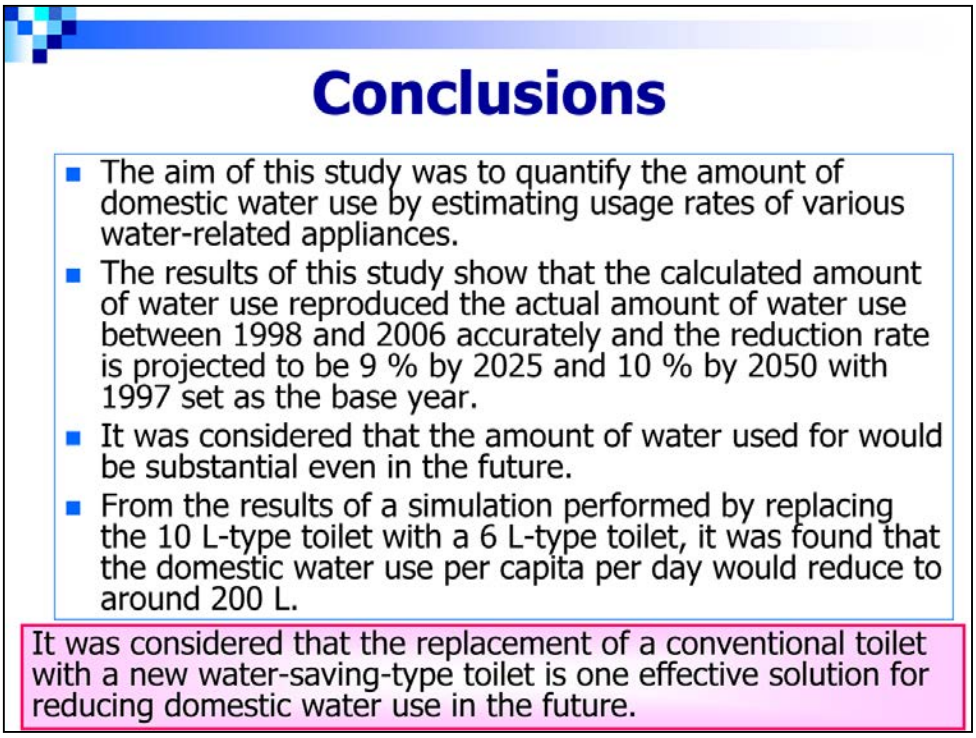

In conclusion,

The aim of this study was to quantify the amount of domestic water use by estimating usage rates of various water-related appliances.

The results of this study show that the calculated amount of water use reproduced the actual amount of water use between 1998 and 2006 accurately and the reduction rate is projected to be 9 % by 2025 and 10 % by 2050 with 1997 set as the base year.

It was considered that the amount of water used for would be substantial even in the future.

From the results of a simulation performed by replacing the 10 L-type toilet with a 6 L-type toilet, it was found that the domestic water use per capita per day would reduce to around 200 L.

It was considered that the replacement of a conventional toilet with a new water-saving-type toilet is one effective solution for reducing domestic water use in the future.

Thank you for your attention.

レポート課題

このpptファイルはテンプレート（ひな型）として作成したものです。このテンプレートを使う場合は日本語で書いてある部分はすべて消して下さい。
このテンプレートを使わずに独自のスライドでpptファイルを作成しても構いません。

最初に学生番号と氏名を英語で明記してください。

Background→ Objective → Materials and Method→ Results and Discussion → Conclusions に沿って、プレゼンのスピーチ（プレゼンのはじめのあいさつから終わりのあいさつまで）を各スライドのこの部分に英語で書いてください。
「An experiment」の文章をそのまま用いても構いません。あいさつやResultで書く表現は今までに配布した資料を参考にして書いてください。

論理的に展開することが重要です。

聴き手にわかりやすいように、また自分が発表しやすいように各スライドにイラストや英語の文章を加えてください(アップロードしていただいたpptファイルを最終日の発表時にそのまま使います)。
すでに記入してある説明文を変えたり、枚数を増やしても構いません。

ご自分の独自の内容で作成される方は，英文の下に和訳も書いてください（時々，英文を読んだだけでは何を伝えたいのかわからないことがあるため）．

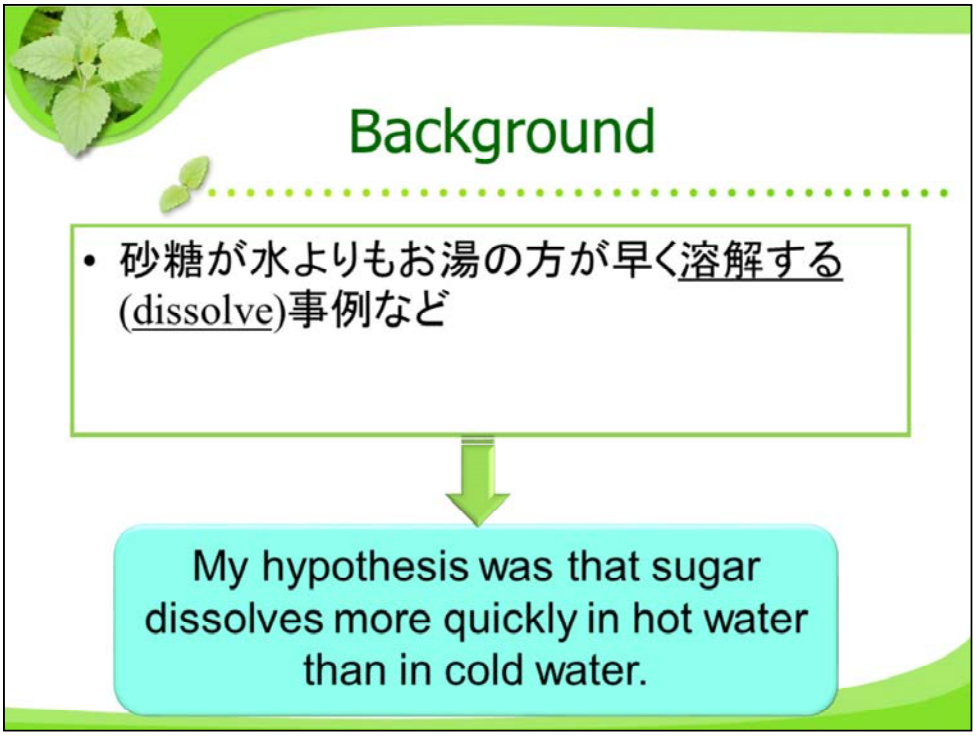

研究の背景を説明するため，例えば砂糖が水よりもお湯の方が早く溶解する(dissolve)事例（「アイスコーヒーよりホットコーヒーの方が砂糖が早く溶けた」など何でもいいです）を手短に書いてください。

研究の目的を書いてください。

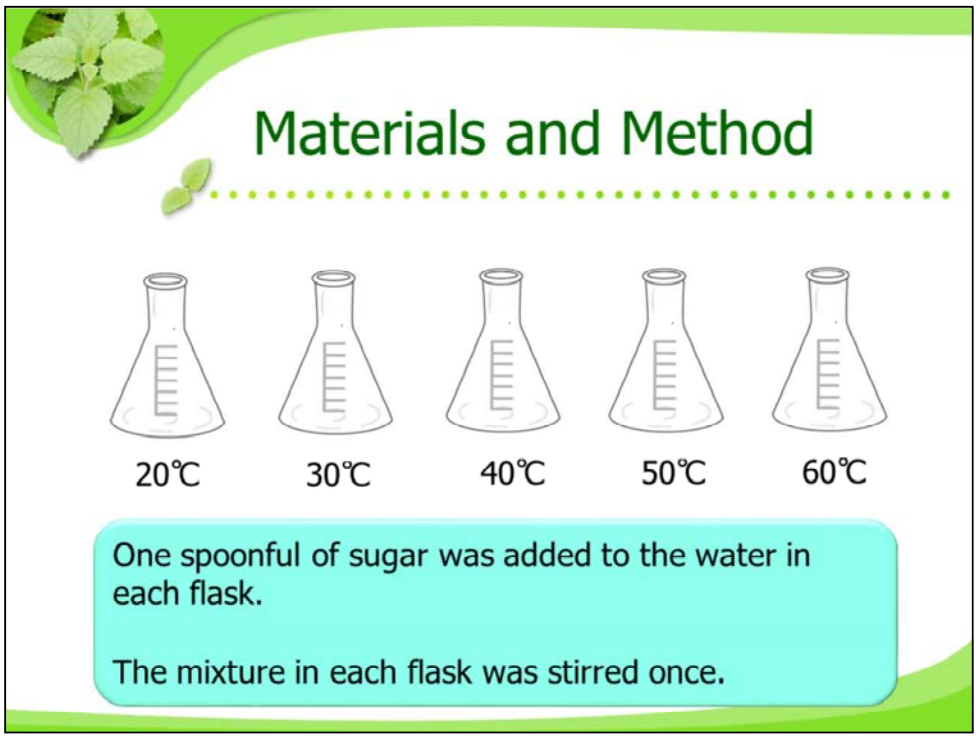

研究に用いた器具や装置,そして研究を遂行するための方法を書いてください。

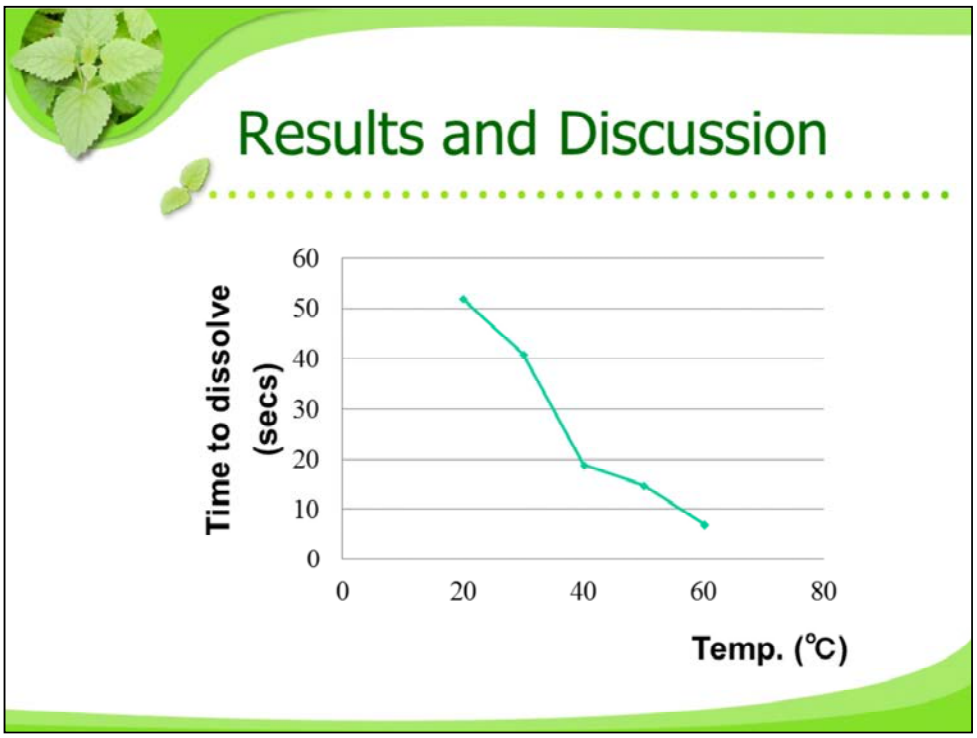

結果を書いてください。

（グラフの説明をしてください。「X軸は水の温度、Y軸は溶ける時間を表す」という説明や、例えば「溶ける時間は20℃から40℃までは急激に下がっているが40℃から60℃までは徐々に下がっている」など何でも結構ですので，グラフから読み取れたことを英語で説明してください。）

あくまでも、「結論」のスライドと同じ記述ではいけません。

結論（この研究のまとめ）を書いてください。
終わりのあいさつも書いてください。

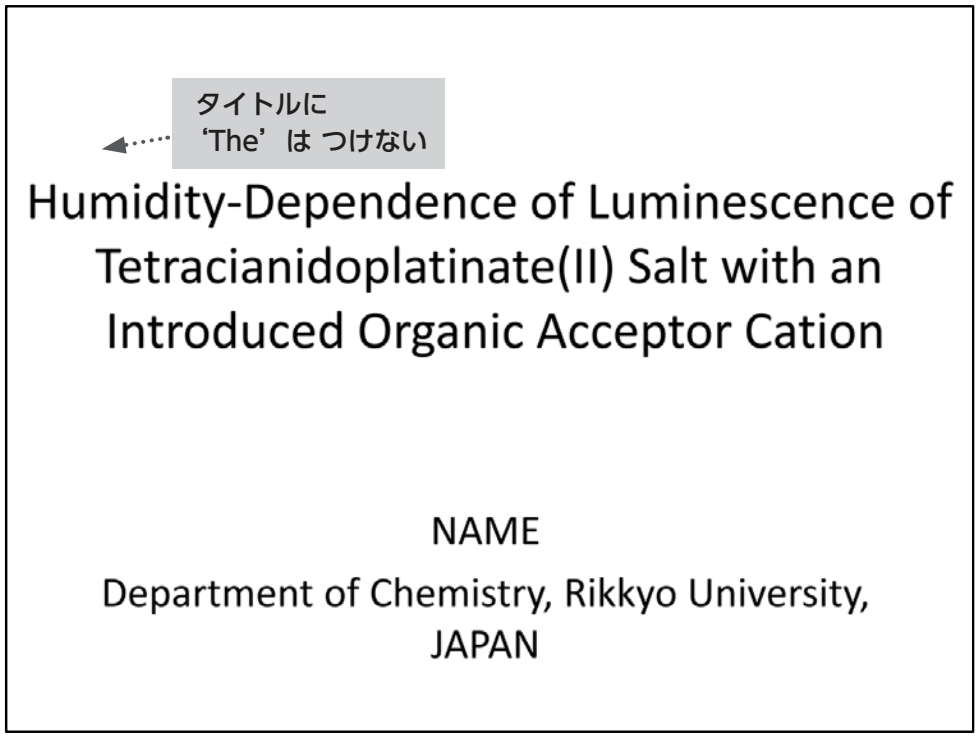

タイトルに
‘The’ は つけない

Thank you, Mr. chairman (Madam. Chairperson).
Good morning(afternoon), ladies and gentlemen.
I’m very glad to have the opportunity to give a presentation here today.
I’m　　from Rikkyo university in(of) Japan.
座長の方ありがとうございます。
おはようございます皆さん。
今日はこのような発表の機会を頂けて光栄です。
日本の立教大学に所属しています　　です。

＊ 太字は良く使用
される語句です
参考にして下さい

The title of my presentation is the Humidity-dependence of luminescence of tetracyanidoplatinate(II) salt with an introduced organic acceptor cation.
発表タイトルは有機カチオンを導入したテトラシアニド白金酸塩の発光色の湿度依存性です。

簡単でよいので英文の下に和訳を入れて下さい。(時々,英文は間違っていなくても，その内容が違っている場合がある為)

catíon[kaetáíon] 陽イオン
aníon [aenáíom] 陰イオン

general background →現在形で書かれている

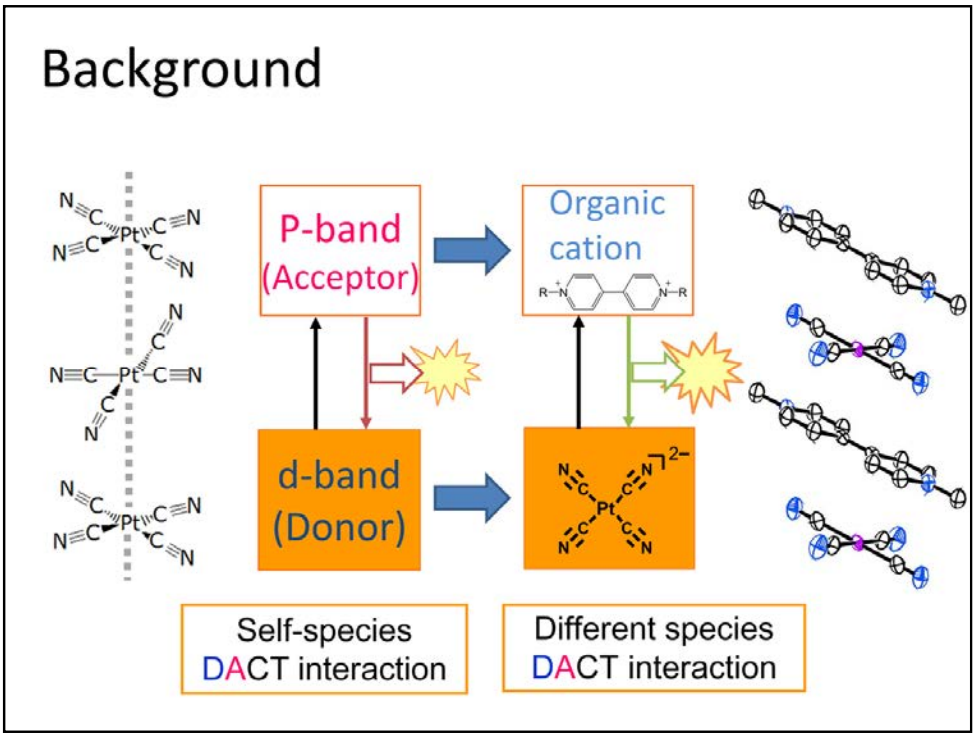

＊冠詞をチェックしてみましょう

First, I'd like to talk about the background of this study.
The tetracyanido platinate salt, for example alkali metal salt, is known as an emissive substance. This emission arises from the interaction between the d-band and the p-band of platinum. It means the d-band is the electron donor and the p-band is the acceptor. So, if the acceptor is changed to other chemicals, for example organic cations, the salt will exhibit emission by the Donor-Acceptor Charge Transfer interaction.

まず、研究の背景について説明します。
アルカリ金属塩のようなテトラシアニド白金酸塩は、発光性の物質として知られています。この塩は白金原子のd-バンドとp-バンドの間の相互作用によって発光します。つまり、d-バンドが電子ドナー、p-バンドがアクセプターとしてはたらいています。
よって、アクセプターの方を異なる化学種に置き換えても、例えば有機カチオンに置き換えてもドナーアクセプター電荷移動相互作用によって発光すると考えられます。

Specific background →過去形，現在完了形
物質の性質など普遍的なことは現在形

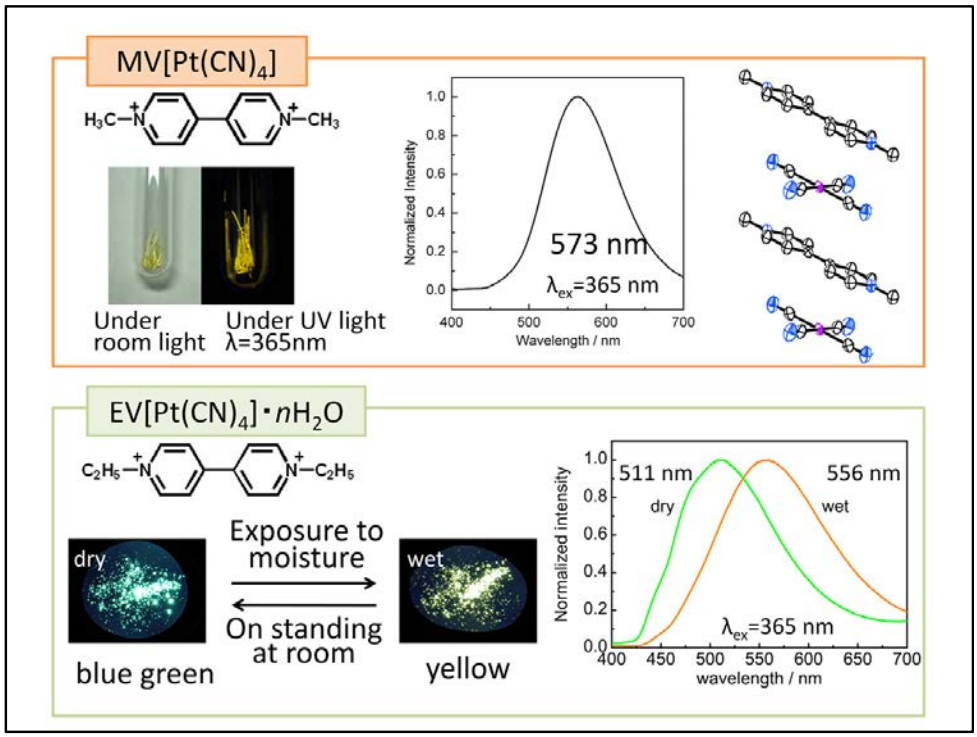

性質を述べているので現在形

つなぎの言葉

Firstly, in the previous work, dimethylviologen **was introduced** to the platinum salt. Dimethylviologen salt exhibits emission, and adopts a columnar structure like this. The donor anions and the acceptor cations stack alternately.
This fact **indicates** the emission of dimethylviologen salt arises from the Donor-Acceptor Charge Transfer interaction.
Secondly, the acceptor cation was extended to diethylviologen. Diethylviologen salt also **exhibits** emission. **In addition,** this salt **shows** vapochromic behavior. In low humidity, this salt has blue-green emission. This is called the dry phase. But, after exposure to moisture, the emission color **changes to** yellow. This is called the wet phase. If the exposure is stopped, this yellow emission **returns to** blue-green.
Therefore we considered this phenomenon **relates to** the adsorption and desorption of H_2O molecules.

先行研究では、まず白金錯体にジメチルビオロゲンが導入されました。ジエチルビオロゲン塩は発光を示し、ドナーとアクセプターの交互積層カラム構造をとっています。このことから、ジエチルビオロゲン塩はドナーアクセプター電荷移動相互作用によって発光していることが示唆されます。
次に、アクセプターカチオンをエチルビオロゲンに拡張しました。ジエチルビオロゲン塩もまた、発光を示します。さらに、この塩はベイポクロミズムを示します。
低湿度下においては、この塩は青緑発光を示します。これをdry相とします。しかし、水蒸気に暴露すると黄色発光に変化します。これをwet相とします。水蒸気暴露をやめると、黄色発光から青緑発光に戻ります。
この現象は水分子の出入りと関係していると考えます。

Objective

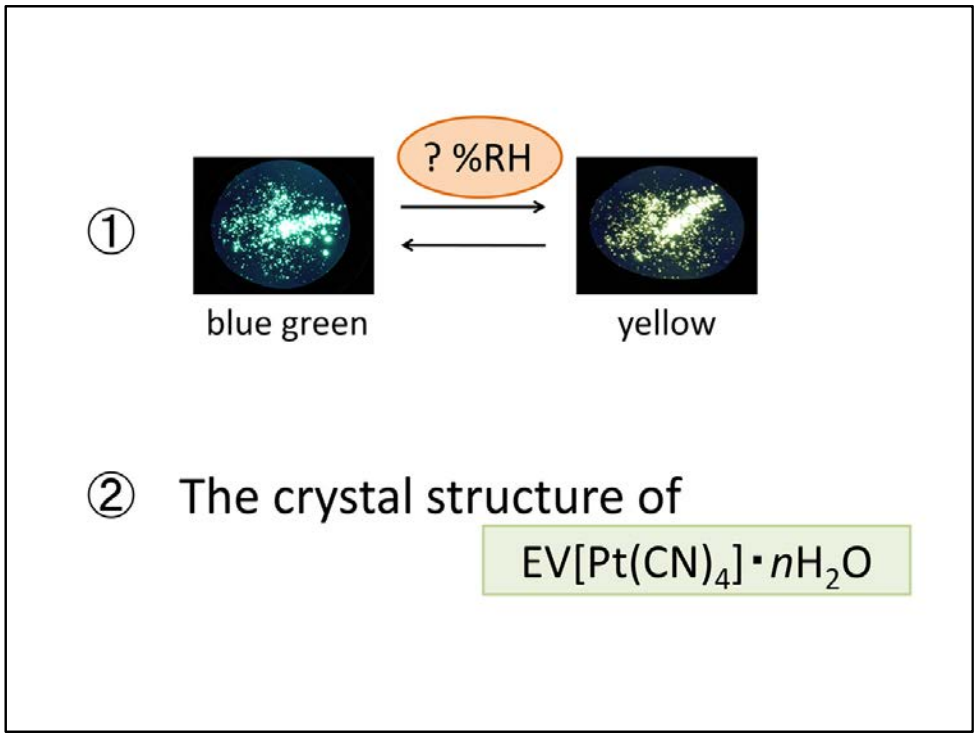

Where is the turning point of the dry phase and the wet phase?
A quantitative investigation **was required**. So a gravimetric analysis **was undertaken**. **Moreover,** the structure of the diethylviologen salt has never been revealed because the single crystal of this salt has never been obtained. **Therefore** the determination of the crystal structure of this salt is also required.

では、dry相とwet相の変化の境目となる湿度は何%でしょう？定量的な調査が必要です。そこで、重量分析を行いました。
さらに、ジエチルビオロゲン塩はこれまで単結晶が得られていなかったため、構造が明らかになっていませんでした。そこで構造を明らかにすることもまた目的の一つです。

Materials and Method

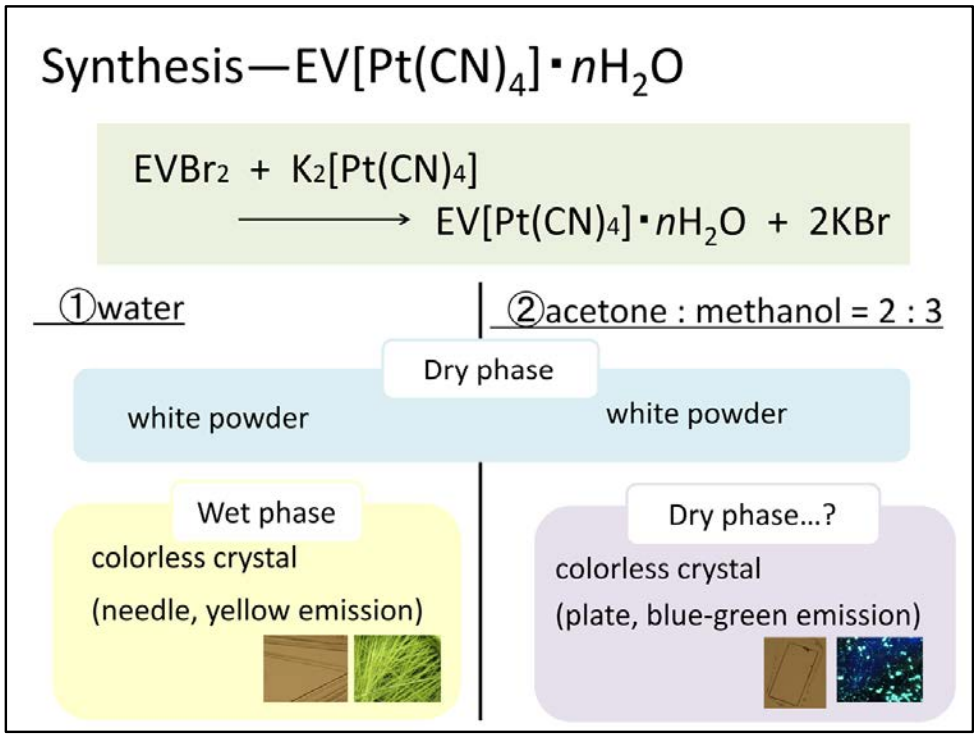

The synthesis of the diethylviologen salt is very simple. An aqueous solution of diethylviologendibromide and potassium tetracyanidoplatinate were mixed. **Subsequently**, white powder or colorless crystals **were obtained**. These single crystals **exhibit** yellow emission. This **corresponds to** the wet phase.
When this procedure **was performed** in a solvent mixture of acetone and methanol, colorless plate crystals **were obtained**. These plate crystals may be single crystals of the dry phase **because of** their blue-green emission.

ジエチルビオロゲン塩の合成法は至って単純です。ジエチルビオロゲン臭化物とテトラシアニド白金酸カリウムの両者の水溶液を混合するだけです。そうすると、白色粉末あるいは無色結晶が得られました。この単結晶は黄色発呼王を示します。つまり、wet相と一致しています。
このような手順をアセトンとメタノールの混合溶媒を用いて行うと、無色板状結晶が得られます。この板状結晶は青緑発光を示すためdry相の単結晶であると考えられます。

Results and Discussion

Single-crystal X-ray analysis

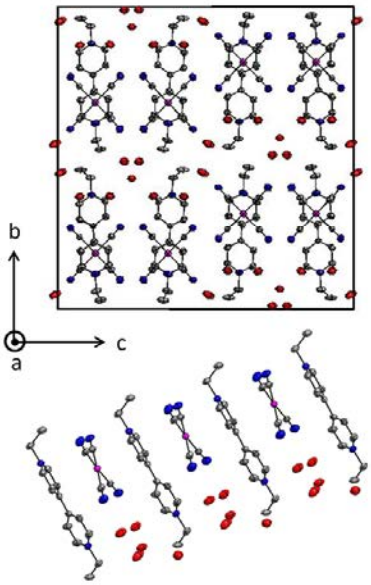

The colorless needles synthesized in water have yellow emission

Wet phase

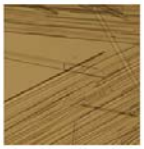

Formula	$EV[Pt(CN)_4]\cdot 5H_2O$
Formula weight	443.751
Crystal system	monoclinic
Space group	*C*2/*c*
a/ Å	6.9479(5)
b/ Å	26.144(2)
c/ Å	25.6450(18)
β/ Å	95.403(2)
V/ Å^3	4637.7(6)
Z	8
R1	0.0542
Temperature / K	173

This time, the X-ray structure analysis of the wet phase succeeded.
This is the structure viewed down the a-axis, and this is the columnar structure. The wet phase includes $5H_2O$ molecules in the structure. **Moreover,** the donor anions and the acceptor cations stack alternately.
This **indicates** the emission is **due to** the Donor-Acceptor Charge Transfer interaction.
This void spaces allow H_2O molecules to move in and out easily.

今回、wet相の単結晶構造解析に成功しました。こちらはa軸投影図で、こちらはカラム構造です。Wet相は水分子を5つ含んでいます。さらに、ドナーとアクセプターの交互積層構造をとっています。
このことはドナーアクセプター電荷移動相互作用による発光を示唆しています。
この空間があることによって水分子が容易に出入りできると考えられます。

Materials and Method ←論文を書くときはまとめてかかなければならない

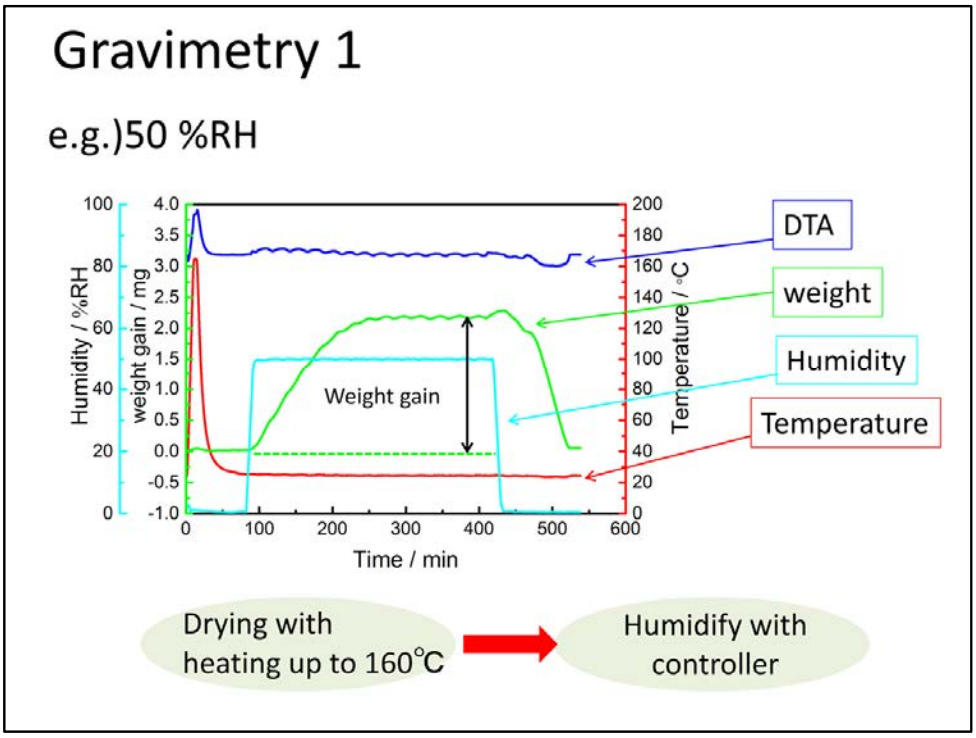

I'd like to explain the gravimetry method. The thermogravimetry machine was combined with a humidity-controller.
This is an example of 50 % RH. The red line is temperature, the green line is weight loss or gain, the sky-blue line is humidity, and the blue line is the Differential Thermal Analysis(DTA).
To set up a completely dry phase, **firstly** the samples were heated up to 160℃. **Subsequently,** it was humidified with the controller. **Then,** the sample absorbed H_2O vapor which was then accompanied by a weight gain. After the weight maximized, the number of H_2O molecules in the salt **were estimated**. The measurements **were conducted** at various humidities.

重量分析の説明をしたいと思います。熱重量分析の装置に湿度管理装置を組み合わせました。
こちらは湿度50%の例です。赤い線が温度、緑が重量変化、水色が湿度、青がDTAを表しています。
完全にdry相にするために、まずサンプルを160℃まで加熱します。その後、加湿を行います。すると、サンプルは水蒸気を吸収し、重量が増加します。重量が飽和したところで取り込まれた水分子の重量を見積もります。このような測定を様々な湿度で行いました。

Results and Discussion

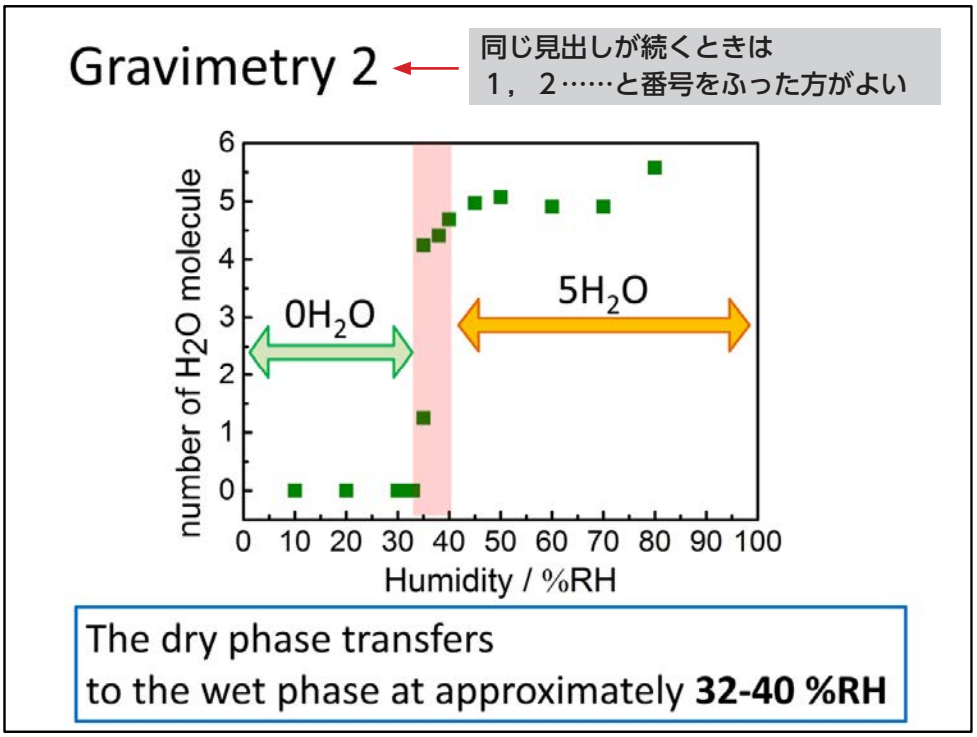

The results are shown in this plot.
The horizontal axis shows the relative humidity, while **the vertical axis shows** the number of H_2O molecule included in the salt.
This plot **indicates** that the dry phase **transfers to** the wet phase at **approximately** 32-40 %RH.
Moreover, the wet phase includes 5 H_2O molecules. This **agrees with** the crystallographic results.

その結果がこちらのプロットです。
こちらの軸が相対湿度、こちらが取り込まれた水分子の数です。このプロットより、dry相からwet相への変化は32-40%RHの間で起こっていることがわかります。さらに、wet相は水分子を5つ含んでおり、これは構造解析の結果と一致しています。

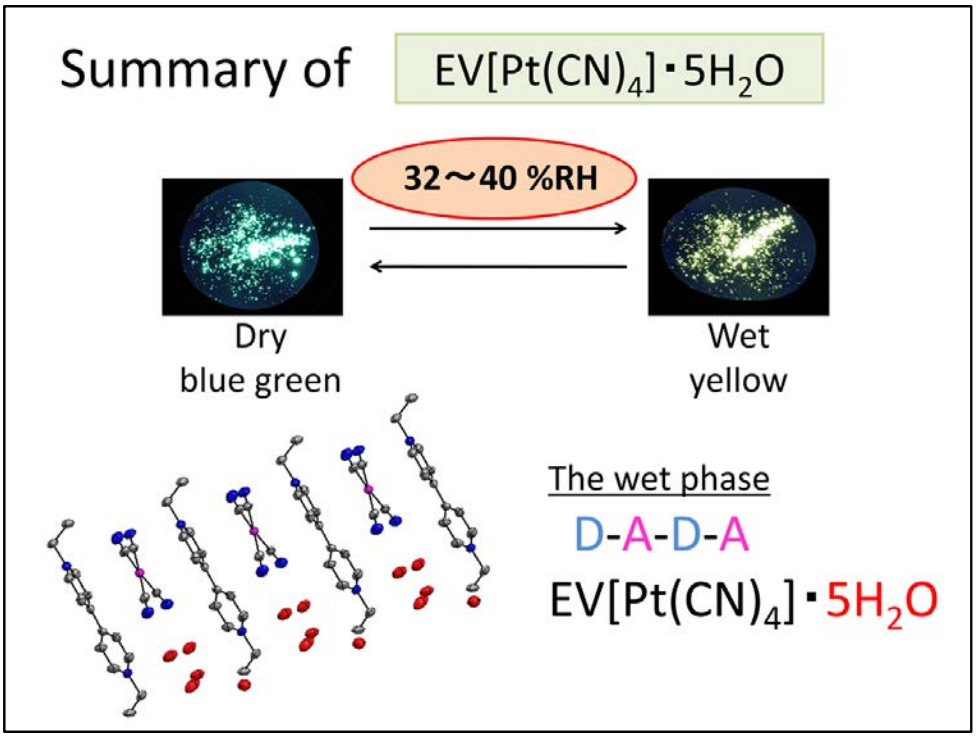

In conclusion, the salt **composed of** tetracyanidoplatinate anions and diethylviologen cations was prepared.
This salt **exhibits** vapochromism of emission. The blue-green emissive dry phase changes to the yellow emissive wet phase at **approximately** 32-40 %RH.
The crystal structure of the wet phase **consists of** a columnar structure **composed of** donor anions and acceptor cations stacked alternately and contains 5 H_2O molecules per asymmetric unit.
The void space **allows** vapochromic behavior, because H_2O molecules can move in and out easily.

Thank you for your attention.

結論としては、
テトラシアニド白金酸イオンとジエチルビオロゲンからなる塩を合成しました。
この塩は発光のベイポクロミズムを示します。青緑発光のdry相は湿度32-40%RHで黄色発光のwet相に変化します。
Wet相はドナーとアクセプターの交互積層構造をとっており、水分子を5つ含んでいます。スペースが空いていることにより水分子が容易に出入りすることができると考えられます。

ご清聴ありがとうございました。

Hello, I am from Rikkyo University in Japan.

As you know, all of us inherited DNA from your parents and will pass it on to our descendants.

This is caused by DNA duplication and this process must be done accurately.

How is it done？

Today, I want to talk about DNA semiconservative replication. Let me begin.

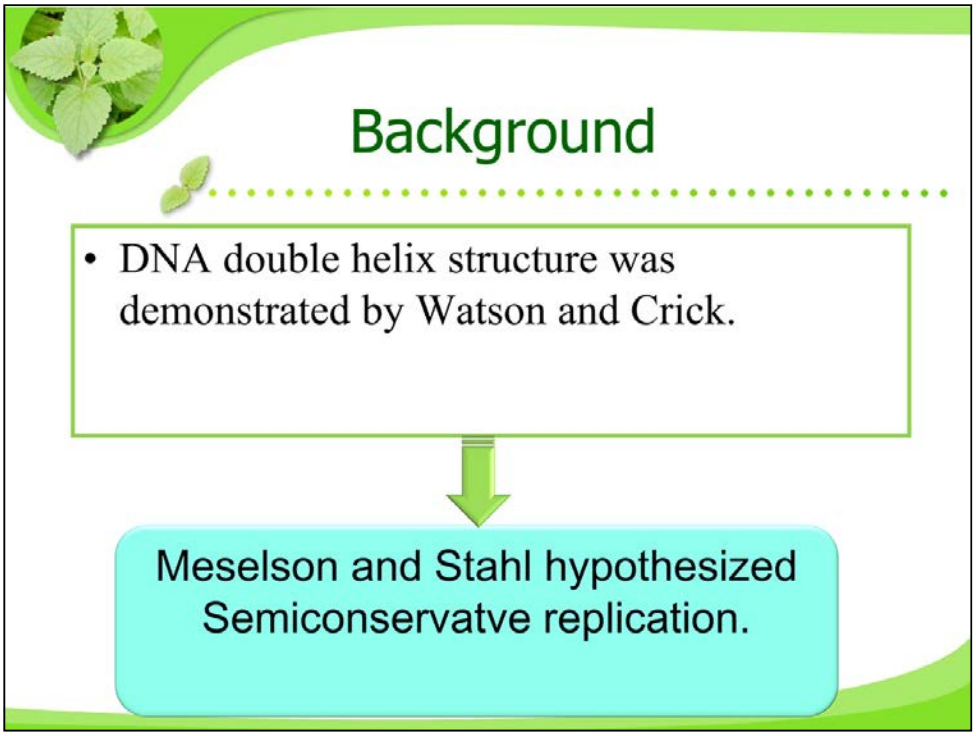

In 1953, DNA double helix structure was first demonstrated by Watson and Crick. And then, 3 DNA replication models were proposed as shown in the next slide.

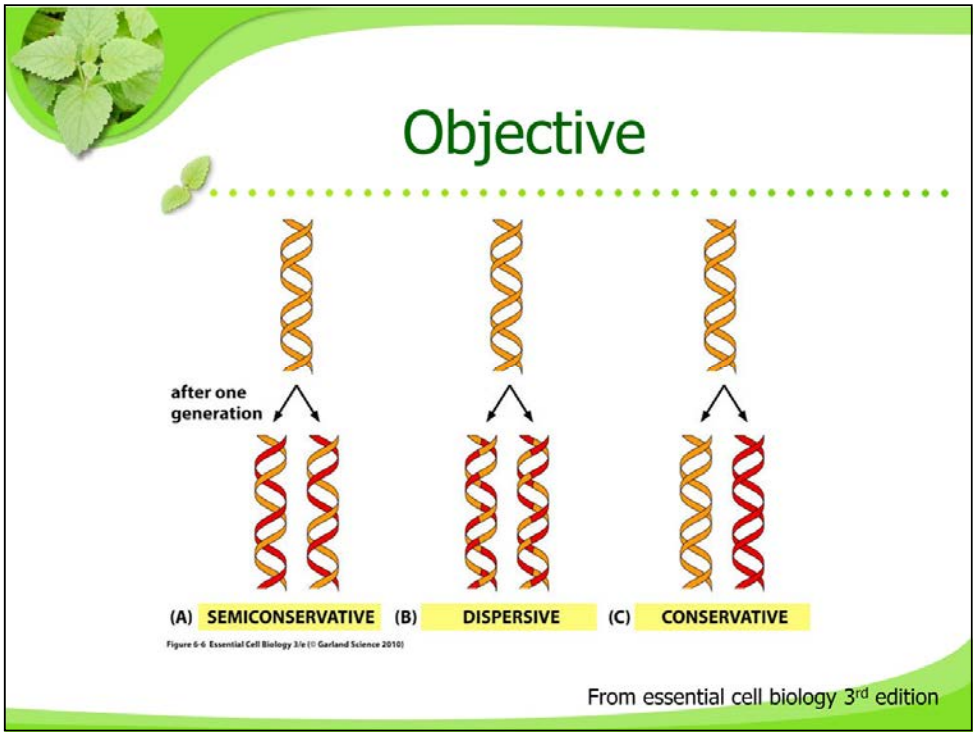

The 3 models are Semiconservative, Dispersive, and Conservative.

In Semiconservative, each strand becomes the template.

In Dispersive, each daughter cell contains both new DNA and fragment from the parent's by mixture.

In conservative, parents DNA is remained after it was replicated. In this case, the parent's DNA and a completely new daughter DNA were proposed.

3つのモデルは、Semiconservative、Dispersive、およびConservativeです。
Semiconservativeでは、各鎖がひな型になります。
Dispersiveでは、各娘細胞は新しいDNAと両親の混合物の両方を含んでいます。
Conservativeでは、親DNAは複製された後も残っている。この場合、親のDNAと完全に新しい娘DNAが提案された。

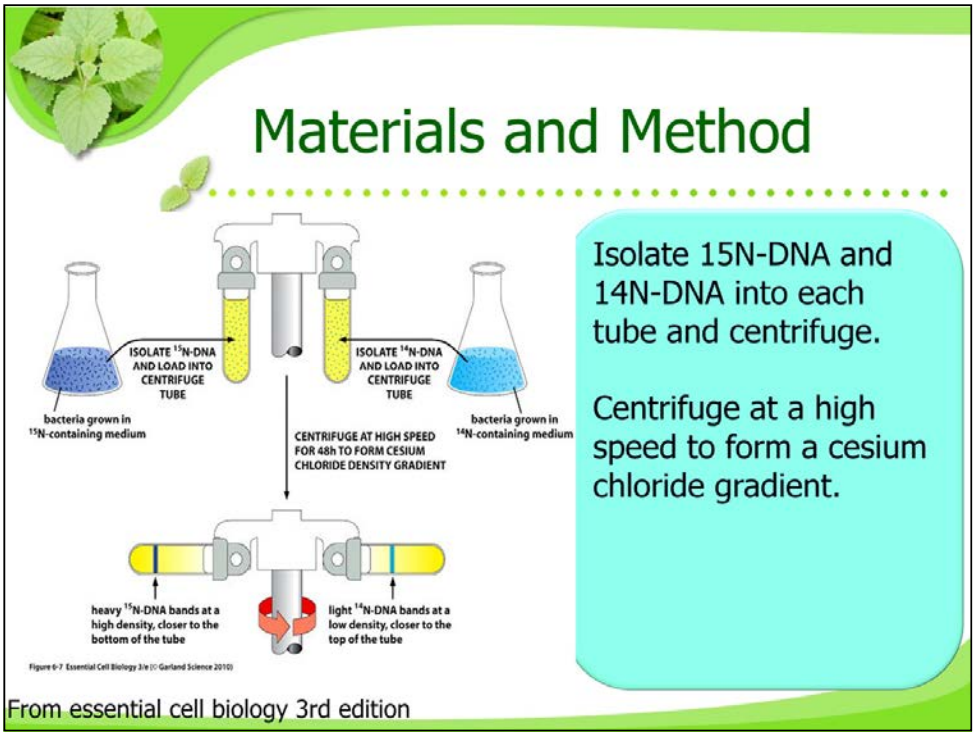

When ^{15}N -DNA and ^{14}N-DNA were isolated into each tube and centrifuged,　a cesium chloride gradient is formed and then developed a band in a different spot.

This process is called density-gradient centrifugation. By using this way, we can distinguish heavy DNA (^{15}N) and light DNA(^{14}N).

The heavy culture medium(^{15}N) was changed to a light culture medium(^{14}N). All DNA was heavy when the experiment started, but it becomes lighter as cell division occurs.

15N-DNAおよび14N-DNAを各チューブに単離し、遠心分離すると、塩化セシウム勾配が形成され、次いで異なるスポットでバンドを発生させた。
このプロセスは密度勾配遠心分離と呼ばれています。このようにして、重いDNA（15N）と軽いDNA（14N）を区別することができます。
重い培地（15N）を軽質培地（14N）に交換した。実験開始時はすべてのDNAが重かったが、細胞分裂が進むにつれて軽くなった。

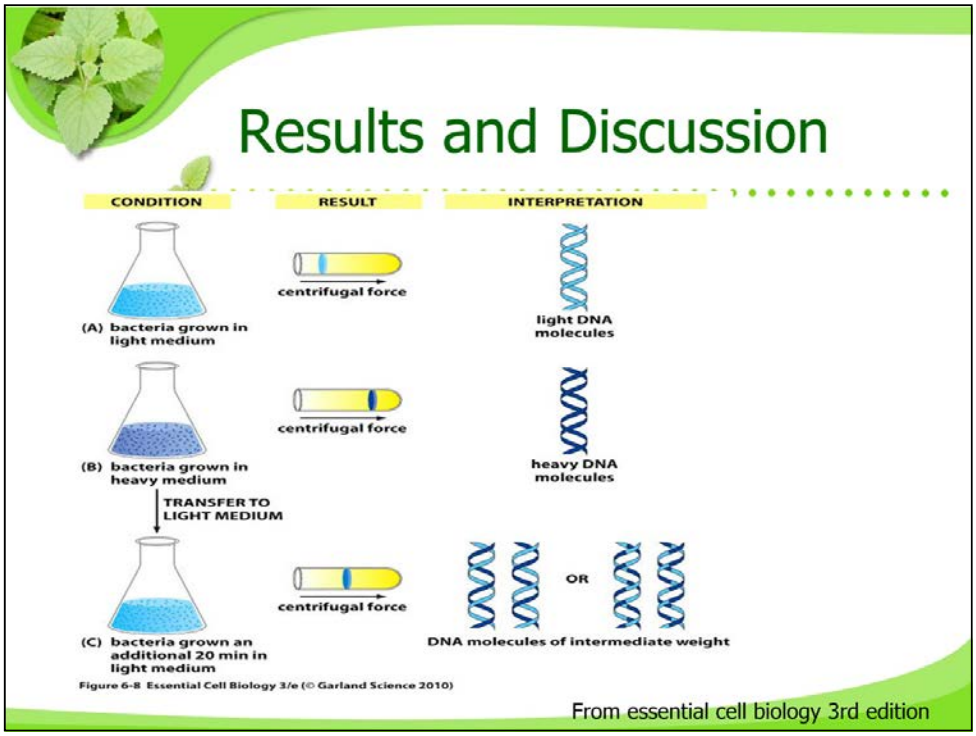

As shown in this figure, bacterias grown in the light medium made a band at a high point in the tube. Bacterias grown in the heavy medium made a band at a low point in the tube. Then, bacterias grown in the heavy medium and transferred to the light medium made a band in the middle of the two bands. This new daughter DNA is thought to be hybrid of heavy and light isolate.

From the results, the conservative model is excluded.

Which one is the true, the semiconservative model or the dispersive model?

Meselson and Stahl heated DNA to identify the way of replication.

As the temperature was raised, the hydrogen bond was cut and single strands were formed.

Then, the hybrid molecules were centrifuged, one strand was heavy and the other was light.

Finally, they found that DNA replication was semiconservative.

この図に示されるように、軽質培地中で生育した細菌は、管内の高い点でバンドを形成した。重い培地で生育したバクテリアは、チューブの低点でバンドを作った。その後、重い培地で増殖し、軽い培地に移された細菌は、2つのバンドの中間にバンドを作った。この新しい娘DNAは、重くて軽い分離株のハイブリッドであると考えられています。
結果から、保存的モデルは除外されます。
どちらが真、半保存的モデルか分散モデルか？
MeselsonとStahlは複製方法を特定するためにDNAを加熱した。
温度を上げると、水素結合が切断され、一本鎖が形成された。
次に、ハイブリッド分子を遠心分離し、一方の鎖は重く、他方の鎖は軽いものであった。
最後に、彼らはDNA複製が半保存的であることを見出した。

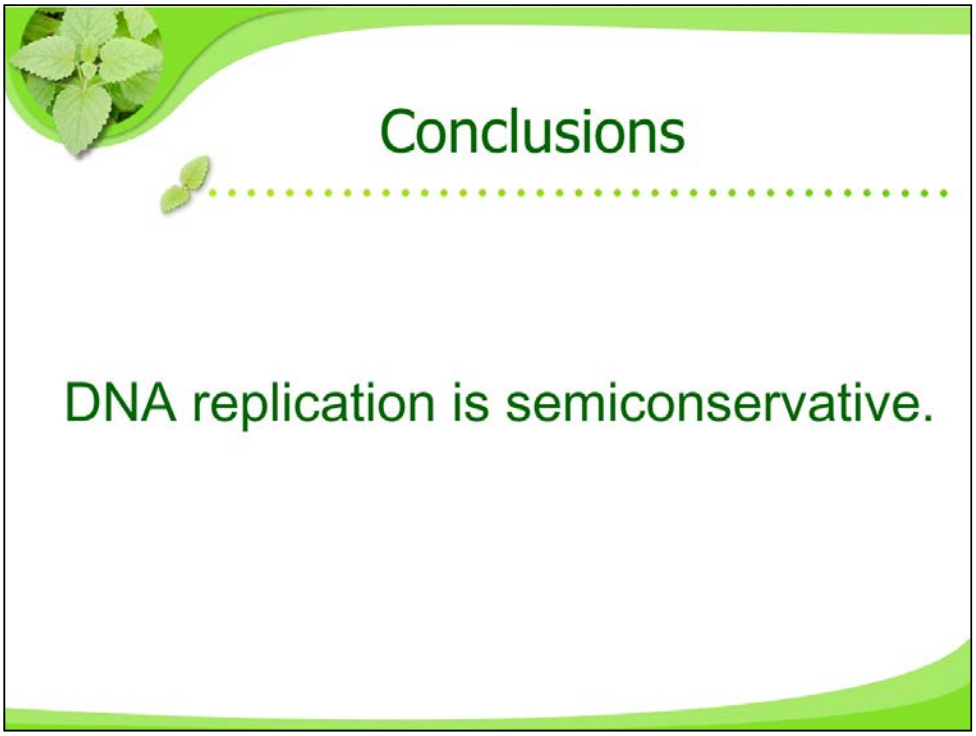

DNA replication is shown to be semiconservative. Each strand in the double helix become a template for the new strand.

And then, two new strands are synthesized.

Thank you for listening.

DNA複製は半保存的であることが示されている。二重らせん中の各鎖は、新しい鎖の鋳型となる。
そして、2つの新しい鎖が合成されます。

ご聴取ありがとうございました。

Good morning, ladies and gentleman. Thank you for attending this presentation.
I'm very glad to meet you.
I'm from Rikkyo University in Japan.
Today, I will talk about the radiation reduction caused by lead plates.

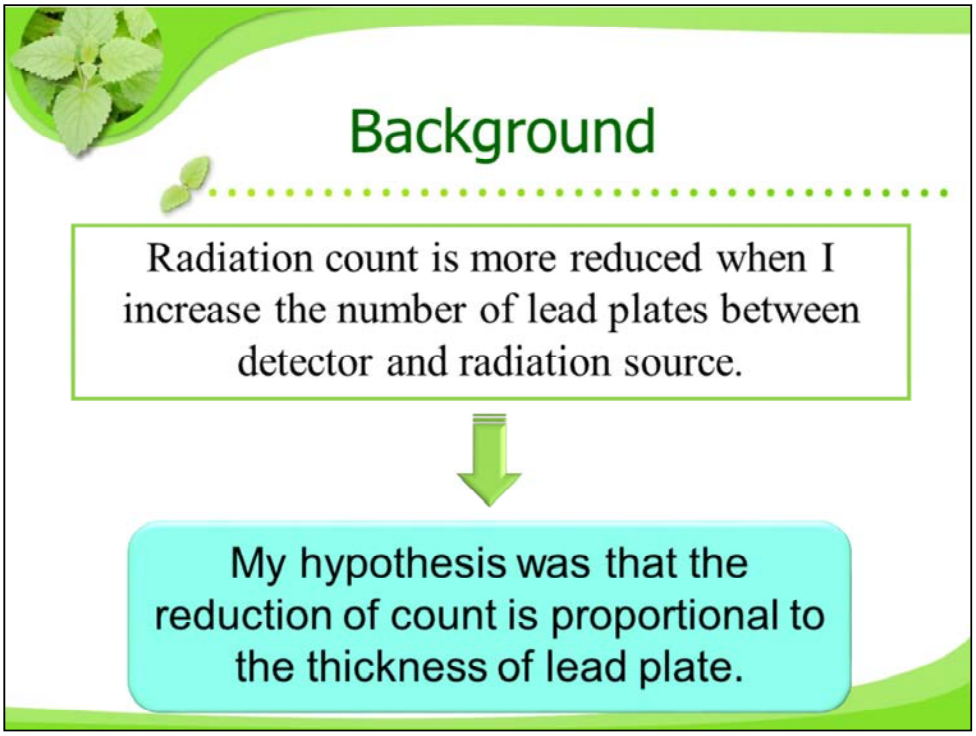

To begin with, I’d like to talk about the background of this study.

When I measured the radiation from a source of cesium137, I found that radiation count was reduced by inserting lead plates between the detector and cesium137.

And then, I also found that if we increase the number of the plates, the radiation count was further reduced.

So, I thought that the reduction of the radiation count is proportional to the thickness of the lead plate.

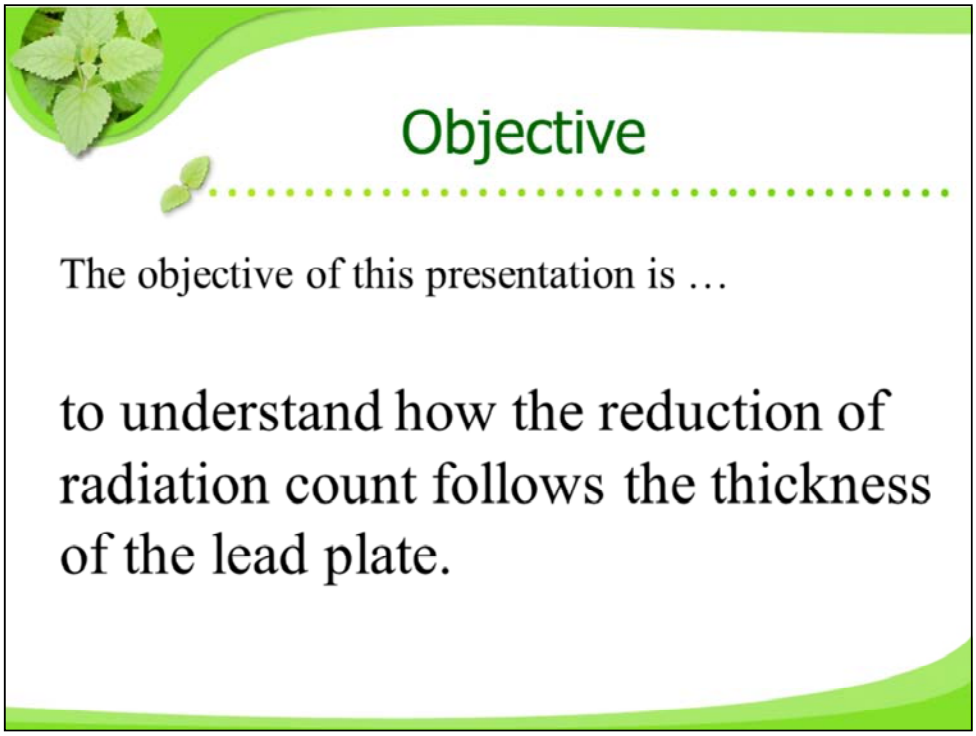

Therefore, **the objective of this experiment is to** understand how the reduction of radiation count follows the thickness of the lead plate between a radiation source and the detector.

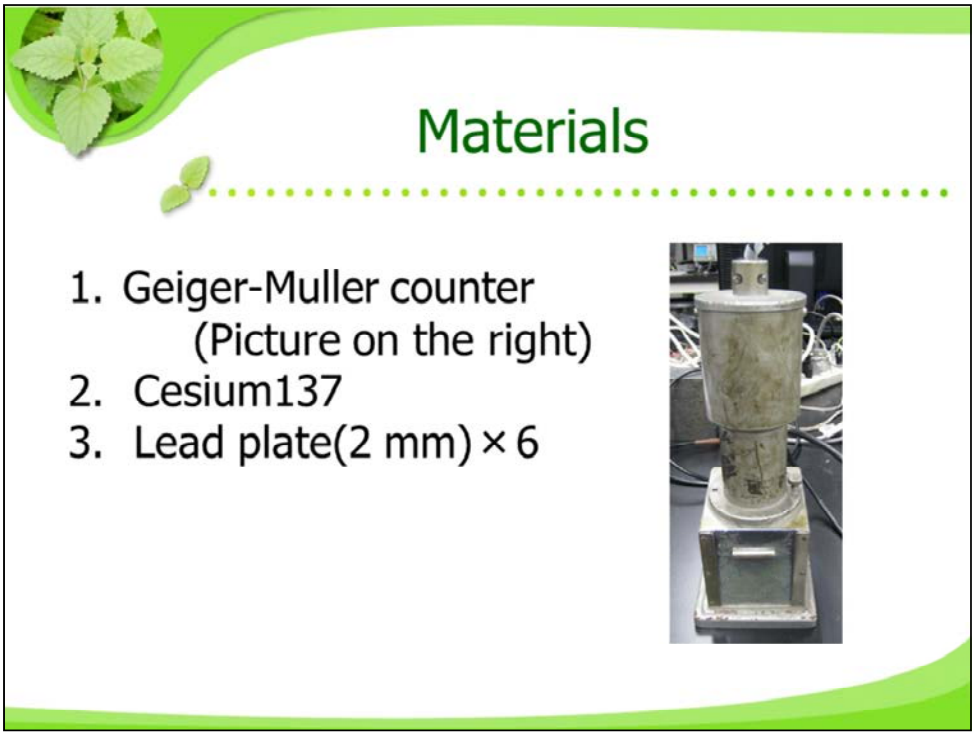

In this research, I used the following materials. **First**, a Geiger-Muller counter, which is used as a detector of radiation. **Second**, Cesium137, which is used as a radiation source. **Third**, 6 lead plates with a thickness of 2 millimeters per plate.

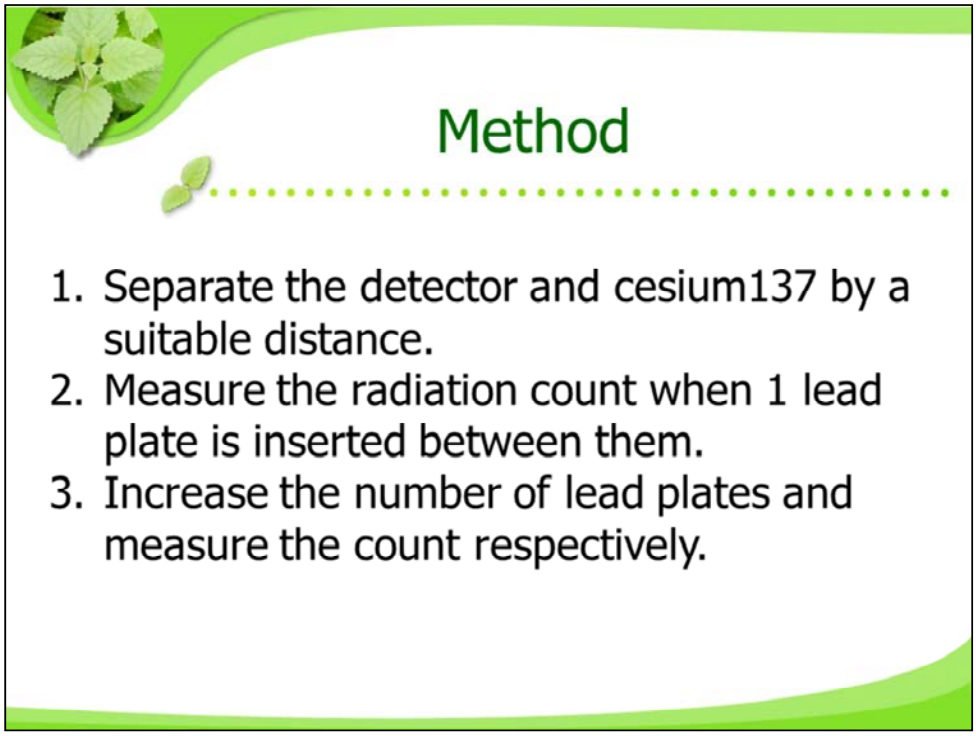

This is the method of this research.

First, I separated the detector and cesium137 by a suitable distance.

Second, I measured the radiation count in the situation when 1 lead plates was inserted between the source and the detector.

Third, I increased the number of lead plates and measured the count respectively.

Last, I graphed the experiment data.

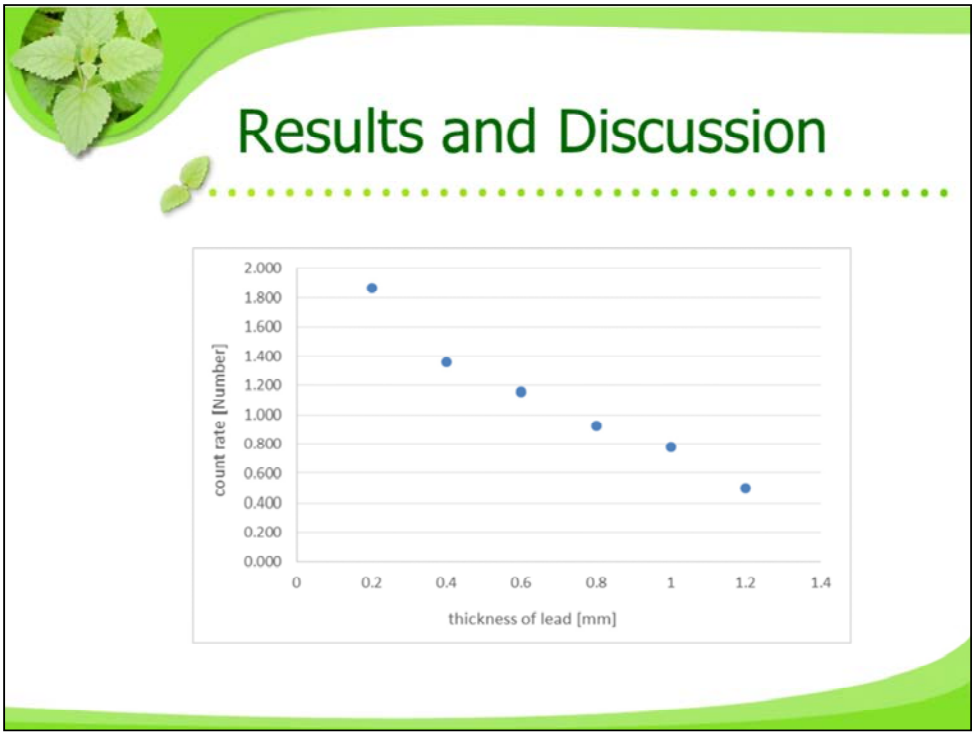

I’d like to talk about the result.

This figure shows the reduction of the count rate by inserting lead plates.

The horizontal axis shows the thickness of lead **and the vertical axis shows** the count rate, which means the radiation count per second.

This figure shows that the count rate was reduced in proportion to the thickness of lead.

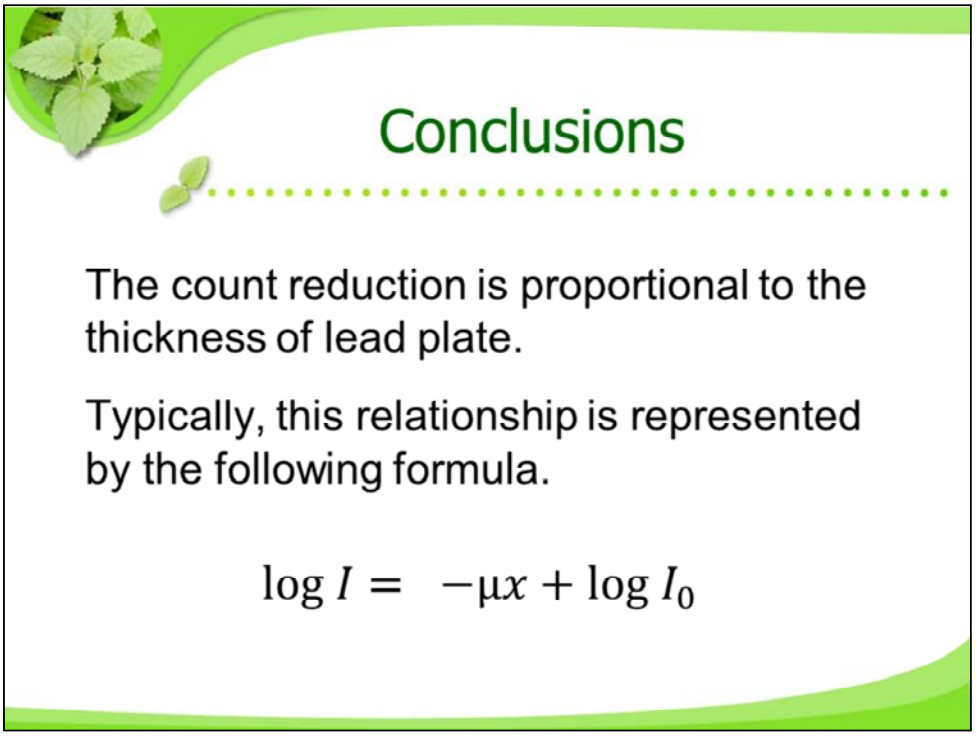

In conclusion, I found that the count reduction is proportional to the thickness of lead plate. Typically, this relationship is already represented by the following formula. "I" is the count rate and "x" is the thickness of lead plates. "I_0" is also the count rate, for the no lead plate situation. μ is called "absorption coefficient". This is different depending on the material used as the blocking plate.

Thank you for your attention.

If you have any question, please raise your hand.

これは私が 2017 年にスペインで国際学会発表した際に，事前に発表者に配られたプレゼンテーションのインストラクションです．参考にしてみましょう．

Wessex Institute of Technology

Ashurst Lodge, Ashurst, Southampton, SO40 7AA, UK
Tel: +44 (0) 238 029 3223 Fax: +44 (0) 238 029 2853
Email: wit@wessex.ac.uk Website: www.wessex.ac.uk

Presentations at WIT Conferences

NOTES TO PRESENTERS

1. When presenting a paper it is essential to consider the type of audience you will be addressing.

2. Having determined your audience the next step is to decide what you want to tell them. In planning your presentation you must first answer the question ***'why do I want to talk to these people?'***

3. Structure your presentation in a similar way to your written paper. ***First introduce yourself and the presentation***, then move to the main body of the paper. Having done that, draw your conclusions and describe future work.

4. The purpose of a presentation is to make the audience want to understand more about your subject. You should assume that people have not read your paper, so ***you should try to make them want to read it.***

5. **Prepare** well in advance. By preparing early, the presentation experience should go smoothly with less anxiety.

6. **Practice** your presentation in front of people who do not understand your work.

7. Marketing presentations and product pitches are not acceptable presentations and will receive poor feedback from delegates.

Presenting

8. ***Under no circumstances should you read your paper.*** Each slide should contain bullet points and you should speak in complete sentences and paragraphs.

9. Speak to the audience not the screen and use the laser pointer.

10. Remember that many of the delegates do not speak English as a first language - **please speak clearly and not too quickly.**

11. Accurate timekeeping is essential to ensure the smooth running of the conference. Remember that the time you have been allocated includes time for Q&A. Delegates do not appreciate long presentations and sessions overrunning.

12. Allow 2 minutes per slide and remember to pause so the audience can read the whole slide. Do not block part of the slide.

Presentation Equipment

13. A computer and LCD projector will be available for your use. If you require other equipment please let us know well in advance and be aware that this may incur an additional charge payable by you. In case of need contact the conference secretariat as soon as possible.

Presentation of your material

14. ***Your presentation will be greatly enhanced with the use of a good slide show.*** Your aim should be to make your presentation as easy to follow as possible.

- Try to use landscape format where possible
- Use colour wherever possible and make sure that the colours can be distinguishable at the back of a large room
- Spacing makes the rest of the slide easier to read — don't cram your slides full.
- Avoid putting important information at the bottom of the page. It can be difficult for some people to see the entire screen.
- Have between 3-5 points per slide and do not use too many equations.
- The first slide should have the name of your presentation, your name and the conference name and date. Your organisation's name should be placed at the bottom corner of each slide along with your own name.
- Remember that a picture or graph is very informative. Check beforehand that your presentation is of good quality and that they can be read from a distance.
- Try the LCD projector in advance to avoid delays or disruptions.
- We would request that all participants bring their presentations on a USB flash drive.
- Meet your session Chairman at least 10 minutes before the session starts.

発表を聴き終わって質問したい時はまず手を挙げて自分の名前と所属を名乗ります.

質疑応答の一例

質問する側：

I’m_____from_____University in Japan.
Thank you for your nice (excellent) presentation.
I’d like to ask a question.
Q（質問内容）: _____.

答える側（発表者）：

That’s a good question.

I didn’t catch your point.（相手の質問の意味が良くわからなかった時）
Could you repeat the question?（もう一度質問を繰り返してほしい時）
Could you speak more slowly ?（もっとゆっくり話してほしい時）
Could you speak more loudly ?（もっと大きな声で話してほしい時）
I have no idea right now, but let’s discuss later.（今すぐには答えられない時）

4–2　英語でポスター発表（Poster presentation）をしてみよう

ポスター発表での決まり文句

呼び込みをする

Hello.　Can I explain my work (study) ?

始まりの挨拶をする

I’m ○○ from Rikkyo University in Japan.

I’m a graduate student at Rikkyo University in Japan.

私は日本の立教大学の大学院生です.

I’m majoring in chemistry (physics, life science) at Rikkyo University in Japan.

私は立教大学で化学（物理，生命理学）を専攻しています.

研究目的を述べる

In this study, we aimed to ~

The aim of this study was to ~

本研究では，～することを目的にしました.

We have been researching ~

我々は～について研究してきました.

What we were doing in this study was ~

本研究で行っていたことは～です.

研究（実験）方法を説明する

Let me explain what we did in the experiment.

どのような実験を行ったかを説明します.

Let me explain how we carried out the experiment (analysis).

どのように実験（分析）を行ったかを説明します.

You can see here the method we used for the experiment (analysis).

実験（分析）で用いた方法をここで説明します.

研究結果を説明する

You can see the results of this study in this Table (Figure) here.

This Table (Figure) here, shows the results of the study.

この表（図）に研究の結果が示されています.

Development of the Circumpolar Stratospheric Telescope FUJIN for Observations of Planets

Introduction

It is important to conduct long-term continuous observations for studies on time-dependent events of the planetary atmospheres and plasmaspheres.We have developed a balloon-borne telescope “FUJIN” that has the purpose of observing the atmospheres of Jupiter and Venus from the stratosphere. We are developing a second telescope “FUJIN-2” aiming the observation of these planets. This telescope took over both the control systems, BBT2009 and FUJIN1.

About Balloon-borne Telescopes

Fig.1; FUJIN-1 appearance

Why do we observe from the stratosphere with a balloon -mounted telescope ?

- Good Visibility (~0.1″)
  At ultraviolet and visible wavelength, the observation at the diffraction limit can be performed.
- Wavelength region
  The observation from 300nm wavelength can be performed.
- Long-term and continuous observation
  In the polar region, there are planets that can be observed continuously for 24 hours
- Observation From unchanged direction
  FUJIN can observe the planet disk from an unchanged direction

Table 1 shows the history of the FUJIN project. The FUJIN project has failed to carry out observations twice in the previous attempts. The weakest point of the FUJIN project is that it does not carry out observations at the optimum time for observations. FUJIN-1, the first model of FUJIN-project, had an unsuccessful flight due to bad climate conditions and a malfunction in the JAXA's bus systems.
However it was concluded that FUJIN-1 can be controlled in the stratosphere from the results of ground tests. The main purpose of the development of FUJIN-1 wasn't to carry out observations but to develop the control systems. Therefore, after the development of FUJIN-1, we started FUJIN-2 development for planet observations.

Table.1:History of FUJIN Project

2002	Start of project
2009	1st experiment was failed due to the onboard CPU failing.
2010	Improvement
2011	Experiment was cancelled due to development delays.
2012	Cancelled due to bad wing condition
2013	Cancelled due to malfunction in the bus system
2014	Start up developing FUJIN-2

FUJIN-2 Optical System

FUJIN-2 is a Schmidt Cassegrain Telescope with a Nasmyth focus and has a mirror that has an effective aperture of 406mm.
Table.2 shows the specifics of FUJIN-2 and Fig.3 shows the light path in the FUJIN-2. The original focal point distance of FUJIN-2 was 3000mm but this distance was extended up to 6000mm using a double sized Barlow lens.

Tab.2: FUJIN-2 telescope specific

Telescope type	Schmidt Cassegrain with a Nasmyth focus	
Effective aperture	406	mm
Focal point distance	~6000	mm
Band-pass filter	8	Sheets
Detector	a CCD	

The end points of the FUJIN-2 light path are separated into two light path through the half mirror. FUJIN-2 can provide multi-wavelength observations using the filter turret in front of a CCD camera. The light into the PMT is used by the attitude control in phase 3 (accurate directivity control). A signal period from PMT to TTM is approximately 1 kHz (FUJIN-1). Tab.3 shows the target wavelengths of FUJIN-2.

Tab.3: Subject of research

Mercury	Venus	Jupiter(main)
	290~320nm SO_2	589nm Na
	320~400nm UV	672nm S
589nm Na	777nm O	800nm NH_3
	900nm NIR	890nm CH_4
	1270nm O_2	920~945nm H_2O

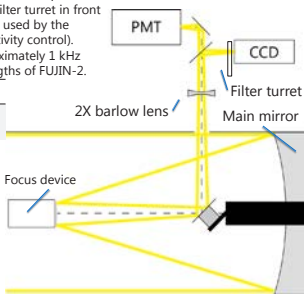

Fig3: FUJIN-2 optical system

FUJIN Control System

For realizing observations at a visibility increment of 0.1″, it is necessary to have highly developed attitude controls and pointing controls.
In the FUJIN-2, the attitude controls were taken from the FUJIN-1 system and are divided into 3 phases with each of these phases performed separately (Fig.2).

○Control phase 1

In the first phase, a gondola of FUJIN-2 is controlled in 3 dimensions by a decoupling mechanism (DCP) and control moment gyros (CMGs).

○Control phase 2

When the FUJIN-2 is not observing targets, the Solar Cell Panels, which are installed on the gondola, are always facing in the direction of the sun to provide electric power for the FUJIN2.

○Control phase 3

In the second control phase, the target is captured by the telescope using two cameras, a wide angle camera and a narrow angle camera.

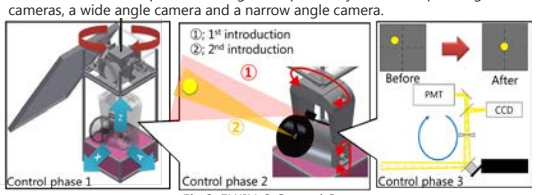

Fig.2: FUJIN-2 Control System

○Results of the attitude control tests in FUJIN-1

Fig.3-a and Fig.3-b show the azimuth and elevation amplitudes respectively, when disturbances are input.
The pointing accuracy as RMS values are shown in Fig.3-c and Fig.3-d, respectively.
In the control phase 3, the light path must be input within the predetermined movable scope of the TTM to be able to use the fine pointing controls of the TTM. The frequency is shown in Table 2. The azimuth ratio is 45.5% and the elevation ratio is 21.7%.
As shown in Fig.3, no significant difference was observed between the case with and without the disturbance. That is, it is identified that the attitude fluctuations of the gondola were sufficiently compensated. Besides, there were constant vibrations every 3~4 seconds.
In the development of FUJIN-2, we introduced the 3

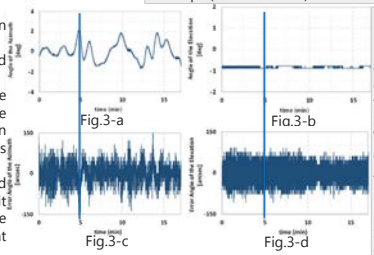

Fig.3: The integrated test results of FUJIN-1 in 2013

Subject of Observation

○Jupiter(Main Target)

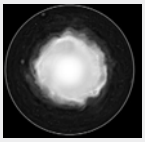

Fig.4: A region of Jovian South-pole at 890nm from Cassini. [Barrado-Izagirre et al., 2008]

- The Rossby wave existing in the Jupiter atmosphere is important for understanding the atmosphere dynamics.
- The white edge in the polar region of Jupiter in Fig.4 shows the Rossby wave with a wave number of 12 as shown in Fig.2.
- Cumulonimbus clouds transport heat vertically in the Jupiter atmosphere and are interactive with the planetary scale zones and belts. There is a hypothesis that these structures were produced via Cumulonimbus cloud activities.

For understanding the Jupiter atmosphere structure, we will obtain the following information .

- Time fluctuations and velocity of the haze wave structures in the polar region of Jupiter for several days.
- The partial distribution of the clouds and the correlation of background wind speeds and time course of these correlation at the troposphere altitude in Jupiter.

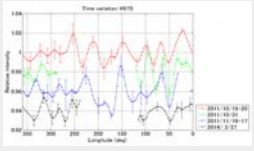

Fig.5: The time fluctuation of the longitudes profiles of the haze brightness in the 67°S in Jupiter taken from Pirka telescope (Hokkaido Univ.).

○Venus(Optional Target)

- Super rotation
- Searching for proofs of unidentified absorbed materials

○Mercury(Optional Target)

- The atmosphere light of Na

Future Plan of FUJIN-2

○The earliest year that the FUJIN-2 can be in operation will be 2017. We are considering 2 operational plans in parallel. One of the plans is that FUJIN-2 will be released from Kiruna, Sweden in the summer in 2017, and observe Venus. The other plan is that Jupiter will be observed from Australia in April of 2017.

This plan is for a 24 hour flight: FUJIN-2 will be released in the morning, and observe the planets in the night. FUJIN-2 will be shipped by September 2017 after the integration of the subsystems.

○イントロダクション

It is important to conduct long-term continuous observations for studies on time-dependent events of the planetary atmospheres and plasmaspheres.
惑星の大気圏やプラズマ圏で起こる変動現象を研究するためには，長時間の連続観測が重要である。

We have developed a balloon-borne telescope “FUJIN” that has the purpose of observing the atmospheres of Jupiter and Venus from the stratosphere.
我々は地上望遠鏡でもなく，また宇宙望遠鏡でもない気球に搭載した望遠鏡によって成層圏から, 木星や金星の大気を観測することを目指した気球搭載型望遠鏡「FUJIN」の開発を行っている。

We are developing a second telescope “FUJIN-2” aiming the observation of these planets. This telescope took over both the control systems, BBT2009 and FUJIN-1.
現在は BBT2009，FUJIN-1 のサブシステムを継いだ，観測することを目的とした望遠鏡 FUJIN-2 の開発を行っている。

○気球搭載型望遠鏡に関して

Why do we observe from the stratosphere with a balloon -mounted telescope ?
・Good Visibility（~0.1”）
なぜ，成層圏から観測するのか
・シーイングがよい（~0.1”）

At ultraviolet and visible wavelength, the observation at the diffraction limit can be performed.
・Wavelength region
紫外，可視光において回折限界での観測が可能
・幅広い観測波長領域

The observation from 300nm wavelength can be performed.
・Long-term and continuous observation
300nm~ の観測が可能
・長期間の連続観測
In the polar region, there are planets that can be observed continuously for 24 hours

・Observation from unchanged direction
FUJIN can observe the planet disk from an unchanged direction
極域でフライトを行った場合，24 時間連続観測が可能な惑星もある
・一定の方向から観測が可能

Table 1 shows the history of the FUJIN project. The FUJIN project has failed to carry out observations twice in the previous attempts.
表 1 は FUJIN-project の歴史である。FUJIN は過去に 2 度, 気候によって観測が出来なかった。

The weakest point of the FUJIN project is that it does not carry out observations at the optimum time for observations
FUJIN プロジェクトの最大の欠点は観測したいときに観測できない点である。

FUJIN-1, the first model of FUJIN project, had an unsuccessful flight due to bad climate conditions and a malfunction in the JAXA's bus systems.
FUJIN プロジェクトの 1 号機である FUJIN-1 は JAXA のバスシステムの不具合や気候の状況が悪く，放球することが出来なかった。

However it was concluded that FUJIN-1 can be controlled in the stratosphere from the results of ground tests.
FUJIN-1 に関して，地上における度重なる試験の結果，成層圏環境下でも十分に姿勢制御ができると結論付けた。

The main purpose of the development of FUJIN-1 wasn't to carry out observations but to develop the control systems.
そもそも，FUJIN-1 の開発目標は観測ではなく，制御システム等の開発が中心だった。

Therefore, after the development of FUJIN-1, we started FUJIN-2 development for planet observations.
FUJIN-1 の開発は 2013 年に終了し，天体の観測を目標とした FUJIN-2 の開発を開始した。

○ FUJIN-2 制御システム

For realizing observations at a visibility increment of 0.1”, it is necessary to have highly developed attitude controls and pointing controls.
0.1”の条件下で観測を実現するには，高精度な姿勢制御と指向精度が必須である。

In the FUJIN-2, the attitude controls were taken from the FUJIN-1 system and are divided into 3 phases with each of these phases performed separately (Fig.2).
FUJIN-2 の姿勢制御は FUJIN-1 の思想を引き継いで３段階に分けて制御を行う。

In the first phase, a gondola of FUJIN-2 is controlled in 3 dimensions by a decoupling mechanism (DCP) and control moment gyros (CMGs).
まず第 1 段階制御ではデカップリング機構（DCP）とコントロールモーメントジャイロ（CMG）を用いて，ゴンドラの３軸制御を行う。

When the FUJIN-2 is not observing targets, the Solar Cell Panels, which are installed on the gondola, are always facing in the direction of the sun to provide electric power for the FUJIN-2.
観測時以外は SCP を常に太陽方向に指向させて電力を確保する。

In the second control phase, the target is captured by the telescope using two cameras, a wide angle camera and a narrow angle camera.
第２段階制御では広角，狭角のカメラを用いて望遠鏡視野内に天体を導入する。

Firstly, the targets are established in the range of the wide angle camera, and then secondly automatically in the narrow angle camera.
まず広角のカメラ内に目標天体を捉え，次に狭角のカメラに自動的に導入させる。

If targets were captured in the narrow camera, the target could then be viewed by the telescope.
このとき狭角カメラ内に天体を導入と同時に望遠鏡視野内にも導入できるようにアライメントしてある。

In the final control phase, the target is established continuously in the center of view field by a Tip/Tilt mirror with 2 axes and a photomultiplier tube (PMT).
第３段階制御では２軸のティップティルトミラー（TTM）と光電子増倍管（PMT）を用いて視野中央に天体を導入し続ける制御を行う。

FUJIN-2 has a half mirror for dividing the incoming light path into 2 light paths.
One is a PMT path, and the other is a CCD path. It is controlled to send the ratio of the light on the four channels in the PMT on time.
FUJIN-2 の光路の最後に CCD カメラと PMT に光線が入射するようにハーフミラーを設置している。４つのチャンネルに分かれた PMT のチャンネル上に入射した光量の比を TTM にリアルタイムで送信することで制御を行う。

Then the TTM is controlled by tipping itself to give equal amounts of light for each of the channels of the PMT.
このとき，各チャンネルの光量が等しくなるように TTM を傾ける制御を行う。

○ FUJIN-1 姿勢制御試験結果

In the experiments of FUJIN-1 in 2013, integrated tests were conducted of all the FUJIN-1 attitude controls, and the controlled performance of FUJIN-1 was evaluated for the stratosphere.
2013 年に行われた FUJIN-1 実験において，第一, 二段階制御のテストを行い，FUJIN-1 が成層圏における姿勢制御の能力を評価した。

Fig.3-a and Fig.3-b show the azimuth and elevation amplitudes respectively, when disturbances are input.
図３-a と図３-b は外乱入力時の方位角と高度角の振幅である。

The pointing accuracy as RMS values are shown in Fig.3-c and Fig.3-d, respectively.
図３-c と図３-d は望遠鏡の指向精度を RMS 値で示したものである。

In the control phase 3, the light path must be input within the predetermined movable scope of the TTM to be able to use the fine pointing controls of the TTM.
第三段階制御では，TTM を使った精指向制御を行うがため，第二段階制御で TTM の駆動範囲内に入射している必要がある。

The frequency is shown in Table 2.
The azimuth ratio is 45.5% and the elevation ratio is 21.7%.
その頻度を表２にまとめる。

As shown in Fig.3, no significant difference was observed between the case with and without the disturbance. That is, it is identified that the attitude fluctuations of the gondola were sufficiently compensated.
方位角に関しては外乱の有無でほぼ差がない。つまり，ゴンドラの姿勢変動は制御によって十分に補償されていることが分かった。

Besides, there were constant vibrations every 3~4 seconds.
また高度角方向は外乱の有無にかかわらず，周期３～４ｓの一定の振動がある。

In the development of FUJIN-2, we introduced the 3 dimensions gondola controls to remove the pendulum movement.
FUJIN-2 の開発では，３軸制御にすることで振り子運動をなくす設計になっている。

When the development of FUJIN-1 was completed, it was established that FUJIN-1 could attain a pointing accuracy of approximately 0.4”,
FUJIN-1 実験において，第 1 段階～第３段階制御では 0.4”程度の指向精度が期待できると確認できたため，FUJIN-1 の開発は終了した。

○ FUJIN-2 光学系

FUJIN-2 is a Schmidt Cassegrain Telescope with a Nasmyth focus and has a mirror that has an effective aperture of 406mm.
FUJIN-2 は有効口径 400mm のナスミス焦点付シュミットカセグレン式望遠鏡である。

Table.2 shows the specifics of FUJIN-2 and Fig.3 shows the light path in the FUJIN-2.
FUJIN-2 の特性を示したものを表２に，FUJIN-2 の光路図を示したものを図３に示す。

The original focal point distance of FUJIN-2 was 3000mm but this distance was extended up to 6000mm using a double sized Barlow lens.
FUJIN-2 の本来の焦点距離は約 3000mm だが，２倍のバローレンズを通すことで，焦点距離を最大 6000mm まで延長している。

The end points of the FUJIN-2 light path are separated into two light path through the half mirror.
光学系の最後はハーフミラーで２つの光路に分けている。

FUJIN-2 can provide multi-wavelength observations using the filter turret in front of a CCD camera.
CCD の直前にフィルターターレットを通すことで，多波長観測を実現させている。

The light into the PMT is used by the attitude control in phase 3 (accurate directivity control).
PMT 側に入射する光は第三段階制御（精指向制御）で用いられる。

A signal period from PMT to TTM is approximately 1 kHz (FUJIN-1). Tab.3 shows the target wavelengths of FUJIN-2.
PMT-TTM の信号周期は 1kHz 程度である。表 3 は FUJIN-2 で観測を予定している波長である。

○研究対象

・The Rossby wave existing in the Jupiter atmosphere is important for understanding the atmosphere dynamics.
・木星大気に存在するロスビー波は，木星大気ダイナミクスを理解するうえで重要である。

・The white edge in the polar region of Jupiter in Fig.4 shows the Rossby wave with a wave number of 12 as shown in Fig.2.
・図 1 の木星南極域で白く見える構造のふちは波構造をしており，図 2 より波数 12 程度のロスビー波と示唆される。

・Cumulonimbus clouds transport heat vertically in the Jupiter atmosphere and are interactive with the planetary scale zones and belts. There is a hypothesis that these structures were produced via Cumulonimbus cloud activities.
・木星内部で熱を鉛直輸送する役割を持つ積乱雲と，ゾーンやベルトなどの大規模構造は相互作用しており，積乱雲によりこれらの構造が形成された説も存在する。

For understanding the Jupiter atmosphere structure, we will obtain the following information .
木星大気のダイナミクスを理解するために，以下の情報を取得する。

・Time fluctuations and velocity of the haze wave structures in the polar region of Jupiter for several days.

・木星極域のヘイズ波構造の数日単位での時間変動及び移動速度。

・The partial distribution of the clouds and the correlation of background wind speeds and time course of these correlation at the troposphere altitude in Jupiter.
・木星対流圏高度での積乱雲の空間分布と背景風速度の相関とその時間変化。

The earliest year that the FUJIN-2 can be in operation will be 2017.
今後の FUJIN-2 の展望は，FUJIN による観測が最も早く行える時期は 2017 年である。

We are considering 2 operational plans in parallel.
現在は２つの計画を平行して検討している。

One of the plans is that FUJIN-2 will be released from Kiruna, Sweden in the summer in 2017, and observe Venus.
一つは 2017 年夏季にスウェーデン・キルナから放球し，金星を観測する計画である。大西洋を渡る 1 週間程度のフライトの後，カナダかアラスカでゴンドラを回収する。

The other plan is that Jupiter will be observed from Australia in April of 2017.
もう一つは，2017 年 4 月にオーストラリアで木星を観測する計画である。

This plan is for a 24 hour flight: FUJIN-2 will be released in the morning, and observe the planets in the night. FUJIN-2 will be shipped by August 2016 after the integration of the subsystems.
こちらは 24 時間程度のフライトで，朝に放球し，夜まで待って夜間に観測を実施する。
2016 年の９月までに全てのサブシステムの統合を終え，実験場所へ向けて搬出する。

４–３　スピーキング（Speaking）のコツ

１．なるべくフレーズをひとかたまりにして覚える．

What do you think ?, I agree with you., You are right...,Let me see..., I’m glad to be here today..., などのフレーズは音楽の歌詞を覚えるように何度も発音して，ひとかたまりにして覚えてしまうと便利です．

２．結論から先に言う．

英語と日本語の語順は逆なので，I think it’s true because... のように，結論から先に言うようにする．英語で何か言いたいときに，日本語が最初に頭に浮かんでしまう場合は，まず，日本語を英語のＳ（主語）＋Ｖ（述語）＋Ｏ（目的語）の順番で言ってみましょう．

３．知らない単語は，知っている単語を使ってなんとか表現する工夫をする．

例えば，「あなたの国では，どのくらいの期間，義務教育があるのですか？」は英語で何と言えばいいでしょうか？もし，「義務教育」という英単語が出てこなかった場合，中学生で習うような簡単な英単語を使ってどう表現すればいいでしょうか？

4–4　論理的なディスカッション（Discussion）をしてみよう

科学分野では，話す時も論理的であることが重要です。

ご自分の意見を言うだけでなく，なぜそう考えるのかという理由，そしてできればご自分の体験など，具体例があると，より説得力が増すと思います。

また，定量的に話すことも重要です。例えば「〜が増加した」と言ってもどのくらい増加したのかわかりません。「〜が 20％増加した」と数字を入れて定量的に述べることで，より具体性が高まります。

ですから，日本語のみならず，英語で話す時も論理的に（logically）かつ定量的に（quantitatively）話すことを心がけましょう。

Discussionの基本表現

1.　Introducing your opinion

I think …….

　　I think it's necessary to/that……..

　　I think it is important that.……

In my opinion,……

It seems to me that……..

To me,……..

2.　Involving other people

What do you think about.……?

What are your thoughts on this ?

Do you have any ideas about.……?

Would you agree with……..?

Do you see what I mean ?

3.　Offering different opinions

Yes, I understand your point but.……

I see your point, but……..

That's good point, but on the other hand.……

OK,…..well I'm not sure, but.……

4.　Other expressions

The reason is that.……

For example,……

This is the reason (why) I think.……

Let me make sure I've got it right. 理解できているかどうか確認させてください .

regarding ～，concerning ～，in terms of ～　～に関しては

because of ～ , due to ～　～のために，～によって

In the case of ～　～の場合

from the viewpoint of ～　～の観点からは

　　from the viewpoint of environment, from the viewpoint of technology,

What is subcritical water?

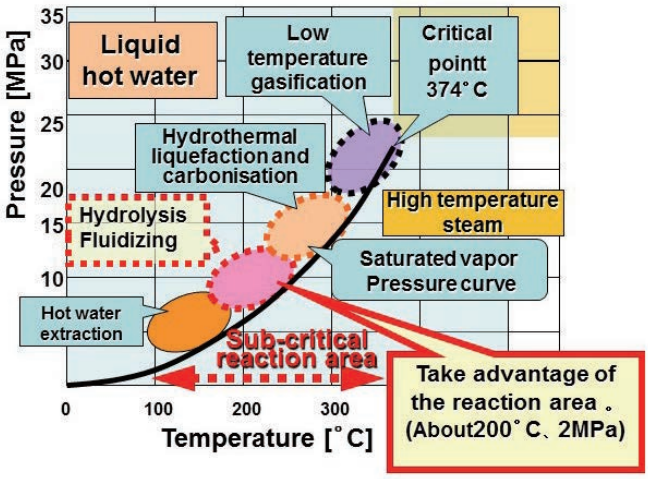

When the temperature and the pressure of water are raised to 374 ℃ and 22 Mpa (220 atmospheres), it becomes an uniform fluid that is neither steam nor water. This condition is called the critical point. Above this point, water is called super critical water. Moreover the hot water where temperature and pressure are lower than the critical point is called subcritical water, and the reaction from this water is called a hydrothermal reaction. Through this reaction the organic molecules such as starch and protein are decomposed into glucose and amino acid as well as being changed into a liquid form from solids. In conclusion this reaction is very safe, good for environment, and obtains valuable resource such as proteins from food waste by a quick and easy process.

To use this subcritical hydrolysis reaction makes recycling of waste easy and gentle on the environment.

What is M RECYCLING MACHINE【MRM】?

The MRM is a future type of subcritical water reactor that processes flammable waste by using high pressure and high temperature in a pressurized vessel.

There is no incineration process; therefore MRM doesn't generate carbon dioxide, dioxin, or nitrous oxide. Odors are not generated because of the sealed process.

This is very good for the prevention of the global warming gases and the protection of the environment. The resulting processed products are in a germ-free condition, with the residual dioxin and heavy metals below government safety standards.

The dimensions of MRM Ⅱ is 4.5 m in height, 8 m in length, and 2.5 m in width. Processing 2 ㎥ of waste takes about an hour. To operate MRM Ⅱ requires 2 to 3 people. The cost to process 2 ㎥ waste is about 3,000 yen including fuel and electricity.

It is able to recycle organic waste such as raw garbage, architectural scrap wood, organic sludge, polystyrene, shredder dust, agricultural vinyl, incineration ash, and any other flammable waste.

Reference:

G-8 INTERNATIONAL TRADING Co., Ltd.

M Miyashiro building 2F,9-26 Daikan-cho,Hiratsuka,Kanagawa,254-0807

TEL 0463-25-0969 FAX 0463-24-2470 Email:info@g8inter.co.jp

http://www.g8inter.co.jp/

[Viewpoint of Discussion]

1．What are the advantages and disadvantages of the M recycle machine ?

Advantages:

Disadvantages:

2．Do you think the M recycle machine business will be expanded throughout the world？ Why？Why not？
Use specific reasons and examples to support your opinion.

Opinion → Reasons → Examples

1．I think the M recycle machine business will be expanded throughout the world.
The reason is that…..

For example,……

2．I don’t think the M recycle machine business will be expanded throughout the world.

The reason is that…..
The M recycle machine is bought not by an individual person but by a large group such as government or public group due to its high cost.
For example,……

The fertilizer generated from the M recycle machine needs to have agricultural lands for it to be used.
For example,……

Dawn of the Dream Toilet –Kenya–

トイレを変えることによって，衛生面を改善するだけでなく，排泄物の肥料化により作物の収穫を増やし結果として住民の貧困も救おうという NGO の取り組みの話．（NHK World TV より）

https://www.youtube.com/watch?v=IrbX7txHxLY

The African nation of Kenya is developing rapidly, but many farmers there continue to subsist below the poverty line on less than US $1.25 per day. Against this backdrop, one Japanese NGO is seeking to promote self-sufficiency in rural communities via a surprising method: the construction of toilets. As well as improving sanitation, organic fertilizers generated by these amazing latrines can dramatically boost crop yields and absolve farmers of the need to buy expensive chemical fertilizers.

Vocabulary

1．背景	
subsist	生きていく，存在する
income	収入
habitant	住人
Sewage system	下水道システム
pit toilet	素掘り式トイレ
overflow	あふれる
swarm of flies	ハエの群れ
infectious disease	伝染病
2．NGO職員Mr.Sendoが登場するシーン	
chamber	便槽
designate	指示する，示す
solid waste	固形排泄物（大便）
liquid waste	液体排泄物（小便）
in terms of~	～の点から,～に関して
hygiene	衛生
dehydrate	脱水する，乾燥する
alkalinity	アルカリ度
eliminate	除去する
insect	虫
detoxify	殺菌する，無害化する

intersperse	まき散らす，散らばらせる，
alkaline compound	アルカリ性化合物
cell membrane	細胞膜
eradicate	根絶する
harmful	害のある
bacteria	細菌
sanitize	衛生的にする
３．エコサントイレにより衛生面の改善がなされるシーン	
hygienic	衛生的な
elementary school	小学校
foster	育てる
patient	患者
cholera	コレラ
diarrhea	下痢
introduction	導入
diagnosis	診断
４．エコサントイレにより作った有機肥料の栄養価が高いことを示すシーン	
related to~	～に関係して
harvest	収穫物
irrigation	灌漑（人工的に用水を引く）
boost	増大する
crop	作物
yield	収穫
chemical fertilizer	化学肥料
organic fertilizer	有機肥料
utilize	使用する
degradation	劣化，退化
fertile	肥沃な
solution	解決
human feces	人糞
dietary fiber	食物繊維
magnesium	マグネシウム
mineral	ミネラル
manure	肥料，肥し
rural village	農村部
affordable way	手ごろな方法
５．地元の住民を集めてセミナーを開くシーン	
skeptical	懐疑的な
be reluctant to~	～することに気が進まない
benefit	利点

cooperation	協力
tackle	タックルする，打ち破る
６．Roseさんに実験協力してもらうシーン	
Ecosan (Ecological Sanitation)	環境に配慮した衛生
Ecosan manure	エコサン肥料=Organic fertilizer
feed	与える，エサをやる
stability	安定性
hang around all day	一日中酔っぱらっている
patch	一区画
be blown over	なぎ倒される
cob	トウモロコシの実
degrade	劣化する
soil	土壌
nutrient balance	栄養バランス
acidic	酸性の
productivity	生産性
In contrast	反対に
massive	大きい，大きくてどっしりした
kernel	核，穀粒
plot	小区画
７．Prof.Matsuiが登場するシーン	
principle	校長
engage in~	～に従事する
protection	保護
cultivation	作物の栽培，土地の耕作
dilute	希釈する
urine	尿
nitrogen	窒素
phosphate	リン酸塩
dilution	希釈
liquid fertilizer	液肥
involve	取り込む，巻き込む
pollution	汚染
contaminate	汚染する
discharge	排出する
water quality	水質
conduct	指揮する
available	利用
sustain	持続する
modern era	近代

extermination	根絶
hallmark	特徴
refine	洗練する
その他	
hygienically	衛生的に
hygiene control	衛生管理
defecate	排泄する

Dawn of the Dream Toilet –Kenya–（ビデオ）の概要

1．背景

ケニアでは近年，都市部（urban area）はめざましく発展している一方で，一日の収入が一人当たり 1.25 ドルより低い，非常に貧しい地域（地名：Bushiangala）がある．ここでは下水道システム（sewage system）もなく，トイレは穴をあけただけの素掘り式トイレ（pit toilet）を使っている．大雨で溢れる（overflow）こともあり，感染症（Infectious diseases）の温床にもなっていて衛生的に（hygienically）良くない．そこで, 2014 年より NICCO という NGO が新しいトイレ，エコサン（EcoSan=Ecological Sanitation）トイレの建設（construction）を行っている．

2．NGO 職員 Mr.Sendo が登場するシーン

尿（liquid waste, urine）と便（solid waste, feces）を分離するエコサントイレの建設（construction）を指導（designate）している．便は排泄（excrete）した後に灰（ash）をまく（intersperse）ことにより，便（solid waste）を脱水し（dehydrate）とアルカリ性にする（alkalize）ことで病害虫（disease-carrying insects）を殺菌し（detoxify），肥料（fertilizer）として使えるように衛生的にする（sanitize）．

3．エコサントイレ（EcoSan Toilet）により，衛生面の改善がなされるシーン

エコサントイレを小学校や公共施設に建設し，小学校では，トイレを使い，灰をまいた後に手を洗う習慣（hand washing habits）を育てている．エコサントイレを導入する（introduce）ことで，コレラ（cholera）や下痢（diarrhea）の患者（patient）が減ったと医者が証言．

4．エコサントイレにより作った有機肥料の栄養価が高いことを示すシーン

化学肥料（chemical fertilizer）を使い続けていると，土壌（soil）が劣化（degradation）し作物がやせてしまう．その解決策（solution）として，人糞（human feces）から作った有機肥料（organic fertilizer) は，食物繊維（dietary fiber）やマグネシウム（magnesium），その他のミネラル（mineral）を含んでいる．農村部（rural village）では，収入（income）も低いので，コストゼロの，エコサン肥料（human waste as manure）を使う（utilize）するのが農業生産（agricultural productivity）を増やす（boost）ための手ごろな方法（affordable way）と Mr. Sendo が言う．

５．地元の住民を集めてセミナーを開くシーン

エコサントイレを各々の家に設置してもらおうと，地元の住民を集めてセミナーを開いたが人糞（human waste）から作った肥料と聞いて住民は懐疑的（skeptical）．人糞から伝染病（infectious disease）が広がることもめずらしくないので，殺菌してあり（detoxified）安全だと説明しても，住民はエコサン肥料には触りたがらない（reluctant to touch）．この状況を打破する（tackle）には，地元の農民（local farmer）に協力（cooperation）を得て実際に実験し，その効果（effectiveness）を評価する（evaluate）してみるしかないと．Mr.Sendo は考えた．

６．Rose さんに実験協力してもらうシーン

Rose さんという女性の協力者を得て，実験をしてみる．Rose さんの畑にて，

① 肥料無し（No added fertilizer）

② 化学肥料を施肥（Chemical fertilizer）

③ エコサン肥料を施肥（EcoSan manure, Manure from toilet, organic fertilizer）

の３つの区画（plot）に分けて，とうもろこしを栽培し，それぞれの区画でとれた収穫物（yield）を比較する．

実験結果：収穫物の重量

①　5.5 kg

②　10 kg

③　91 kg

となり，エコサン肥料の栄養価が高い（rich in nutrient）ことが示された．

７．Prof.Matsui が登場するシーン

下水処理（sewage treatment），有機農業（organic farming）の専門家であり，この組織のディレクター（director）である Matsui 教授がこの地を視察しに来る．Matsui 教授はエコサントイレの第一人者であり，世界中でエコサントイレを推進してきた．小学校の校庭（school garden）では，子供たちが，尿（urine）を希釈し（dilute），液肥（liquid fertilizer）にして作物に施肥する（fertilize）練習（training, practicing）をしている．子供たちも尿から作った液肥の効果に驚いている．Matsui 教授はビクトリア湖の汚染（pollution）の一因は屎尿であると言う．日本の琵琶湖の水質（water quality）にもずっと関わってきた．屎尿は水環境に排出せずに農業利用すべき（Excrement should be discharged not into water environment but back onto fields for agriculture.）日本の近代（江戸時代）は人間の屎尿を肥料として有効利用していた特徴（hallmark）があり，それをアフリカに合う形で適用すべきと言う．

[Viewpoint of Discussion]

Do you think the Ecosan toilets should be used in Japan ?

Why? Why not ?

Use specific reasons and examples to support your opinion.

Opinion → Reasons → Examples

1 . I think the Ecosan toilets should be used in Japan.

The reason is that….

We have a problem of shortage of phosphate which is contained in excrements and one of the elements required for crops.

For example,……

From the viewpoint of environment, I think excrements should be discharged not into the water environment but back onto fields for agriculture.

For example,……

2 . I don't think the Ecosan toilets should be used in Japan.

The reason is that…….

Sewerage systems are already installed in urban areas in Japan.

For example,……

Japanese people are too busy to deal with Ecosan toilets properly.

For example,……

From a hygienic viewpoint, Ecosan toilets might not be suitable for Japan.

For example,……

Let’s discuss about toilets !

Vocabulary

flushing toilet	水洗トイレ
urine(liquid waste)	小便，尿
f(a)eces (solid waste)	大便
require	要求する
septic tank	浄化槽
sewage system	下水道システム
advantage	長所
disadvantage	短所
comfortable	快適な，心地よい
hygienic	衛生的な
sewage disposal	汚水処理
excrement	屎尿
household environment	住環境
waste pipe	下水管
contaminated wastewater	汚染された下水
downstream infrastructure	下流のインフラ（下水道システムなど）
untreated wastewater	未処理下水
outflow	流出物
groundwater	地下水
treatment	処理
irrigating crops	灌漑作物
developed countries	先進国
developing countries	発展途上国
urban area	都市域
rural area	郊外，田舎
sustainable	持続的な
disaster	災害
earthquake	地震
electricity	電気
water works	水道設備

Let’s discuss about toilets !

Over the years the toilet has developed into its present form, the **flushing toilet.** It has a flushing mechanism to wash the **urine, faeces** and toilet paper away with water. This type of toilet **requires** a constant and sufficient (enough) water supply. The force of the water from the flushing mechanism washes the urine, faeces and toilet paper out into a **septic tank** or **sewage system.**

Advantages and disadvantages of the flushing toilet.

Advantages: The flushing toilet that is highly popular provides a **comfortable**, safe and **hygienic** method of **sewage disposal**. They are easy to use and keep clean and they remove **excrement** from the **household environment**. The water seal prevents flies and smells from entering the house through the **waste pipe**.

Disadvantages: The flushing toilet can produce substantial quantities of heavily **contaminated wastewater** which then requires **downstream infrastructure** to avoid environmental and public health problems. **Untreated wastewater** can pose risks to health if the **outflow** may pollute **groundwater,** or even more critically, is used without **treatment** for **irrigating crops**.

Viewpoint of Discussion

Do you think flushing toilets should be replaced with other toilets in Japan?
Use specific reasons and examples to support your opinion.

レポート課題

Please summarize your opinions regarding the discussion topic.
Your opinion needs to be supported with logical reasoning.

Student number_____

Name_____

e.g.

In my opinion,_____for the following reasons.

Firstly,_____.

For example,_____.

Secondly,_____.

For example,_____.

Therefore, I think._____

長くてもこの **A4** 用紙一枚以内にまとめてください．また，英語の下に日本語訳も書いてください．

このファイルは期日までに，**Blackboard** にアップロードしてください．

著者略歴

中川 直子

東京都文京区生まれ.
お茶の水女子大学理学部物理学科卒業.
卒業後は㈱東芝総合研究所にて勤務.
海外在住の後，お茶の水女子大学に再入学し2007年お茶の水女子大学博士後期課程修了，博士（理学）取得．その後，お茶の水女子大学，首都大学東京にて勤務した後，現在，立教大学理学部特任准教授として科学英語教育に携わる.

Let's enjoy Scientific English !

2018年９月15日発行

著　者　中川直子
発行所　学術研究出版
〒670-0933　姫路市平野町62
TEL.079（222）5372　FAX.079（223）3523
http://bookway.jp
印刷所　小野高速印刷株式会社

ISBN978-4-86584-332-3

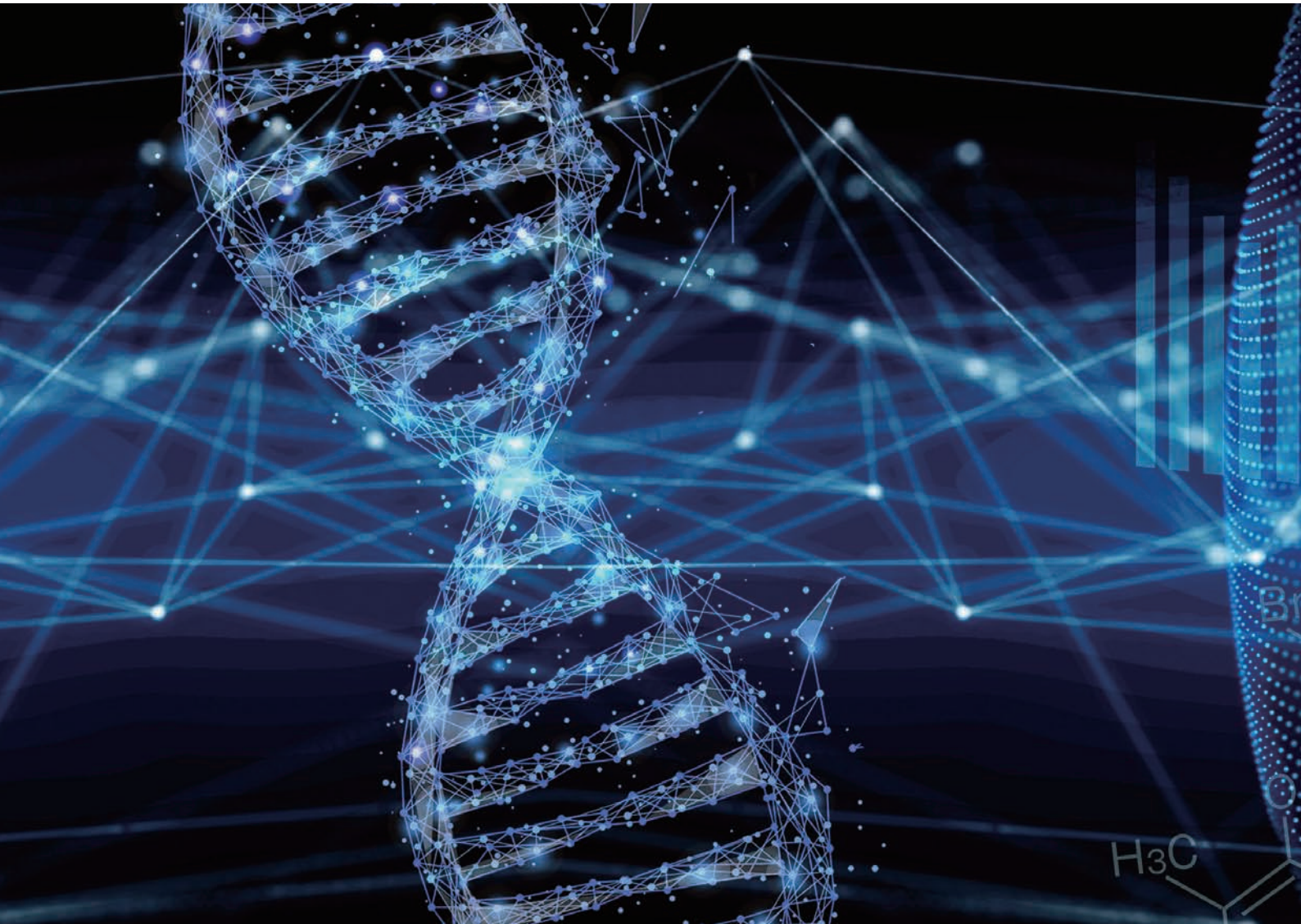
H3C